Propriétés électriques, optoélectroniques et thermoélectriques de matériaux à base de poly (3,4-éthylènedioxythiophène)PEDOT

Magatte Gueye

Communauté
UNIVERSITÉ Grenoble Alpes

THÈSE

Pour obtenir le grade de

DOCTEUR DE LA COMMUNAUTE UNIVERSITE GRENOBLE ALPES

Spécialité : **2MGE : Matériaux, Mécanique, Génie Civil, Electrochimie**

Arrêté ministériel : 25 mai 2016

Présentée par

Magatte Niang GUEYE

Thèse dirigée par **Jean-Pierre SIMONATO,** Directeur de recherche CEA Grenoble
Encadrée par **Renaud DEMADRILLE,** Ingénieur de recherche CEA Grenoble
Et par **Alexandre CARELLA,** Ingénieur de recherche CEA Grenoble

Préparée au sein du **Laboratoire systèmes moléculaires et nanomatériaux pour l'énergie et la santé (DRF/INAC/SyMMES/STEP)**
Et du **Laboratoire de synthèse et d'intégration des nanomatériaux (DRT/Liten/DTNM/SEN/LSIN)**

Dans **l'École Doctorale IMEP-2 – Ingénierie, Matériaux, Mécanique, Environnement, Energétique, Procédés, Production**

Propriétés électriques, opto-électroniques et thermoélectriques de matériaux à base de poly(3,4-éthylènedioxythiophène) (PEDOT)

Thèse soutenue publiquement le **18 décembre 2017**
devant le jury composé de :

Madame, Laurence VIGNAU
Professeur, IMS, Bordeaux INP, Rapporteur
Monsieur, Adam PRON
Professeur, Warsaw University of Technology, Rapporteur
Monsieur, Jean-Luc DUVAIL
Professeur, IMN, Université de Nantes, Examinateur
Monsieur, Daniel BELLET
Professeur, LMGP, UGA Grenoble, Président du jury
Monsieur, Renaud DEMADRILLE
Ingénieur de recherche, INAC, CEA Grenoble, Encadrant
Monsieur, Alexandre CARELLA
Ingénieur de recherche, Liten, CEA Grenoble, Encadrant
Monsieur, Jean-Pierre SIMONATO
Directeur de recherche, Liten, CEA Grenoble, Directeur de thèse

« L'homme s'ennuie du bien, cherche le mieux,
trouve le mal, et s'y soumet par crainte du pire. »
Duc de Lévis

Remerciements

Ces trois dernières années furent marquées, entre autres, par la découverte de la présence d'eau sur Mars, la détection des ondes gravitationnelles, la création d'un cristal temporel à l'échelle du laboratoire, mais aussi, dans une moindre mesure certes, mais néanmoins importante pour moi, par toutes ces personnes qui ont été impliquées dans mes trois années de thèse. Avant de clore ce chapitre de ma vie, j'aimerais prendre quelques lignes et leur exprimer toute ma gratitude, et j'espère sincèrement n'oublier personne.

Mes premiers remerciements vont au labex LANEF qui a bien voulu financer mes travaux de thèse. Mes remerciements vont tout particulièrement à Joël Cibert et Xavier Thibault qui ont suivi mes travaux avec des entretiens réguliers tout au long de ces trois années. Merci pour les discussions enrichissantes qui ont toujours accompagné ces entretiens.

Je tiens aussi à remercier les membres du jury pour avoir accepté d'évaluer mes travaux de thèse. Je remercie ainsi Madame Laurence Vignau et Monsieur Adam Pron pour avoir accepté d'être les rapporteurs de ma thèse, Monsieur Jean-Luc Duvail pour avoir examiné mon travail et Monsieur Daniel Bellet pour avoir présidé ma soutenance de thèse. Merci beaucoup pour l'intérêt que vous avez porté à mon travail, et merci aussi pour vos questions et remarques intéressantes, ainsi que la discussion enrichissante qui a suivi ma soutenance de thèse !

Je souhaite ensuite adresser mes profonds sentiments de gratitude à mon directeur de thèse Jean-Pierre Simonato et à mes encadrants, Renaud Demadrille et Alexandre Carella. Merci J-P pour le suivi régulier, malgré le travail parallèle de chef de labo qui n'était pas de tout repos ! Je retiens surtout ton pragmatisme et ta disponibilité grâce auxquelles je n'ai jamais perdu le nord ! Merci Renaud pour ton encadrement. Suivre une thésarde qui dépend de ton labo mais évolue dans un autre ayant une politique différente n'a pas été sans complexité ! Grâce à ton important bagage scientifique, couplé à ta facilité de communication, je ressortais plus instruite après chaque passage à l'INAC. Merci aussi Alex pour ton encadrement. Depuis nos entretiens téléphoniques jusqu'au moment où je rédige ces remerciements, tu as toujours appuyé mes projets et m'en as proposé bien d'autres. Ton optimisme infaillible a constitué un cadre serein pour ma thèse. J-P, Renaud, Alex, merci beaucoup pour votre confiance et vos conseils ! A vous trois, vous avez formé une synergie formidable qui m'a permis de finir ma course sans jamais perdre mon souffle. Les futurs thésards que vous encadrerez ont bien de la chance, ils peuvent me croire ! Au plaisir de retravailler ensemble !

J'aimerais aussi remercier Peter Reiss pour m'avoir accueilli dans son laboratoire, et merci à Frédéric Chandezon et Jean-Pierre Travers pour le suivi et l'intérêt que vous avez manifesté pour mon sujet de thèse.

Un remerciement très spécial à Stéphanie Pouget, Jérôme Faure-Vincent, Hanako Okuno, Anass Benayad, François Rieutord pour toutes ces études et caractérisations que l'on a faites et qui ont enrichi ma thèse. Moi qui adore la caractérisation, ce fut un plaisir d'apprendre de votre expertise et de partager toutes ces discussions scientifiquement et humainement très instructives.

De gros gros gros remerciements à tous ceux de la fosse à thésards (les anciens comme les nouveaux), les alternants du E et notre mamie-détective. Pour cette expérience unique (joie, petits coups de stress, fous rires, travail –plus ou moins acharné, sorties, débats scientifico-politico-philosophiques… mais pas que ☺), merci beaucoup Lou, Hugo, Thomas S., Djadidi, Anthony, Etienne. Partager le même bureau que vous m'a permis de grandir ! Merci beaucoup Lucie, notre détective-mamie-pas-si-vieille-que-ça aux blagues… disons… curieuses. Et merci aussi aux tout nouveaux, Amélie (ce labo manquait un peu de filles, mais quelle idée de n'arriver que maintenant :/) et Arnaud (tu le fais exprès ou tu n'as vraiment pas de chance ?). Bon courage pour la suite !

Je remercie chaleureusement tous mes collègues du SyMMES qui n'ont jamais été avares en gentillesse, bons conseils et encouragements ! Plus particulièrement, merci Olivier B., pour le cours de remise à niveau sur le photovoltaïque organique, et pour tout en fait. Merci beaucoup Damien, Florent, Maxime et Cyril, et bon courage pour vos travaux et post-docs respectifs ! Merci Yann K., Ben, Jérôme P., Clément, David, Sandrine et Pascale. Je ne vous oublie pas Charlie, Joëlle, Sarah et Christine. Je vous ai souvent embêtés pour tous mes papiers administratifs et vous suis très reconnaissante de votre aide toujours dans la bonne humeur.

Dans cette même optique je remercie tous mes collègues du LSIN qui m'ont aidée à évoluer autant scientifiquement que humainement. Merci tout particulièrement à Caro et Bruno ! Mes remerciements vont aussi à Sakina, Sonia, Florence, Charlotte, Aurélien, Jacqueline, Konstantin et Stéphanie !

Un remerciement très spécial à tous ceux du bâtiment E dont la présence, les blagues, les discussions et surtout les gâteaux (ah ça va me manquer ça ☺) au quotidien ont rythmé mes trois années de thèse et lui ont donné la douce saveur qu'il me reste aujourd'hui ! Merci Olivier ! Tisane thym miel, thé à la menthe et tous ces KWIINK me manquent déjà ! Merci

beaucoup Myriam, Elise, Camille, Gaëlla, Sophie, Julie, Thomas P., Michel, Stéphane, Marilyne, Denis, Cyril, Marc, Sorana et Nathalie.

Grâce à vous tous, j'ai vécu 3 belles années et je vous en remercie énormément !

Ces remerciements ne seraient pas complets sans toutes ces personnes externes au labo mais dont la présence ces trois dernières années ont été importantes pour moi ! Merci beaucoup Hélène et Jenni ! It was a real pleasure knowing you and sharing that weird passion for socks ;)! See you around somewhere in the world, and very soon I hope ☺! Thank you!

Un grand merci à Marie-So ! J'ai adoré vivre avec toi, dommage que cette fin de thèse rime avec la fin de notre coloc'! On retiendra qu'on n'a toujours pas compris le principe du salon…

Un merci très spécial à Solène, pour ton amitié, pour ton soutien inconditionnel durant toutes les phases de ma vie ces dernières années, pour avoir été une énorme bouée pour moi, et pour ne pas avoir pris tes jambes à ton cou malgré le danger ambulant que je constitue :p, Merci beaucoup Rémy, j'ai hérité d'un nouvel ami grâce à Solène ! Et bon courage à vous deux pour la rédaction et pour la suite après la thèse ! Les beaux jours reviennent ! French pour garder la motivation et bastille pour se donner bonne conscience ?

Je finis enfin ces remerciements en exprimant toute ma profonde et sincère gratitude à Tapha, Fatou, Papa et Maman. Je suis infiniment reconnaissante de vous avoir comme famille, et je vous remercie énormément pour tout le soutien que vous me prodiguez depuis que je suis toute petite, et malgré mes idées farfelues qui vont parfois à l'encontre de ce dont vous avez l'habitude. Je ne vous remercierai jamais assez… Merci beaucoup !

List of abbreviations

AFM	Atomic force microscopy
AgNWs	Silver nanowires
C-AFM	Conductive atomic force microscopy
CB	Conduction band
CNTs	Carbon nanotubes
CV	Cyclic voltammetry
DMF	Dimethylformamide
DMSO	Dimethyl sulfoxide
EA	Electron affinity
EDOT	3,4-ethylenedioxythiophene
EG	Ethylene glycol
EPR	Electron paramagnetic resonnance
GIWAXS	Grazing-incidence wide-angle X-Ray diffraction
HOMO	Highest occupied molecular orbital
HRTEM	High resolution transmission electron microscopy
IE	Ionization energy
IPA	Isopropyl alcohol
ITO	Indium tin oxide
LUMO	Lowest unoccupied molecular orbital
MDOT	Methylene dioxythiophene
NMP	N-Methyl-2-pyrrolidone
NMR	Nuclear magnetic resonnance
OLED	Organic light emitting diode
OPV	Organic photovoltaics
OTf	Triflate, Trifluoromethanesulfonate
PC	Poly-carbonate
PEDOT	Poly (3,4-ethylenedioxythiophene)
PEG-PPG-PEG	Poly(ethylene glycol) – poly(propylene glycol) – poly(ethylene glycol)
PEI	Polyethylene imine
PET	Polyethylene terephthalate
PSS	Polystyrene sulfonate
QCM	Quartz crystal microbalance
SCP	Solution cast polymerization
SEM	Scanning electron microscopy

Sulf	Hydrogenosulfate
Tos	Tosylate
UV-Vis-NIR	Ultraviolet – Visible – Near infrared
VB	Valence band
VPP	Vapor phase polymerization
XANES	X-Ray absorbtion near edge structure
XPS	X-Ray photoelectron spectroscopy
XRD	X-Ray diffraction

General Introduction

To make a long story short, organic electronics is a field of materials science that deals with the design, synthesis and study of organic materials whose electrical properties are interesting enough to consider them for technical applications. To give that same story its fullest insight, we have to go through more than a half century of materials science research, beginning with the discovery of conducting polymers, or rather the keen interest that arose after the pioneering work of Hideki Shirakawa, Alan Heeger and Alan MacDiarmid.

In 2000, these three researchers were awarded the Nobel Prize in chemistry "for the discovery and development of conducting polymers" as they managed to increase the conductivity of polyacetylene by 10 million times through doping.[1,2] Actually, they did not discover conducting polymers as partly evidenced by Naarmann's conference talk given in 1969.[3] The discovery of conducting polymers dates back from more than a century ago with polyaniline, which was electrically insulating at that stage, but whose conductivity was stated as early as 1967.[4,5] Polypyrrole was also proved to be electrically conductive as early as 1963.[6–8] But the real excitement behind conducting polymers and the possible routes that they opened through organic electronics truly begun with the Nobel Prize awardees' discovery, that is the conductivity of polyacetylene could be increased over several orders of magnitude.[1,2] Was it because of the dramatic increase in conductivity, because of the international collaboration between Hideki Shirakawa (Tokyo, Japan) and Alan Heeger and Alan MacDiarmid (Pennsylvania, Philadelphia), or because of the serendipity in their work (as at first they were not interested in polyacetylene itself)? In any case, from that point, scientists considered conducting polymers as "a new generation of materials which exhibit the electrical and optical properties of metals or semiconductors *and* which retain the attractive mechanical properties and processing advantages of polymers". Conducting polymers were then interesting in a "characterization" point of view due to their "intermediary" position, as well as an "application" point of view as they opened the route to "plastic electronic devices".[9] Therefore studies mainly focused on the synthesis, engineering and processing of conducting polymers with good electrical and optoelectronic properties as well as the understanding of the charge transport mechanisms.

After some years of research, poly(3,4-ethylenedioxythiophene) (PEDOT) stood out from the huge family of conducting polymers which were studied (polyaniline, polyacetylene, polypyrrole, polythiophene, poly(*para*-phenylene vinylene) and their derivatives) due to its interesting properties, high stability and processability. From all the conducting polymers, PEDOT is probably the most known, it is commercialized and is now present in numerous organic electronics applications such as anti-static coating, hole injecting layer or active layer in organic light emitting diodes (OLEDs), transistors, solar cells, electrochromic devices.

However, the fact that PEDOT is already present in those applications does not mean that there is no room for further investigation, development of new materials and novel applications. That is what we intended to achieve during this thesis by developing new PEDOT materials, fully characterizing them, implementing new applications while always comparing ourselves to the state of the art and the commercial PEDOT materials.

Therefore, the first chapter will lay the groundwork with definitions of conducting polymers, PEDOT, its applications and its properties. We will try to understand why such popularity around PEDOT, what makes it so special, what the existing and potential applications are, in other words, why we directed this thesis through its thorough study.

Subsequently, the second chapter will present PEDOT materials developed within our group, as well as their interesting structure and electrical properties. This chapter is basically showing the results which have been already published in part in the journal Chemistry of Materials, in the article entitled : “Structure and dopant engineering in highly conductive PEDOT thin films: practical tools for a dramatic conductivity enhancement”.[10]

The interesting electrical properties posed in Chapter 2 are also accompanied with appealing optical properties as will be presented in Chapter 3. This combination of transparency and high conductivity / low sheet resistance is strongly sought in optoelectronics, especially for transparent electrodes. This is proved by already existing applications and continuous research in this field as exposed in this chapter. We however directed ourselves into a novel application for conducting polymers dealing both with their optoelectronic and non-reversible thermoelectric properties for heat generation, namely transparent heaters. Chapter 3 will hence focus on the study, characterization and application of PEDOT as flexible transparent heater. This work

has been published in ACS Applied Materials & Interfaces in 2017 under the title “All polymeric flexible transparent heaters”.[11]

The Chapter 4 will deal with thermodynamically reversible thermoelectric properties of PEDOT. Indeed, PEDOT is also currently intensively investigated for its potential thermoelectric applications for waste heat harvesting. As it will be shown in this chapter, a high electrical conductivity is a requirement for a good thermoelectric material, but not exclusively. We then investigated some properties that could make our PEDOT materials good thermoelectric ones (namely the electrical conductivity and the Seebeck coefficient), in order to optimize the power factor, a datum that provides information on the thermoelectric efficiency of the material as it will be defined therein.

With the electrical, optoelectronic and thermoelectric properties exposed in this thesis, we direct ourselves to the potential use in thermoelectric devices, transparent heaters and/or transparent electrodes. Any practical application would certainly require a stable functioning material. PEDOT is known to be stable. That does not mean indefinitely stable and in all kinds of environments, especially for the newly synthesized PEDOT materials presented in this study (along with commercial ones). In the last chapter, we explored their ageing and stability when exposed to harsh conditions, observed their degradation and attempted to unravel the mechanisms behind such degradation.

This work will finally be completed with a general conclusion that will most likely show the contribution of this thesis to the better comprehension of PEDOT based materials and some of their applications.

An Appendix is also provided, resuming all the experimental methods and the characterization techniques, as well as some references.

Table of contents

Chapter 1
Literature review on PEDOT materials

This short review of the literature is expected to be slightly historical so that one can understand the frame of the works. However, even if most of the synthesis methods and transport or structure studies were previously used for earlier conducting polymers before PEDOT development, we limited this work to the scope of PEDOT for the sake of conciseness.

The purpose of this chapter is to introduce PEDOT, that electrically conductive polymer that aroused, and still does, great interest in all fields of organic electronics' applications. The notion of conjugated and conducting polymers is presented hereinafter as well as that of PEDOT. Subsequently, progresses on the electrical conductivity enhancement are reported and the origin of such improvement is explained. An overview of the structure is given and finally the transport mechanisms are presented. We purposely directed the work through elements that might help to have a better understanding of the electrical, optoelectronic and thermoelectric properties of the polymer films that we will develop hereinafter. Though the literature presented dealt particularly with the electronic conduction and related aspects, optoelectronic and thermoelectric properties of PEDOT will be presented in Chapter 3 and 4, the work being voluntarily chopped for the sake of clarity.

1. Conjugated polymers, semiconductors and conducting polymers

1-1. π-electrons and conjugation

We begin with reminding few basics about semiconducting and conducting organic materials.

Carbon atom's electronic ground state configuration is $1s^2 2s^2 2p^2$. The valence electrons are those available in the most external atomic orbitals $2s^2$ and $2p^2$, the third 2p orbital being unfilled. The system is however more stable with only half filled orbitals, if not fully filled. Therefore, the appropriate electronic configuration is $1s^2 2s^1 2p^3$ with one valence electron per atomic orbital. When involved in the formation of covalent bonds with surrounding atoms, the atomic orbitals 2s and 2p combine in order to evolve into hybridized orbitals. Depending on the number of surrounding atoms, the carbon can be sp^3, sp^2 or sp hybridized.

- sp^3 hybridization (Figure I.1a): when the carbon is surrounded by four atoms, the 2s orbital is hybridized with each 2p orbitals, resulting in four sp^3 orbitals. All valence electrons take part in σ bonds constituted from the overlapping of one sp^3 orbital with one neighboring one. The structure is tetrahedral and the obtained molecule is three dimensional.

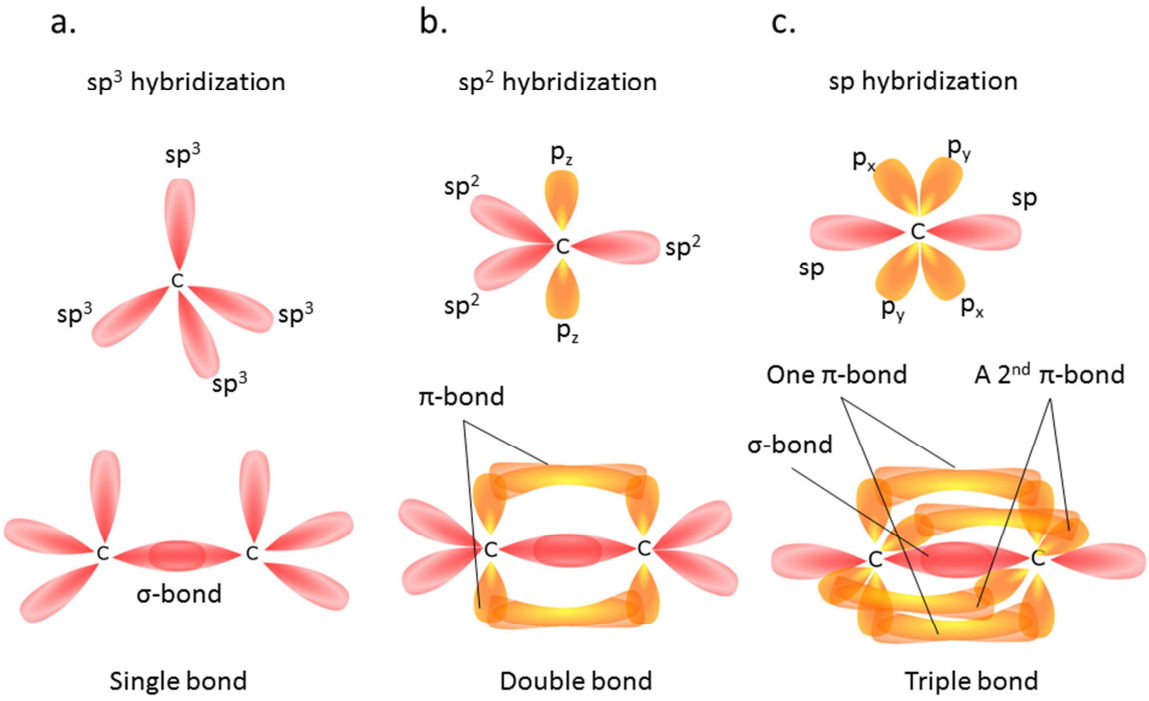

Figure I.1. Diagram summarizing the orbital hybridization in carbon atoms. a) sp^3 hybridization. b) sp^2 hybridization and c) sp hybridization.

- sp^2 hybridization (Figure I.1b): when the carbon is surrounded by three atoms, the 2s orbital is hybridized with two of the 2p orbitals, resulting in three sp^2 orbitals and one $2p_z$ orbital. Three σ bonds are created by overlapping a sp^2 orbital with a neighboring orbital and the remaining $2p_z$ orbital is perpendicular to the plane of the σ bonds. Especially if two sp^2 hybridized carbons are close, $2p_z$ orbitals overlap to create a weaker π bond from both sides of the stronger bond. The pair created by the σ and π bonds is described as a double or conjugated bond while the sole σ bond is called a single bond. Single bonds are longer (0.154 nm) than double bonds (0.134 nm). The structure is planar as well as the obtained molecule, which is unsaturated.

- sp hybridization (Figure I.1c): the 2s orbital is combined with only one of the 2p orbitals, hence giving two hybrids sp orbitals and two 2p orbitals. Therefore if two sp hybridized carbons atoms get close, a σ bond and two π-bonds are created between them, which constitute a triple bond. The structure is linear and so is the obtained molecule which is unsaturated.

1-2. Conjugated polymers

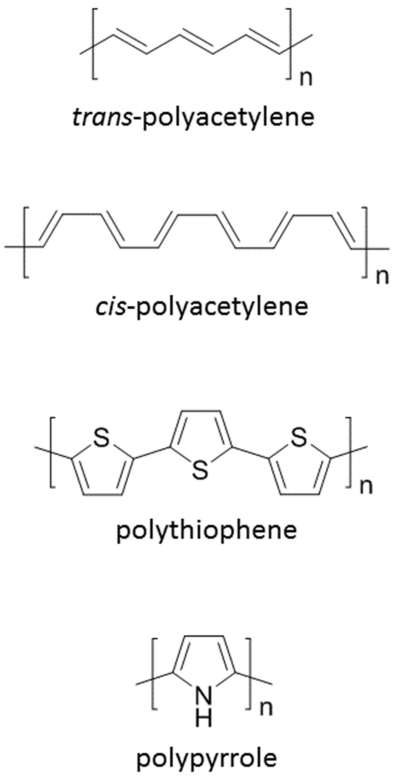

Figure I.2. Some examples of conjugated polymers.

According to *The Free Dictionary*, a polymer is "a naturally occurring or synthetic compound, (…), that has large molecules made up of many relatively simple repeated units".[1] A conjugated polymer is a polymer characterized by a backbone chain of units containing π electrons. The p-orbitals overlap and create a system of delocalized π-electrons. Some examples of conjugated polymers can be found in Figure I.2. The delocalization of π-electrons can be understood as a railway for π-electrons, which do not belong to only one carbon atom since each carbon atom can create π bonds with

[1] http://www.thefreedictionary.com/polymer

one of its neighbors independently. Therefore, p orbitals are overlapping and electrons are delocalized.[12,13] Due to defects that can occur along the chains, the delocalization occurs on a certain number of monomer units and that limited delocalization space is called a conjugation length.

1-3. Semi-conducting polymers

In saturated polymers (all carbon atoms are sp^3 hybridized), the atomic orbitals merge into molecular ones and quantum physics predicts the arrangement of the energy levels into σ bonding and σ* antibonding states. Energy bands are created and the gap between the filled valance band (σ bonding) and the empty conduction band (σ* antibonding) is too high, typically higher than 6 eV, which renders the polymer insulating.[14]

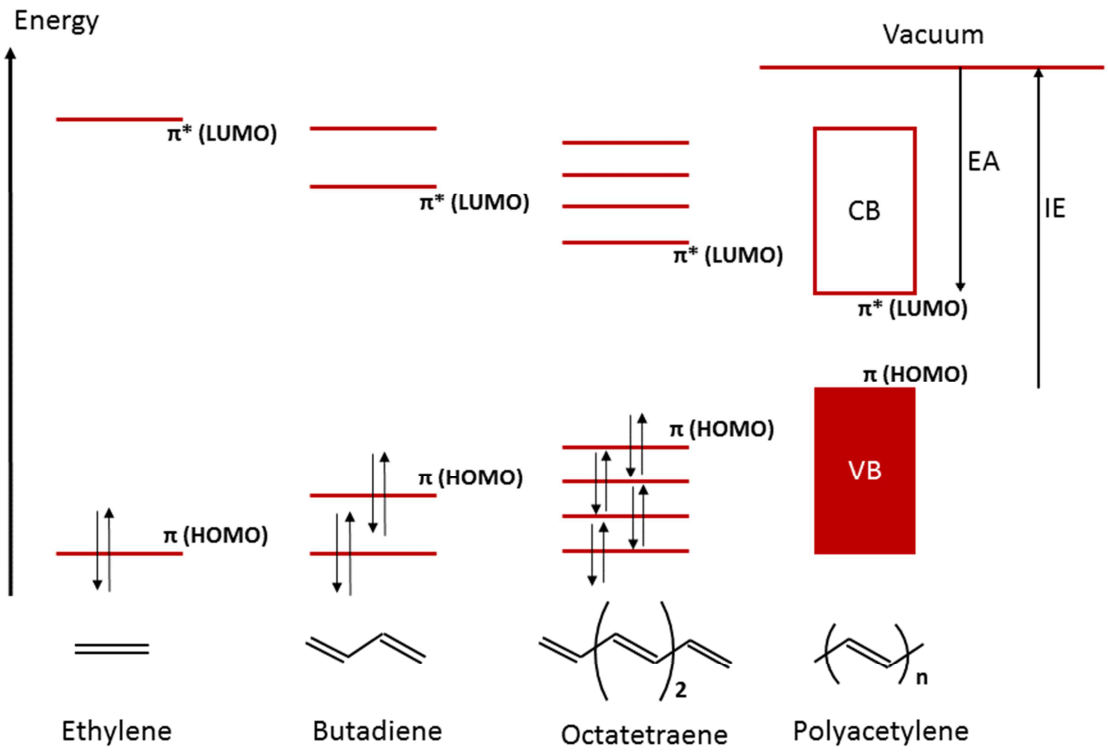

Figure I.3. Band structure building in conjugated polymers. Reproduced after[14].

In conjugated polymers, quantum physics also predicts the formation of π bonding and π* antibonding states after the creation of a molecular orbital from the p atomic orbitals. These states are respectively the highest occupied molecular orbital (HOMO) and the lowest unoccupied molecular orbital (LUMO). The longer the chain becomes,

the more states are created within these states and the energy gap between the HOMO and the LUMO decreases (Figure I.3). When the chain becomes long enough (supposedly infinite) the molecular orbitals are so close that discretization ceases and energy bands are created, a completely filled valence band (VB) whose highest energy is the HOMO and a completely empty conduction band (CB) whose lowest energy is the LUMO. The energy gap between the HOMO and the LUMO is comprised between 1 and 4 eV, hence rendering conjugated polymers semi-conductors (Figure I.4).[15]

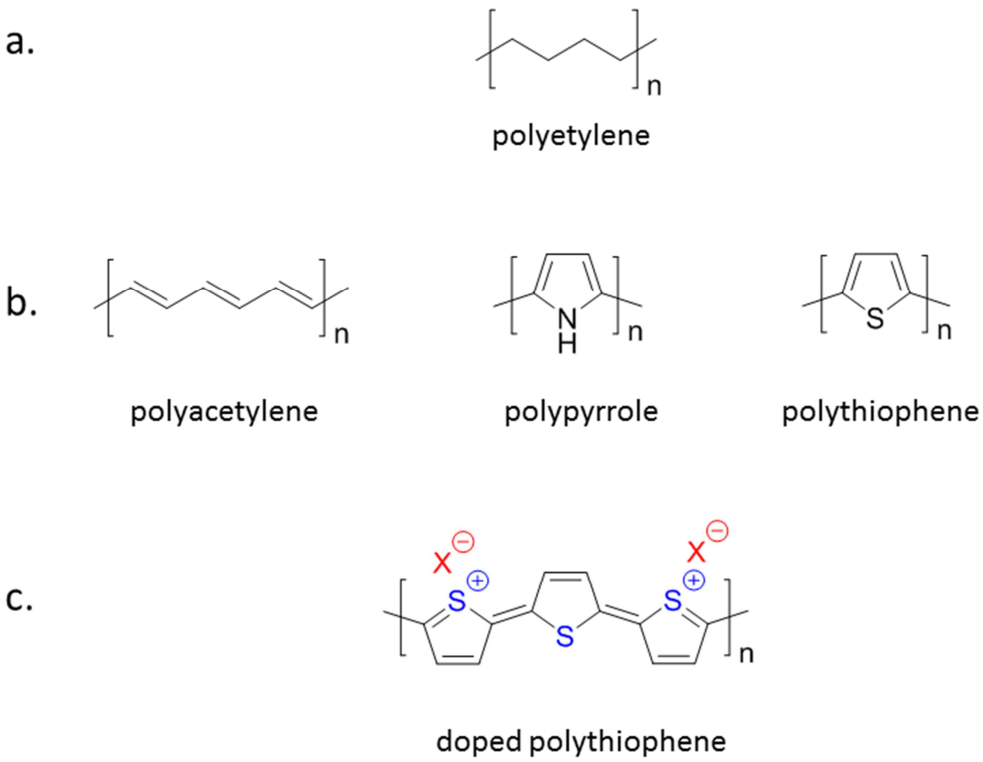

Figure I.4. The difference between insulating polymers (saturated) (a), conjugated (semiconducting) polymers (b) and conducting polymers (c), as reproduced from Evans et al.[16]

Electronic conduction is achievable if electrons are easily extracted from the HOMO (low ionization energy (IE)) or easily injected in the LUMO (high electron affinity (EA)). Given the delocalized π-electrons in semi-conducting polymers, π-electrons can efficiently be injected (reduction) or extracted (oxidation). Therefore, semi-conducting polymers can be doped, charges carriers created and charges' conduction favored.

1-4. Conducting polymers

Doping in semiconducting polymers consists of the introduction of an electron (injected electron) or a hole (extracted electron) in the polymer chain. With the presence of such a charge within the π-system, a local deformation of the conjugated chain occurs in order to reduce its energy. The charge is then localized around the deformation of the chain. This defect, namely the coupling between the charge and the deformation, is at the origin of the conduction mechanisms in semi-conducting polymers. The defect appears as an alternation of simple and double bonds on some units around the charge and differently from the rest of the chain. Depending on the polymer, the system can be degenerated or not.

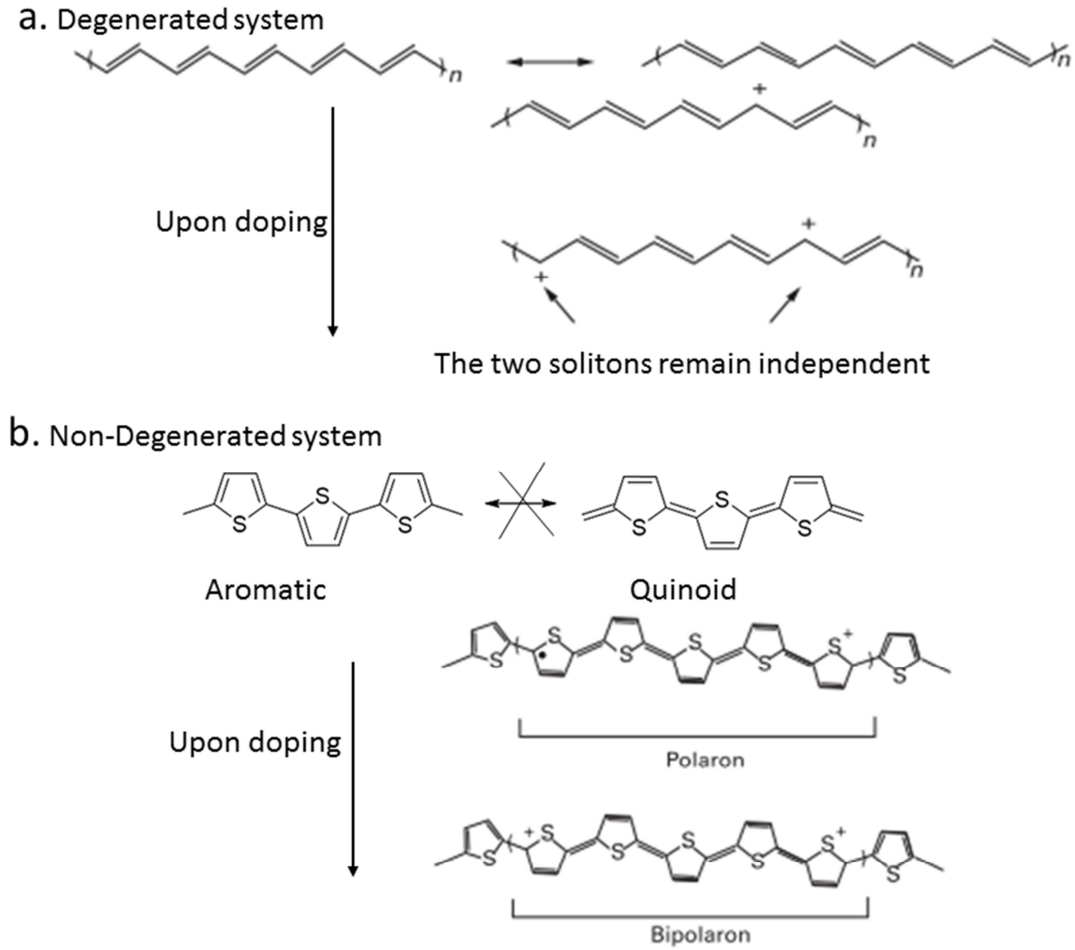

Figure I.5. Charge carriers in degenerated and non-degenerated systems, reproduced after[14].

The only degenerated system is *trans*-polyacetylene as represented in Figure I.5. The defect delimits two zones with differently alternating single and double bonds. The permutation of the bonds all along the chains does not alter the energy of polyacetylene and the charge carrier is called a soliton in physics (radical ion in chemistry) because it is similar to a wave that can propagate without deformation and dissipation.[17]

If the system is non-degenerated, the permutation of the bonds in the polymer changes its energy. Indeed, if a charge is introduced in polythiophene (Figure I.5) which has a benzenoid structure, a local deformation is induced with a quinoid structure and expands on some units. The polymer recovers its benzenoid structure from both sides of the defect in order to lower its energy. The defect is called a polaron (or radical ion). If another charge is injected, it will preferentially get localized around the deformation in order not to increase the energy of the polymer chain. This new defect is called a bipolaron (radical dication).[17]

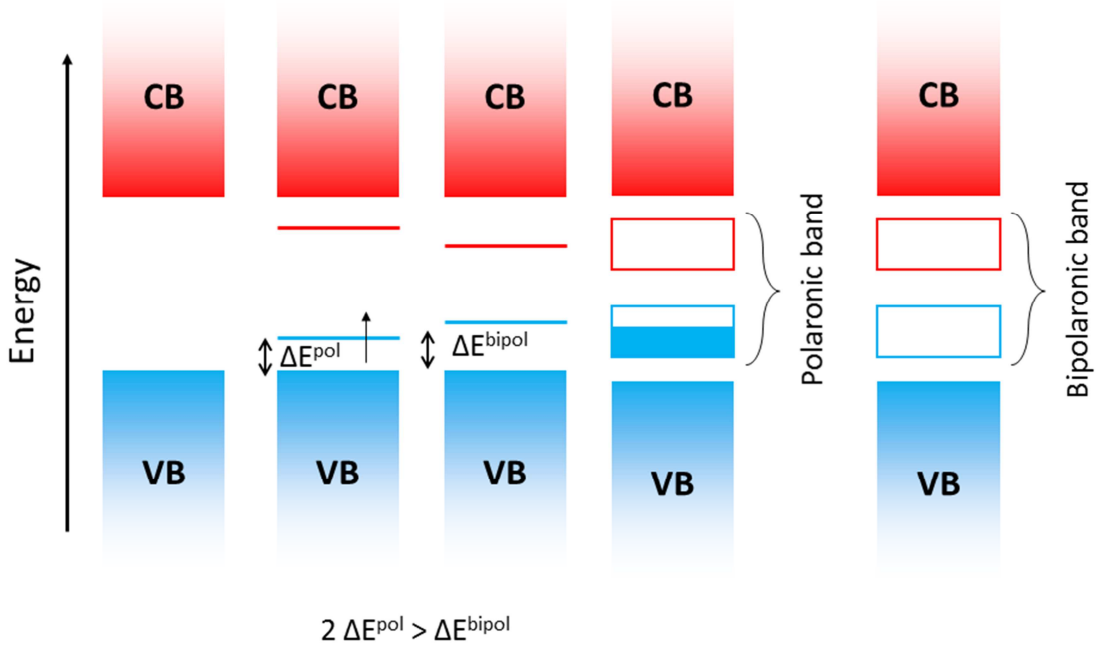

Figure I.6. Band structure in conjugated polymers. From left to right: neutral, 1 polaron, 1 bipolaron, polaronic band and bipolaronic band.[18]

The nature of the defect, polaronic or bipolaronic, can be assessed through electron paramagnetic resonance spectroscopy (EPR) which detects the presence of unpaired electrons in solids. Polarons possess a spin of ½ due to the unpaired electron while bipolarons possess no spin.[19,20]

The introduction of defects in the semiconducting polymer film corresponds to the apparition of states in the band gap. With increasing doping levels, these states overlap and create soliton, polaron or bipolaron bands within the band gap (Figure I.6).[17]

1-5. Optical properties in conducting polymers

With an energy gap between 1 and 4 eV, semiconducting polymers can absorb light in the ultraviolet, visible and near infrared regions. Therefore, UV-Vis-NIR spectroscopy has intensively been used to assess the doping state of the conducting polymers as well as the electronic processes that occur in the doped and un-doped states and the nature of the charges. If the energy gap is greater than 3 eV, the semiconducting polymer is transparent. When doped, charges (solitons, polarons or bipolarons) appear in the band gap (Figure I.6) and the obtained conducting polymer highly absorbs in the visible region. On the other hand, if the energy gap is small (typically 1.5 eV), the un-doped polymers absorbs the visible light whereas it will be transparent when doped.[15] Such characteristics has made the use of conducting polymers in electrochromic devices appealing[21–23].

1-6. Disorder in conducting polymers

Conducting polymers are inherently disordered materials. In fact, the material is constituted with polymer chains with various lengths, defects non-uniformly distributed within the chain, thus various conjugation lengths (the effective distance whereby the electrons are delocalized along the chains).

π -π interactions between chains can give rise to weak Van der Waals forces so that polymer chains are more or less well stacked. The overall materials then have crystalline domains whose size can reach tens of nm and amorphous domains, as illustrated in Figure I.7.[12,24,25] In such disordered materials, the charge transport is high along the chains, moderate between the chains and low between the lamellar planes (Figure I.8).[25,26] Also, the chains can be randomly oriented through the x, y or z axis. We can easily understand that transport properties would be optimized in the case of Figure I.7a rather than Figure I.7c. In fact, it is commonly thought that a high carrier mobility is linked to the degree of order and the relative stacking between the chains. Both high carrier mobility and/or efficient intra-chain transport are therefore sought in order to optimize the transport properties in conducting polymers.

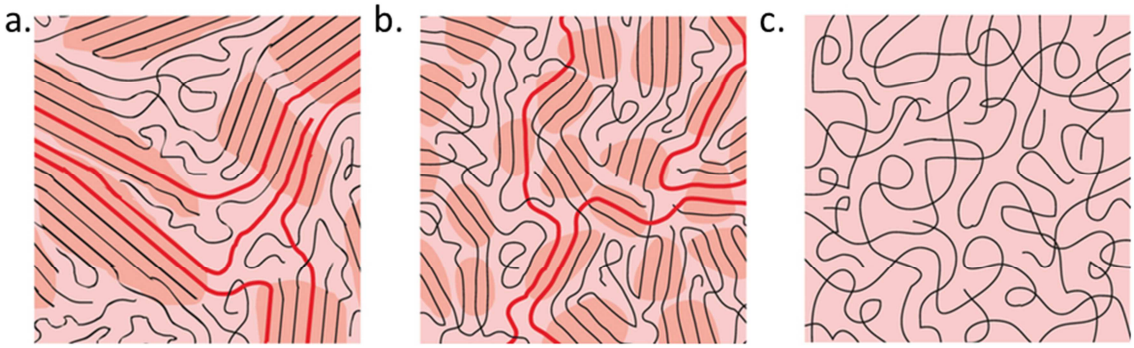

Figure I.7. Schematic structure of polymers with different disorder levels. a) Very ordered, b) disordered aggregates and c) completely disordered. Depending on the density of the polymer, long chains (highlighted in red) can connect ordered regions (darker orange ones) without significant loss of the conjugation length. Reproduced after[25].

As enlightened by Anderson, lack of crystal symmetry and lack of long distance order induce localization of the charges' wavefunctions so that charge transport is only possible through quantum mechanical jumps from a localized site to another.[27] Transport in conducting polymers can be different from that in metals or classical semiconducting materials.

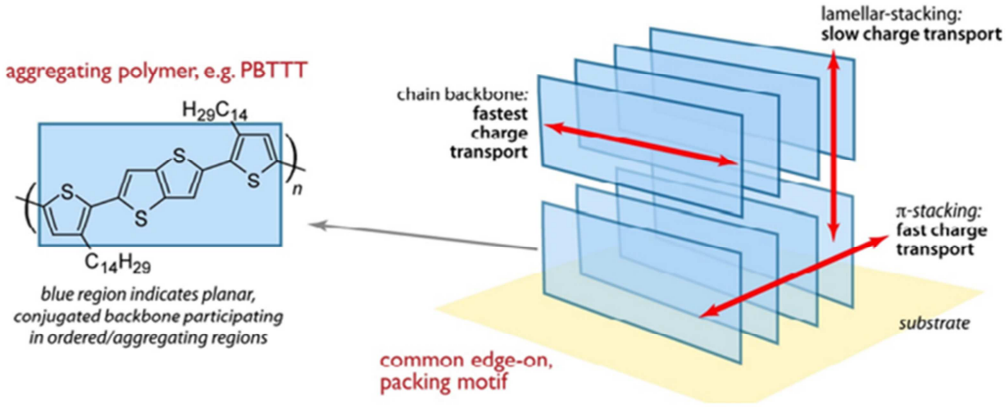

Figure I.8. Fast, moderate and slow transport along the chain backbone, the π-π stacking and the lamellar stacking respectively in conducting polymers. Reproduced after[25].

1-7. Transport properties in conducting polymers

The electrical conductivity σ of a material is given by Equation I.1:

$$\sigma = ne\mu \tag{I.1}$$

With n the charges carriers' density, e the electronic charge and μ the mobility of the charges.

In metals, the band theory predicts no band gap between the highest occupied energy level and the lowest one. Therefore, electrons can be easily excited to unoccupied state. Without thermal energy at T = 0 K, the highest occupied energy level is called the Fermi level and there is no sharp distinction between occupied and unoccupied states. Above T = 0 K, more and more electrons are excited into higher unoccupied states, which would lead to an increased electrical conductivity. This is however not the case since the increase number of excited electrons is compensated by their thermal motions. Collisions between electrons and atoms hinder the charge transport so that the mobility μ is decreased, and therefore the mean free path, as well as the electrical conductivity σ (Figure I.9). The conductivity does however not decrease indefinitely and the minimum metallic conductivity compatible with a minimum free path is called the Mott-Ioffe-Regel limit (see Figure I.10).

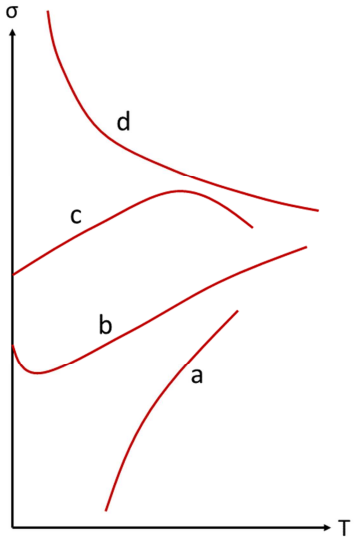

Figure I.9. Temperature dependence of conductivity from a semiconductor to a metal: a) semiconductor, b) & c) semiconductor or disordered metal with metallic behavior, d) metal.

A different mechanism is observed in classical semiconductors (Figure I.9). At T = 0 K, the band gap between the valence band and conduction band does not allow the extraction of charges. Above T = 0 K, more and more valence electrons are excited into the conduction band and n increases. As the density of charge carriers is lower than in the case of metals, collisions do not hinder the transport mechanism and the electrical conductivity increases with temperature.

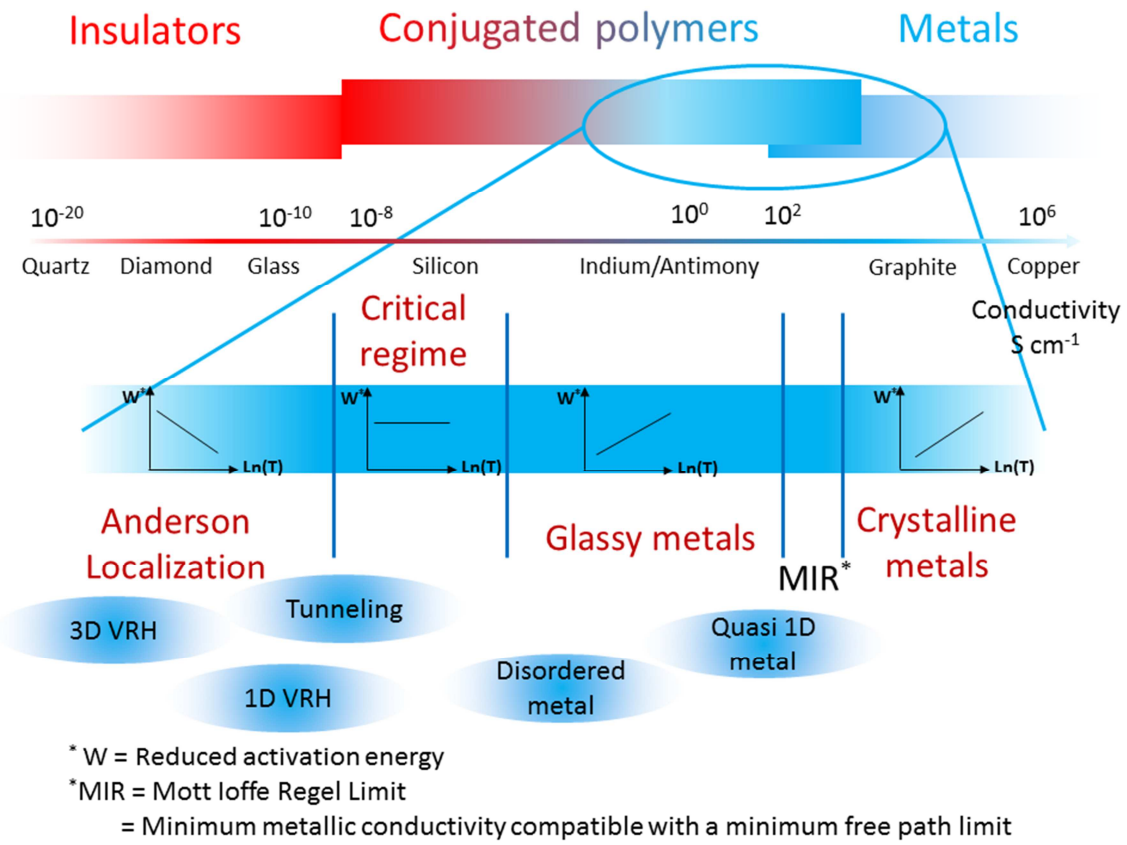

Figure I.10. Scheme representing the place of conjugated polymers between metals, semiconductors and insulators. Examples of materials are given as function of their electrical conductivity. The inset corresponds to conducting polymers and schematizes the different transport regime that can be found around the critical regime of the insulator to metal transition.

Contrarily to classical semiconductors in which charges carriers' density n increases with temperature as more and more electrons are excited, in conducting polymers the density is constant (solitons, polarons and bipolarons). Above T = 0 K, the mobility of the charge carriers is increased due to thermal motion and so is the electrical conductivity. In highly disordered materials, the Anderson localization predicts the absence of diffusion of the charges all over the material and the localization of their

wavefunctions. Based on this theory, Mott's variable range hopping (VRH) theory gave a first insight of transport mechanisms in strongly disordered semiconductors. Such model states that the transport of charges is function of the distance between two localized sites and the difference between the associated energies.[24,28] Thus in conducting polymers hopping between two localized states occurs when the thermal vibration of the chain changes the energy of these states. The mobile charge (soliton, polaron or bipolaron) hops from a site to another. This hopping is possible if there is no charge in the terminal site, and if there is a fixed charge nearby (the counter-ion) as there is a strong coupling between the mobile and fixed charge. The conductivity is given by Equation I.2:

$$\sigma_{VRH}(T) = \sigma_0 \exp\left[-\left(\frac{T_0}{T}\right)^{\frac{1}{n+1}}\right] \quad (I.2)$$

With σ_0 characteristic of the overall conductivity, T_0 related to the activation energy (depending both on the physical distance and the energy barrier between two sites) and n the dimension of the conduction. When n decreases, some directions are favored, meaning that a certain order/anisotropy has appeared.

This hopping model describes the behavior of semiconductors in the left side of the Anderson localization in Figure I.10, but is however not totally satisfactory as it cannot explain the relatively high conductivity (> 10 S cm^{-1}) or some metallic behavior in conducting polymers like highly doped polyacetylene or PEDOT.[29–33] In 1980, Sheng revisited the hopping model and proposed a model called *fluctuation induced tunneling* inspired from his previous *charging-energy-limited tunneling.*[34,35] The *charging-energy-limited tunneling model* was developed for granular metals dispersed in a dielectric matrix. Contrarily to Mott's VRH, the charge carriers are thermally activated and an electron is removed from a neutral grain and injected to another neighboring neutral grain *via* tunneling. For semiconductors, Sheng inferred that transport was dominated by charge transfers between large conducting segments rather than hopping between localized states. Thermal vibrations were thought to induce energy fluctuations between two close segments of the polymer which were highly doped so that tunneling of the charges could occur. Such model, given in Equation I.3, could explain the metallic behavior noticed in polyacetylene and which was contradictory to the negative resistivity coefficient typical in nonmetallic systems (as the conductivity increases with temperature).

$$\sigma_{Sheng}(T) = \sigma_S \exp\left(-\frac{T_1}{T+T_2}\right) \quad (I.3)$$

Where σ_S, T_1 and T_2 are constant parameters, and , T_1 and T_2 the tunneling temperatures dependent on the barrier geometry and energy.

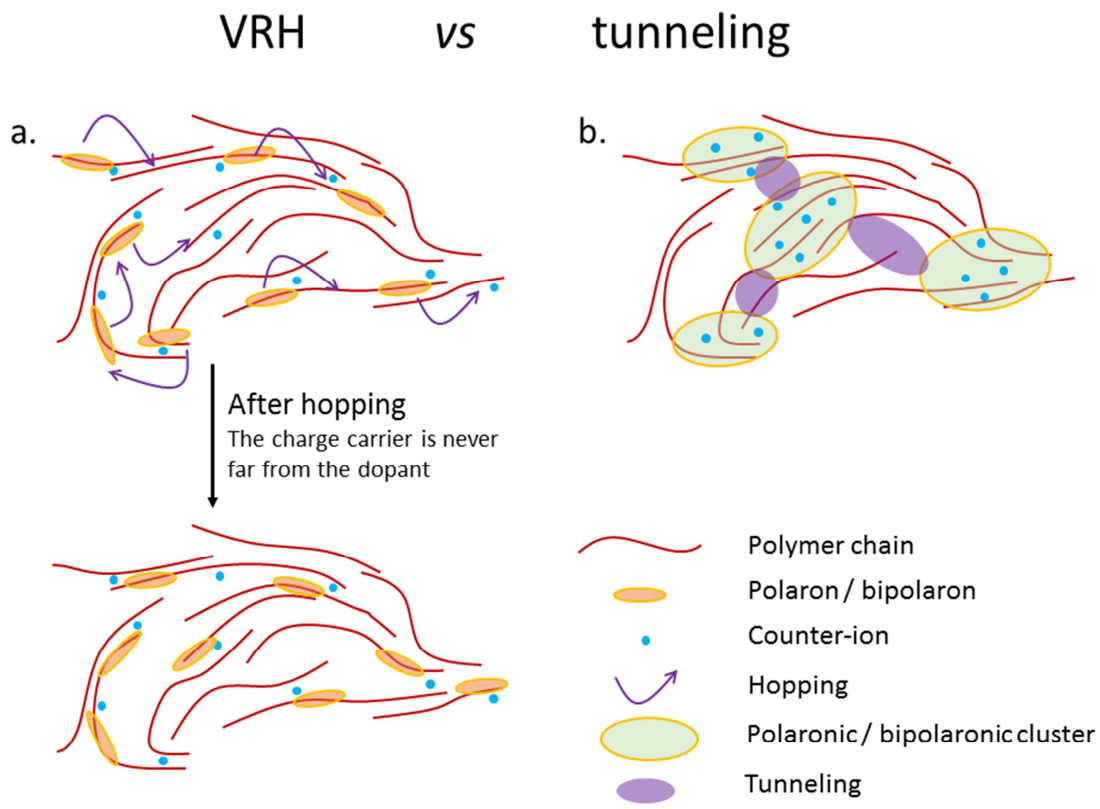

Figure I.11. Schematic representation of the variable range hopping model (a) *vs* the tunneling model (b). Due to the disorder, Anderson localization predicts the localization of the charges carriers‘ wavefunctions. While charges are strongly delocalized in the first place, inducing VRH, a less pronounced disorder in the second case results in charges that are close enough to induce a local delocalization, the formation of more densely charges zones (polaronic and bipolaronic clusters) and therefore another transport mechanism.

In 1994, Zuppiroli and coworkers, inspired from the fluctuation induced tunneling model, enlightened the arrangement of charges that could lead to such a model. They showed through calculations and temperature dependence conductivity measurements that transport does not occur solely from hopping between single polarons and bipolarons along the chains. Instead, polaronic clusters dispersed in the polymer matrix are created, and similarly to Sheng's model, hopping can take place between two strongly doped polaronic clusters separated by less doped domains. At T = 0, charge carriers stay in the vicinity of the dopants from which they originate. Above zero

temperature, hopping depends both on the probability of creating an excited state from an extra electron from one cluster and an extra hole from another, and the probability for the tunneling between clusters (Figure I.11).

Another school of thought was more responsive to the metallic features in some heavily doped conducting polymers. Their temperature dependence of conductivity had a finite value at zero temperature and sometimes depicted a negative slope (Figure I.9 and Figure I.12). Their temperature dependence of thermopower showed a linear behavior, typical of metals (Figure I.12). No energy gap was visible with optical spectroscopy techniques in highly doped polyacetylene. Moreover, it was shown that the counter-ions in the polymer film were spatially removed from the conduction path and that π-π interactions were strong enough to avoid localization of charges.[36] Therefore, polyacetylene was described as an anisotropic metal in which the charge density is high enough to create the overlapping of their wavefunctions on long distances and the coupling between the dopant and the charge is weakened. Other polymers such as PANI and PEDOT were also reported to depict such metallic behavior.[9,32] In such systems, charge transport is similar to that of metals, namely free charges diffusing in the polymer matrix. These are usually very conductive polymers with a high degree of order and a high doping level, following the conductivity law in Equation I.4.[36]

$$\sigma_{metal} = \sigma_m \exp\left(\frac{T_m}{T}\right) \quad (I.4)$$

Where σ_m is a constant parameter and T_m represents the energy of the phonons that can backscatter the charges.[37]

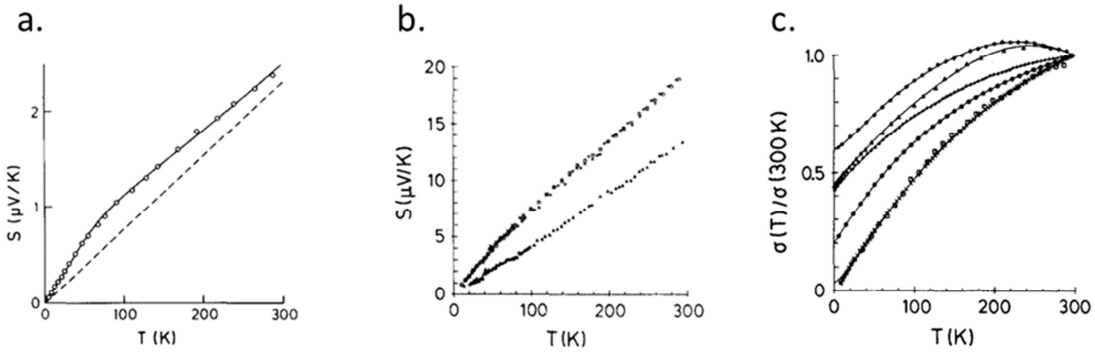

Figure I.12. a) Typical metallic thermopower in Zr-Ni alloy. b) Approximately linear thermopower in doped polyacetylene. c) Temperature dependance of conductivity in doped polyacetylene. Reproduced after[37].

Simply put, as summarized in Figure I.10 and Figure I.11, in disordered conducting polymers, charges are localized and transport is facilitated by hopping from a site to another. In more ordered polymers, polaronic clusters (in crystalline domains or disordered chains) are found and tunneling can occur between two highly doped segments separated by less doped ones. In heavily doped or very well ordered conducting polymers, coherent transport can occur without the coupling of charge carriers with the counter-ions. Hence, depending on the disorder or the degree of doping, transition from insulator to metal can be observed.[37,38] This metal-insulator transition can be assessed through the reduced activation energy W(T) in Equation I.5, which increases (respectively decreases) in the metallic (respectively insulator) regime, as illustrated in Figure I.10.[30]

$$W(T) = \frac{d[\ln(\sigma)]}{d[\ln(T)]} \quad (I.5)$$

Actually, these are not the sole models for conducting polymers. The transport mechanisms may differ from one polymer to another and several theoretical approaches were led for different conducting polymers. These three models however give a first insight of the different transport mechanisms that can occur.

1-8. Mechanical properties

Due to the π-π interactions between chains, polymers are rigidified, but they stay flexible when deposited into films. Conducting polymers are generally poorly insoluble. That hinders their processing and alkyl chains or solubilizing agents are needed to be added to their backbone or to the counterion.[12] When dispersed in a solution, they tend to aggregate due to the Van der Waals interactions between the chains and surfactants are needed to be added.[18] Nonetheless, when deposited as films, despite their high degree of disorder, π -π interactions between chains favor a local ordering so that the polymer is robust and semi-crystalline.

2. The breakthrough of PEDOT

2-1. From conducting polymers to PEDOT

Polyacetylene is the first conducting polymer reported with conductivities exceeding 10^5 S cm^{-1}, close to that of copper, and transport properties similar to that of a metal.[39]

It is however air-sensitive and not processable, hence not appropriate for industrial applications.[40] Regarding the lack of stability of the π -electron system in the doped state, strategies to solve the issue include the addition of electron donating heteroatoms such as nitrogen (N) or sulfur (S) either in the main chain or as carbon substituent in the cycles. Researchers have then turned their attention to polyaniline, polypyrrole and polythiophene
(Figure I.2).[41,42] Polyaniline is low cost and can be obtained in bulk amounts. However, aniline which is the precursor of polyaniline is known to be a hazardous compound for human health and environment. The benzidine moieties that appear upon degradation are also toxic, so that polyaniline is not preferred for practical applications. Polypyrrole is the first heterocyclic polymer whose electrical conductivity has been reported. [6–8] It also has been used as anode in capacitors.[12] However, its toxicity, high vapor pressure and strong color delayed the researches for its industrial applications. Polythiophenes are environmental friendly with interesting conductivities.[43] They are unstable, infusible and insoluble, the same way as all doped conducting polymers, but more stable derivatives can be developed.[44]

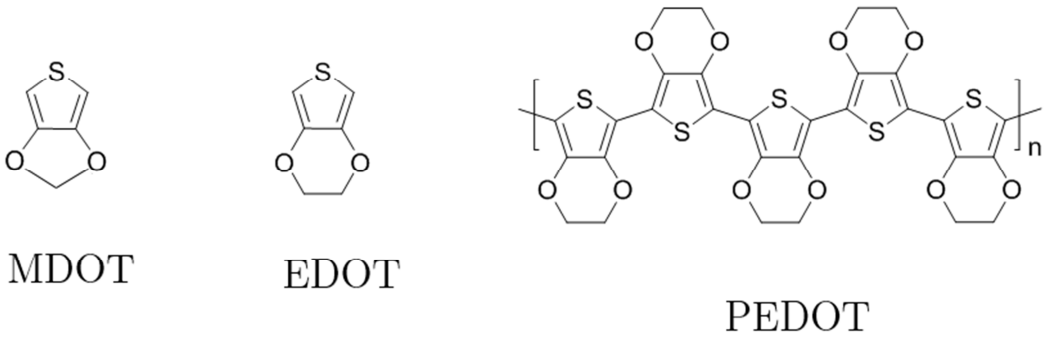

Figure I.13. a) Methylene dioxythiophene, b) 3,4-ethylene dioxythiophene and c) poly(3,4-ethylene dioxythiophene).

In the search to stable conducting polymers that are relevant for industrial applications, the German Bayer Central Research Department has been highly active. When their first attempts to stabilize polyacetylene failed and their works on polypyrrole were aborted, they focused on monoalkoxy and 3,4-dialkoxy substituted thiophene in order to increase the stability, and on bicyclic rings structures in order to decrease the steric hindrance associated.[45] Their first efforts on the synthesis of 3,4-methylenedioxythiophene (MDOT, see Figure I.13) was unsuccessful as they did not manage to isolate a workable amount of the monomer. Subsequently, they focused

on 3,4-ethylenedioxythiophene (EDOT), whose success was immediate. After polymerization with iron(III) chloride, the obtained poly(3,4-ethylenedioxythiophene) (PEDOT) appeared as a breakthrough in conducting polymers, since it is stable in its doped state and depicts conductivities up to 200 S cm^{-1}. [42,45,46] The synthesized PEDOT straightforwardly found applications in capacitors.[47] After the first oxidative polymerization of PEDOT reported by researchers from Bayer Ag in 1988, they also investigated the first electro-polymerized PEDOT the same year.[48]

The conductivity of PEDOT was interesting and it was air and water stable. However, chemically synthesized PEDOT is black, insoluble and infusible while electrochemically synthesized PEDOT can only be formed on conductive substrates. An alternative processable solution was strongly expected. Bayer's engineers found it shortly after during a collaboration with engineers from Agfa, who were researching on new antistatic coatings for their photographic films. As a matter of fact, the available material they used as antistatic coating, namely the sodium salt of polystyrene sulfonate) (PSSNa), suffered from humidity dependence of its conductivity. Oxidizing EDOT with persulfates and polymerizing in the presence of PSS in water, they obtained an aqueous dispersion of PEDOT stabilized with PSS^- as counter-anion, and which showed high stability.[49] Subsequently, PEDOT:PSS, and PEDOT in general, became interesting as an industrial material as well as an academic one.

2-2. Importance of PEDOT: industrial applications

Since its first year of discovery, PEDOT found applications as cathode in capacitors and antistatic coating in photographic films.[45,47] Not long after, their electroluminescence was demonstrated and OLED using PEDOT as active materials were developed.[50,51] Organic photovoltaics and transistors are not outdone and PEDOT is used as hole injection layer, active layer, buffer layer or electrode in OPV, OLED, transistors and electrochromic devices.[51–54]

In parallel to the different applications of PEDOT that have emerged through the years, intensive research on the spintronic, electrochromic, and thermoelectric properties of PEDOT are a fair perception of the tremendous importance it has gained since its first synthesis in 1988. PEDOT is present in many products used in modern life and continues gaining interest due to the emergence of plastic, soft and flexible electronics[55,56]:

3. Synthesis of PEDOT

PEDOT is not the first synthesized polymer. Its development benefitted therefore from all the expertise already accumulated from the first developed polymers. The techniques that will be presented hereafter were previously already used for other polymers, but we limited ourselves to the scope of PEDOT for the sake of conciseness.

PEDOT can be synthesized through three main polymerization reactions:

- Transition metal-mediated coupling of dihalo derivatives of EDOT
- Electrochemical polymerization of EDOT-based monomers
- Oxidative chemical polymerization of EDOT-based monomers

Only the latter one has been carried out during the thesis and will be developed hereinafter. The interested reader can refer to more specialized articles, reviews or books.[12,44,55]

3-1. Transition mediated coupling of dihalo derivatives of EDOT

In the synthesis routes that will be presented hereinafter, PEDOT is mainly present in its more stable oxidized p-doped form and is hard to de-dope due to the stabilizing effect of the electron donating dialkoxy groups. Regarding the interest to study the neutral PEDOT, Yamamoto et al. carried out polycondensation of 2,5-dichloro-3,4-ethylenedioxythiophene, following Figure I.14.[57] The dark purple product was however not soluble and therefore not amenable for molecular weight calculations, similarly to other doped PEDOT.

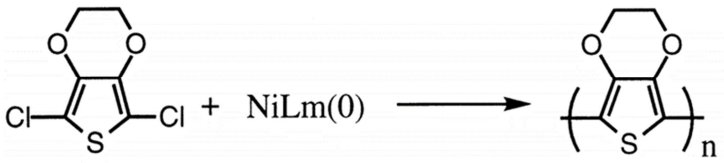

Figure I.14. Dihalogenation polycondensation for neutral PEDOT synthesis. Reproduced after[57].

3-2. Electrochemical polymerization of EDOT-based monomers

PEDOT can be electrochemically polymerized in a three electrode cell containing an electrolyte (such as PSSNa or water), the monomer (EDOT or EDOT derivatives) and the oxidant which can be added in the form of salts. PEDOT is formed on the anode's surface, commonly used ones being indium tin oxide (ITO) and Au.[58] This method needs only a small amount of the monomer, the reaction is fast and both supported and free-standing films can be obtained. The obtained product is transparent-blue with conductivities up to 780 S cm^{-1}.[59,60]

3-3. Oxidative chemical polymerization of EDOT-based monomers

Only routes using the EDOT monomer are presented hereinafter. Roncali et al. reviewed various synthesis methods for EDOT-based systems.[55]

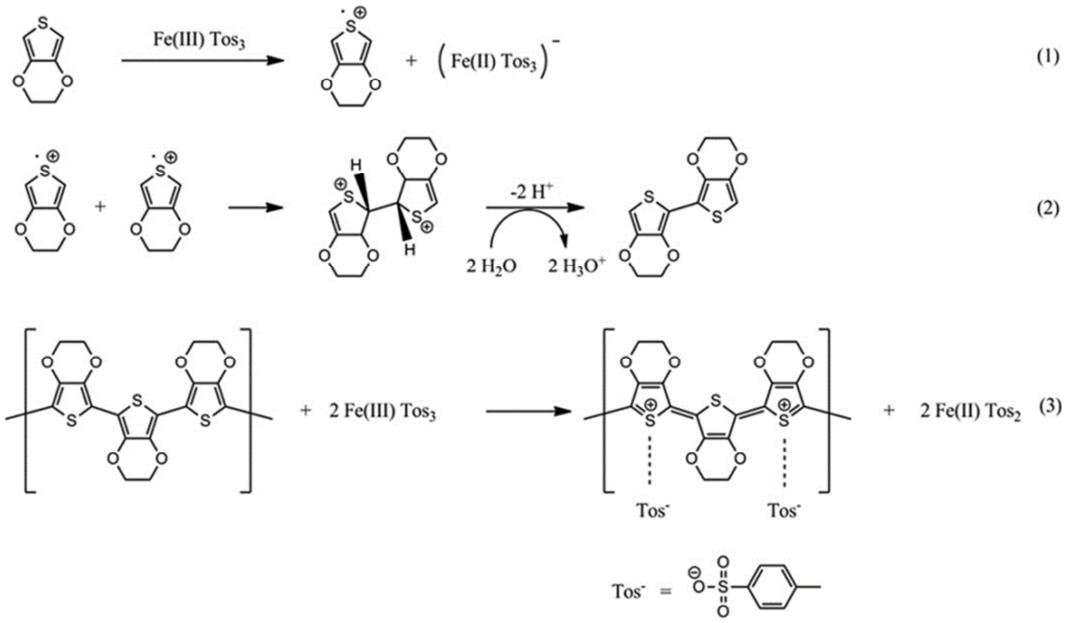

Figure I.15. Proposed mechanism for the synthesis of PEDOT:Tos as reproduced from Mueller and coworkers' work.[61]

PEDOT can be polymerized from the monomer EDOT, which is commercialized. Iron (III) complexes were proved to be efficient oxidants since the standard electrode potential of the cation is high (0.77 V).[16] They also provide the counter-anion to

stabilize the oxidized PEDOT as well.[18] Iron complexes that can be found in the literature are:

- Iron(III) chloride ($FeCl_3$)
- Iron(III) *para*-toluenesulfonate or tosylate ($Fe(Tos)_3$)
- Iron(III) camphor sulfonate ($Fe(C_7H_7O_4S_3)_3$
- Iron(III) methanesulfonate ($Fe(CH_3SO_3)_3$)
- Iron(III) trifluoromethanesulfonate or triflate ($Fe(OTf)_3$)

The most commonly used in the literature is $Fe(Tos)_3$, which is even commercialized in a solution ready to use for the synthesis of PEDOT (Baytron C from HC Stark). The polymerization mechanism, although not fully understood, can be described as in Figure I.15:[18,61]

- (1) Fe(III) oxidizes EDOT and is reduced to Fe(II)
- (2) Two oxidized EDOT combine into an 2-EDOT dimer which is further deprotonated by surrounding water molecules
- (3) Steps (1) and (2) are repeated in order to form polymer chains. Remaining Fe(III) ions dope the formed PEDOT and Tos^- ions are inserted as counter-anions in order to stabilized the doped PEDOT.

Several oxidative chemical polymerization methods can be found in the literature. The most classical one, introduced with the first synthesis of PEDOT by Bayer AG in 1988, consists of introducing oxidizing agents in a mixture of the monomer and a solvent. A dark and insoluble product is precipitated. It is insoluble and infusible, and therefore not processable. Conductivities of some tens S cm^{-1} were first reported.[45] In 2001, Hohnholz and coworkers revisited this method by suspending substrates in a beaker containing the polymerization mixture so that polymerization occurs at the interface with the substrates.[62] This lead to the film formation of PEDOT.

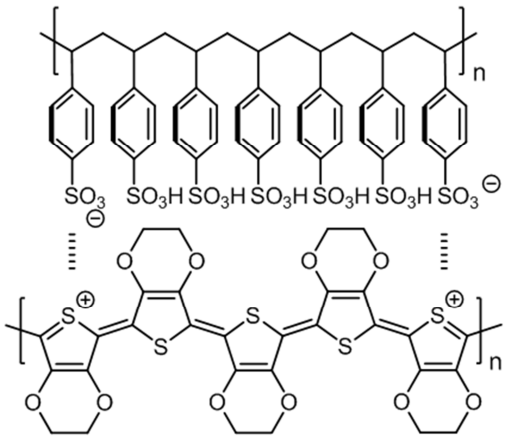

Figure I.16. Chemical structure of PEDOT:PSS

In 1990 a second processable method was introduced by the same company, as stated in section 2-1. EDOT is polymerized in an aqueous polyelectrolyte solution (typically PSS) in the presence of $Na_2S_2O_8$ as the oxidizing agent. PEDOT is then stabilized by the counter-anion PSS^- and the blue dispersion resulting from that reaction, namely PEDOT:PSS whose structure can be found in Figure I.16, is processable so that thin (~100 nm) to thick (> 1 m) films can be deposited. The mechanically robust, transparent (depending on the thickness) and insoluble film has a high intrinsic conductivity up to 10 S cm^{-1} which, through decades of research, was improved up to 4839 S cm^{-1}.[63] Moreover, it is commercialized so that several applications were able to emerge.

In 1994 a third polymerization method suitable for surface films formation was reported by de Leeuw and coworkers since the commercially available PEDOT:PSS did not reach conductivities exceeding 10 S cm^{-1} at that time.[64] A solution containing *n*-butanol as a solvent, $Fe(Tos)_3$ as an oxidant, EDOT as the monomer and imidazole as a base inhibitor was spin-coated on a glass or plastic substrate. Polymerization occurred when the deposited film was heated up to 110 °C. The black, insoluble and infusible film obtained after rinsing with water and n-butanol exhibited conductivities up to 550 S cm^{-1}.[65] This method did however not allow reproducible and homogeneous films.

In 2004 Winther-Jensen et al. reported a new oxidative polymerization route with conductivities exceeding 1000 S cm^{-1}.[66] That vapor phase polymerization (VPP) consisted of exposing a surface covered with a mixture of $Fe(Tos)_3$ as the oxidant and pyridine as a base to EDOT vapors (Figure I.17).[67,68] Winther-Jensen and coworkers

noticed that EDOT could participate in an acid initiated polymerization, whereby a partially conjugated polymer was formed, which leads to short conjugation lengths. The addition of a base is therefore of interest in order to prevent unwanted acidic side reactions. As a consequence, they added pyridine in the VPP chamber.

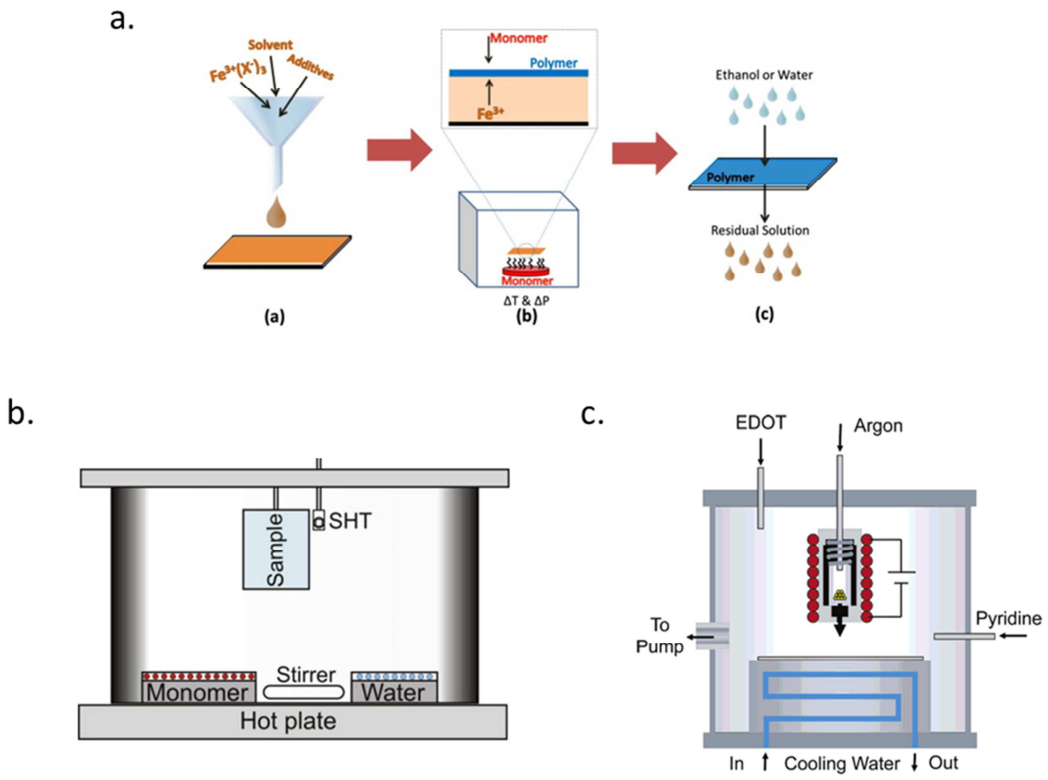

Figure I.17. a) Vapor phase polymerization principle (VPP). b) VPP chamber, as reproduced from Murphy and coworkers' work.[69] Vacuum VPP is a variant that has the advantage to allow working with bigger chambers (the even distribution of the EDOT monomer being easier) so that large areas substrates can be used.[61] b) Another quite similar principle (chemical vapor deposision_CVD) principle as reproduced from Gleason and coworker's work.[67] It is slightly different from VVPP. In here, no solvents are used and the oxidant is heated in the crucible that faces the substrate on which EDOT is adsorbed.

They further developed de Leeuw's solution-cast polymerization (SCP) method in 2005.[70] Actually, de Leeuw and coworkers primarily added imidazole as a base to control the speed of polymerization as stated hereinbefore. However, the polymerization does not start before the removal of imidazole which required high temperature heating

(> 105 °C). Moreover, imidazole builds ligands with Fe(III), hence leading to the formation of crystals in the film. By using pyridine instead of imidazole and by controlling the acidity of the oxidative solution, good film forming properties were demonstrated and conductivities exceeding 1000 S cm^{-1} were routinely demonstrated.

These two new routes, surpassing by far all the previous routes reported in terms of conductivity (> 1000 S cm^{-1}), have been dominating the synthesis field of PEDOT in the academic field ever since and were in competition with the commercialized PEDOT:PSS.

In the following work, when oxidative chemical polymerization with counter-anions other than PSS^- is encountered, the classical one will be referred to as chemical oxidation, the vapor phase polymerization as itself (VPP) and the polymerization on a substrate from a deposited oxidative solution as solution-cast polymerization (SCP). It is important to understand that all three methods can be referred to as "*in-situ* oxidative chemical polymerization" in the literature and that the distinction we suggest here is only for the sake of clarity in this work.

4. Chemical properties

PEDOT chains are short, only a few to few tens monomer units.[71,72] Neutral PEDOT is in an aromatic state. It undergoes a distortion from aromatic to quinoid form during doping, as schematized in Figure I.18.[12,18,56]

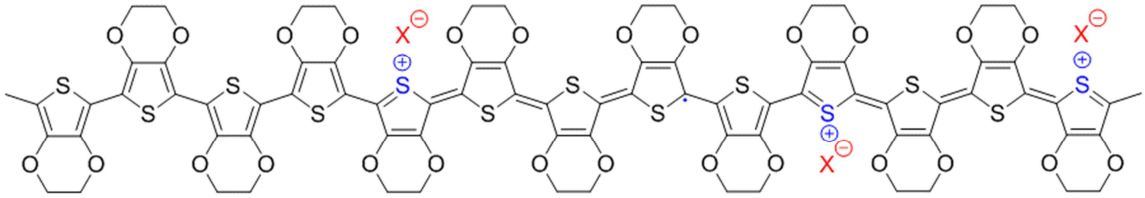

Figure I.18. PEDOT in different states: a) neutral, b) polaron, c) bipolaron. Reproduced from[18].

The polymerization results in a polymer whose doping level is approximately 33 % (one dopant for 3 monomer units).[56] PEDOT being insoluble in any common solvent, "standard" solution characterization techniques (such as NMR) cannot be used, and

features such as their molecular weight remain unraveled. Electronic and vibrational spectroscopies are however possible on the thin or thick formed films and information such as their energy gap, their elemental composition, their doping level or their chemical state can be assessed.

4-1. Optical properties

The optical features of PEDOT at various oxidation levels are schematized in Figure I.19A and can be assessed using ultraviolet-visible-near infrared (UV-Vis-NIR) spectroscopy. Figure I.19B gives the evolution of the optical characteristic from a neutral chain to a fully polymerized film. Neutral PEDOT is dark purple/blue and has an optical absorption gap around 1.5 eV.[58,73] When oxidized, new energy states are introduced in the band gap in the NIR region outside the visible range, and PEDOT becomes transparent.

This confers to PEDOT good electrochromic properties which can be controlled electrochemically with the doping level.

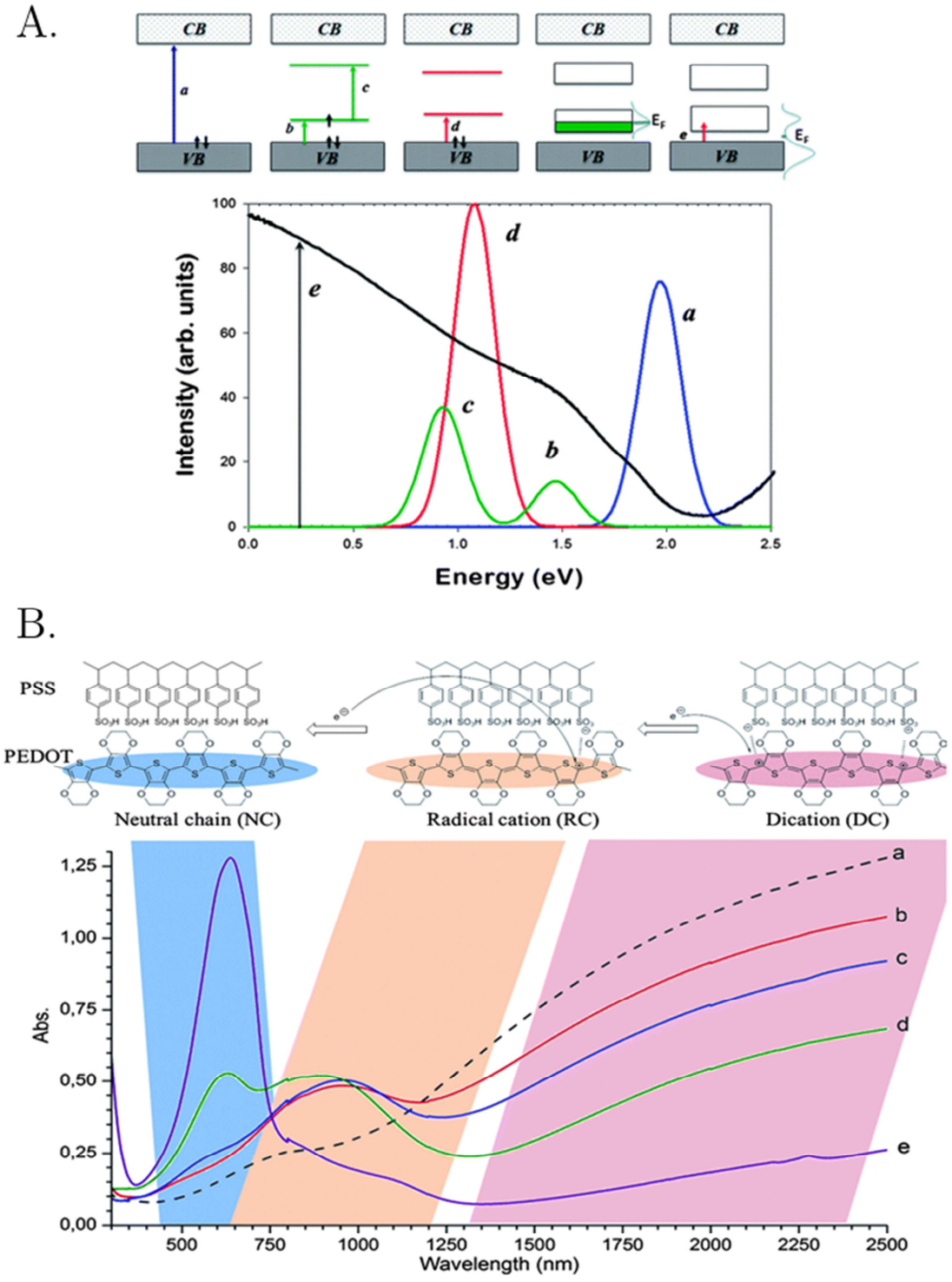

Figure I.19. Evolution of the electronic characteristic of PEDOT at different doping levels.

A) Upper image: from left to right: a neutral chain ('**a**' no charges are present in the chain and the corresponding transition in UV-Vis-NIR in the lower image is a band in the visible range), a chain with a polaron ('**b** & **c**' in UV-Vis-NIR, the energy transitions that are detected correspond to the transition from the VB to the polaronic

band and the transition from the occupied state to the non-occupied state of the polaronic band. Those transitions appear at the end of the visible range), a chain with a bipolaron ('**e**' the transition in the bipolaronic band occurs in the NIR region), an intrachain or interchain polaron network inducing a polaronic band and an intrachain or interchain bipolaron network inducing a bipolaronic band ('**e**' in these last two cases, all transitions that can occur and which are due to the neutral chains, the polarons and the bipolarons are represented, hence giving such so know UV-Vis-NIR spectrum of PEDOT).

B) PEDOT chains with different doping states (upper image) and their corresponding UV-Vis-NIR spectra (lower image).

Reproduced from[74,75]

4-2. Doping level

In parallel to UV-Vis-NIR spectroscopy that gives information on the doping state, the doping level can be assessed through X-Ray photoelectron spectrometry (XPS).[71,72]

As can be seen in Figure I.20, the sulfur S2p contribution originates from the thiophene rings and the counter-anion as they have different chemical environments (see Materials & Methods in the appendix for more details). Therefore, using XPS surface elemental analysis technique, one can have access to the ratio PEDOT to counter-anion. In the case of PEDOT:PSS, PSS consists of a few hundreds of monomers whereas PEDOT only consists of some units to some tens.[71,72] Using XPS studies, combined with AFM imaging, Jönsson and coworkers suggested a grain-like structure for the PEDOT:PSS films, with a non-homogeneous distribution of PEDOT and PSS in the grains and an excess of PSSH around the grains. They inferred that those grains were probably defined by PSS random coils with PEDOT chains ionically attached to them, and that the areas between the grains were probably filled with excess neutral PSS.[72] Thus the PEDOT to PSS ratio only gives information on the quantity of PSS in the films.[60] In the case of PEDOT stabilized with small counter-anions such as tosylate, the non-polymeric nature of the counter-anion prevents it from being in excess. Therefore, the ratio PEDOT to counter-anion gives direct access to the doping level of PEDOT, which has been calculated to be between 25 and 35 %.[44,60,76]

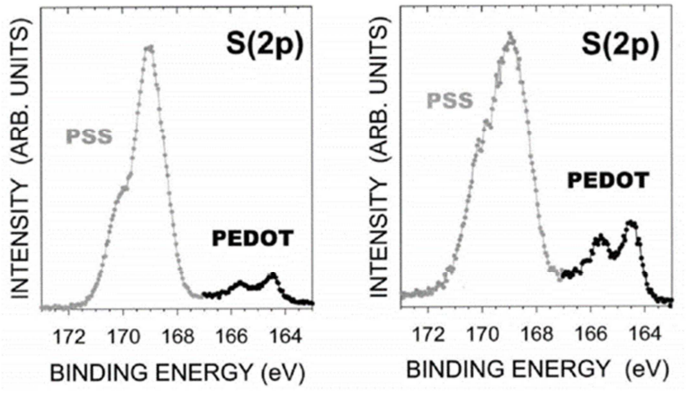

Figure I.20. Typical sulfur doublet response of PEDOT:PSS polymer blends probed using XPS. The shift of S2p doublet between thiophene and PSS is clearly represented. Reproduced from Greczynski et al.'s review[77].

5. Electrical properties

Since the discovery of PEDOT:PSS, its processability, its conductivity and its good film forming properties, several applications have emerged. For all these applications, highly stable, processable and conductive PEDOT films have been researched. In that respect, some researchers focused on improving the electrical conductivity of PEDOT:PSS, available commercially, while other directed their attention to PEDOT stabilized with smaller counter-anions such as tosylate.

5-1. PEDOT:PSS

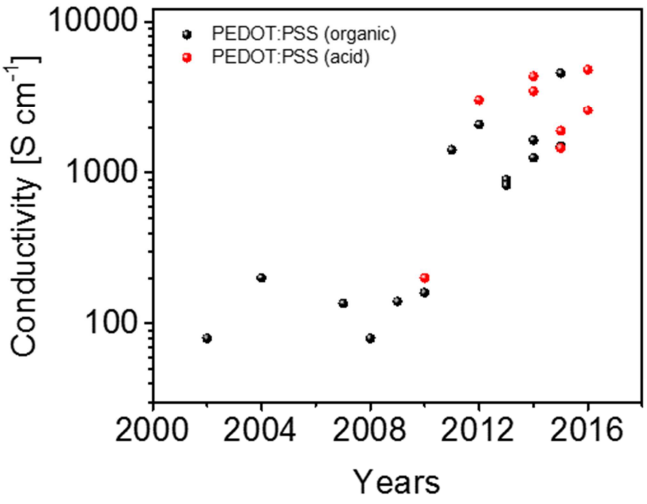

Figure I.21. Conductivity enhancement of PEDOT:PSS through years. References are given in Table B1.

At first, commercialized PEDOT:PSS exhibited conductivities from 0.1 to 10 S cm^{-1}. In order to increase its conductivity, strategies include pre- and post-deposition treatment. Pre-treatment consists of adding ionic liquids, anionic surfactants, salts and organic solvents such as dimethyl sulfoxide (DMSO), N,N-dimethylformamide (DMF), 1-methyl-2-pyrrolidone (NMP) or ethylene glycol (EG) in the PEDOT:PSS dispersion.[71,72,77–83] The conductivity enhancement over 2000 S cm^{-1} is attributed to the phase separation between PEDOT-rich and PSS-rich domains, hence inducing a better connectivity between conductive domains. Post-treatments consist of dipping the PEDOT:PSS film in organic solvents, organic acid or inorganic acids. In that case, the increase in conductivity is attributed to the removal of the excess insulating PSS of the films.[84–87] With such treatments, the conductivity was enhanced up to 4840 S cm^{-1} as summarized in Figure I.21.

5-2. PEDOT with small counter-anions

In 2004, Winther-Jensen works on VPP demonstrated conductivities exceeding 1000 S cm^{-1}, hence arousing great interest among researchers.[66] PEDOT:PSS is processable, but conductivities were barely reaching 200 S cm^{-1} at that time.[88] PSS, the stabilizer counter-anion which allows dispersion in water, is insulating and in excess,

thus hindering the conduction mechanisms. The new method proposed by Winther-Jensen et al. allowed not only to get free from the insulating PSS, but also to have highly conductive films which can be coated on any substrate, insulator or not. With such technique, the conductivity of PEDOT reached up to 4500 S cm^{-1} for thin films and 8797 S cm^{-1} for single crystals.

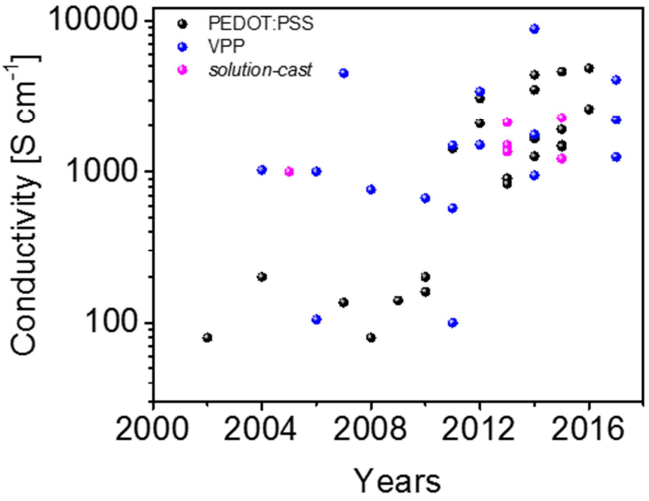

Figure I.22. Comparison of the conductivity in PEDOT films using different synthesis approaches. References are given in Table B1.

No long after Winther-Jensen pioneering works on VPP, they also reported SCP of PEDOT with conductivities exceeding 1000 S cm^{-1} using the same reactants, but deposited by spin-coating. Even though such method was previously reported, the conductivities did not exceed 550 S cm^{-1}. The over 1000 S cm^{-1} conducting PEDOT:Tos deposited by spin-coating yet did not arouse as much interest as the VPP method despite its inherent advantages: deposition on both conducting or insulating substrates, films as homogeneous, conducting and transparent as in VPP, solution processable and highly ordered, no vacuum needed.[64,70,89] Only few reports dealing with increasing the conductivity using SCP method were published, as shown in Figure I.22.[32,90]

6. Structural properties

The research on increasing the conductivity of PEDOT was systematically carried out while investigating the morphology and the structure of the deposited films. Since the

conductivity depends on both the mobility and the charge carriers' density, and since this latter is mainly contingent on the synthesis methods, increasing the mobility seems to be the key parameter to deal with. By synthesizing more ordered structures, the mobility is expected to increase and the transport properties optimized. The morphology and structure of the films were then investigated in order to understand the conductivity enhancement and the inherent transport mechanisms.

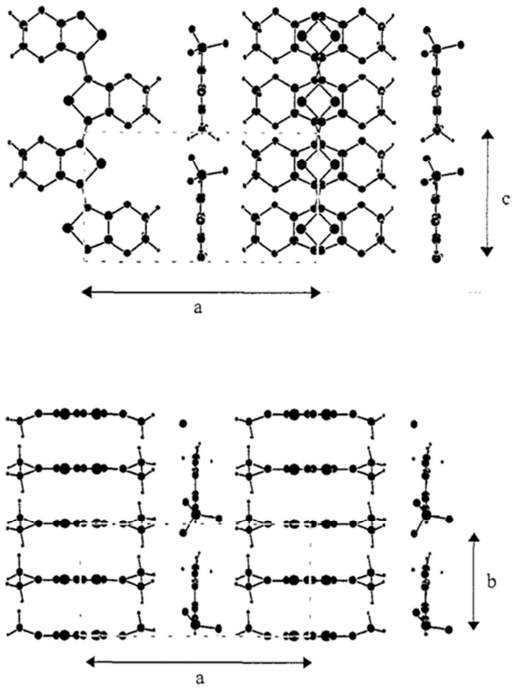

Figure I.23. Structure model of PEDOT:Tos. The substrate is normal to the a-axis.[89]

Inganäs and coworkers gave the first comprehensive study of the structural characteristics of PEDOT.[89] They studied SCP PEDOT:Tos using grazing incidence wide angle X-Ray scattering (GIWAXS) with synchrotron radiation (this technique is explained in Materials & methods). The spin-coated material was smooth, homogeneous, and the oxidation level was calculated to be 25 % using XPS. Their results also showed that the material was highly anisotropic and in a paracrystalline state, with dopant anions forming distinct planes that alternate with stacks of the polymer chains as in Figure I.23. The lattice parameters in the orthorombric structure as depicted in Figure I.23 were calculated to be a = 14.0 Å, b = 6.8 Å and c = 7.8 Å. A metallic behavior was found in the plane and a dielectric behavior out of the plane of the films.[89] Such structure for PEDOT was further proved through years and remained the same for all PEDOT films, whatever the counter-anions.[18,32,91–93] The lattice

parameters as well as the crystalline degree (relative order) however change from a PEDOT material to another, from a deposition technique to another, and even from a sample to another.

Comparisons between VPP PEDOT, chemically oxidized PEDOT and PEDOT:PSS (non-acid treated) prove that VPP PEDOTs exhibit the highest conductivity and optical transmission, attributed to increased molecular ordering and smoother morphology as confirmed by XRD, SEM and AFM.[94]

The importance of engineering a fine structure on the conductivity of PEDOT was evidenced by Cho et al.[91] Given the fact that disorder in PEDOT films highly affects chains alignment which hinders the inter-chain transport, they grew PEDOT single nanocrystals in nano-sized molds. The high conductivity obtained, namely 8797 S cm^{-1} with a doping level as small as 10 %, was associated to the entirely crystalline nature of the synthesized PEDOT.

7. Transport properties

When deposited, PEDOT chains organize in a disorder or crystalline way. In highly disordered PEDOT films, such as untreated PEDOT:PSS or chemically oxidative deposited PEDOT with other counter-anions, the too high disorder induces the localization of the charges also known as Anderson localization (Figure I.10). In such systems, 3D VRH has been reported.[79,86,88,95] Upon secondary doping, acid treatment, or VPP and SCP of PEDOT with small counter-anions, a systematic improvement of the transport properties has been observed. For example, after organic solvent or acid treatment, the decrease of disorder in PEDOT:PSS films induced better ordering and preferred charge transport orientation leading to 1D VRH.[79,96] With increasing order, charges were found to be less localized so that tunneling between highly doped regions was possible as explained in Figure I.11b.[97,98] Interestingly, with the growing progress made on the conductivity and structure/order of PEDOT films, they were also reported to approach the critical regime of the metal insulator transition, and even to cross it depicting disordered-metallic or metallic behavior.[20,32,33]

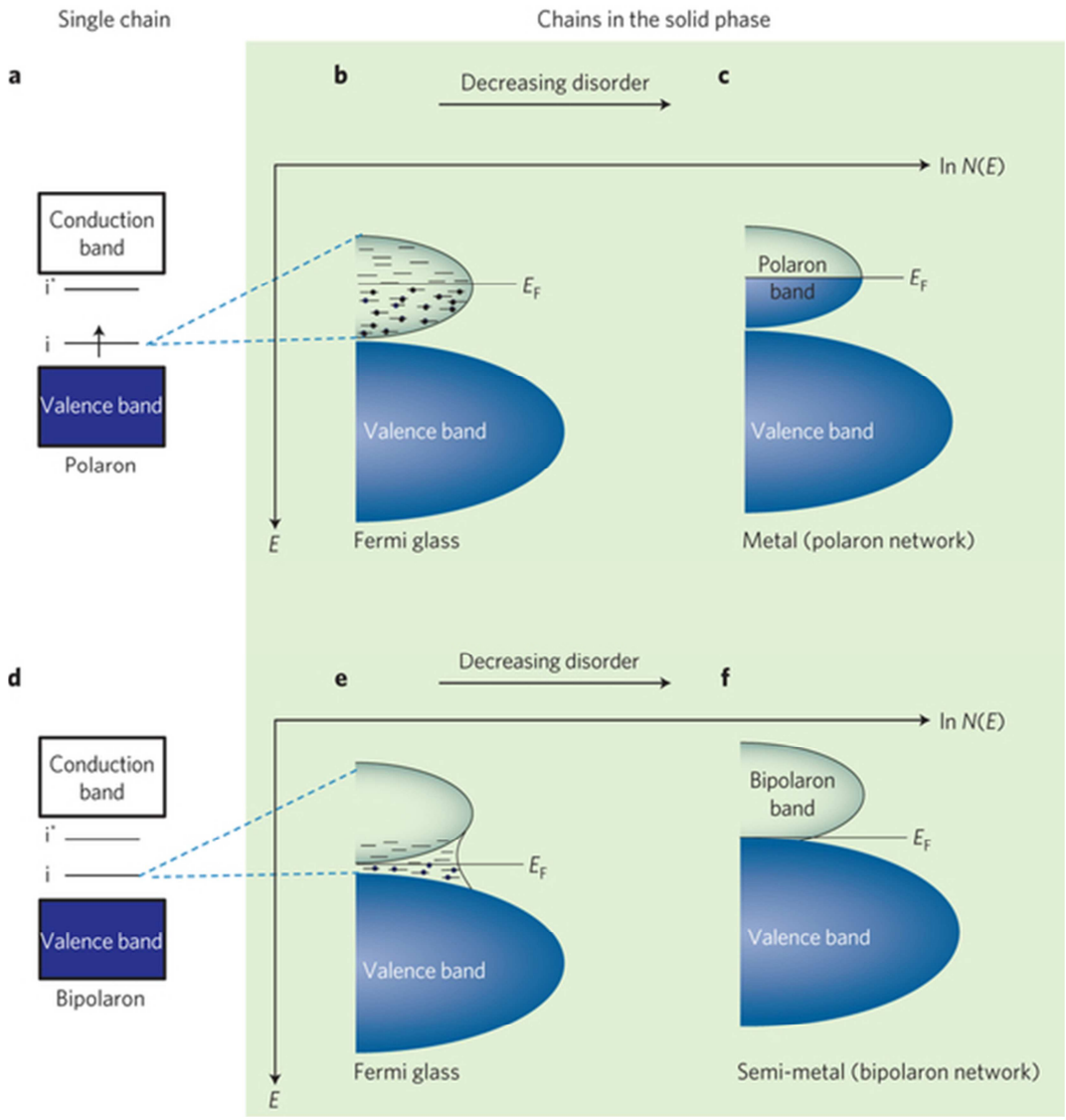

Figure I.24. Representation of the electronic structure in PEDOT materials and in conducting polymers in general. a–c, If the majority charge carriers are polarons: (a) a polymer chain with one polaron, (b) the logarithm of the density of states (DOS) lnN(E) disordered material (c) as well as for a more ordered (metallic) system. In the latter case, the Fermi level lies in a delocalized polaron band while it was surrounded with localized states in the former case. d–f, If the majority charge carriers are bipolarons: (d) a polymer chain with one bipolaron, (e) lnN(E) for an disordered bipolaronic polymer solid, (f) as well as for a more ordered (semi-metallic) solid. The Fermi level lies between the valence band and the empty bipolaron band in the latter case.[20]

Such large variations in the transport properties in various PEDOT samples have recently been explained in terms of the nature of the majority charge carriers and the content of disorder.[20] In highly disordered materials, charges are distributed and do not

form a continuous band. In an energy point of view, the Fermi energy lies in the middle of the polaronic band if charges are polarons or between the valence band and the bipolaronic band in the case of bipolarons. We therefore obtain a Fermi glass as illustrated by Bubnova et al. (Figure I.24), that is a material in which charges are localized at the Fermi level and whose wave functions do not possess any long range interaction. In such systems, the transport mostly takes place by hopping, following the 3D Mott VRH model as introduced hereinbefore.[20]

With increasing order, polymer chains are better stacked and the charges are more delocalized. The majority charge carriers' wave functions overlap over several chains. In polymers where polarons are the majority charges' carriers, a polaronic band is created, in the middle of which the Fermi level lies. The polymer hence depicts a metallic behavior as depicted in Figure I.24 and observed in conducting polymers such as polyanaline.[37,99,100] In polymers where bipolarons are the majority charge carriers, a bipolaronic band is created and the Fermi level lies within its interface with the valence band.[20,32,101] Such system is described as a semi-metal, a material in which metallic and hopping transport compete and where the leading mechanism is directed by the degree of order and the ratio between polarons and bipolarons.[20,102]

PEDOT is known to have more bipolarons defects than polarons ones as evidenced by EPR. In highly disordered PEDOT films (such as non-treated PEDOT:PSS), bipolarons are delocalized and the material is a Fermi glass. In that respect, several studies reported VRH transport properties in PEDOT:PSS films.[79,80,103] In highly ordered PEDOT films (such as PEDOT:Tos or PEDOT:OTf reported by Murphy's, Crispin's, Evans' or Simonato's groups), Crispin claims the delocalization of the charges leads to a semi-metal, a material in which both metallic and semiconducting behaviors compete.

8. Summary and strategy

With the rising demand of flexible, low cost and environmental friendly materials for future technologies (for energy, for the internet of things, for smartphones, and so on), the world is going "organic". Organic photovoltaics, organic light emitting diodes, organic field effect transistors, organic thermoelectricity, organic transparent electrodes are just as much evidences of how organic materials are sought for tomorrow. Materials which can fulfill the requirements specifications of future technologies are conducting

polymers, which owe their popularity to their interesting electrical, optoelectronic, thermochromic, lighting and mechanical properties, coupled with their good processability even on flexible and large substrates, their high stability and their low environmental impact.

Among conducting polymers, PEDOT has undoubtedly stood out as we have shown in this first chapter. The first excitement around PEDOT aroused from its stability, the second its processability (PEDOT:PSS), the third its optoelectronic properties and the fourth the numerous applications whereby it participates or it opens the route to. PEDOT based materials (PEDOT stabilized with PSS^- or smaller counter-anions such as tosylate) represent an interesting class of materials. They are stable in their doped state as they are readily oxidized in air and are present in numerous every-day-life applications. In less than two decades, conductivities from 0.1 S cm^{-1} for the highly disordered PEDOT:PSS materials to 8797 S cm^{-1} for single crystal PEDOT nanowires have been reported as summarized in Figure I.22 and Table B1. That figure gives an overview of the remarkable progress done on the conductivity enhancement, and at the same time, the dispersion of the data suggests that there is still room for a better understanding of that material. As a matter of fact, there are almost as much PEDOT materials as research groups working on them, which is due to the disordered and semi-crystalline nature of the material itself.

My thesis is born in that context and has four main objectives:

- The synthesis of PEDOT materials with and optimized and controlled structure for good electrical properties
- The thorough characterization of the as-synthesized PEDOT for a better understanding of the material and its transport mechanisms
- The study of its thermoelectric properties and optimization directions
- The validity of its practical use by studying its stability under different environments and stresses

For that purpose, the next chapter will deal with the synthesis and characterization of PEDOT-based materials. Our literature review showed us that PEDOT:PSS, even though it is processable and can have its conductivity enhanced over several orders of magnitude, is also highly disordered and with a structure difficult to assess because of the counter-anion PSS. Its presence in excess hinders the electronic transport mechanisms. On the other hand, in PEDOT with small counter-anions, the hindering

PSS counter-anions are *de facto* absent. Therefore, better carriers' mobility is favored, a higher charges carriers density is reached, better transport properties take place and an enhanced electrical conductivity is acknowledged. We directed then our study into PEDOT obtained with the salt iron(III) trifluoromethane sulfonate ($Fe(OTf)_3$). We will report the development of highly conductive PEDOT films by controlling the crystallization of the PEDOT chains and by a subsequent dopant engineering approach using $Fe(OTf)_3$ as oxidant, N-methyl pyrrolidone (NMP) as polymerization rate controller and sulfuric acid as dopant. XPS, HRTEM, Synchrotron GIWAXS analyses and conductivity measurements down to 3 K will allow us to unravel the organization, doping, and transport mechanism of these highly conductive PEDOT materials, and to understand the role that NMP and sulfuric acid played in the morphology and the electronic properties of the films. We will finally propose a charge transport model that fully corroborates our experimental observations.

Subsequently, after a thorough characterization of our materials and their electrical and transport properties, the following third and fourth chapter will be directed into the study of their thermoelectric properties. Thermoelectricity refers to any physical phenomenon relating heat transfer to electrical energy. The most known examples are Joule heating (governing electrical heaters) and Peltier effect (for electrical cooling). We here focus only on two of them because of the appealing applications that can derive from those, namely the Joule heating (Chapter 3) and the Seebeck effect (Chapter 4). While the former one creates heat for the user's convenience, the latter one harvests heat for global energy consumption savings. In Chapter 3 then, the heating properties that arise from the application of an electrical potential on our PEDOT films will be investigated. Very high areal power densities, up to 10 times that of an electrical heater, are measured on very thin PEDOT films. The thermal conduction mechanisms will be investigated and a thermal model implemented. Such great heating performances are actually interesting when combined with good optical ones, because apart from acting a heater, PEDOT can especially be a transparent one. That being the case, we will demonstrate the first all polymeric flexible transparent heater, solely made of PEDOT, and demonstrate its use in a thermochromic display and as a visor deicer.

In Chapter 4, we will focus on another thermoelectric effect, the Seebeck effect. We will see that contrarily to Joule heating, the Seebeck effect is a thermodynamically reversible phenomenon, very similar to the Peltier one (actually the reverse phenomenon), so that thermoelectric generators can be developed using that physical

feature. After a rapid overview of the state of the art of organic thermoelectric materials, and especially PEDOT ones, our preliminary results on the thermoelectric performances will be presented.

With the appealing properties and applications that will be shed light on in the next three chapters, the fifth chapter will deal with features without which no industrial applications can be considered, that is the ageing and stability of our PEDOT based materials under different environmental stresses. We will investigate the impact of both humidity and light exposure on the electrical properties of PEDOT. Raman, XPS, GIWAXS and electronic transport measurements will all be characterization techniques that will allow us to study the mechanisms (be they chemical, structural or electronic) that take place during the ageing of PEDOT films. This chapter is an ongoing work and therefore additional experiments are required in order to confirm the degradation mechanisms.

Finally, the work will be completed with conclusive remarks summarizing the main studies that have been developed during this thesis and opening perspectives to future works for always a better understanding of our PEDOT based materials and appealing applications that can stem from them. This will allow us to introduce the Appendix, which will expose the experimental methods.

Chapter 2
Structure and dopant engineering in PEDOT thin films

1. Introduction

In this chapter, novel PEDOT materials will be developed and their electrical properties thoroughly studied.

We will first explain the choice of the materials as well as the structure and dopant engineering that will be implemented for better electrical properties. The experimental details will only be roughly explained but more information can be found in Materials & methods in the appendix.

The electrical properties will be presented and different characterization techniques will be used in order to unravel the electronic conduction in our PEDOT films, so that a transport model can finally be implemented and the transport mechanisms fully understood.

2. Strategy

Because of the properties and applications targeted, researches have put tremendous efforts on increasing, if not optimizing and even maximizing, the electrical conductivity of PEDOT as illustrated in Figure I.22 and Table B.1. Reported conductivities spread over a wide range and reach nowadays routinely conductivities exceeding 1000 S cm^{-1}.[20,32,61,101,104–107] The origin of such differences lies in the semi-crystalline nature of the material itself, strongly correlated with the synthesis method and the counter-anions.[26,108] PEDOT:PSS, although commercially available and easily processable, retains however an excess insulating polystyrene sulfonic acid (PSSH) which hinders its conductivity. PEDOT with small counter-anions, such as tosylate (Tos), genuinely show better electrical properties due to the absence of the sterically hindering polymeric counter-anion which leads to a better crystalline structure.[32,101] They can mainly be synthesized through vapor phase polymerization (VPP) or solution cast polymerization (SCP).

The water uptake is another issue for good film forming properties. As a matter of fact, the two more common oxidants for VPP are $FeCl_3$ and $Fe(Tos)_3$, which are known to form crystallites in the presence of water, which is detrimental to the conduction properties. But at the same time, the presence of water within the VPP chamber was shown to be crucial since it was helping deprotonating the EDOT-dimer and hence

allowing polymerization to occur (see Figure I.15).[109,110] Murphy and coworkers introduced an interesting solution to that issue. Water being mandatory, and at the same time detrimental to the polymerization process, they added a surfactant in order to inhibit the crystal formation of the oxidant. The surfactants used in their work are glycol based, typically the amphiphilic copolymers poly(ethylene glycol)-*ran*-poly(propylene glycol) (PEG-*ran*-PPG) and poly(ethylene glycol) – poly(propylene glycol) – poly(ethylene glycol) (PEG-PPG-PEG) , consisting of hydrophobic PPG blocks and hydrophilic PEG blocks.[109,110] These surfactants, besides suppressing the crystallization of the oxidant, also moderate the polymerization rate as proved by quartz crystal microbalance measurements (QCM), so that a base is no longer necessary.[69,110] They further demonstrated that the glycol-based surfactant complexes the oxidant and controls the reaction rate.[61,111] In VPP however, due to the processing technique itself, the glycol copolymer remains in the film, leading to the same problem as in PEDOT:PSS, or in other words the presence of an insulating phase in the film. This is however not the case for SCP in which the bottom-up polymerization process allows an easy rinsing of the copolymer.[18,110]

That is in that context, in order to avoid any undesired insulating phase in the PEDOT (PSSH or PEG-PPG-PEG) films and in order to optimize the electronic conduction properties by using non bulky counter-anions, that our group investigated the solution-cast polymerization of PEDOT using the oxidant iron (III) trifluoromethane sulfonate (iron(III) triflate or $Fe(OTf)_3$).[32] Using $Fe(OTf)_3$ as the oxidant, PEG-PPG-PEG as the acidic side reactions inhibitor and polymerization rate controller, EDOT as the monomer and ethanol as the solvent, PEDOT:OTf (PEDOT stabilized with triflate counter-anions) was then successfully synthesized and a conductivity of 1200 S cm^{-1} is obtained.[18,32]

The objective of this chapter is to increase that conductivity to the state of the art ideally and above all to understand the origin of the high conductivity and the transport mechanisms occurring within the films. For that purpose, our attention has turned toward aprotic polar solvents. As a matter of fact, it is known that aprotic polar solvents easily coordinate with Fe(III).[112] Using such coordinating solvents in the oxidative solution for PEDOT:OTf, we intend to reduce the number of nucleation centers at the surface of the substrate during the film formation. We then expect the limited number of nuclei to lead to the formation of longer polymer chains, and hopefully longer conjugation lengths. For that purpose, three coordinating co-solvents

are tested, namely N-Methyl-2-pyrrolidone (NMP), dimethyl sulfoxide (DMSO) and dimethyl formamide (DMF) in Figure II.1.

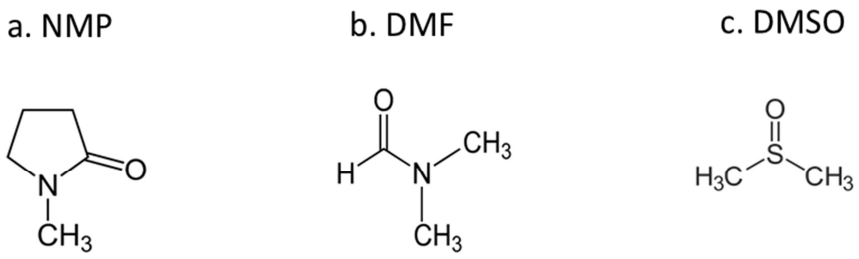

Figure II.1. Aprotic polar solvents used as co-solvent for PEDOT polymerization.

3. Results and discussion

3-1. Electrical conductivity

PEDOT:OTf films were obtained by spin-coating an ethanolic solution containing 3,4-ethylenedioxythiophene (EDOT), the oxidant Fe(III)$(OTf)_3$ and the polymerization rate controller PEG-PPG-PEG[101], on glass substrates as illustrated in Figure II.2.

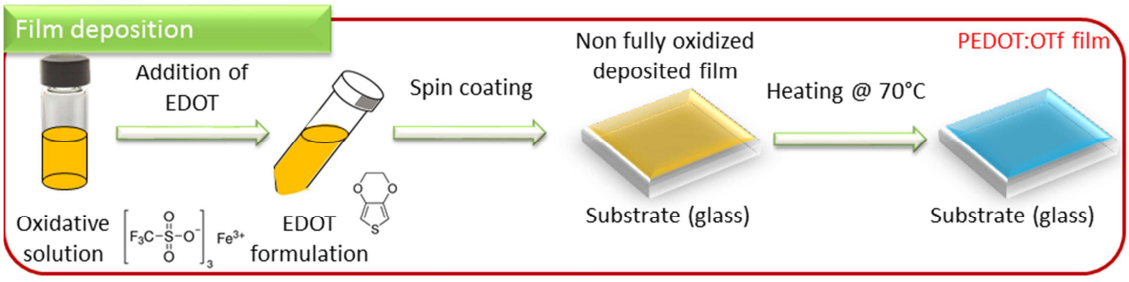

Figure II.2. Illustration of the synthesis of PEDOT:OTf thin films.

3-1-1. Co-solvent addition

The formulation with the co-solvents was obtained by adding NMP, DMF or DMSO in the aforementioned oxidative solution, hence obtaining PEDOT:OTf-NMP, PEDOT:OTf-DMF or PEDOT:OTf-DMSO films respectively.

Figure II.3a shows conductivity values obtained on PEDOT:OTf-co-solvents with different amounts of co-solvents. The conductivity was calculated from the measured

thickness e (with atomic force microscopy (AFM)) and the measured square resistivity Rs (with a four point probe apparatus). Subsequently, the electrical conductivity σ is calculated using Equation II.1

$$\sigma = \frac{1}{Rs.e} \tag{II.1}$$

The details can be found in Materials & methods in the appendix.

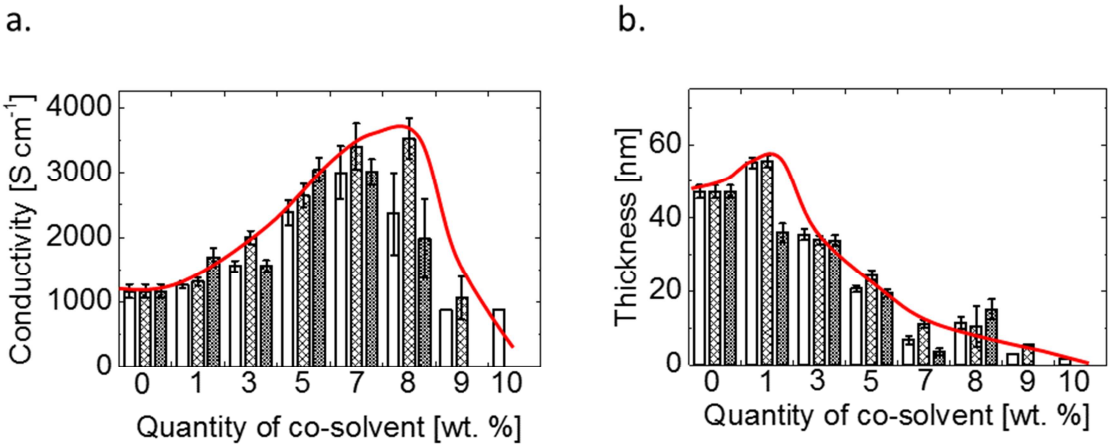

Figure II.3. Electrical properties of PEDOT materials with different amounts of co-solvents. Room temperature conductivity (a) and thickness (b) measurements of PEDOT:OTf-co-solvent thin films. The co-solvents used are DMF (empty columns), NMP (medium filled columns) and DMSO (densely filled columns). Error bars include the average value over three samples.

The conductivity increases with increasing co-solvent quantity and maximum values are reached for a loading of 7 – 8 wt. % of co-solvent. The highest conductivities achieved with DMF, DMSO and NMP loaded PEDOT films are 3000 ± 400, 3000 ± 200 and 3600 ± 200 S cm^{-1} respectively. These values are among the highest reported for conducting polymer films. While the conductivity increases, the thickness decreases as shown in Figure II.3b. After a loading amount superior to 10 wt. %, the film is not continuous anymore or simply polymerization does not occur and neither the thickness nor the square resistivity could be assessed properly.

From loading amounts of co-solvents superior to 5 wt. %, the thickness is lower than 10 nm. In order to avoid any miscalculation of the electrical conductivity, multilayers up to 3 layers were deposited in order to be comparable in thickness with PEDOT:OTf (~40 nm). For each co-solvent-treated film, the conductivity is greater than 2500 $S.cm^{-1}$, even reaching 3500 and 3600 $S.cm^{-1}$ for a bilayer and a monolayer

deposition of PEDOT:OTf-NMP (7%) respectively as depicted in Figure II.4. Finding the same conductivity for all layers from the same co-solvent proves that the conductivity is independent of the thickness for a given material, and that the measured electrical conductivities at co-solvent loading superior to 7 wt. % are reliable.

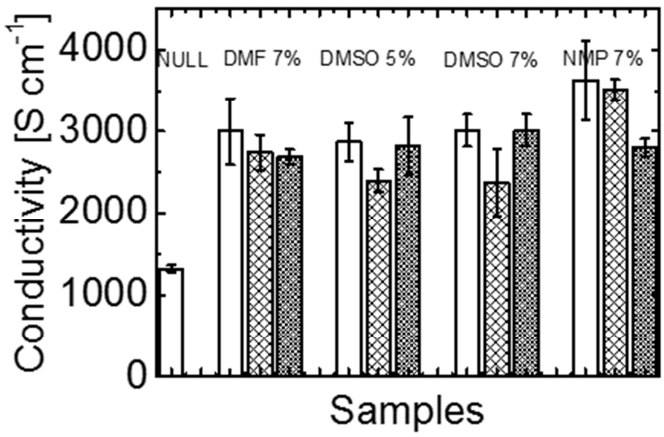

Figure II.4. Room temperature electrical conductivity of PEDOT films with different amounts of co-solvents (in wt. %). For each co-solvent containing film one layer (empty columns), two layers (medium filled columns) and three layers (densely filled columns) were deposited. Error bars include measurements errors.

3-1-2. Acid treatment

PEDOT films were also treated with diluted sulfuric acid in order to further enhance the conductivity as illustrated in Figure II.5. Such treatment has been proven efficient on both PEDOT:PSS and PEDOT:Tos as reported in the first chapter and also on PEDOT:OTf films as shown by our group.[32,54,87,113] PEDOT:OTf and PEDOT:OTf-co-solvent films were immersed into 1 M sulfuric acid aqueous solution for 30 min before being heated at 120 °C for 20 min without rinsing. Resulting samples were named PEDOT:Sulf and PEDOT:Sulf-co-solvent respectively.

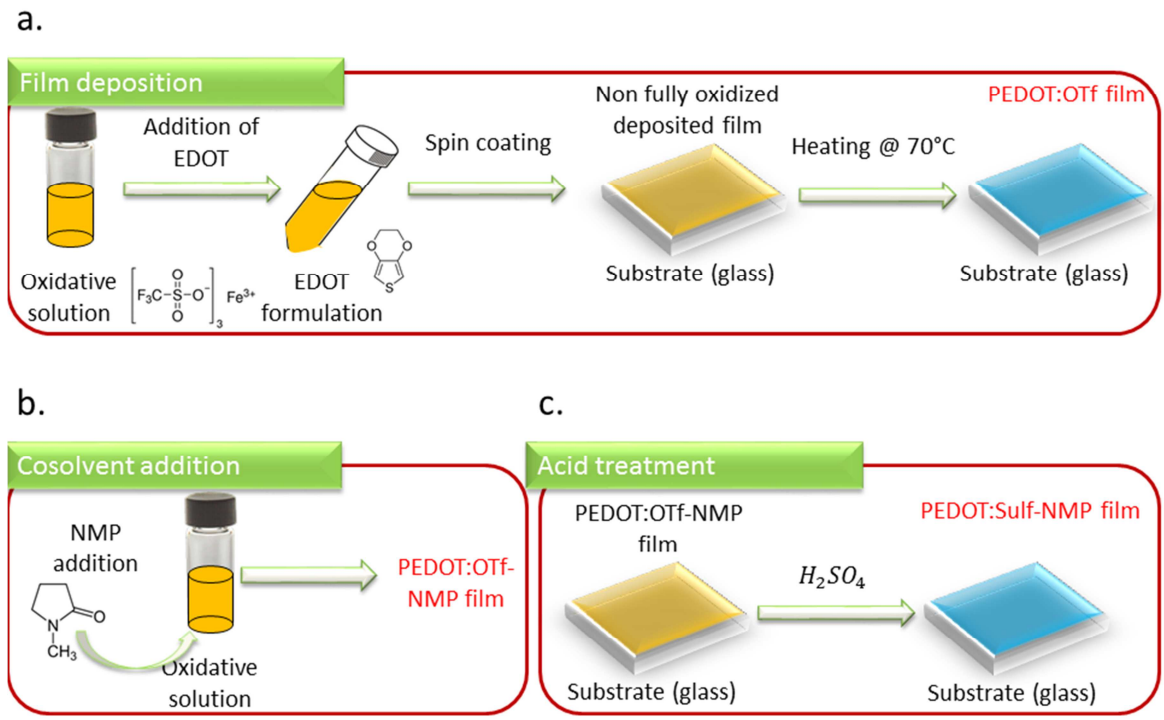

Figure II.5. From the synthesis of PEDOT:OTf and PEDOT:OTf-NMP to its treatment with sulfuric acid. a) Synthesis of PEDOT:OTf. b) Synthesis of PEDOT:OTf-NMP. After the addition of EDOT, all previous steps are the same. c) Treatment with sulfuric acid: the obtained PEDOT:OTf (with or without a co-solvent) is dipped into diluted sulfuric acid.

The conductivities of the acid treated PEDOT films are given in Figure II.6. Without prior co-solvent addition, the conductivity reaches 2270 ± 50 S cm^{-1} and goes up to 5190 ± 880 S cm^{-1}, 4020 ± 400 S cm^{-1} and 5400 ± 470 S cm^{-1} after the addition of DMF, DMSO and NMP respectively. The acid treatment leads then to a conductivity increase between 40 and 70 %. It is interesting to note that the conductivity of PEDOT:Sulf-NMP was measured at 5400 ± 400 S cm^{-1}, which is the highest reported value for PEDOT films so far. Explanation of the chemical and structural mechanisms responsible for this extensive enhancement is presented hereafter.

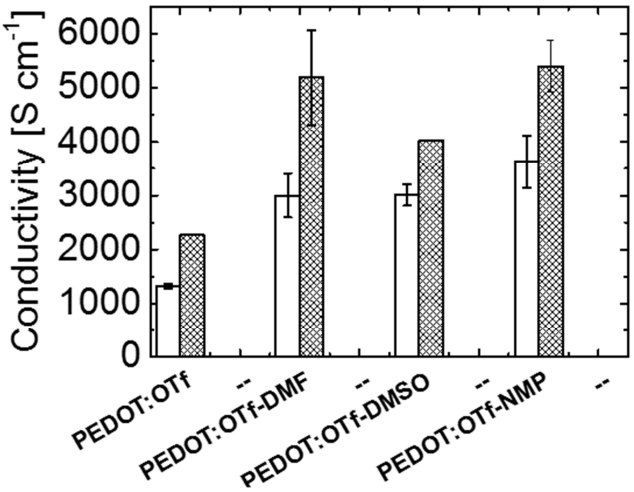

Figure II.6. Room temperature conductivity of PEDOT:OTf and its derivatives before acid treatment (empty columns) and after acid treatment (filled columns). Error bars include the average value over two samples and measurement errors.

For the sake of clarity, only the effect of loading with 7 wt. % NMP is studied (Figure II.7). DMF and DMSO are expected to have similar actions during the synthesis.

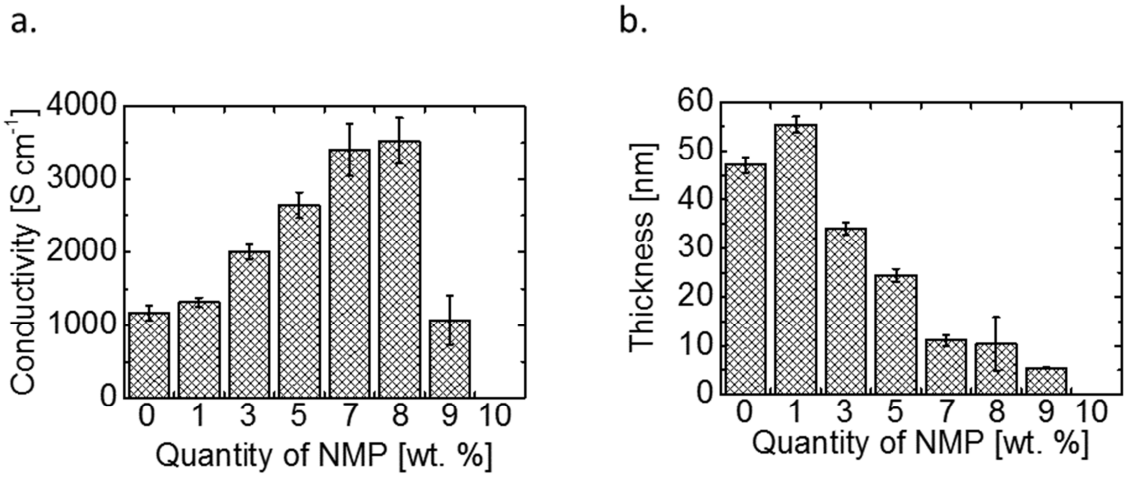

Figure II.7. Electrical properties of the PEDOT:OTf-NMP materials. a) Conductivity and b) thickness of PEDOT:OTf-NMP thin films as a function of the quantity of NMP. Error bars include the average value over three samples.

3-2. Oxidation state

UV-Vis-NIR absorption spectra of PEDOT:OTf as well as its acid treated counterparts can be found in Figure II.8. In all samples broad bands at $\lambda \sim 750$ nm and $\lambda > 1250$ nm correspond respectively to the polarons and bipolarons charges carriers in PEDOT films (see Figure I.19).[60] PEDOT:OTf films are light blue with the transmittance at 550 nm being 87.2 %. With the addition of NMP highly transparent films are obtained (T = 96.9 %). The absorbance of polarons and bipolarons is also smaller but this is mostly due to the thinner film obtained (10 nm compared to 40 nm). When treated with sulfuric acid the bipolaronic absorbance increases to the detriment of the polaronic one. According to Crispin et al. theory about semi-metallic polymers that has been presented in Chapter 1, that trend could promote a more pronounced semi-metallic behavior as will be more discussed later.[20]

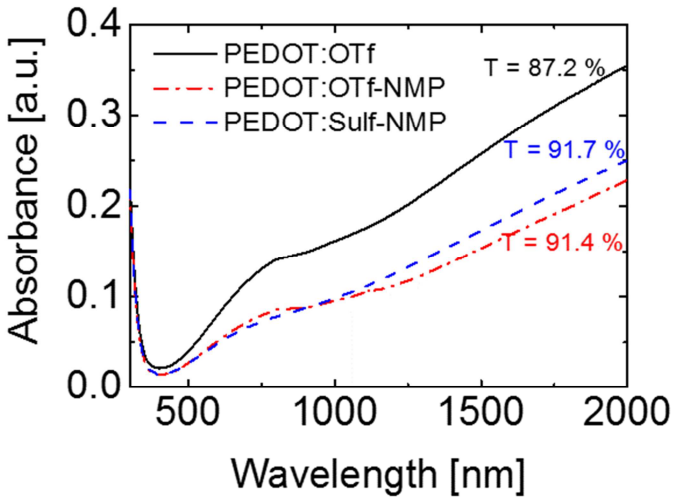

Figure II.8. UV-Vis-NIR spectra of PEDOT:OTf and its treated counterparts. The transmittance is taken at 550 nm.

X-Ray photoelectron spectroscopy (XPS) provides insights into the chemical composition at the surface of the films and their oxidation states.[60] We investigated PEDOT:OTf-NMP and PEDOT:Sulf-NMP in order to determine the effect of the co-solvent addition and the influence of the acid treatment.

Typical high resolution core level spectra were obtained and confirmed the presence of nitrogen, carbon, oxygen and sulfur in both PEDOT:OTf-NMP and PEDOT:Sulf-NMP in Figure II.9. Fluorine was only detected in PEDOT:OTf-NMP.

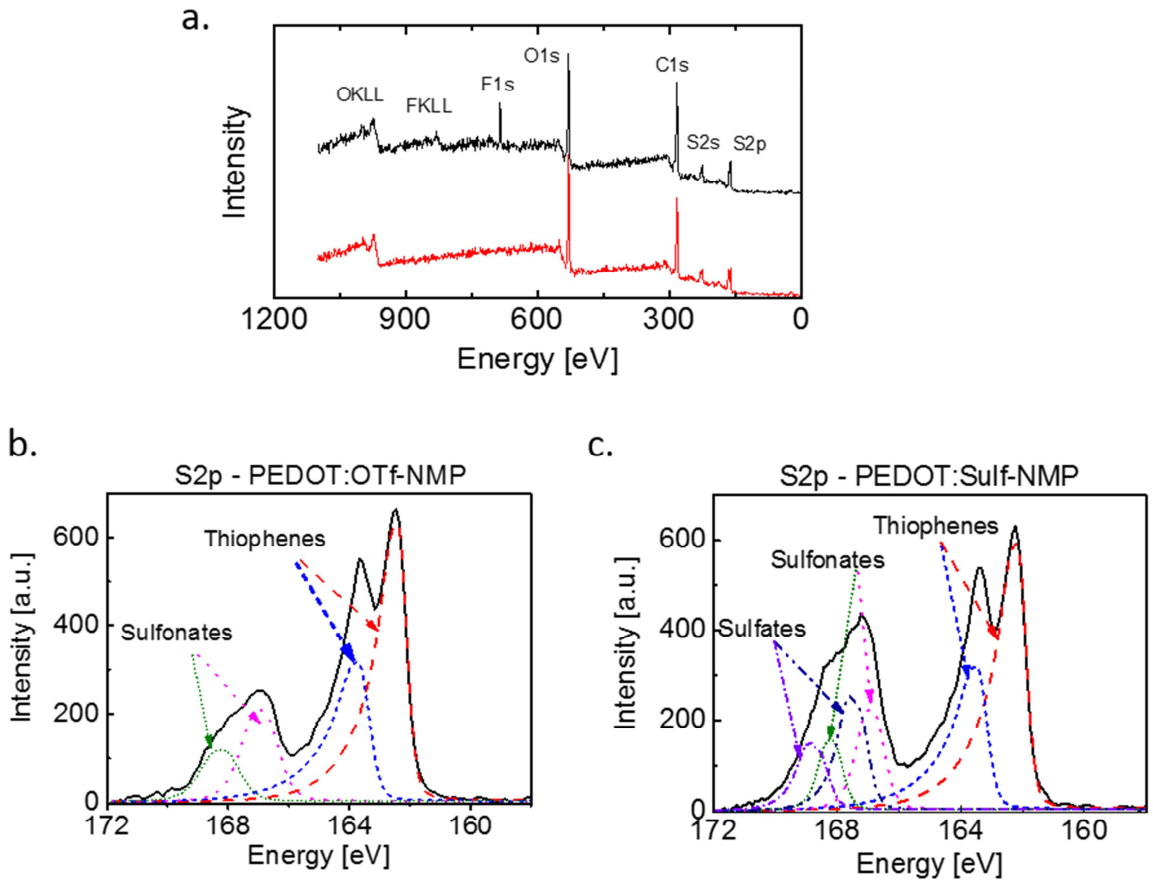

Figure II.9. Chemical analysis of the PEDOT materials using X-Ray photospectrometry. a) Survey spectra of PEDOT:OTf-NMP (black curve) and PEDOT:Sulf-NMP (red curve). b) S2p XPS spectrum of PEDOT:OTf-NMP. c) S2p XPS spectrum of PEDOT:Sulf-NMP.

Though it is a surface technique, the films are thin enough (< 10 nm) to be investigated in their whole thickness as evidenced in Figure II.10 by the Si contribution originated from the glass substrate. Therefore, the results presented here represent the films in their whole thickness. Moreover, Figure II.10 shows the presence of nitrogen, confirming that NMP is still present in the film and was not totally eliminated during the washing step. It was however barely detected and the remaining NMP is not expected to be substantial.

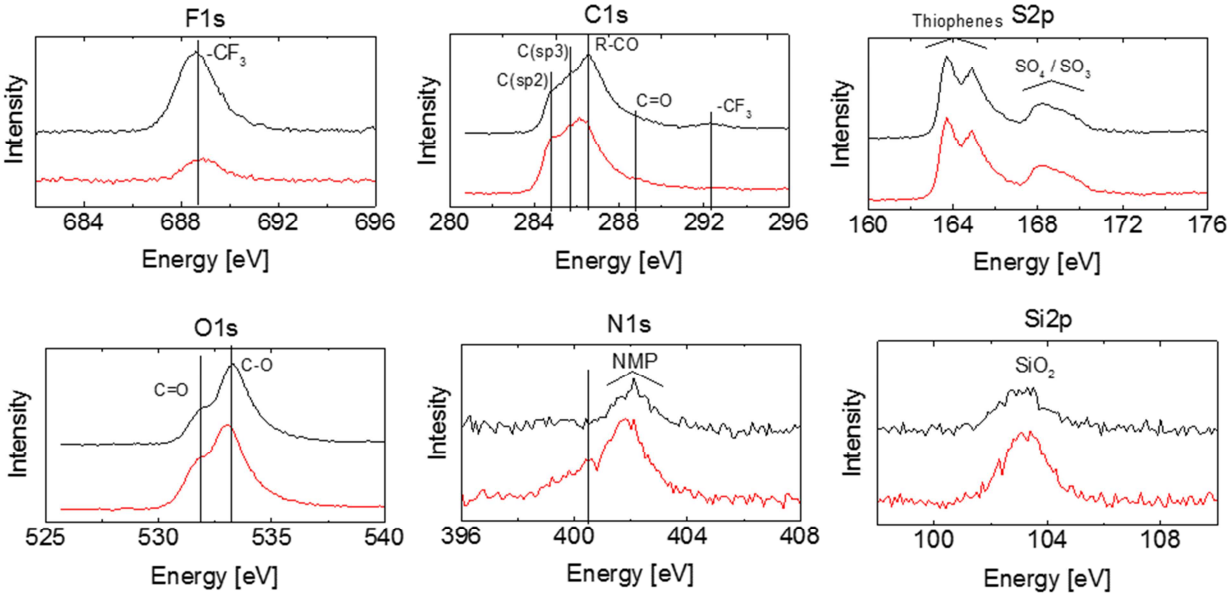

Figure II.10. XPS spectra of different elements present in the films.
PEDOT:OTf-NMP (black line) and PEDOT:Sulf-NMP (red line).

The survey spectra in Figure II.9a show the presence of fluorine in PEDOT:OTf-NMP whereas it could not be identified in PEDOT:Sulf-NMP, and was scarcely present in the high resolution core level spectra in Figure II.10. This suggests that triflate counter-anions have been washed off the film, at least partially.

The oxidation level of PEDOT films can be estimated thanks to the ratio of thiophene units to other sulfur based components.[76] The S2p spectra of PEDOT:OTf-NMP and PEDOT:Sulf-NMP are depicted in Figure II.9b,c. Due to different oxidation states, the $S2p_{3/2\text{-}1/2}$ doublet from the thiophene units of PEDOT is distinct from that of the counterions.

Both thiophenes and sulfonates are detected in the S2p spectrum of PEDOT:OTf-NMP. By using deconvolution on both peaks, information on the oxidation level can be obtained as explained in Materials & methods. An oxidation level of 38 % was measured, which is in good agreement with the oxidation level of PEDOT:OTf which is about 28 %.[32] The co-solvent addition enhances the oxidation of PEDOT.

Regarding the acid treated films, not only were thiophenes and sulfonates detected, but also sulfates. This, along with the reduced amount of fluorine found in the films, can be explained by the replacement of triflate by hydrogenosulfate as counter-anions. The ratio of sulfonates and sulfates over thiophene is about 64 % which means that not

only are some $CF_3SO_3^-$ replaced by HSO_4^-, but also the film undergoes further oxidation and sulfates from the acid are still present after the treatment. The deconvolution of these different spectra poses that more than ¾ of the triflate anions have been replaced. The use of a less steric counter-anion introduced after acid treatment, combined with a higher oxidation level, allows a substantial conductivity enhancement from 3600 to 5400 S cm^{-1}.

Thus, the co-solvent and the sulfuric acid are both suspected to induce changes in the charge carriers's density.

3-3. Role of the co-solvent

In order to shed some light on the role of the co-solvent, UV-Vis-NIR spectroscopy was used to monitor the PEDOT synthesis with and without NMP. The UV-Vis-NIR spectra of the oxidative solutions used for the synthesis of PEDOT:OTf and PEDOT:OTf-NMP, were recorded before and after the addition of the EDOT monomer. These solutions were contained in sealed vials. Figure II.11a,b displays these spectra. The absorbance was given at 650 nm in order to schematize the kinetics of the reaction with and without the co-solvent (Figure II.11c). Before and just after the addition of EDOT monomer, both solutions have the same absorption spectra. 17 minutes after the addition of EDOT, the absorbance was greater in the case of the non-NMP containing solution. Saturation of the absorption, here attributed to a too high PEDOT concentration in the solution, was reached within less than 34 minutes in the case of PEDOT:OTf, while it was reached after 100 minutes in the case of PEDOT:OTf-NMP. This experience shows that the co-solvent NMP slows down the polymerization reaction. This may cause a lower polymerization rate, and hence more time for morphological changes in the structure of the films.

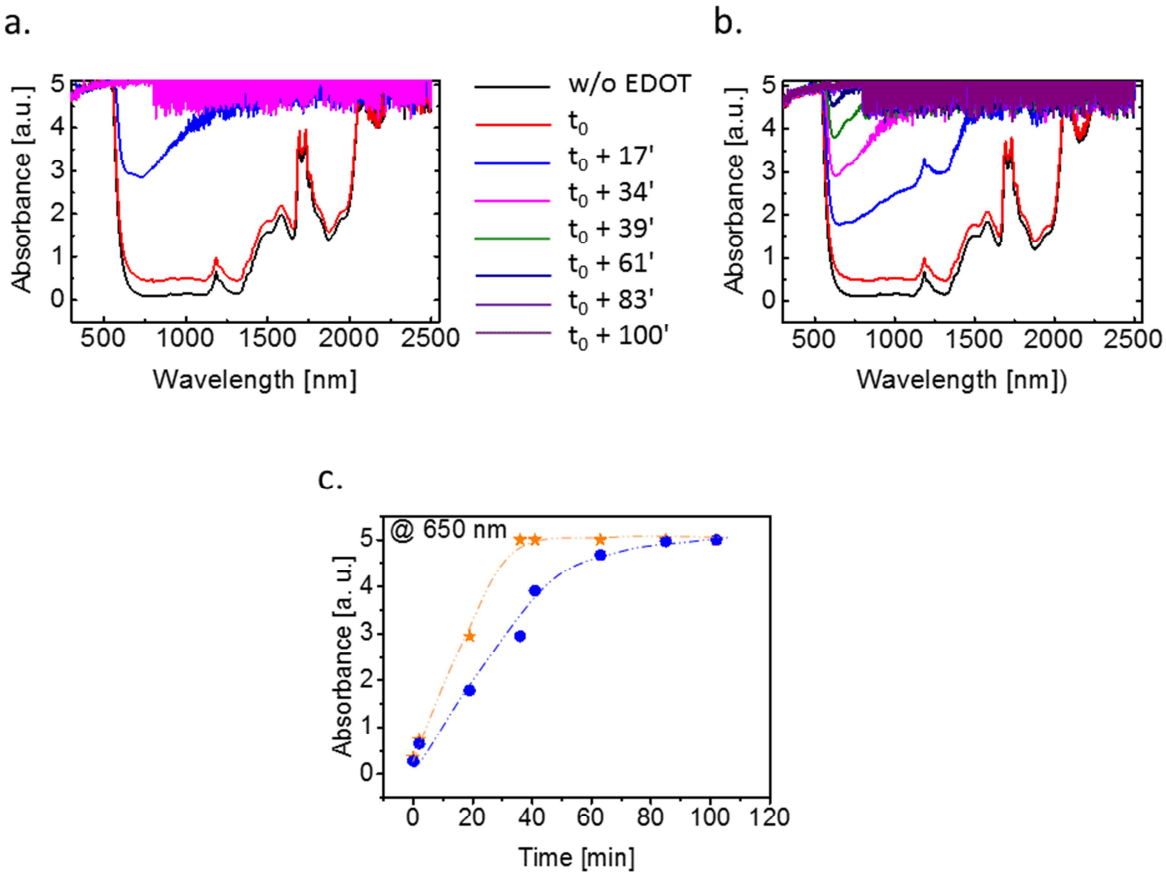

Figure II.11. UV-Vis-NIR spectra of a) PEDOT:OTf and b) PEDOT:OTf-NMP at different polymerization times. Above an absorbance of 4.5, saturation is reached. c) Reaction rate without (orange stars) and with (blue circles) NMP. The dashed lines are a guide for the eyes.

3-4. Structure of the PEDOT films

3-4-a. X-Ray measurements

GIWAXS measurements give access to the structure of the PEDOT films and their crystallinity. This technique is well suited for investigating our films which are between 10 and 40 nm thick (Figure II.7b). More information on this technique is given in the Materials & methods. Measurements were led both in the European Synchrotron Radiation Facility (ESRF) at Grenoble using beamline BM 32 and in our laboratory using a recently acquired Smartlab diffractometer equipment. The GIWAXS intensity profiles of commercial PEDOT:PSS (Clevios PH1000) doped with EG, PEDOT:OTf, PEDOT:OTf-NMP and PEDOT:Sulf-NMP obtained with the Smartlab diffractometer are presented in Figure II.12. Those obtained with synchrotron radiation are presented in Figure II.13a,b. Both in-plane and out-of-plane measurements reveal the structure of

the as-deposited films. The different peaks were indexed according to previous works.[32,93,101] All samples have been characterized directly on their glass substrate.

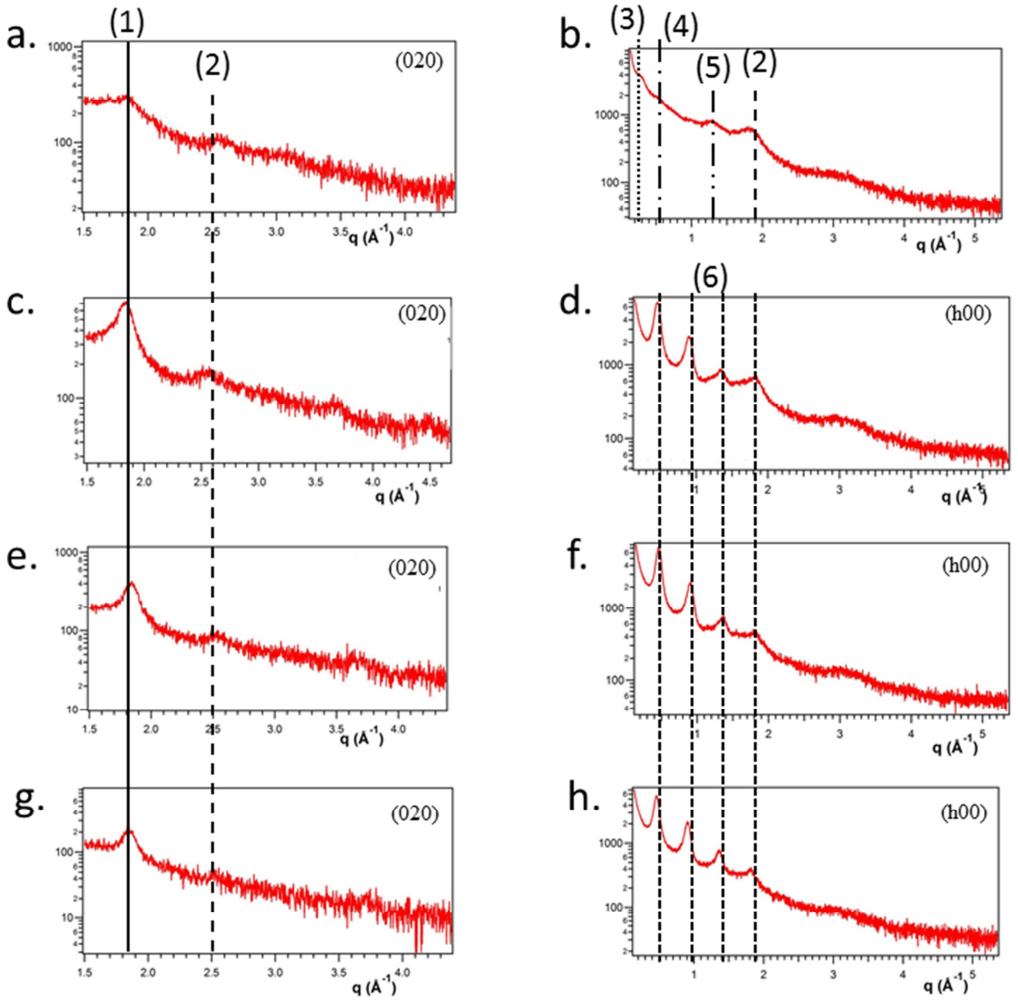

Figure II.12. GIWAXS patterns of different PEDOT films: PEDOT:PSS a) in-plane & b) out-of plane. PEDOT:OTf c) in-plane & d) out-of plane. PEDOT:OTf-NMP e) in-plane & f) out-of plane. PEDOT:Sulf-NMP g) in-plane & h) out-of plane. For PEDOT:OTf, PEDOT:OTf-NMP and PEDOT:Sulf-NMP, (020) peak can clearly be observed on in-plane measurements and (100) peak and higher orders on out-of-plane scans. Diffraction peaks were fitted assuming a pseudo-Voigt profile with fixed shape parameter $\eta = 0.7$.

The main diffraction peaks' parameters can be found in Table II.1. On in-plane measurements (Figure II.12a,c,e,g), PEDOT:PSS exhibits a weak bump at around q = 1.82 Å^{-1} (d = 3.45 Å). This bump becomes a sharp intense peak in the case of PEDOT:OTf, PEDOT:OTf-NMP and PEDOT:Sulf-NMP at q = 1.85 Å^{-1} (d = 3.40 Å), q = 1.85 Å^{-1} (d = 3.40 Å) and q = 1.87 Å^{-1} (d = 3.39 Å) respectively. This peak is

attributed to the Bragg diffraction of the π-π stacking of the PEDOT thiophene rings (1), representing the face to face oligomers stacking in the b-direction as described in Figure II.13c. It corresponds to the (020) diffraction peak of the PEDOT orthorhombic structure. The disappearance of the bump in PEDOT:PSS, replaced by a peak in PEDOT:OTf, is due to the replacement of the excess PSS by small triflate anions, which, with less steric hindrance, leads to a more crystalline structure. Another bump appears in the in-plane scanning of all PEDOT films at q = 2.57 $Å^{-1}$ (d = 2.45 Å). As this Bragg diffraction appears in all patterns, it is independent of the PSS counter-anion and belongs therefore to the PEDOT structure. Moreover, being smaller than the π-π stacking of the PEDOT thiophene rings, it is attributed to the second order of another distance, which is thought to be the EDOT/EDOT repetition (2), and is coherent with the distance measured from the HRTEM images (see below).

Table II.1. Diffraction distances and grains' size of the studied samples.

		q [$Å^{-1}$]	d [Å]	τ [nm][1]
π-π stacking of PEDOT (d020)	PEDOT:PSS	ND[2]	ND	ND
	PEDOT:OTf	1.846 ± 0.005	3.403 ± 0.005	4 ± 0.5
	PEDOT:OTf-NMP	1.847 ± 0.005	3.401 ± 0.005	5 ± 0.5
	PEDOT:Sulf-NMP	1.856 ± 0.005	3.385 ± 0.005	5.5 ± 0.5
Lamellar stacking of PEDOT	PEDOT:PSS	ND[2]	ND	ND
	PEDOT:OTf	0.461 ± 0.002	13.629 ± 0.002	7.5 ± 1
	PEDOT:OTf-NMP	0.465 ± 0.002	13.512 ± 0.002	9 ± 1
	PEDOT:Sulf-NMP	0.466 ± 0.002	13.483 ± 0.002	10 ± 1

[1] Comments on the crystallites' size calculation can be found in Materials & methods.
[2] Not defined. Peaks in PEDOT:PSS diffractograms are too broad to allow to extract reliable quantitative results.

In the out-of-plane diffraction patterns, PEDOT:PSS exhibits four broad bumps at q = 0.29 $Å^{-1}$ (d = 21.86 Å), q = 0.45 $Å^{-1}$ (d = 13.96 Å), q = 1.22 $Å^{-1}$ (d = 5.15 Å) and q = 1.82 $Å^{-1}$ (d = 3.45 Å). According to previous research the first peak results from

both PEDOT and PSS contributions and corresponds to the lamellar stacking between PEDOT and PSS chains (3).[32] The peak at q = 1.82 Å^{-1} has already been assigned to the π-π stacking of PEDOT chains (1), which implies that PEDOT chains are face-on as well as edge-on the glass substrate in PEDOT:PSS where no preferred orientation is noticed. The remaining peaks at q = 0.45 Å^{-1} and q = 1.22 Å^{-1} are attributed to the interdigitation packing (4) and π-π stacking of PSS chains (5) respectively. PEDOT:OTf and its treated counterparts exhibit also several peaks. Here, the appearance of narrow and sharp intense peaks suggests a more crystalline structure with bigger crystallites size. A first peak at q = 0.46 Å^{-1} (d = 13.65 Å) represents the Bragg diffraction of the lamellar packing of PEDOT chains in the a-direction, corresponding to the (100) diffraction plan (6). The other following peaks at q = 0.92 Å^{-1}, 1.38 Å^{-1} and 1.84 Å^{-1} are the second, third and fourth order (6).

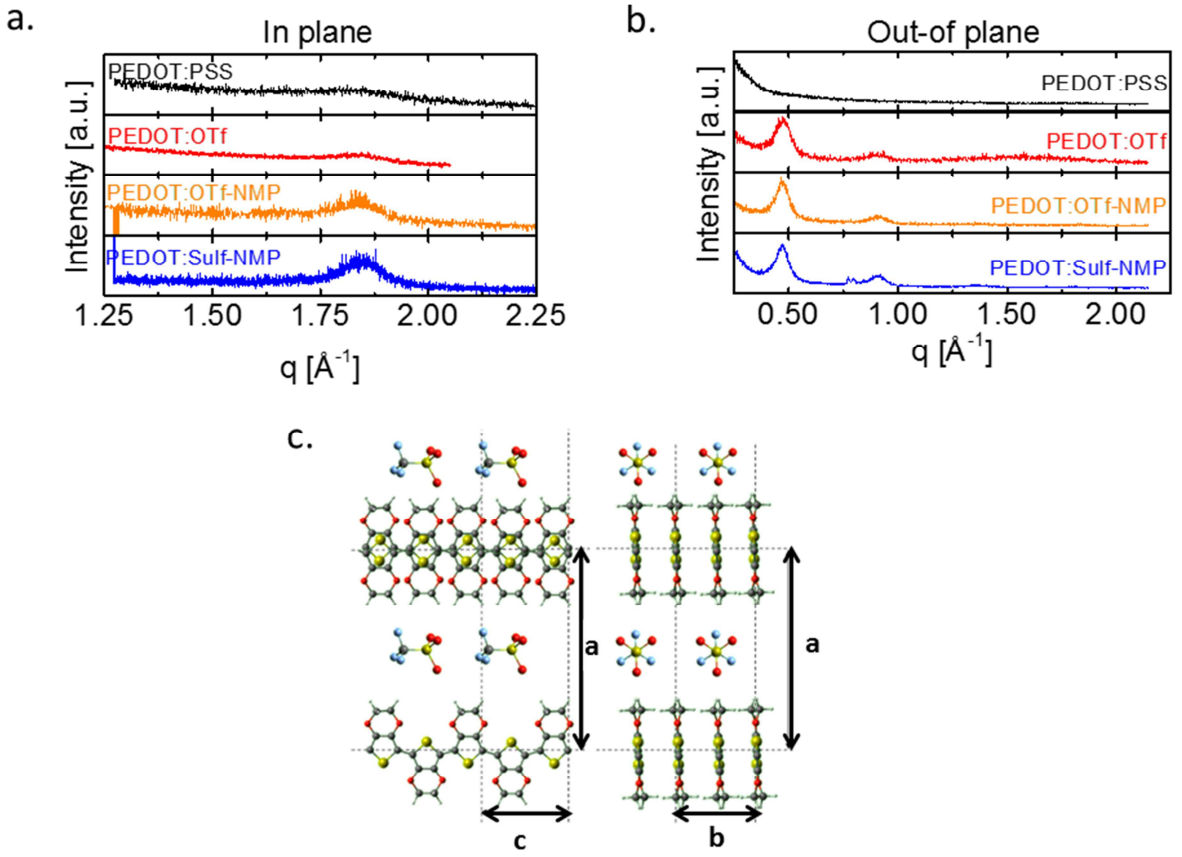

Figure II.13. Structural characteristics of the PEDOT materials. a) In-plane and b) out-of plane synchrotron GIWAXS diffractograms of PEDOT:PSS, PEDOT:OTf, PEDOT:OTf-NMP and PEDOT:Sulf-NMP. c) Scheme of stacking in the crystallites.

By using synchrotron radiation, in both PEDOT:PSS diffractograms, no clear diffraction peak is noticeable. However, the bump at q = 1.82 $Å^{-1}$ in the in-plane scan can similarly be associated with the (020) diffraction peak of the PEDOT orthorhombic structure. The broadness of the bump reveals the high degree of disorder in PEDOT:PSS and prevents the determination of the mean size of the crystallites.[32,108] Nonetheless previous studies suggested a 4.5 nm crystallite size along the b axis.[93]

The crystallites' size obtained from in-plane measurements are 4, 5 and 5.5 ± 0.5 nm for PEDOT:OTf, PEDOT:OTf-NMP and PEDOT:Sulf-NMP respectively; out-of-plane diffractograms give 7.5, 9 and 10 ± 1 nm. Interestingly for PEDOT:OTf-NMP and PEDOT:Sulf-NMP the film thickness is very close to the crystallite size deduced from out-of plane measurements, suggesting that the film is approximately one crystallite thick.

3-4-b. HRTEM images

These GIWAXS characteristic lengths and distances are corroborated by HRTEM images. Figure II.14 and Figure II.15 give HRTEM images of PEDOT:OTf-NMP deposited on a copper grid coated with graphene in order to support the PEDOT film. The images clearly infer the presence of crystalline domains surrounded by amorphous regions. In the crystallites, characteristic π-π stacking distances can be measured at 3.46 Å, consistent with GIWAXS data. These HRTEM images provide also clear information about the length of PEDOT chains forming the crystallites, typically around 10 nm as inferred from Figure II.14 and Figure II.15. Moreover, another characteristic length about 2.72 Å (Figure II.14) in the direction perpendicular to the π-π stacking can be attributed to the EDOT monomer size.[55] Given the fact that PEDOT chains are actually oligomers and supposing that the chain is not much longer than the crystallite size, the number of repeating units in the PEDOT chains in the crystallite in Figure II.14 can be approximated to 23 EDOT units.

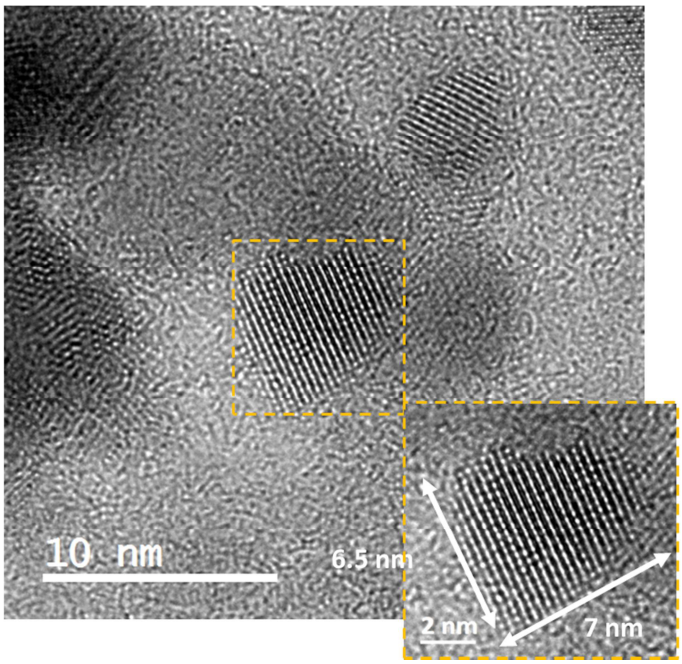

Figure II.14. HRTEM images of PEDOT:OTf-NMP. The inset image is the magnification of the outlined square. The (100) direction, as defined in Figure II.13, is perpendicular to the plane of the film.

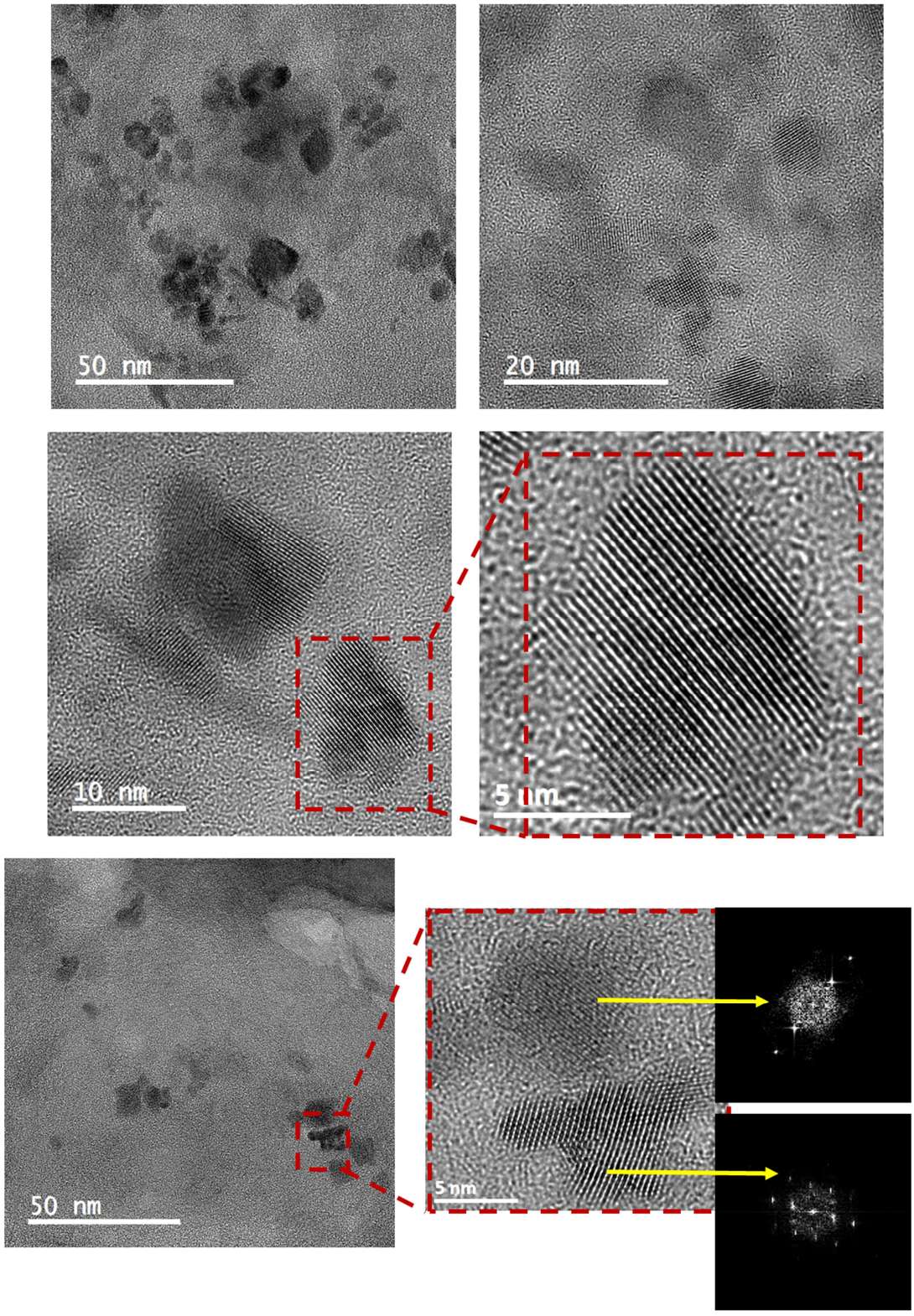

Figure II.15. Figure S10: HRTEM images at different magnifications.

3-4-d. Conclusion

As NMP is added to the oxidative solution, the polymerization rate slows down, probably due to a lower number of nuclei.[112] This may lead to the formation of longer and better stacked chains with better conjugation lengths, as deduced from the higher doping level from XPS, the bigger crystallites size calculated from GIWAXS data and the tighter diffraction parameters from GIWAXS data. It then seems reasonable to assume that the increase of crystallites' mean size noticed between PEDOT:OTf and PEDOT:OTf-NMP together with the more ordered film obtained and the higher doping level might be a reason for the dramatic improvement of the conductivity from 1200 to 3600 S cm^{-1}.

On the other hand, with acid treatment, the parameters deduced from the diffraction patterns are the same order so that a noticeable structure change cannot be assessed. There seems to be no significant structure change but a chemical one is suggested by the replacement of some triflate counter-anions by hydrogenosulfate ones.

With the structure highly enhanced by NMP addition and the steric hindrance of the counter-anion reduced, better transport properties are expected in these PEDOT films.

3-5. Transport properties

Transport mechanisms in conducting polymer films remain highly impacted by the degree of disorder inherent to these materials.[30,108] The degree of disorder and the transport properties in conducting polymers are generally assessed by the resistivity ratio $\rho_r = \frac{\rho(0\ K)}{\rho(300\ K)}$ and the temperature dependence of conductivity as explained in Chapter 1.[32,114] A lower ρ_r corresponds to a more ordered film. Indeed, since the drop between the room temperature and the 0 K resistivity is moderate, the temperature dependence of the resistivity (or conductivity) is modest meaning that high energy barriers induced by a heavy disorder are not encountered. PEDOT:PSS typically follows a variable range hopping (VRH) transport mechanism due to the Anderson localization of the charge carriers induced by the high disorder in those films as explained in Chapter 1.[115] PEDOT:OTf and its treated counter parts however do not.

3-5-a. Co-solvent effect

Figure II.16a,b depicts the temperature dependence of conductivity of PEDOT:OTf without and with addition of NMP at various quantities. The data are also compared to that of commercial PEDOT:PSS (Clevios PH1000) without any solvent treatment.

The data given for PEDOT:PSS and PEDOT:OTf without NMP were not recorded during this thesis and are those published by Massonnet et al.[32] The conductivities are normalized for the sake of comparisons.

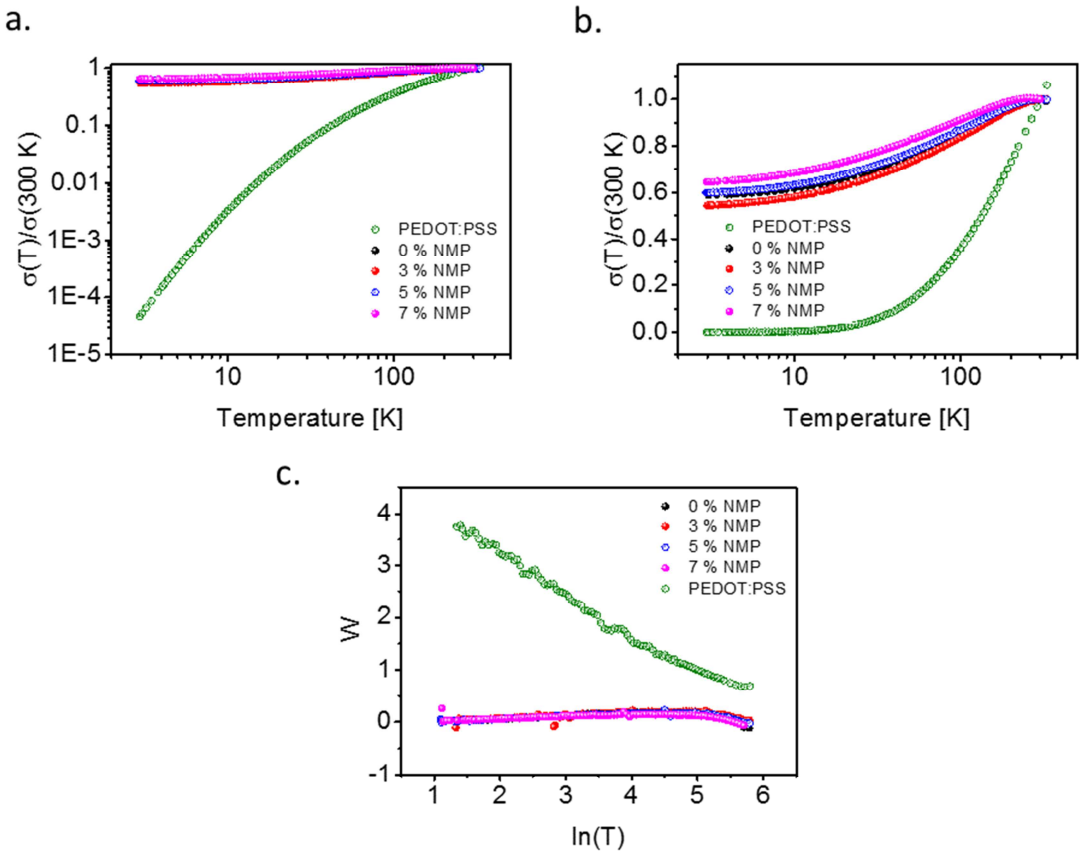

Figure II.16. a) Log-scale and b) linear scale of the temperature dependence of conductivity of commercial PEDOT:PSS (PH1000) and PEDOT:OTf with different amounts of NMP. c) Reduced activation energy

The difference between PEDOT:PSS and PEDOT with small counter-anions is striking. While the former one is strongly temperature dependent with a resistivity ratio superior to 20000, the one of PEDOT:OTf and its NMP-treated counterparts are comprised between 1.55 and 1.84. This smaller value means that their structure is far more ordered and that they stand in the metallic side of the metal-insulator transition. This assertion is confirmed by (1) the crossover noticeable near room temperature with the increasing quantity of NMP in Figure II.17, (2) by the non-null conductivity at low temperature and (3) by the slope of the reduced activation energy as introduced in Chapter 1 and depicted in Figure II.16c. While its slope is negative for PEDOT:PSS proving that it is on the insulator side of the metal insulator transition (Figure I-10),

the slope is mainly positive for PEDOT:OTf and its NMP-treated counterparts. Figure II.17 focuses on these latter ones. The resistivity ratio decreases while increasing the quantity of NMP as shown in Figure II.17a and Table II.2. This means that the more NMP is added, the more the structure is ordered. This trend does however not include PEDOT:OTf without addition of NMP, which could be due to the fact that that material was not synthesized at the same time than the three other ones and that differences can appear from a batch to another.

Table II.2. Resistivity ratio as function of the quantity of NMP in the oxidative solution for the polymerization of PEDOT:OTf.[30]

NMP quantity	0 %	3 %	5 %	7 %
Resistivity ratio ρ_r	1.70	1.84	1.67	1.55

The materials seem slightly better ordered after the addition of NMP, but the energy barriers seem similar when comparing their reduced activation energy in Figure II.18b. Despite their metallic behavior, the crossover indicates at least the occurrence of two competing transport mechanisms.

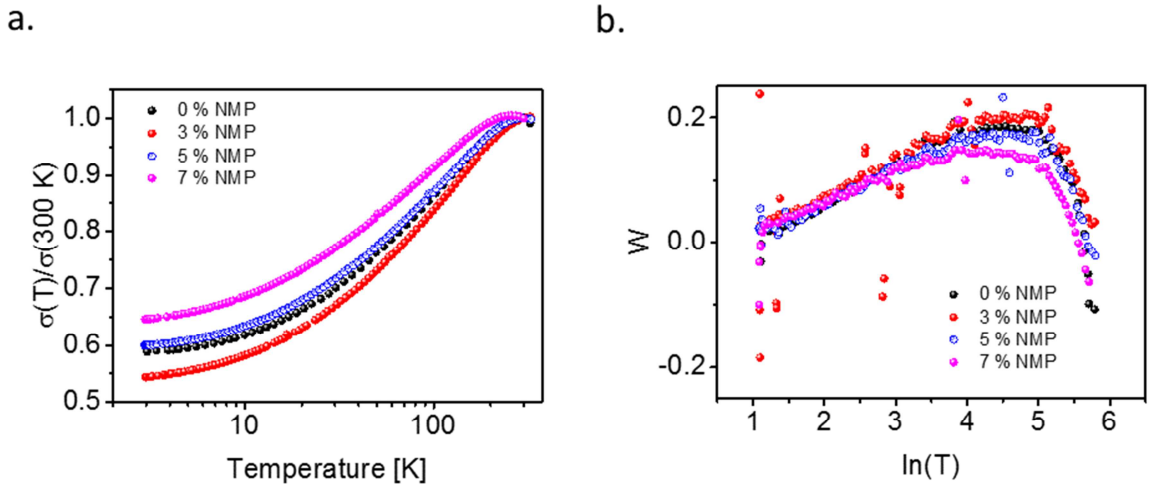

Figure II.17. Electrical conductivity and b) reduced activation energy W of PEDOT:OTf with different amounts of NMP (wt. %). PEDOT:OTf without NMP (at 0 %) was synthesized previously outside the scope of this thesis.[32]

3-5-b. Acid treatment

Figure II.18 presents the transport properties of PEDOT:OTf-NMP (7wt. %) after acid treatment. Here too, a metallic behavior is noteworthy, evidenced by (1) the positive slope of the activation energy, (2) the low resistivity ratio (down to 1.22), (3) a crossover near room temperature introducing a negative slope of the conductivity, (4) the non-null conductivity near 0 K as well as (5) the negative slope of the electrical conductivity near 0 K. This latter one is mainly noticed when the experiments were not lead under vacuum. Indeed, in order to reach temperatures down to 3 K, liquid Helium is used and in order to avoid the presence of water which could lead to ice formation, experiments have to be conducted under vacuum. We however noticed that the pumping lowered the electrical conductivity as also reported by others.[116]

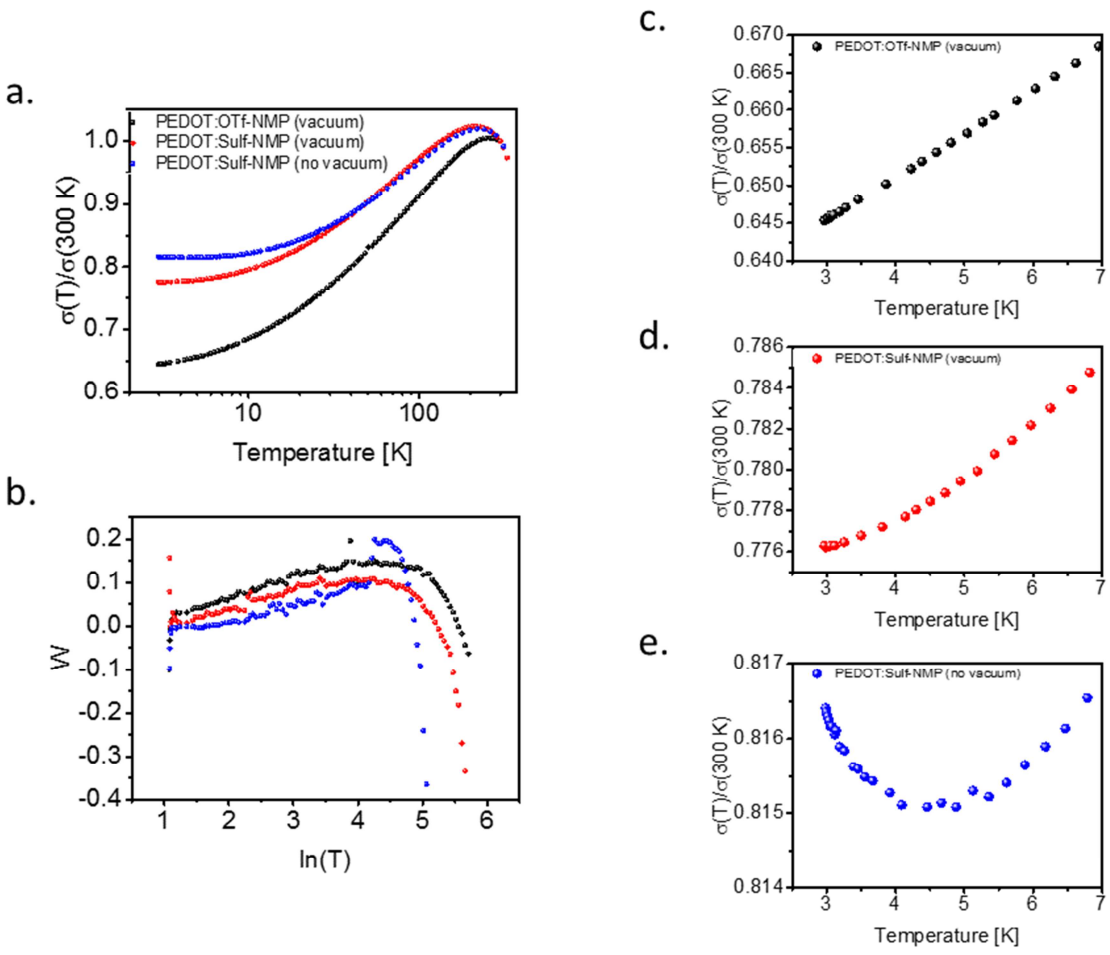

Figure II.18. a) Temperature dependence of conductivity of PEDOT:OTf-NMP before and after acid treatment and b) their reduced activation energy. A magnified image of their conductivity is given for low temperature (c, d and e).

In Figure II.18, PEDOT:OTf-NMP presents a positive slope near 0 K while PEDOT:Sulf-NMP presents either a null slope under pumping, or a negative slope without pumping, signature of a more pronounced metallic transport. The more pronounced metallic behavior after acid treatment could be due to the increase of bipolarons to the detriment of polarons as evidenced by UV-Vis-NIR, which might render the polymer more semi-metallic.[20] We also attribute the difference observed between the samples measured under vacuum and without vacuum to desorption of some counter-anions from the surface of the film when pumping.

3-5-c. Conduction model

In this section, we would like to develop a model in order to better understand the transport properties in PEDOT films. Therefore, PEDOT:OTf, PEDOT:Sulf, PEDOT:OTf-NMP and PEDOT:Sulf-NMP are studied. All experiments were done in the same conditions as explained in Materials & Methods and under vacuum. Only PEDOT:OTf was measured prior to this thesis. Figure II.19 gives the temperature dependence of conductivity as well as the reduced activation energy of these four materials.

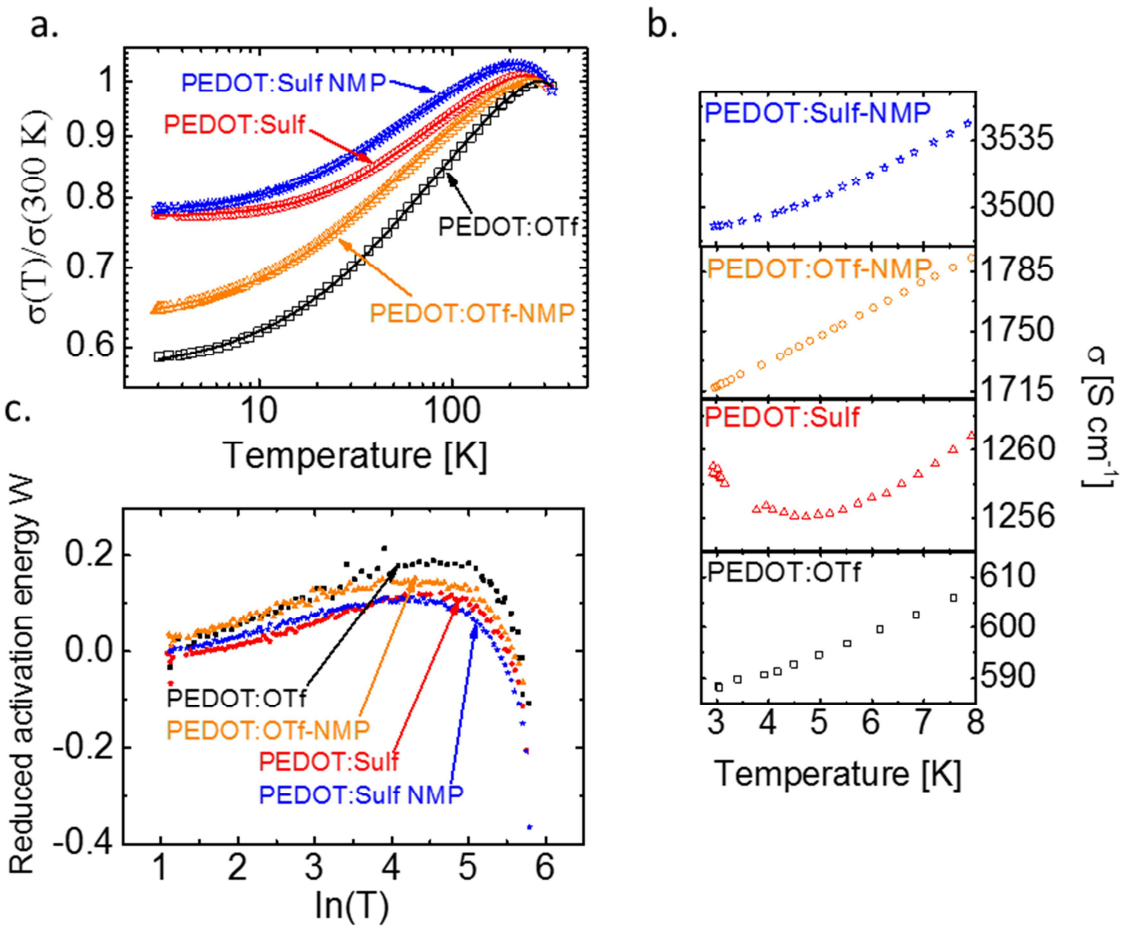

Figure II.19. Transport properties of the PEDOT materials. a) Temperature dependence of electrical conductivity (symbols) and heterogeneous model of conduction (solid lines), b) Low temperature dependence of electrical conductivity and c) Reduced activation energy (W) of PEDOT materials vs ln(T).

Compared to PEDOT:PSS with a highly disordered structure ($\rho_r > 20000$), PEDOT:OTf and its treated counter-parts appear very ordered ($\rho_r = 1.72$, 1.49, 1.54 and 1.28 for PEDOT:OTf, PEDOT:Sulf, PEDOT:OTf-NMP and PEDOT:Sulf-NMP repectively). For all four samples, non-zero conductivity for T → 0 K suggests the presence of charges at the Fermi level allowing conduction without thermal activation, and hence sweeps out the hypothesis of VRH conduction. The samples appear to be in the metallic side of the metal-insulator transition as further proved by the positive slope of the reduced activation energy $W = \frac{d(\ln(\sigma))}{d(\ln(T))}$ plotted in Figure II.19.[30,117] Interestingly, PEDOT:Sulf depicts a metallic behavior with a positive temperature coefficient of resistivity for T < 5 K. Such metallic behavior is not present in other

samples at low temperature, although a slight inflection is noticeable in PEDOT:Sulf-NMP around 3 K. All samples show a metallic sign for their temperature dependence of conductivity at room temperature and within a large temperature range (down to 215 K for PEDOT-Sulf-NMP). It is noteworthy that only very few reports of metallic behavior at low and room temperature are present in the literature in polymeric materials (PF_6-doped polypyrroles CSA-doped polyaniline and PEDOT:OTf).[30–32,100]

With the very high conductivity, the metallic behavior observed, the semiconducting behavior (increasing conductivity with temperature) and the crossover temperatures near 0 K and at room temperature suggest several transport mechanisms that compete in the films:

- The metallic behavior, together with the quality of the atomic arrangement in crystalline parts seen in Figure II.12 and Figure II.13 and the interestingly oriented structure conjecture a metallic conduction in the crystallites along the conjugated backbone,[26] supposedly quasi one dimensional (1-D).
- The imperfect crystallinity of our polymers, the still existing disordered regions, the grain-like structure surrounded by disordered regions and the zero-limit of the activation energy at 0 K suggest a tunneling conduction as introduced in Chapter 1 (Sheng model).[20,35,100,118,119]
- The large disordered regions (as shown in HRTEM) images suggest that the tunneling might not always take place between two grains particularly if they are far apart ($>$ 100 nm). The tunneling could also take part between more densely charged parts in the disordered regions and should take place together with a conduction along or between chains aside. Therefore, a disordered metallic conduction could take place in parallel to the tunneling one.

In fine the resistivity of our films can be described as the sum of two components: the resistivity of the crystalline regions (quasi 1-D metallic resistivity, first term in Equation II.2) plus the resistivity of the amorphous regions (a tunneling mechanism, second term in Equation II.2, in parallel with a disordered metal transport model, third term in Equation II.2). This corresponds to the heterogeneous model where highly conductive crystalline regions are connected by less conductive disordered ones.[29] With this model, the resistivity is described by the following equation:

$$\sigma^{-1} = \rho = f_m \rho_m \exp\left(-\frac{T_m}{T}\right) + \left\{\left[f_S \rho_S \exp\left(\frac{T_1}{T+T_0}\right)\right]^{-1} + [f_{dm}\rho_{dm}]^{-1}\right\}^{-1} \quad \text{(II.2)}$$

where f_m, f_S and f_{dm} are form factors corresponding to intrinsic resistivities ρ_m, ρ_S and ρ_{dm}, T_m represents the energy of the phonons that can backscatter the charges;[37] and T_0 and T_1 are the tunneling temperatures dependent on the barrier geometry and energy.[35]

Table II.3. Fitting parameters of the heterogeneous model describing the conduction mechanisms in our PEDOT films*.

Materials	M	Tm [K]	N	T0 [K]	T1 [K]	DM
PEDOT:OTf	15 ± 6	1907 ± 129	1.15 ± 0.09	61 ± 6	76 ± 3	0.32 ± 0.06
PEDOT:OTf-NMP	13 ± 8	1813 ± 197	1.27 ± 0.17	46 ± 5	46 ± 5	0.33 ± 0.10
PEDOT:Sulf	5.97 ± 1.57	1501 ± 84	2.86 ±0.03	14.4 ± 0.7	81 ± 2	0.7700 ± 0.0007
PEDOT:Sulf-NMP	3.79 ± 0.37	1268 ± 33	2.73 ± 0.03	18.3 ± 0.8	60 ± 1	0.752 ± 0.002

*The temperature dependent conductivity curves were fitted with the following equation.

$$\frac{\sigma(T)}{\sigma(300)} = \left\{ M\exp\left(-\frac{T_m}{T}\right) + \left[(N\exp(\frac{T_1}{T+T_0}))^{-1} + DM \right]^{-1} \right\}^{-1}$$

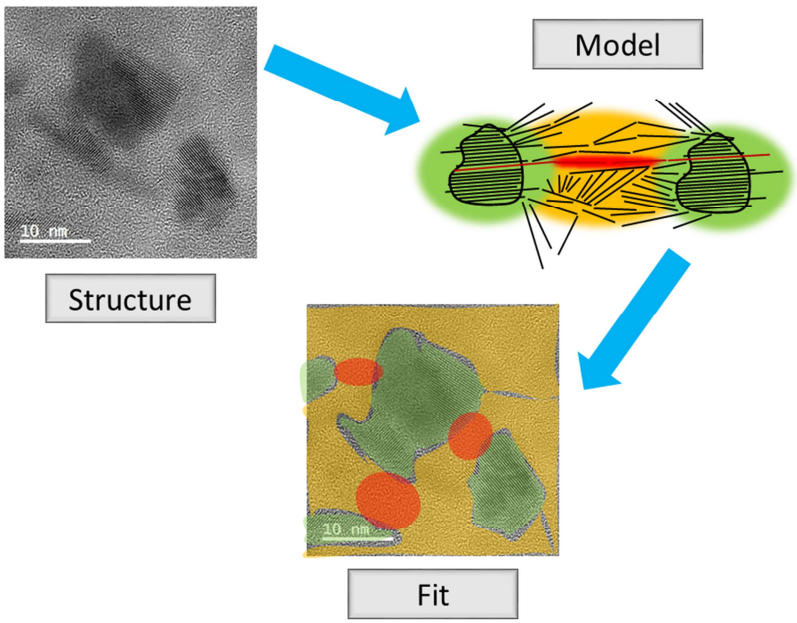

Figure II.20. Illustration of the conduction model.

Equation II.2 was used to fit the temperature dependence of conductivity in Figure II.19 and the fitting parameters are summarized in Table II.3. Figure II.19a shows an excellent agreement between the theory and the experiment, successfully fitting the model to the conductivity within 2 orders of magnitude of temperature (schematized in Figure II.20). The phonons being excited with temperature, the 1-D metallic dependence of conductivity becomes significant at room temperature with low values of T_m. The energies of phonons relative to the metallic conduction in the crystallites are 1907 K, 1813 K, 1501 K and 1268 K for PEDOT:OTf, PEDOT:OTf-NMP, PEDOT:Sulf and PEDOT:Sulf-NMP respectively, hence significantly broadening the metallic behavior from room temperature down to lower temperatures only for the acid treated samples. Table II.4 details different contributions of conductivities as derived from the fitting parameters in Table II.3. The metallicity, defined as the ratio of the 1-D metallic resistance to the total resistance at 300 K,[120] points out that the crystallites are responsible for 2.7 %, 4.0 %, 3.0 % and 5.5 % of the total resistance in PEDOT:OTf, PEDOT:OTf-NMP, PEDOT:Sulf and PEDOT:Sulf-NMP respectively. Taking into account the 300 K conductivity, this leads to high intrinsic conductivity inside the grains up to approximatively 88000 S cm^{-1} for PEDOT:OTf-NMP (see Table II.4). Even if one can wonder the real physical meaning of this value, it is not absurd since single crystals of PEDOT have been reported to have a conductivity up to 8797 S cm^{-1} at only 10 % oxidation level.[91]

Table II.4. Detailed conduction contributions deduced from the fitting parameters. These values are given for room temperature.

Materials	Metallicity [%]	Quasi 1D-metallic [S cm^{-1}]	Amorphous region [S cm^{-1}]		Sheng barrier T_1 [K]
			Sheng-like	Disordered metal	
PEDOT:OTf	2.7	37224	707	319	76
PEDOT:OTf-NMP	4.0	88371	1846	895	46
PEDOT:Sulf	3.0	40473	439	1249	81
PEDOT:Sulf-NMP	5.5	81187	1362	3384	60

Upon co-solvent addition, the quasi 1-D metal contribution increases by 137 % and 100 % for PEDOT:OTf and PEDOT:Sulf respectively, indicative of the strong impact of the co-solvent on the crystallites due to a slower polymerization rate yielding bigger crystallites. The disordered metal contribution is also strongly enhanced as well as the Sheng contribution (originating from the decrease of the Sheng barrier temperature T_1). As a result the total contribution of the amorphous regions increases by 167 % and 181 % respectively.

The acid treatment has a lower impact on the crystallites as confirmed by the slight changes in the quasi 1D-metallic part of the conductivity. The contribution of amorphous regions is raised by 64 % for the PEDOT:OTf and a similar increase is observed for PEDOT:OTf-NMP (73 %), probably because the replacement of triflate ions by hydrogenosulfate ions distort the PEDOT chains and then alter the sizes of the amorphous and crystalline regions.[121] After acid treatment (see Table II.4), the metallic contribution remains in the same order of magnitude, the Sheng contribution decreases in accordance with the previous assumption, while the disordered metal conduction is more than three times higher. The dramatic increase in total conduction with acid treatment originates then from the amorphous regions, meaning that the replacement of counter-anions has mainly taken place in those domains. Such information cannot be deduced from GIWAXS or TEM experiments.

3-5-d. Conclusion

This analysis reveals the influence of the co-solvent addition and acid treatment on both the crystallites and disordered regions in PEDOT films and is illustrated in Figure II.21. Due to the polymerization rate slowdown resulting from the co-solvent addition, longer chains (and possibly conjugation lengths) could have grown both in the crystalline and in the amorphous regions so that bigger grains are obtained as evidenced with GIWAXS. As a result, the total conductivity enhancement is roughly the same both for the crystalline and amorphous domains. After acid treatment, hydrogenosulfate ions replace the original triflate ions, but mainly in the amorphous regions since the too well packed structure in the crystallites does not allow the diffusion of ions. Therefore, the conductivity enhancement is more pronounced on amorphous regions after acid treatment.

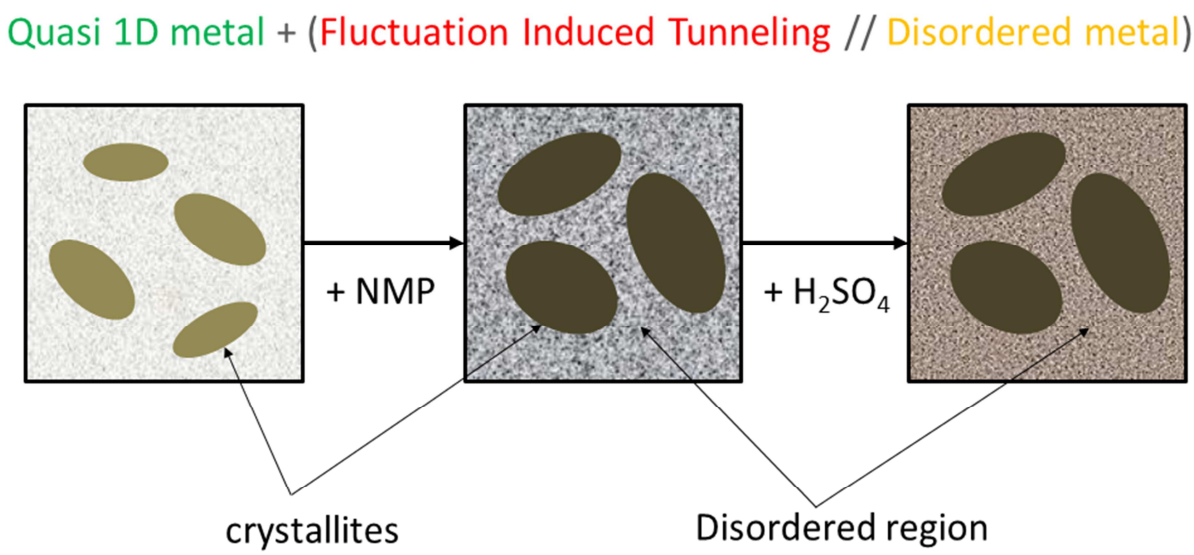

Figure II.21. Illustration of the conductivity enhancement of PEDOT:OTf after co-solvent addition and acid treatment. After the addition of NMP, both the crystallites and the amorphous regions show better electronic transport properties. This is coherent with a slower polymerization reaction that leads to a better structure all along the film. After acid treatment the crystallites are not affected and the transport is enhanced only in the amorphous regions. This is coherent with the replacement of triflate counter-anions mainly in the amorphous regions.

In addition, in these amorphous regions where conductivity is driven by the tunneling and disordered metal models, the co-solvent and the acid have a stronger impact on the disordered metal contribution, hence comforting longer chains or smaller counter-anions along the chains.

Therefore, compared to PEDOT:PSS with a highly disordered structure and a VRH conduction model, PEDOT:OTf and its treated counterparts, thanks to the better ordered structure and the smaller counter-anions, depict a behavior leaving the Anderson localization and shifting more towards the metallic side of the metal insulator transition (Figure I.10).

4. Conclusion

We managed to synthesize PEDOT materials stabilized with small counter-anions triflate. Because of their dimensions, conductivities up to 1200 S cm^{-1}, which are better

than that of the commercial PEDOT:PSS, are obtained. Furthermore, through an adequate structure engineering with coordinating solvents and dopant engineering with acid treatment, the conductivity was risen up to 5400 S cm^{-1}, currently representing the state of the art for PEDOT films. Through different characterization techniques, the mechanisms behind such dramatic enhancement was unraveled.

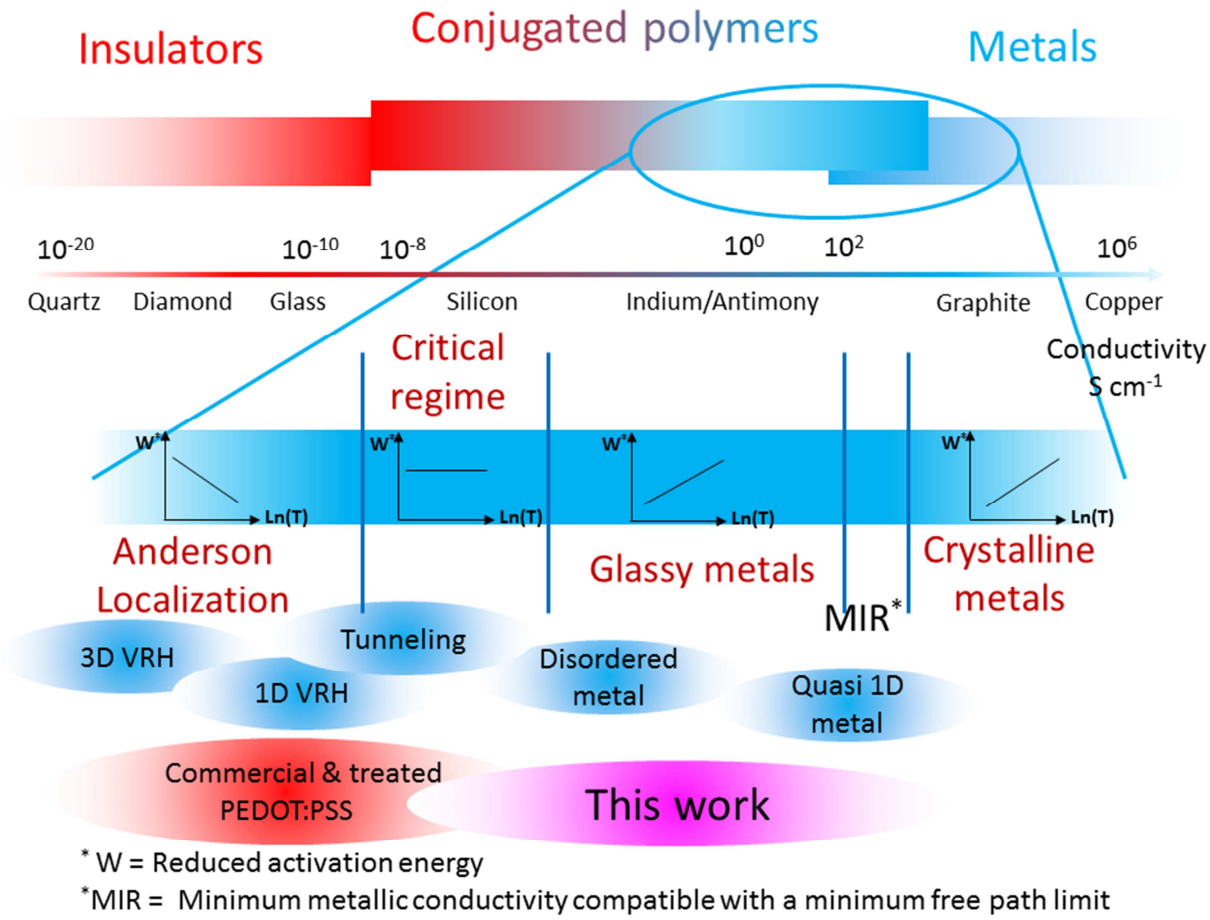

Figure II.22. Illustration of our materials among metals, conjugated polymers and insulators.

The addition of coordinating solvents such as NMP, DMF or DMSO in the oxidative solution leads to longer polymerization reactions. We believe that the oxidant is complexed and the number of nucleation sites on the substrate is reduced. As a result, longer and better packed chains are grown. The structure is semi-crystalline, with bigger crystallites, and the transport mechanisms are enhanced both in the crystallites and in the less well ordered domains.

Upon sulfuric acid treatment, hydrogeno-sulfonate ions from the acid interact preferentially with the amorphous regions and replace thereby the original triflate ions. As a result, the transport mechanisms are mainly improved in the disordered regions. Moreover, bipolarons are favored in front of polarons which lead to a more metallic polymer.

We also succeeded in explaining the electronic transport mechanisms in our polymer films with a heterogeneous transport model, a model in which metallic conduction along the chains and inside the crystallites compete with a tunneling transport typical of semiconducting materials with localized highly conductive domains. Upon each treatment, the proportion of the metallic conductivity increases to the detriment of the semiconducting one. The highest transport takes place in the crystallites (up to 80000 S cm^{-1}) but that contribution is limited by the amorphous regions (they participate only up to 5 % of the total conduction mechanism). With the increasing degree of order that appears after each treatment, the organized structure and the smaller counter-anions that supposedly lead to better mobility, our materials leave the Anderson localization in Figure II.22 and move towards metallic systems. This tendency was also recently proved by Farka et al., who synthesized PEDOT:Sulf and showed that it stands at the Mott-Ioffe-Regel limit with electronic transport mechanisms not far from that of crystalline metals (Figure II.22).[33] A heterogeneous conduction model takes place, whereby metallic and semi-conducting transport mechanisms compete.

The structure and dopant engineering conducted in this study lead to a total conductivity enhancement from 1200 to 5400 S cm^{-1}. With such metal-like conductivity and behavior, PEDOT:OTf-NMP and PEDOT:Sulf-NMP are highly suitable for next generation transparent electrode applications

Chapter 3
Electrical to thermal energy conversion in PEDOT based conducting polymers: application in flexible transparent heaters

From here onwards, since PEDOT:OTf and PEDOT:OTf-NMP are the same materials, and similarly for PEDOT:Sulf and PEDOT:Sulf-NMP, the terminology “NMP” will not be added anymore. All following PEDOT:OTf and PEDOT:Sulf are synthesized with a certain amount of NMP which will be introduced beforehand.

The work presented in this chapter has been published in the journal ACS Applied Materials & Interfaces.[11]

1. Introduction

This chapter will deal with some thermoelectric properties of the PEDOT materials that have been developed in Chapter 2 as well as some PEDOT materials available commercially, especially the conversion of electrical energy to thermal one via Joule heating and the thermal conduction mechanisms within the conducting films.

Thermoelectricity refers to any transport of heat combined with electrical energy. When the system recovers its initial state after the electrical or thermal stress without energy loss or entropy creation, the system is thermodynamically reversible; irreversible otherwise. In that respect, Joule heating and thermal conduction phenomena are thermodynamically irreversible thermoelectric processes. Given the highly conductive materials that we reported in Chapter 2, the study of such mechanisms is mainly interesting in the field of heaters.

After a brief overview of Joule heating observations in PEDOT materials, we will study the thermal conduction mechanisms that take place in our PEDOT materials when an electric current flows through them and confront our experimental observations to a theoretical model that will allow us to define the phenomena that occur during the thermal conduction.

Subsequently, a novel application for PEDOT using their heating properties will be introduced, namely transparent heaters.

2. Strategy

Joule heating is a physical process by which heat is produced when an electric current flows through a resistive material. In the literature, the resistive Joule heating of

PEDOT is mainly sought for electroactive, thermochromic and fabric heaters applications.[122–124] As a matter of fact, PEDOT:PSS was shown to undergo contraction upon application of a voltage bias. That contraction is due to desorption of water in the film after Joule heating. This lead mainly to electroactive applications in which PEDOT is used as an actuator that contracts or expands when subjected to a bias and in a relatively humid atmosphere.[13,122,123,125,126] Also, despite its electrochromic properties, it is easier to use the resistive Joule heating of PEDOT to cause the color changing of a thermochromic material since an electrochromic device requires a whole system to be fabricated (with at least an electrode and an electrolyte).[127] Another field that is arousing great interest for the conversion of electrical energy to thermal energy using PEDOT and conductive materials in general is that of wearable fabric heaters.[123,124]

In these heating applications where low voltage, high response time, flexibility, stability and stretchability are needed, a clear understanding of the mechanisms behind the electrical to energy conversion in these PEDOT heaters is however lacking in the literature.

We here then propose to study the thermal response of PEDOT upon an application of a bias. Subsequently, a novel application for PEDOT as heater will be proposed.

3. Joule heating and thermal conduction in PEDOT films

3-1. Materials

This study was carried out with four different polymers based on PEDOT. Commercial PEDOT:PSS (Clevios PH1000) was used as deposited, or after being treated with ethylene glycol, which is known to increase carrier density and the carrier mobility (this material was named PEDOT:PSS-EG).[88,128] Two other PEDOT materials presented in Chapter 2, namely PEDOT:OTf and PEDOT:Sulf, with unprecedented conductivities were also used for this study (see Table III.1).[10]

Table III.1. Thickness, sheet resistance and conductivity of the studied materials. Two to three layers were deposited in order to achieve such properties.

Materials	PEDOT:PSS	PEDOT:PSS-EG	PEDOT:OTf	PEDOT:Sulf
Thickness [nm]	156	108	41	44
Sheet resistance [Ω sq^{-1}]	361	68	81	57
Conductivity [S cm^{-1}]	178	1361	3011	3987

The chemical structure of these materials can be found in Figure III.1.The solvent NMP was added at 7.75 wt. % in the oxidative solution as reported in Materials & methods. The materials were deposited by spin coating the solutions either on a Planibel glass or on PET substrates and the sample sizes were 2.5 cm x 2.5 cm and 10 cm x 10 cm as shown in Figure III.2. A detailed explanation of the synthesis methods is given in Materials & methods. In the following, the resistance and/or the sheet resistance of the materials are given because this physical property is more adequate than the conductivity for Joule power calculations.

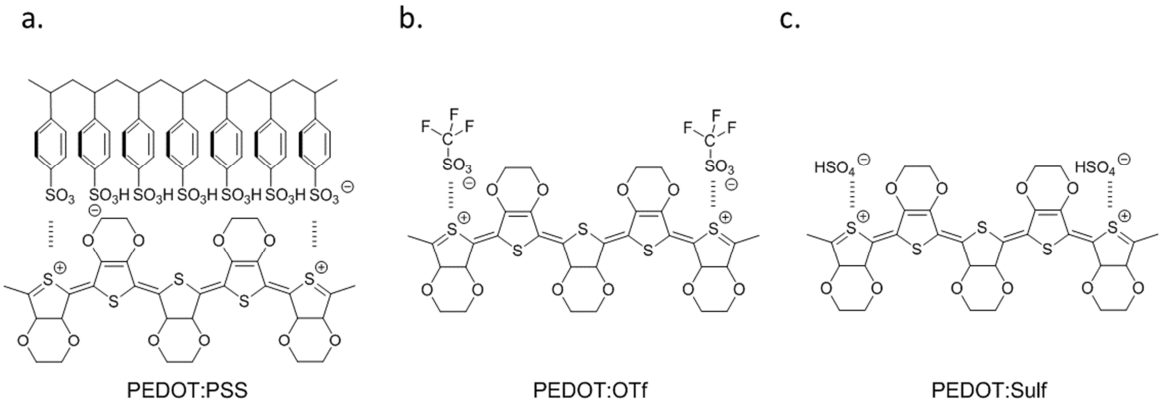

Figure III.1. The studied materials: a) PEDOT:PSS or PEDOT:PSS-EG. b) PEDOT:OTf. c) PEDOT:Sulf.

As reported in Table III.1, the materials have different sheet resistances and thicknesses. In order to be able to compare their heating properties, the materials are compared according to their transparency in the visible range, so that electrical properties given in this chapter correspond to materials whose transparency is around 90 % at 550 nm (this wavelength is widely acknowledged for transparency measurements as it corresponds to the maximum sensitivity of human eye).[129] When

dealing with the couple sheet resistance/transparence, a figure of merit (FOM) is a good indicator that helps comparing materials. A FOM is basically a relationship between the transmittance T and the sheet resistance Rs that is controlled by the conductivity ratio, σ_{DC}/σ_{OP} where σ_{DC} is the electrical conductivity and σ_{OP} the optical conductivity. A FOM is therefore a good indicator to rank different materials.[130,131] A FOM has been defined by De et al. as given in Equation III.1, and it gives a good ranking for transparent conductive materials in general.[130]

$$FOM = \frac{\sigma_{DC}}{\sigma_{OP}} = \frac{Z_0}{2.R_S(\frac{1}{\sqrt{T}}-1)} \quad \text{(III.1)}$$

with Z_0 = impedance of free space = 377 Ω, T the transmittance, Rs the sheet resistance.

3-2. Experimental observation of the heating performances

Figure III.2. Picture of PEDOT:Sulf deposited on (a) a 2.5 cm x 2.5 cm glass substrate with silver paints for contacts, (b) a 10 cm x 10 cm glass substrate and (c) a 10 cm x10 cm flexible PET substrate.

Small strips of silver ink were deposited on the opposing edges of the materials in order to ensure a better contact between the films and the external circuit as presented in Figure III.2a,b. In order to evaluate the heating properties of these PEDOT materials, voltages from 4 to 12 V were applied on the four films. The temperature elevation, as recorded with a K-type thermocouple affixed under the substrate for all four materials, is displayed in Figure III.3. The main electrical and heating properties are summarized in Table III.2. PEDOT:PSS, whose resistance is the highest, shows the poorest temperature increase (Figure III.3b). At 10 V bias, PEDOT:OTf and PEDOT:PSS-EG have performances twice higher than PEDOT:PSS (Figure III.3a,d), reaching 88 °C and

94 °C respectively. PEDOT:Sulf shows even better heating properties reaching 120 °C at 10 V bias, and 138 °C at 12 V bias.

Though the possibility to heat at temperatures above 200°C is demonstrated (Figure III.4 hereinafter), we focused the study in a temperature range below 100°C, which is more compatible with the thermal stability of organic materials.

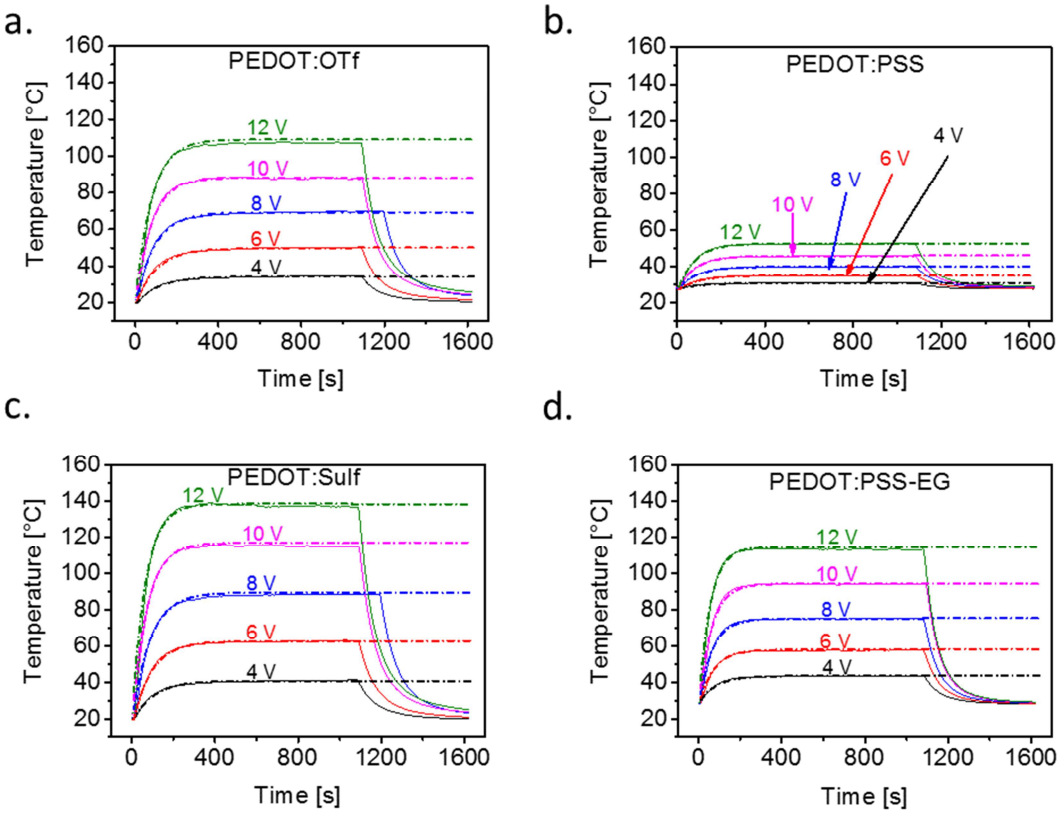

Figure III.3. Heating performances of PEDOT materials. Temperature elevation of PEDOT:OTf (a), PEDOT:PSS (b), PEDOT:Sulf (c) and PEDOT:PSS-EG (d) deposited by spin-coating on glass substrates. Voltages from 4 to 12 V were applied and shut off after ca. 1000 – 1200 s. Curves were fitted with the model from Equation III.3. Solid lines represent the experimental curves and dash lines the calculated fits.

From the curves presented in Figure III.3, we can correlate the trend of the heating ability to the electrical resistances. As expected, the temperature elevation follows the same trend as the resistive Joule heating, specifically an increase when the resistance decreases. But in order to compare the different materials, it is better to correlate the heating ability with the figure FOM as defined by De et al. and given in Equation III.1 and Table III.2.[130] It appears in Table III.2 that PEDOT:PSS-EG and PEDOT:Sulf have equivalent FOM, and hence optoelectronic properties. In other words if equivalent

transmittances are achieved, equivalent sheet resistances will also be achieved and the same thermal responses would likely be expected as well. The better thermal responses are however obtained with PEDOT:Sulf whose resistance is the lowest. The FOM still remains the most adequate tool to classify them and despite their different conductivities, PEDOT:Sulf and PEDOT:PSS-EG should have equivalent heating properties.

Table III.2. Optical, electrical and heating properties of the studied PEDOT based materials.

Materials	Sheet resistance [Ω sq^{-1}]	Total transmission @ 550 nm [%]	Haze [%]	FOM	Temperature at 10 V [°C]	Heating rate at 10 V [°C s^{-1}]
PEDOT:PSS	361	90.1	0.1	10	45	0.2
PEDOT:PSS-EG	68	89.6	0.7	49	94	1.0
PEDOT:OTf	81	88.4	0.5	37	88	0.9
PEDOT:Sulf	57	87.8	0.7	50	114	1.2

3-3. Modelling the temperature elevation

Being able to theoretically anticipate the temperature elevation in these PEDOT films would allow to better understand the thermal properties of the material and to finely tune the properties' choice at an applied voltage. This would be helpful for optimizing the properties of PEDOT in view of potential heater applications. Sorel et al. developed a relevant and comprehensive model that describes the temperature dependence of the system {material + substrate} with their physical characteristics.[131] That model was given for silver nanowires networks but can be extended to our polymer films as it is an energy balance between the dissipated power by Joule heating and the power losses through conduction, convection and radiation. When applying a voltage U to a film, a current I flows through it and the power dissipated by Joule heating is given by $P_{Joule} = RI^2 = \frac{U^2}{R}$, assuming that the sample does not alter with time (which is the case when looking at the stable thermal responses in Figure III.3). That heat is dissipated *via* conduction, hence raising the temperature of both the material and its substrate, *via* convection and *via* radiation. By neglecting the losses through the electrodes,

thermocouples and other wires in the circuits and assuming a uniform temperature all over the sample (which is true for small areas as exposed later in Figure III.12), the energy balance is given by Equation III.2.

$$\frac{U^2}{R} = (m_1C_1 + m_2C_2)\frac{dT(t)}{dt} + A(h_1 + h_2)(T(t) - T_0) + \sigma A(\varepsilon_1 + \varepsilon_2).(T(t)^4 - {T_0}^4) \quad \text{(III.2)}$$

The indexes 1 and 2 refer to the PEDOT material and the substrate respectively. C_1 and C_2 are the specific heat capacities, m_1 and m_2 the masses, h_1 and h_2 the convective heat transfer coefficients and ε_1 and ε_2 the emissivities from both sides of the studied system. σ is the Stefan-Boltzmann constant and A the area of the film. T(t) is the instantaneous temperature and T_0 the ambient temperature. Since $m_1 \ll m_2$, the conduction loss term can be reduced, hence giving $mC\frac{dT(t)}{dt}$. Moreover, as such equation does not have any simple analytical solution, it is simplified by hypothesizing small temperature variations and by applying a Taylor expansion that gives $T(t)^4 - {T_0}^4 \approx 4T_0^3(T(t) - T_0)$. The following solution can be demonstrated:

$$T(t) = T_0 + \frac{1}{\alpha}.\frac{U^2}{RA}.\left(1 - e^{-\frac{\alpha A}{mc}t}\right) \quad \text{(III.3)}$$

Here, $\alpha = (h_1 + h_2) + 4T_0^3(\varepsilon_1 + \varepsilon_2)$ and stands for the heat transfer coefficient related to convection and radiation losses. It is also defined as the thermal conductance.[132]

Equation III.3 was used to fit the temperature elevation curves in Figure III.3. The dashed lines correspond to the calculated fits and are superposed to experimental data. Thus it appears that the model reflects quite accurately the heating capability of the PEDOT-based materials. The rare deviations observed, particularly above 80 °C, can be attributed to the hypotheses of the model.

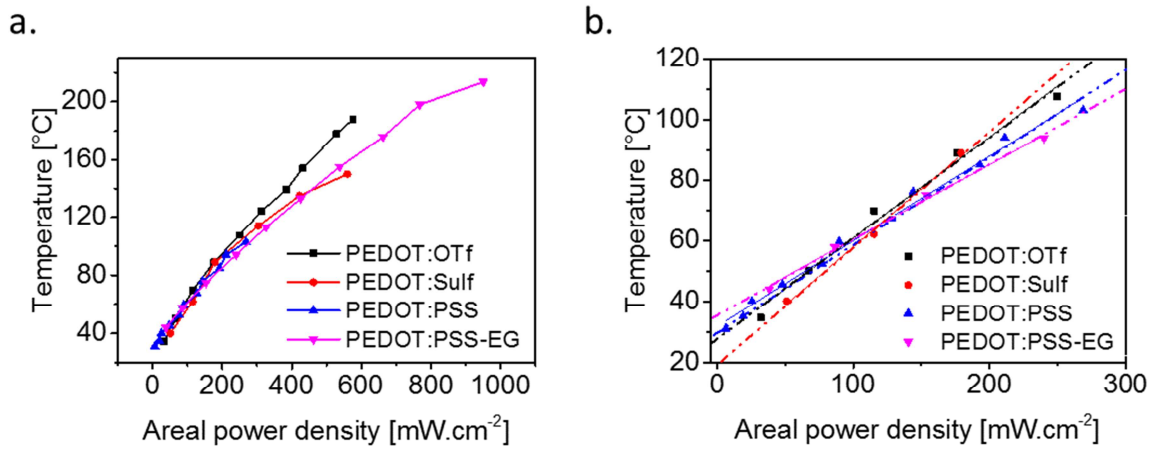

Figure III.4. Areal power density of PEDOT materials on the whole range of reached temperature (a) and on the linear dependency range (below 150 °C) (b). The linear dependency above 150 °C disappears, probably due to polymer degradation.

At steady state temperature, the temperature is given in Equation III.4 and depends solely on the areal power density $\frac{U^2}{RA}$ and the heat transfer constant α.

$$T_{max} = T_0 + \frac{1}{\alpha}.\frac{U^2}{RA} \quad \text{(III.4)}$$

That linear dependency is shown in Figure III.4. The proportionality coefficient $1/\alpha$ is the thermal resistance and is defined as the resistance of the material against the flow of heat outside the system as it is related to the convective and radiative losses. It is found to be greater for PEDOT:Sulf, followed by PEDOT:OTf, PEDOT:PSS and PEDOT:PSS-EG. In comparison to electrical resistance, one can easily understand that best heaters should depict high thermal resistance in order to reduce losses. The thermal resistance is found to be 380, 330, 280 and 250 K cm² W^{-1} for PEDOT:Sulf, PEDOT:OTf, PEDOT:PSS and PEDOT:PSS-EG. These values are comparable to those reported for silver nanowire based film heaters.[131,133,134] Since the studied system is only constituted of PEDOT and the substrate, and since the substrates are identical for all four PEDOT materials, the differences noticed in the thermal resistances may be inherent to the materials themselves. Losses as maximized for PEDOT:PSS-EG and minimized for PEDOT:Sulf. The origin of such differences is still unknown but hypotheses comprise materials features such as their thickness or their composition.

In the linear dependency region in Figure III.4, areal power densities up to 240 mW cm^{-2} are reached for PEDOT:PSS-EG under 10 V bias. This power density can

be further increased up to near 1000 mW cm^{-2}, i.e. 10 000 W m^{-2}, when 22 V are applied, the steady state temperature being then 214 °C (Figure III.4a). Even though high steady state temperature (> 200 °C) and very high areal power density can be achieved, these conditions are not recommended because of the potential degradation of the organic polymer.

As the steady state temperature depends on the areal power density, moving to large areas substrates will inevitably induce a drop of heating performances unless the total resistance of the PEDOT material is modulated, geometrically for instance, since the dissipated power depends on the electrical resistance and not the sheet resistance. Indeed, Figure III.5 gives the temperature responses of PEDOT:Sulf deposited on a 10 cm x 10 cm glass substrate, to be compared with Figure III.3. The resistance is measured to be 57 Ω for the small area material and 68 Ω for the large one. The area being 16 times larger, we expect from Equation III.4 that a voltage 3 to 4 times higher should be applied in order to reach the same steady state temperature (supposing the losses being approximately the same). That is what is achieved experimentally, when 20 V is needed for a 10 cm x 10 cm film to reach 70 °C, while only around 7 V were needed for the small size material (2.5 cm x 2.5 cm).

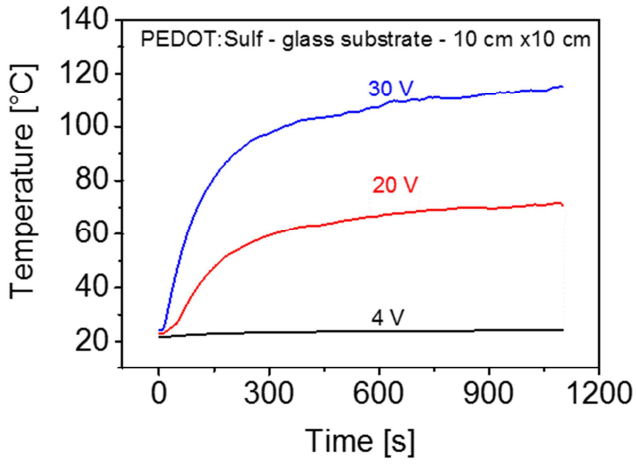

Figure III.5. Temperature elevation of PEDOT:Sulf deposited on a 10 cm x 10 cm (Rs = 62.6 Ω sq-1, $T_{550\ nm}$ = 89.0 %) glass substrate when different voltages are applied.

We showed, both experimentally and theoretically, that the resistance and the area are both key features that achieve a good steady state temperature. The properties making

a good heater are however not restricted to those characteristics and heaters should in addition have a fair response time for practical applications, high thermal stability and a good resistance to environmental stresses.

3-4. Heating rate

Equation III.3 was derived in order to evaluate the heating rate, so that the material and voltage dependence of the heating rate can be inferred from Equation III.5:

$$\frac{dT(t)}{dt} = \frac{U^2}{RmC} e^{-\frac{\alpha A}{mC}t} \qquad \text{(III.5)}$$

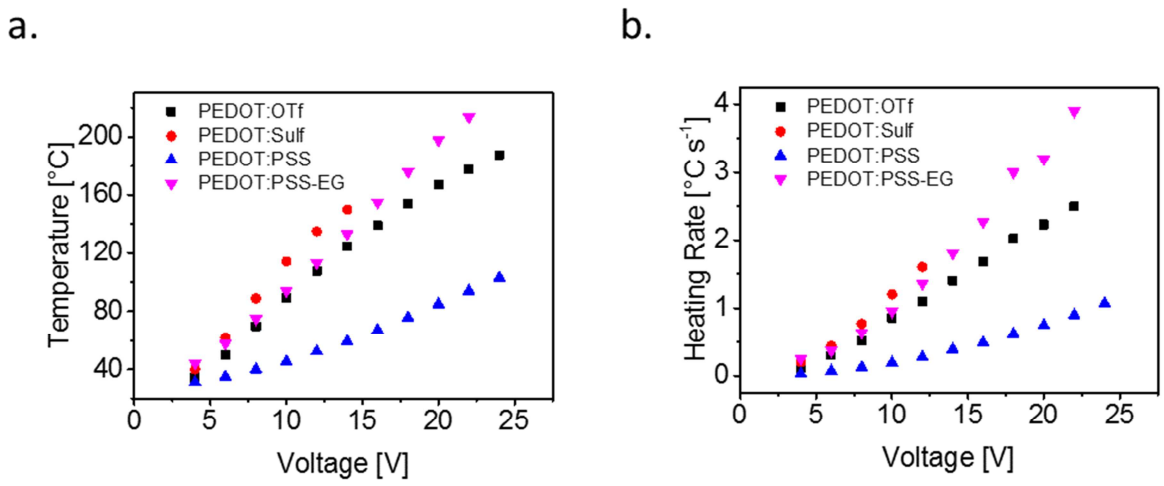

Figure III.6. Steady state temperature and maximum heating rate as function of the applied voltage for the four PEDOT based materials studied.

Figure III.6 gives the steady state temperatures and the maximum heating rates over the whole range of applied voltage while Table III.2 gives the steady state temperatures and the maximum heating rates when 10 V are applied on our all-polymeric film heaters. At such bias the heating rate ranges from 0.2 °C s^{-1} for PEDOT:PSS to 1.2 °C s^{-1} for PEDOT:Sulf. This parameter is material dependent and temperature dependent as can be seen in Figure III.6 and it can be as high as 4 °C s^{-1} for PEDOT:PSS-EG when 22 V are applied. These values remain slightly lower than those found in the literature for heating fabrics using PEDOT. Heating rates of PEDOT heaters made of fibers or microfilms for textiles are generally from 1 to 6 °C s^{-1} for low voltage bias (< 12 V) and the response time is usually lower than 100 s.[123,124] For example, Yeon et al. reported a steady state temperature of 99.6 °C upon 12 V, which

was reached within 60 s.[124] Their material, PEDOT:PSS, was loaded in a cotton fabric (thus was not used as a thin film), with a sheet resistance of 24 Ω sq^{-1}. Ours being far thinner, their properties should be compared to those of transparent heaters such as carbon nanotubes or silver nanowires. Heating rates for transparent heaters based on graphene, CNTs or metallic nanowires are typically in the range 0.1 to 2.0 °C s^{-1} for low voltage bias (< 12 V), hence comparable to our materials.[135–137]

At such heating rates, the steady state temperatures are reached after less than *ca.* 400 s for all materials, which can be observed in Figure III.3. The response time of heaters can be measured using the 99 % response time ($t_{99\,\%}$) which is the time needed to reach 99 % of the steady state temperature. It is given by $t_{99\,\%} = 2\frac{mC}{\alpha A}\ln 10$, deduced from Equation III.3 which is theoretically between 250 and 385 s for all for materials, given the thermal resistance found previously and the mass and specific capacity of the glass substrate. This is consistent with observations in Figure III.3. This concordance between the experiments and the theory confirms the relevance of the model and sheds some light on the parameters that could improve the response time of PEDOT for heating applications.

In other words, given the low thickness of PEDOT films, the maximum value of the rate depends solely on the power (thus the applied voltage and the material's resistance), the substrate's weight and its specific heat capacity. Therefore, the time response is mainly function of the substrate's properties (mass, area and specific heat capacity). Thus, heavier, larger or less thermally conductive substrates will induce a longer response time. For that reason, compared to the 1 mm thick glass substrate, a 125 µm PET (polyethylene terephthalate) substrate will show faster thermal response times (as low as 140 s, see Figure III.7 and Table III. 3). It is interesting to note that depositing PEDOT on thin PET substrate (125 µm) not only increases the response time as expected, but also leads to a flexible heating material.

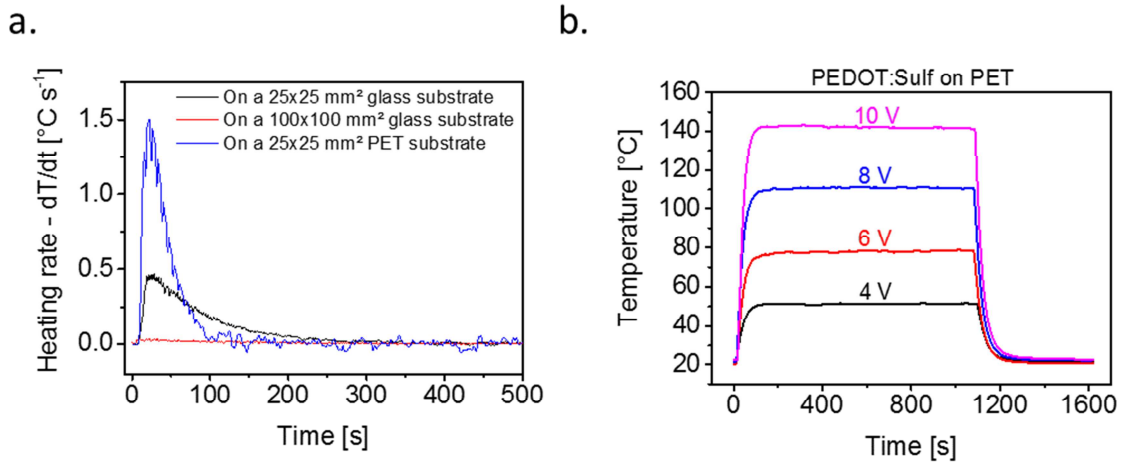

Figure III.7. a) Comparison of heating rates of PEDOT:Sulf. b) Temperature elevation of PEDOT:Sulf on a 2.5 cm x 2.5 cm PET substrate ($Rs = 40.0\ \Omega\ sq^{-1}$, $T_{550\ nm} = 86.5\ \%$).

The response time can further be improved by increasing the heating rate. Apart from being function of the surface characteristics (mass and specific heat capacity), this latter is also dependent on the input power as inferred by Equation III.5. Therefore, the time response can be increased by applying a high voltage in the first seconds before reducing the voltage to reach the required temperature. For example, in Figure III.8, 15 V were applied in the first 20 s before reducing the voltage to 6 V. The target temperature 52 °C is reached in less than 50 s. On the other hand, the 50 °C setpoint temperature was reached within 300 s by applying 5 V. Hence, by modulating the input power, the time response can be drastically improved.

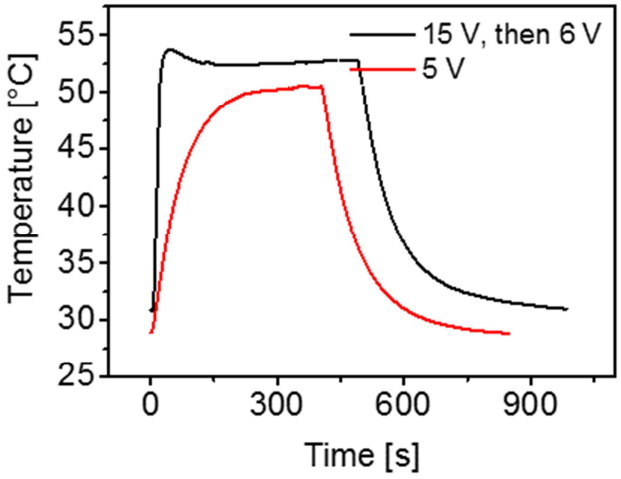

Figure III.8. Improved response time via input power adjustment. The experiment was done on PEDOT:PSS-EG based heaters, deposited on 2.5 cm x 2.5 cm glass substrates.

3-5. Stability

For practical applications, more than the physical characteristics that can be engineered and optimized, stability is a key issue to be dealt with. Stability through cycling (Figure III.9) and the ageing during 200 h (Figure III.10) have been investigated.

Heating and cooling cycles on PEDOT heaters have been performed. The results are presented in Figure III.9. The active materials were deposited on 2.5 cm x 2.5 cm glass substrates and the required voltages to reach a 50 °C steady state temperature were applied and shut down every 400 s. No significant changes were noticed and the temperature remained stable after 20 cycles for each PEDOT based material.

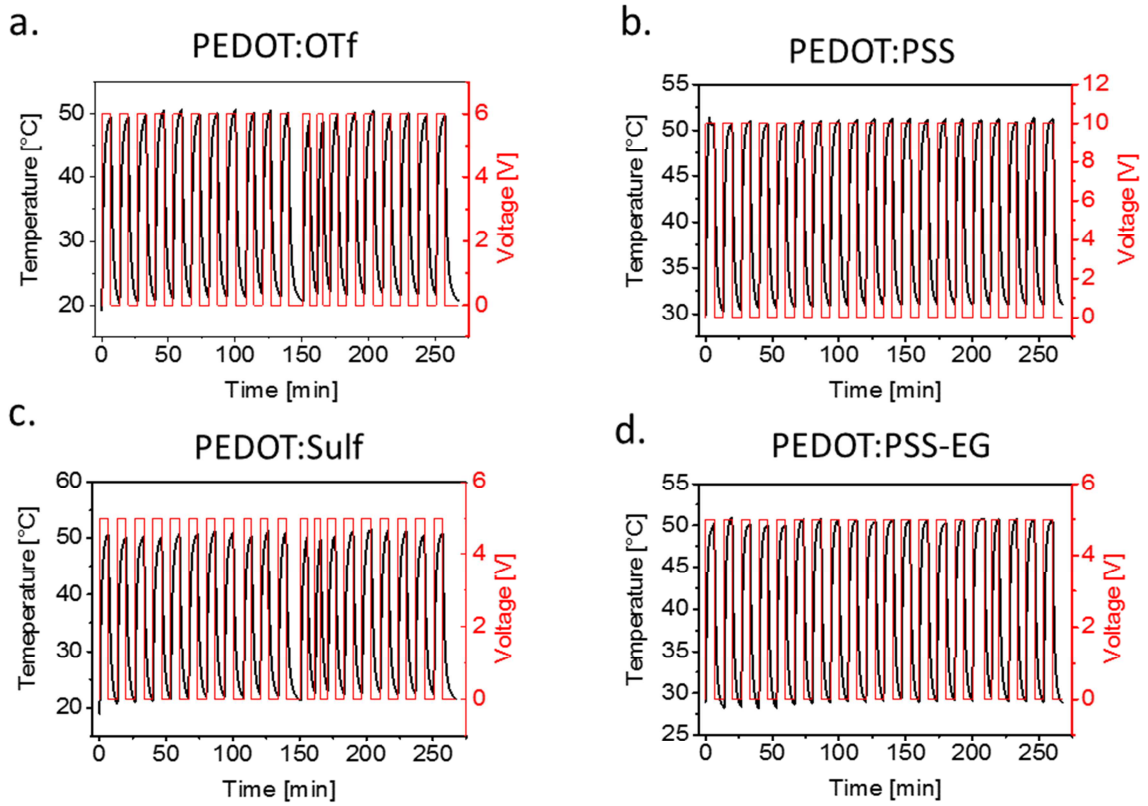

Figure III.9. Stability while cycling of a) PEDOT:OTf (Rs = 72.8 Ω sq^{-1}, $T_{550\ nm}$ = 87.4 %), b) PEDOT:PSS (Rs = 315 Ω sq^{-1}, $T_{550\ nm}$ = 89.4 %), c) PEDOT:Sulf (Rs = 49.2 Ω sq^{-1}, $T_{550\ nm}$ = 88.6 %) and d)PEDOT:PSS-EG (Rs = 67.5 Ω sq^{-1}, $T_{550\ nm}$ = 90.1 %).

PEDOT:PSS-EG and PEDOT:Sulf, which are the materials exhibiting the best heating properties, were also subjected to a constant bias for 200 h (i.e. continuously for more than 8 days), at 22 °C and under 30 % relative humidity, targeting a 50 °C steady state temperature. The results are given in Figure III.10. The variations observed in Figure III.10a are due to the day/night and seasonal temperature variations. Therefore, the room temperature (Figure III.10a) was subtracted to the samples' temperature (Figure III.10b,c) so that the only influence of the Joule heating is displayed. It was observed that under constant bias stress, PEDOT:PSS-EG heating capability decreases from 63 °C to 54 °C (-15 %) while PEDOT:Sulf's decreases from 59 °C to 44 °C (-25%).

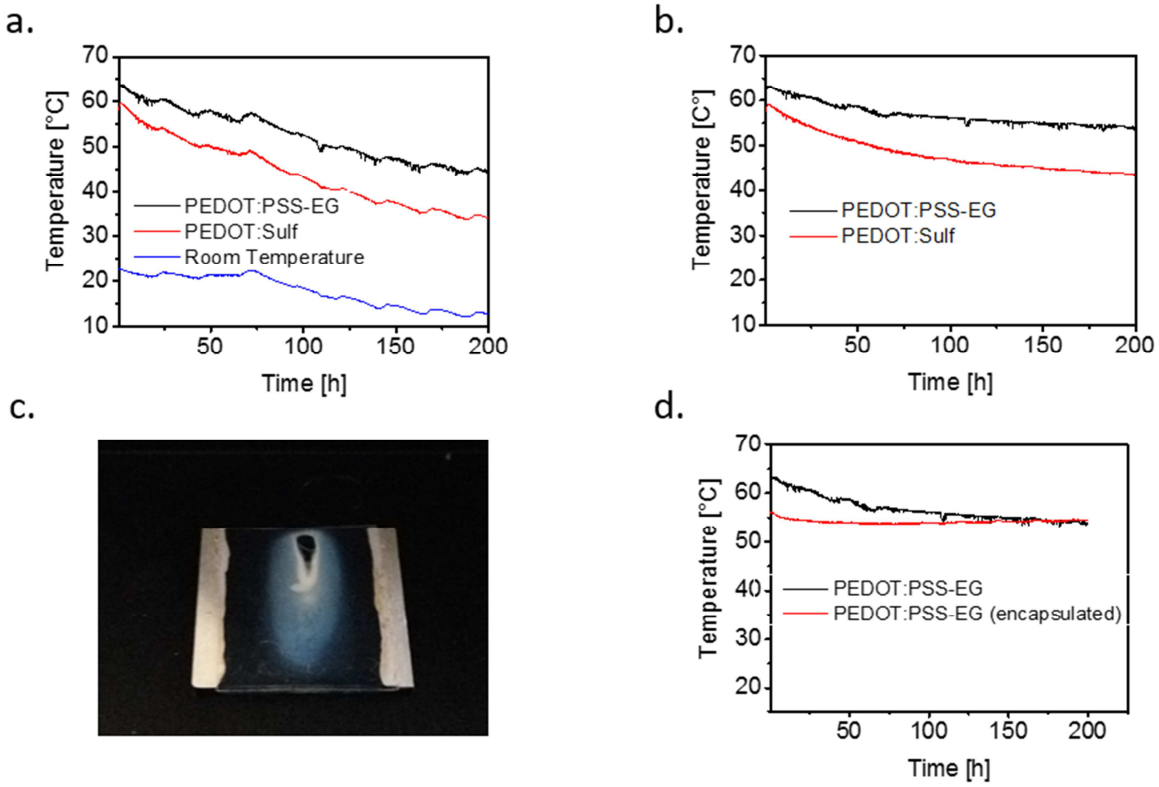

Figure III.10. 200 h ageing of PEDOT:PSS-EG and PEDOT:Sulf when 50 °C are targeted. a) Ageing of PEDOT:PSS-EG (Rs = 53.7 Ω sq^{-1}, $T_{550\ nm}$ = 87.5 %) and PEDOT:Sulf (Rs = 53.5 Ω sq^{-1}, $T_{550\ nm}$ = 87.5 %) as well as the room temperature fluctuations during the measurement. b) Ageing of PEDOT:PSS-EG and PEDOT:Sulf after correction taking into account the fluctuations of the experimental room's temperature. c) Encapsulation of PEDOT:Sulf showing the incompatibility of this film barrier. d) Ageing of PEDOT:PSS-EG after encapsulation with a film barrier.

The reasons for this moderate drop have not been clearly established so far, but more than temperature instability, the environment could also play a significant role as PEDOT materials are known to be moisture-sensitive.[80] Consequently we decided to encapsulate the heater with a film barrier, whose WVTR (water vapor transmission rate) is given at 5.10^{-5} g m^{-2} d^{-1} at 40 °C and 90 % RH, thanks to an optically clear adhesive (OCA).[138] In the case of PEDOT:Sulf, a destructive chemical reaction occurred between the film and the OCA (Figure III.10c), probably due to the acidity of the material, so that such encapsulation is not preferred and other ones should be investigated. In the case of PEDOT:PSS-EG, the encapsulation resulted in a very efficient stabilization of the functional system (Figure III.10d), less than 1 °C variation being observed after 200h.

3-6. Flexibility

In order to demonstrate the flexibility of polymeric heater, we performed 500 bending cycles at approximately 9 mm bending radius on a 2.5 cm x 2.5 cm PEDOT:PSS-EG based heater. PEDOT:Sulf also could be deposited on flexible substrate but since the sulfuric acid treatment could be detrimental to the PET substrate, the flexibility of this material was not investigated but was supposed to be similar to that of PEDOT:PSS-EG.

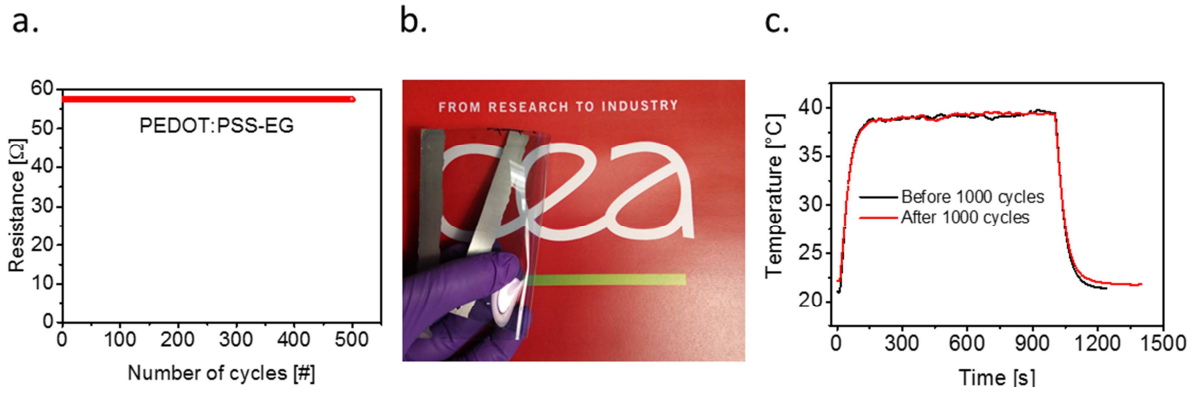

Figure III.11. a) Electrical stability of PEDOT:PSS-EG (2.5 cm x 2.5 cm electrode, Rs = 53.7 Ω sq^{-1}, $T_{550\ nm}$ = 87.5 %) after 500 bending cycles under 9 mm bending radius. b) PEDOT:PSS-EG (Rs = 97.1 Ω, $T_{550\ nm}$ = 94 % , applied voltage = 15 V, I = 150 mA, steady state T = 39 °C) deposited on a flexible PET substrate (125 m) and c) the stability of its heating properties after 1000 flexions under 10 mm bending radius.

The resistance was measured after each cycle. The results presented in Figure III.11a show that the resistance remains constant after 500 cycles. For practical applications we performed more than 1000 flexions at 10 mm bending radius, on a 10 cm x 10 cm PEDOT:PSS-EG based heater (Figure III.11b,c) without altering the heating properties. As the electrical resistance is not altered after the bending cycles, the heating properties remain unchanged as shown in Figure III.11c.

3-7. Uniformity of the heating

The uniformity of temperature distribution across these PEDOT-based heaters can be a good indicator for some heating applications. PEDOT:PSS-EG was deposited on both a flat small area glass substrate and a curved large area polycarbonate substrate (a

motor visor). Only PEDOT:PSS-EG was investigated because it is easily processable for deposition on large and curved surfaces and has good heating performances similar to that of PEDOT:Sulf.

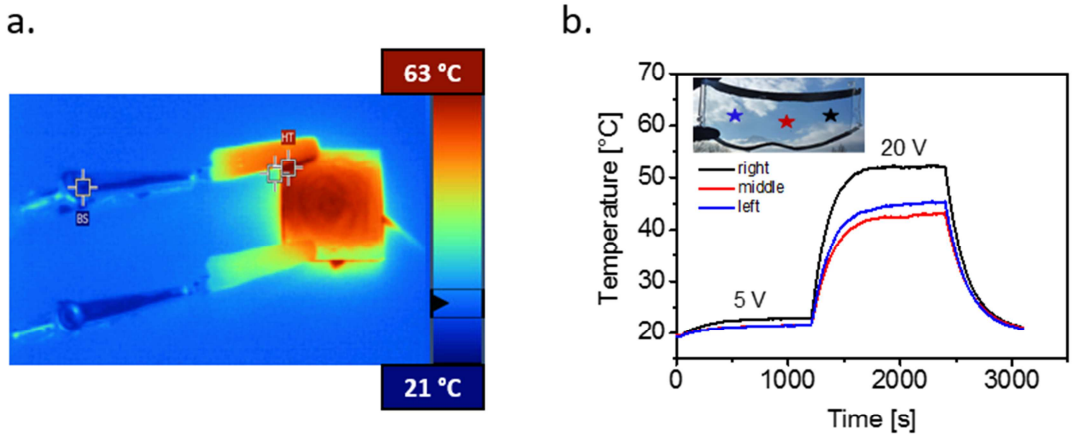

Figure III.12. a) IR image of a PEDOT:PSS-EG heating at 63 °C (applied voltage = 6 V). The heat losses in the electrodes' contacts (left side), the thermocouple's wire (right side) and the Kapton® tape (lower side) are visible. b) Temperature response when 5 V followed by 20 V bias are applied on a visor covered with a thin PEDOT:PSS film. Three K-type thermocouples were placed at three different spots on the visor and the temperature raise was recorded. R = 18 Ω.

For small area materials, typically 2.5 cm x 2.5 cm, the temperature rise as well as the steady state temperature are uniform all over the sample as illustrated with the IR thermal image in Figure III.12a where one can see the increased temperature throughout the film and the connecting wires. However, with larger surfaces, an uneven temperature can be noticed (Figure III.12b). This non uniformity can be due both to the geometry of the visor, or losses over large surfaces. Further works are focusing on explaining these losses more thoroughly and optimizing the uniformity of the heating.

4. Application as transparent heaters

4-1. PEDOT as transparent conductive materials

Transparent conductive materials (TCMs) are needed in a myriad of applications such as antistatic coatings, electromagnetic shielding, touch panel controls, transparent electrodes in solar cells or OLEDs, low emissivity windows and transparent heaters.[139] A good TCM is characterized by its low sheet resistance ($R_s < 100\ \Omega\ sq^{-1}$) combined with a high transparency ($T_{550\ nm} > 90\ \%$), a very low blurriness (measured by the haze factor as introduced later) for applications whereby high visibility is needed, and an appropriate stability and response time. Furthermore, the processing methods and cost should be harnessed. In order to acknowledge materials as good TCM, the FOM should be at least greater than 35.

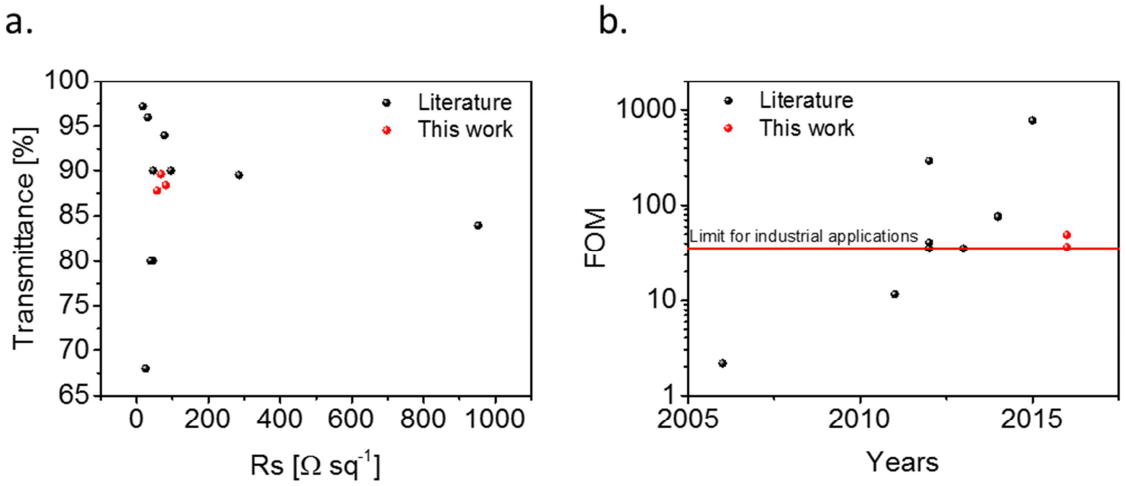

Figure III.13.a) Transmittance *versus* sheet resistance of PEDOT materials and b) FOM of PEDOT materials *versus* years. Black points are literature data and red points are data of this work, corresponding to PEDOT:OTf, PEDOT:Sulf and PEDOT:PSS-EG. References can be found in the Appendix.

Transparent conducting oxides have long been the reference for such applications due to their good optoelectronic properties and stability. However, their brittleness and their cost become an issue regarding the growing demand on flexible devices.[140] PEDOT, among others, has made itself a reliable candidate through the increasing electrical performances reported as shown in Chapter 1 and Chapter 2.

PEDOT was proposed as electromagnetic shield as well as transparent electrode anode in order to replace indium tin oxide (ITO) in organic solar cells and lighting devices.[50,81,84,85,94,101,112,113,141,142] It was also shown to replace platinum and fluorinated tin oxide in dye sensitized solar cells.[143] Figure III.13 shows the optoelectronic properties of PEDOT materials studied as transparent electrodes in the literature.

Though preliminary works revealed the relevance of PEDOT as a TCM, they were mainly focused on transparent electrode applications. We here aim to demonstrate a novel TCM application for PEDOT materials and for conducting polymers in general.

4-2. Transparent heaters

The first use of transparent heaters (THs) dates back from the World War II when they were applied for defrosting the windows of airplanes at high altitudes.[139] Nowadays ITO is the most employed TCM in general and for TH in particular, the foremost uses being for defrosters and defoggers in vehicles, advertisement boards, avionics and displays.[137,139,144] Due to the growing market of TCMs and the increasing demand on flexible devices, the brittleness of ITO and the scarcity of indium stimulated research for alternative materials. In that respect, THs made of metal oxides, carbon nanotubes, graphene, metallic nanowires (NWs), metal meshes and hybrid materials have been investigated.[134,135,145–154] After seminal studies focused only on metal oxides, carbon nanotubes (CNTs) and graphene based heaters refreshed the attention on THs.[136,155,156] The high sheet resistances in CNTs require however a too high input voltage and the numerous defects in graphene induce some local hot spots and hence a non-uniform heating over large areas. These materials do not allow to reach excellent trade-off between conductivity and transparency and require high bias to be activated. Metallic nanowire-based networks were proved to be efficient THs only few years ago.[135,157] They are solution-processable and exhibit low sheet resistance, high transparency, excellent flexibility and hence are convenient for flexible transparent film heaters.[132,133,135,137,144,158,159] They however have a too high haze factor and hence diffuse too much light.[134] Hybridizing AgNWs with conducting polymers such as PEDOT:PSS allows to reduce the sheet resistance, the haze factor and to homogenize the heating.[134] However, it was demonstrated that these hybrids show moderate stability.[160–162] Metal meshes also depict interesting optoelectronic properties for transparent heaters applications, but the fabrication process can be costly and the haze factor remains high.[152,154] Conducting polymers, including PEDOT, are well-known to be relevant TCMs for OLEDs, photovoltaics, sensors and other optoelectronics devices.[56,112,150,163]

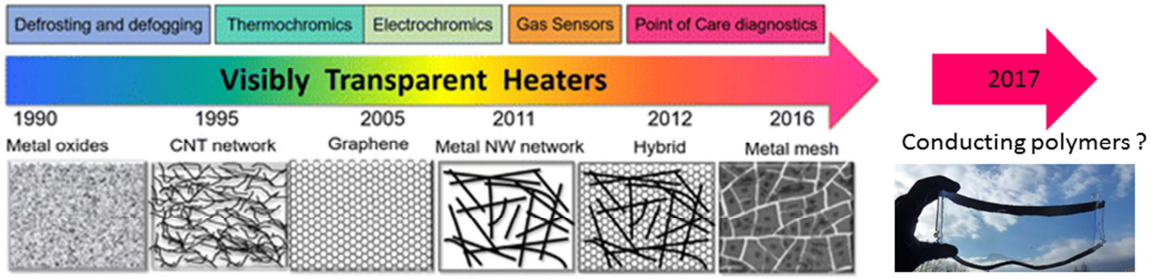

Figure III.14. Next generation transparent heater. Reproduced from[137].

Surprisingly, to the best of our knowledge, no TH solely based on conducting polymers has ever been reported, although these materials can exhibit outstanding optoelectronic properties (Figure III.13) and interesting thermal response as introduced in 3-3.[74,91,123] We here investigate PEDOT as the next generation of transparent film heaters (Figure III.14).

4-3. Optoelectronic properties

Besides their outstanding electrical properties as presented in Chapter 2, these materials also exhibit high transparencies in the visible spectrum (see figure II.7), which are two key properties for transparent thin film heaters. Their main optoelectronic properties are reported in Figure III.15a,b. The high conductivity associated to the low thickness of PEDOT:OTf and PEDOT:Sulf films are at the origin of the excellent trade-off between sheet resistance and high transparency in the visible range (Table III.1). PEDOT:PSS and PEDOT:PSS-EG on the other hand are less conductive materials (178 and 1361 S cm^{-1} respectively), which is mainly due to the excess of insulating PSS present in the films. However, this excess of PSS does not absorb in the visible range, and hence is not detrimental for the transparency of these materials. Figure III.15a shows the specular transmission values at 550 nm of the four materials as a function of their sheet resistances. Transparencies higher than 80 % associated with sheet resistances below 100 Ω sq^{-1} are very good features to achieve high performance THs.[137] This can be easily accomplished by stacking two to three layers of PEDOT films. In addition to these optoelectronic properties, these materials barely diffuse light, as evidenced by the very low haze factor, namely the amount of diffuse light over the total transmitted light, which remains below 1 % in the entire visible range (Figure III.15b).

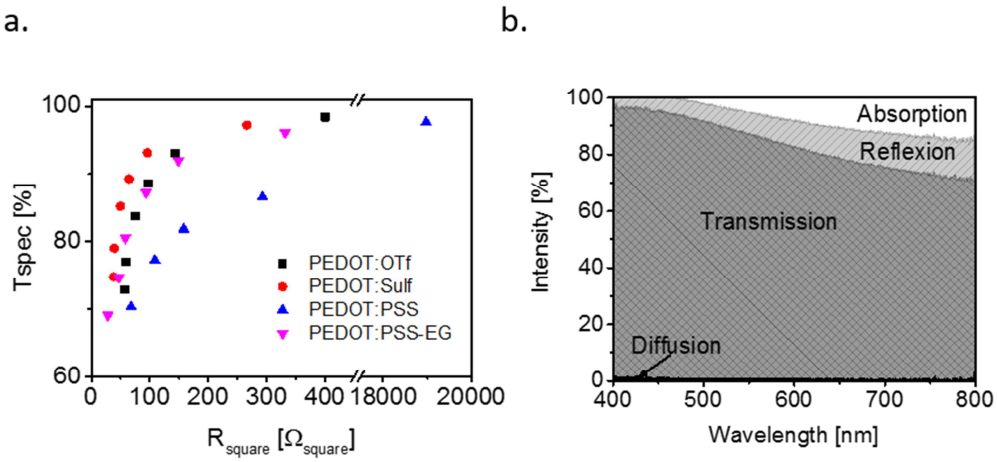

Figure III.15. Optoelectronic properties of PEDOT materials. a) Dependence of the transmittance at 550 nm as function of the sheet resistance of the materials. b) Optical properties of PEDOT:Sulf in the visible (Haze = (Diffuse transmittance)/(Total transmittance) < 1 %).

4-4. Applications

Combining the good heating properties as reported hereinbefore and the good optoelectronic properties of PEDOT:PSS-EG and PEDOT:Sulf particularly, their heating performances are compared to the state of the art materials for THs in Table III. 3. Based on these results, it appears that PEDOT-based materials are very competitive in the field of THs with heating properties even better than those of CNTs, graphene and metal oxides and almost comparable to that of silver nanowires and derived hybrids.[137,155,156]

In Table III.3, it appears that for FOM equivalent to that of our materials, the steady state temperature reached is similar. The thermal response is however higher for our PEDOT materials compared all other THs. Also, the thermal resistances are lower than that of carbon and metal oxide based heaters and similar to that of metal nanowires, hybrids or meshes. The losses are therefore lower in the case of carbon materials and metal oxides and are still to be minimized for the remaining materials. Losses in PEDOT are too high and supplementary works are required in order to localize the origin of these losses so that they can be minimized. Nonetheless, those losses do not hinder the steady state temperature reached and the thermal response can be optimized by modulating the applied bias as stated hereinbefore. PEDOT-based films appear then to be suitable for TH applications at low voltages, and are even scalable as long as the TH device is designed in a way to minimize the total electrical resistance.

Table III.3. A non-exhaustive list of state of the art materials for transparent heaters.

Materials	Substrate	Area [mm²]	T_{total} [%]	R_{sheet} [Ω sq^{-1}]	Haze [%]	FOM	Voltage [V]	T_{peak} [°C]	Thermal resistance [°C cm² W^{-1}]	Response time [s]
ITO[164]	Glass	N/A	> 95	633	N/A	11[a]	10	62	N/A	40
SWCNTs[165]	PET	40 x 40	76	356	N/A	4[a]	12	N/A	N/A	< 50
MWCNT[146]	PET	13 x 9	71	349	N/A	3[a]	10	58	406[a]	N/A
Graphene[147]	Glass	20 x 20	92	403	N/A	10[a]	24	80	645[a]	~300
$AuCl_3$ doped graphene[147]	Glass	20 x 20	90	66	N/A	53[a]	10	80	645[a]	~300
$AuCl_3$ doped graphene[155]	PET (sandwiched)	40 x 40	89	43	N/A	73[a]	12	100	494[a]	~150
AgCP1[132]	PET	40 x 30	86	6	5	401	5	~100	515	20
CuNWs encapsulated[148]	Glass	N/A	84	17	N/A	122[a]	10	110	N/A	< 100
Metal Meshes (Ti + Pt)[154]	PET 125 m	7 x 11	89	94	5	34	5	69	258	~15
AgNW + PEDOT:PSS[134]	Glass 150 m	300	70	4	~30	241[a]	4	> 85	313[a]	~50
Ag Mesh + ITO[166]	PET 150 m	30 x 40	88	300	N/A	100[a]	12	43	N/A	30
PEDOT:PSS-EG[b]	glass	25 x 25	89.6	68	0.7	49	10	94	247	249
PEDOT:Sulf[b]	Glass	25 x 25	87.8	57	0.7	50	10	114	383	383
PEDOT:Sulf[b]	PET 125 m	25 x 25	86.5	40	0.7	62	10	142	308	140

[a] Calculated from authors' data

[b] This work

Aside from their performances, development of polymeric THs is particularly beneficial because PEDOT polymers are easily processable. Consequently large area, flexible and curved devices can be built easily and at significantly lower cost when compared to TCOs. As a matter of fact, PEDOT dispersion or oxidative solution can be deposited on flexible substrates, for instance transparent polymer films such as PET. Their thermal properties are even better as explained hereinbefore, and demonstrated in Figure III.7b.

In order to demonstrate the interest of PEDOT in future TH applications, integration in thermochromic displays (on glass) and visor defoggers/deicers (on polymer substrate) has been carried out. Figure III.16a shows a thermochromic display. PEDOT:Sulf was deposited on a 10 cm x 10 cm glass substrate (58 Ω sq^{-1}, 88 % transmittance). The thermochromic ink (activation temperature 43°C) was spray-coated through a shadow mask on a film barrier. The latter was used to encapsulate the PEDOT thin film using the same film barrier and OCA as described previously. When 15 V bias is applied, the temperature increases until the pattern color turns from blue to white at 43 °C. When the voltage is switched off, the temperature decreases, inducing the recovery of the blue color. This was realized for dozens of cycles without any alteration.

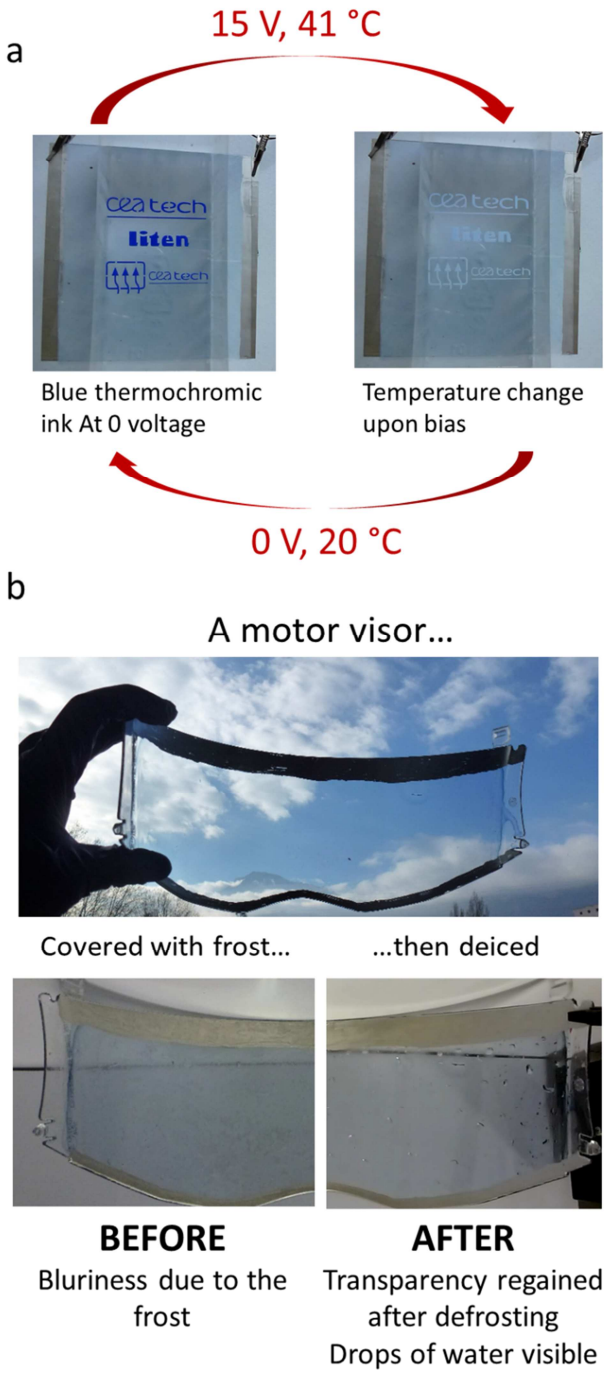

Figure III.16. a) Application as thermochromic display. Due to the increase of temperature of the film when a voltage is applied, the color of the thermochromic ink turns from blue to white. This process is reversible b) Application as visor deicer. The frost formation at the surface of the transparent heater renders it blurry, but the transparency is promptly regained after application of a voltage as the ice melts.

In the second example of application PEDOT:PSS-EG was drop-coated on a polycarbonate motorcycle visor (20 Ω, 92 % transmittance, Figure III.16b). Contacts were printed up- and down-side the visor (Figure III.16b) rather than on the left and right sides in order to minimize the resistance between the electrodes. The external surface was then slightly humidified and the visor was iced in a fridge at -26 °C. Deicing was then performed in few seconds by applying 15 V to heat up the surface. These demonstrators evidence the relevant use of PEDOT based thin films as THs.

5. Conclusion

In summary, we studied in this chapter the conversion of electrical energy into thermal energy through the resistive Joule heating of PEDOT thin films. In particular, PEDOT:Sulf thin film depicts outstanding properties, with a sheet resistance of 57 Ω sq^{-1} at 87.8 % transmittance, 1.6 °C s^{-1} heating rate and a steady state temperature of 138 °C under 12 V bias.

It is also shown that heaters can be realized from thin films of commercially available PEDOT:PSS solutions if the film is post-treated with EG. For instance PEDOT:PSS-EG (68 Ω sq^{-1} at 89.6 % transmittance), shows also excellent heating performances, and stability after cycling and after 200 h at 50 °C was evidenced. Very high areal power density was measured with this material, reaching up to 10 000 W m^{-2}.

The heating performances were successfully explained with a power model resulting from an energy balance between the {film + its substrate} system and its surrounding. We showed that the steady state temperature depends on the applied voltage, the film resistance, the substrate area and the convective and radiative losses. On the other hand, the time response, which was always greater than 300 s, depends mainly on the applied voltage, the film resistance and the substrate physical features (its mass and specific heat capacity). The substrate is then the main obstacle for a fast response time. Overall, the performance of PEDOT thin heaters can be modulated through their resistance, the applied voltage and the substrate's characteristics.

Subsequently, transparent heaters based on thin films of PEDOT polymers are demonstrated for the first time, with performances similar to those of the state of the art THs' materials. They even surpass them regarding their very low haze factor, always smaller than 1 %. Thanks to a straightforward deposition process, in particular

on large and curved surfaces such as a visor, PEDOT transparent thin films can be integrated into various functional devices, such as thermochromic displays or de-icing of visors.

After metal oxides, CNTs, graphene, metallic nanowires, metal meshes and hybrids, conducting polymers stand as the next generation of low cost, easily processable, flexible transparent heaters. The obtained results rank them at the very best level when compared to the state of the art materials (Table III.3).

Chapter 4
Thermal to electrical energy conversion: thermoelectricity

1. Introduction

In this chapter, we will introduce a thermodynamically reversible thermoelectric phenomenon, namely the Seebeck effect and particularly in PEDOT films. We will see how such phenomenon can allow heat harvesting and which properties the material should have in order to be efficient.

Compared to the resistive Joule heating studied in the last chapter, the Seebeck effect is far less unknown. Therefore, in the following, we will first present the reason why the study of such effect is interesting. Thermodynamically reversible thermoelectric effects will also be presented and the accent will be put on the Seebeck effect. Materials that depict fair thermoelectric properties will be introduced, as well as the state of the art thermoelectric properties of PEDOT materials.

After having presented those notions, we will expose the preliminary works about the thermoelectric properties of our PEDOT materials.

2. Reversible thermoelectric effect in PEDOT materials

2-1. Context

Around 90 % of the energy produced is converted into heat, most of which being lost during transportation, in households or during industrial processes.[167,168] At the same time, numerous sources of natural heat such as anthropogenic heat, solar and geothermal energy remain largely unexploited. Given the depletion of fossil energy and the growing global demand for clean and renewable energy, both new sources and a more economical use of the produced energy are strongly desired. The latter one could be realized by harvesting the paramount heat losses, what can be made possible using thermoelectric devices.

Thermoelectricity refers to any transport of heat combined with electrical energy. In that respect, Joule heating and thermal conduction phenomena observed in the previous chapter are thermoelectric effects, but non-reversible ones as they correspond to energy losses. Howerver, only three reversible thermoelectric effects exist which are

the Seebeck effect, the Peltier effect and the Thomson effect. These effects are behind the conversion of heat into electricity, and vice versa, and explain the functioning of the commonly known thermocouple or Peltier device.

This chapter reports on the thermoelectric properties of PEDOT based materials, their optimization and give insight in their use in thermoelectric generators.

2-2. Some notions and state of the art

2-2-a. Thermoelectricity: what and what for?

The first reversible thermoelectric effect, the Seebeck effect, was discovered in 1821 by Thomas Johann Seebeck. He noticed that a compass needle deflects when it is placed in a closed loop of two dissimilar materials which are jointed and whose junctions are set at different temperatures, as in Figure IV.1a.[169,170] Such deflection is due to the apparition of a Seebeck voltage that creates an electric current and then a magnetic field following Ampere's law. However, at first, Seebeck accounted the deflection of the needle to a magnetic force and called the effect "thermomagnetic effect". Some years later, Hans Christian Orsted recognized that an electric field is actually created and corrected it to "thermoelectric effect".[171] The assembly in Figure IV.1a is called a thermocouple and the produced voltage between the cold side and the hot side is found proportional to the temperature gradient following Equation IV.1.

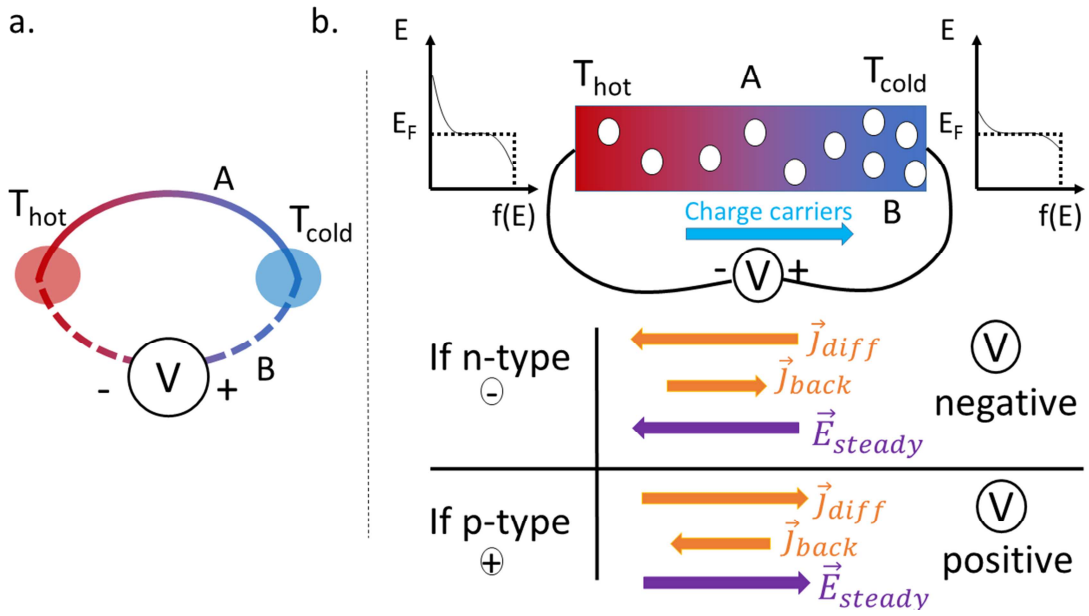

Figure IV.1. a) A thermocouple made of two dissimilar materials whose junctions are set at two different temperatures. b) Illustration of the Seebeck thermoelectric effect in material A.

$$V_{hot} - V_{cold} = S_{AB} \cdot (T_{hot} - T_{cold}) \quad \text{(IV.1)}$$

Where $S_{AB} = S_B - S_A$ the Seebeck coefficient or thermopower of the thermocouple and S_A and S_B the absolute Seebeck coefficient of materials A and B respectively.

In each material in Figure IV.1a, the temperature gradient induces a higher energy of the charge carriers at the hot side (Figure IV.1b). Subsequently, the charges diffuse from the hot to the cold size. When charges accumulate at the cold side an electrical potential is created. Due to the electrical charges of the charge carriers, an electrical field that drives back the charge carriers is created. At steady state, a constant potential difference depending only on the temperature gradient remains, namely the Seebeck voltage. If the Seebeck coefficient of material A is very high compared to B, it can be directly assessed through Equation IV.1. That is how absolute thermopower of a material is assessed, by coupling it with a known material which was previously coupled with a supraconductor (a material with a zero thermopower). If the majority charge carriers are negative, the voltage given by the voltmeter is negative and so is the Seebeck coefficient of material A; conversely if the majority charge carriers are positive. Seebeck coefficient is the entropy per charge carrier in the solid, therefore, its

study can indicate whether charge carriers move freely or whether they are trapped due to disorder.[172]

Thirteen years after Seebeck's discovery, Jean Charles Athanase Peltier discovered the complementary phenomenon, named after him, the Peltier effect. Using the same set-up as Seebeck, Peltier did not apply a temperature gradient but rather a current was passed through the loop of the thermocouple, hence causing heating and cooling at the junctions.[173]

The Peltier effect can be described as in Figure IV.2b&c. The heating or cooling of the junction is dependent on the current flow direction. In Figure IV.2b, as electrons flow from higher to lower energy levels, they lose energy which is transferred as heat to the surrounding environment, and conversely in Figure IV.2c.

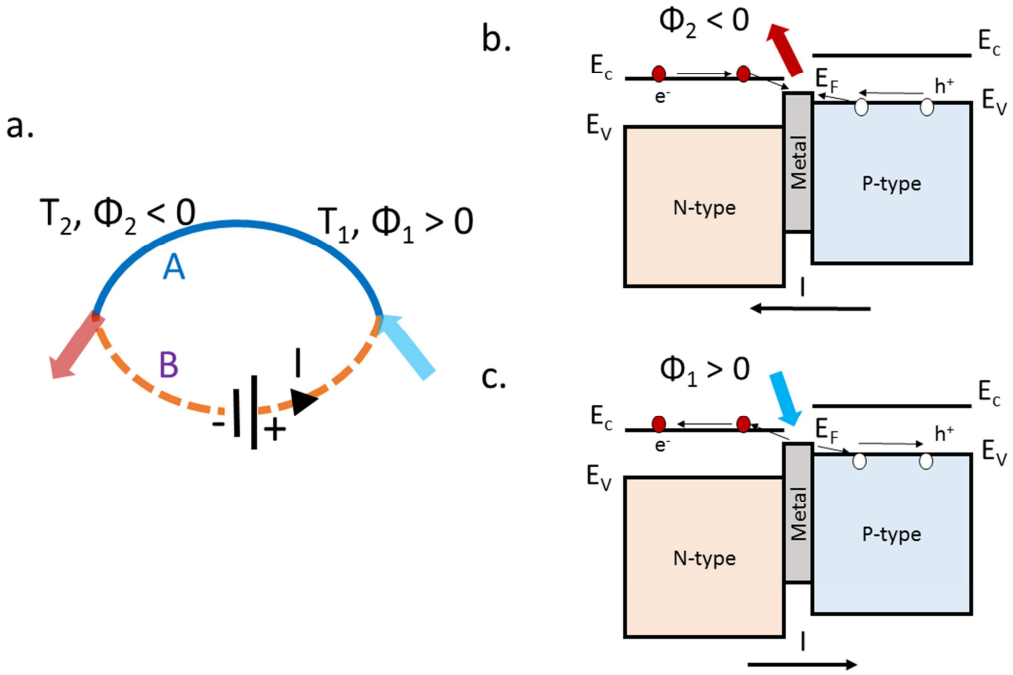

Figure IV.2. a) Two different materials A (p-type) and B (n-type) with current flowing from B to A. b) Illustration of the Peltier thermoelectric effect, reproduced from [174].

The interdependency between the Seebeck effect and the Peltier effect was stated in 1850 by William Thomson who was studying their thermodynamics. He established the relationship between the Seebeck and Peltier effects and discovered the third

thermoelectric effect, the Thomson effect in which a material undergoes reversible heating and cooling when subjected to both an electrical current flow and a temperature gradient as in Figure IV.3.[175]

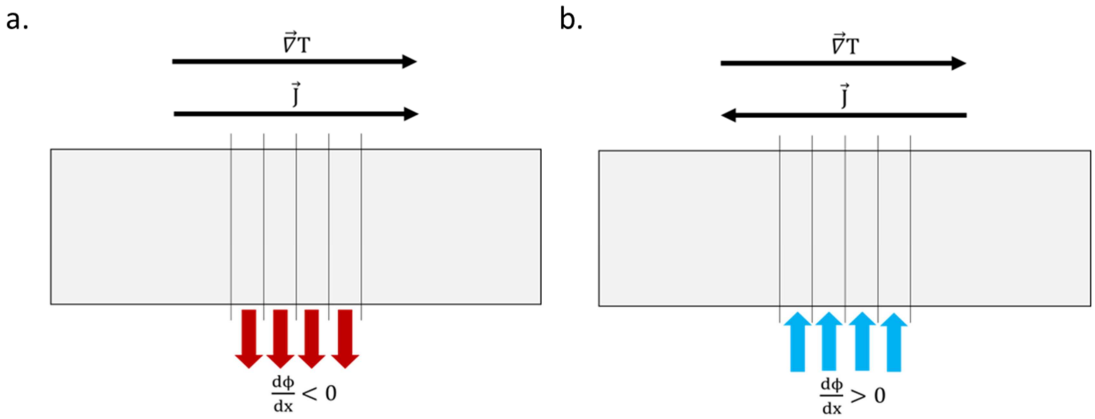

Figure IV.3. Illustration of the Thomson when the temperature gradient and the current density are in the same (a) or different (b) directions. Reproduced from[174].

Similarly to the Seebeck coefficient, the Peltier and Thomson coefficients are negative for n-type materials and positive for p-type ones. However, contrarily to the Seebeck and Peltier effect, the Thomson effect does not hold any practical application.

2-2-b. Thermoelectric devices

While studying thermoelectric effect, Thomson inferred that a thermocouple can act as a heat engine which could be used for heat harvesting (Seebeck effect) or as heat pump or refrigerator (Peltier effect).[176] The irreversible phenomena that occurred alongside the reversible ones induce however too much losses and thermocouples are not efficient. In 1911, Edmund Altenkirch investigated such device performance and showed that the efficiency could be improved by increasing the magnitude of the differential Seebeck coefficient between the two branches of the thermocouple, by increasing their electrical conductivity and by reducing their thermal conductivity.[177] The lack of reasonably efficient materials at that time was not advantageous for such device implementation. The suggestion of semiconductors as efficient thermoelectric material in the nineteen fifties opened the route to Peltier refrigerators and thermoelectric generators.

The aforementioned devices operate following the scheme in Figure IV.4. A thermoelectric device is constituted of p and n-type legs which are electrically

connected in series and thermally in parallel. The alteration of n and p type materials allows to optimize the Seebeck coefficient of the as-formed thermocouple. The system can be made from as much legs as necessary in order to increase the efficiency of the system.

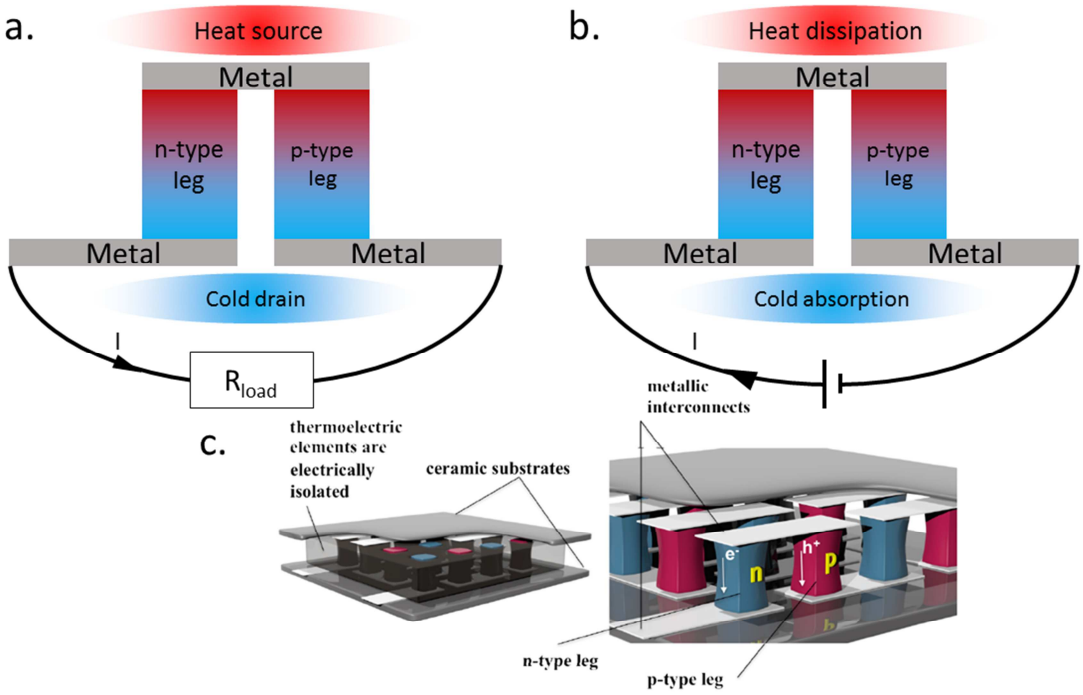

Figure IV.4. a-b) Functioning principle of a thermoelectric generator (a) and a Peltier device (b). c) A thermoelectric module made of p-type and n-type legs reproduced after [74].

Thermoelectric generators have gained tremendous attention in the past decades. They have no moving parts and hence require no maintenance, and they can be used in any environment, all they need being a temperature gradient. Therefore, they were the effective solution for spacecraft missions. Their main problem remains in their low efficiency, so that they are only used in niche applications.[176] The efficiency η of such device is given in Equation IV.2 :[18,176,178]

$$\eta = \frac{T_h - T_c}{T_h} \cdot \frac{(\sqrt{1+zT_m}-1)}{(1+zT_m+\frac{T_c}{T_h})} \quad \text{(IV.2)}$$

Where T_h and T_c are the temperature at the hot side and cold side respectively, T_m the mean temperature and zT_m the figure of merit given by Equation IV.3:

$$zT_m = \frac{(S_p - S_n)^2}{\left[(\lambda_p \cdot \rho_p)^{1/2} + (\lambda_n \cdot \rho_n)^{1/2}\right]} \cdot T_m \quad \text{(IV.3)}$$

With p and n indices referring to the p- and n-type material respectively, S the Seebeck coefficient, λ the thermal conductivity and ρ the resistivity.

The figure of merit reflects then directly the efficiency of thermoelectric generators as given in Figure IV.5. It appears that when the temperature gradient is set at 100 K and the cold side of the device at room temperature (300 K), the efficiency is barely 5 % if zT_m values 1. Despite such low efficiency, the fuel of such devices is lost heat and the produced voltage is enough to power devices in the growing market of the internet of things for instance.

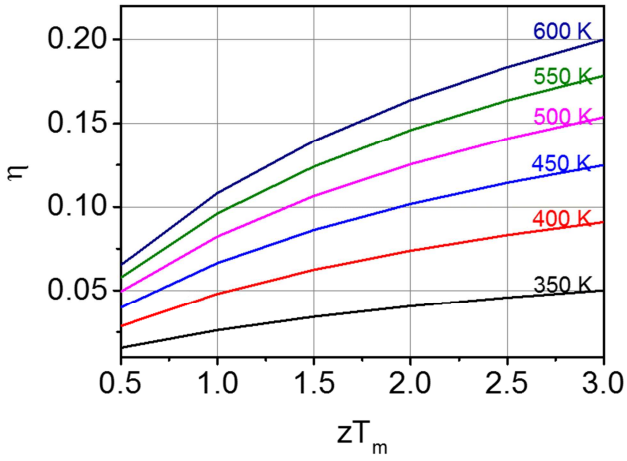

Figure IV.5. Maximum efficiency of a thermoelectric device as function of the hot temperature and the figure of merit. The cold temperature is set at room temperature (300 K) and the hot temperature is ascribed near the corresponding curves.

In spite of studying the whole device or the whole thermocouple, dealing with only one of the materials (one leg) is more convenient for the study of the material. Therefore, we introduce in practice the figure of merit of a material given by Equation IV.4 :

$$ZT = \frac{S^2}{\lambda.\rho}T = \frac{\sigma.S^2}{\lambda}T \qquad \text{(IV.4)}$$

With σ the electrical conductivity of the considered material.

3. Thermoelectric materials

As inferred previously by Edmund Altenkirch, as one can guess intuitively and also as proved in Equation IV.4, the efficiency of a thermoelectric material depends on its

propensity to conduct electricity (its electrical conductivity), its propensity to convert a temperature gradient into electricity (its Seebeck coefficent) and its propensity to keep the temperature gradient the longest (its thermal conductivity). In other terms, a high electrical conductivity, a high Seebeck coefficient and a low thermal conductivity are required in order to optimize ZT and subsequently the efficiency. A major issue remains however in the interdependency of these three parameters, which are all function of the charge carriers' concentration, as shown in Figure IV.6.

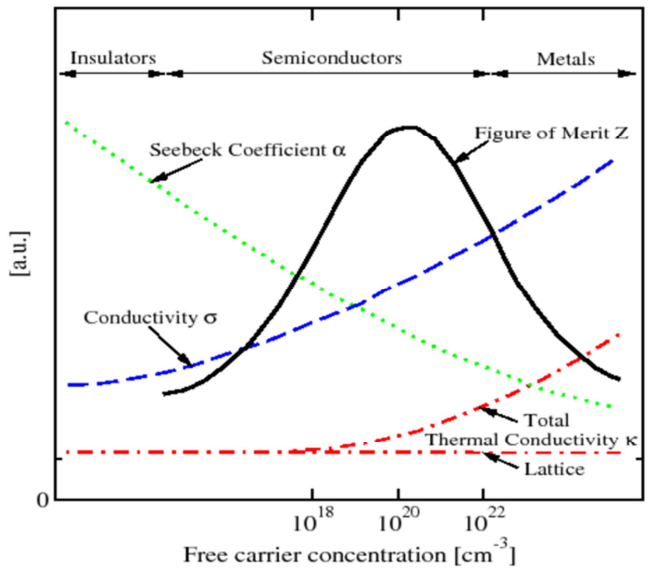

Figure IV.6. Seebeck coefficient, electrical and thermal conductivity as a function of free carrier concentration for different classes of materials, after[178].

Table IV.1. Comparison of the thermoelectric properties of metals, semiconductors and insulators at room temperature, reproduced from[179].

Metals	Semiconductors	Insulators
S ~ 5 μV K^{-1}	S ~ 200 μV K^{-1}	S ~ 1 mV K^{-1}
σ ~10^6 S cm^{-1}	σ ~ 10^3 S cm^{-1}	σ ~ 10^{-12} S cm^{-1}
λ ~ 10-1000 W m^{-1} K^{-1}	λ ~ 1-100 W m^{-1} K^{-1}	λ ~ 0.1-1 W m^{-1} K^{-1}
ZT ~ 10^{-3}	ZT ~0.1-1.0	ZT ~ 10^{-14}

As summarized in Table IV.1, metals have high conductivity, but their Seebeck coefficient is too low to consider them as viable thermoelectric materials. Insulators possess high Seebeck coefficient, up to some mV K^{-1}, but their too low conductivity do

not allow reasonable efficiency. As for semiconductors, they depict a set of properties letting expect ZT around 1. In fact, thermoelectric materials belong to a special class of materials described as "phonon glass and electron-crystal" materials.[180] Such materials should inhibit the conduction of phonons like a glass, thus resulting in a lessening of the thermal conductivity, while behaving like crystals for electrons, hence increasing the electrical conductivity.

In that respect, early researches have focused on the engineering of inorganic semiconductors in order to optimize the figure of merit and subsequently, the efficiency. Thermoelectric materials appear to have a temperature range of functioning as depicted in Figure IV.7. State of the art materials have figure of merit ranging between 1 and 2.6, which, at high temperatures (> 900 K), correspond to efficiencies higher than 20 %.[172]

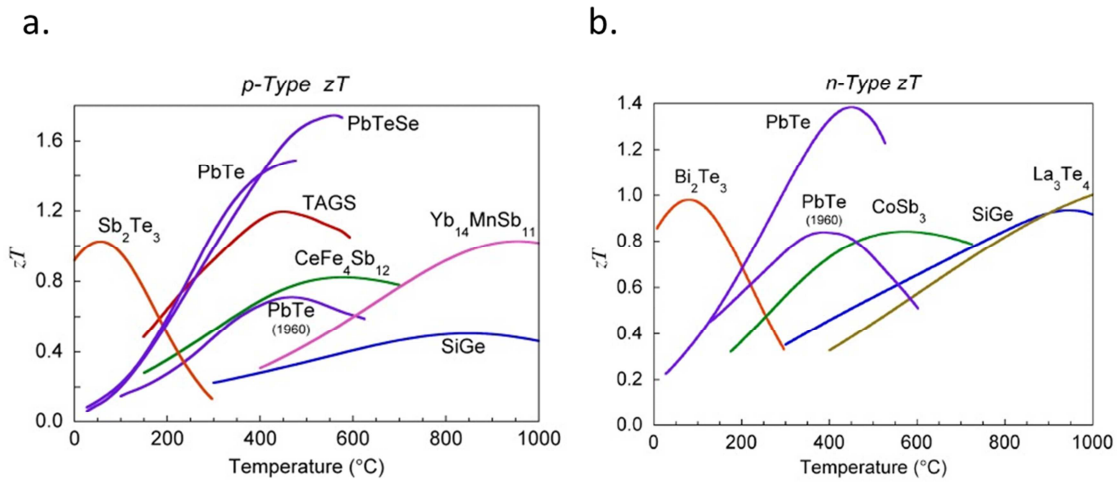

Figure IV.7. P-type and n-type thermoelectric materials at different working temperature, after[2].

Interesting progress in that field have been made, especially for power generation for space exploration. Radioisotope thermoelectric generators (RTEG) powered NASA missions such as Voyager 1 and 2, which were launched in 1977 and are still fulfilling their mission.

However, coming back to earth and the tremendous heat losses in our energy consumption, around 60 % of the losses are present at temperature below 100 °C, available, but not harvested.[167,168,181] Main efficient materials at such low temperature

[2] http://thermoelectrics.matsci.northwestern.edu/thermoelectrics/index.html, last visited in July 2017

(< 100 °C) and with good thermoelectric properties for practicability (ZT > 1) are based on tellurium as shown in Figure IV.7, a brittle, rare and toxic material whose process is expensive.[172,176]

Alternatives are needed, and organic semiconductors have emerged as satisfactory ones.

4. PEDOT among thermoelectric materials

4-1. Advantages of PEDOT as thermoelectric materials

Due to their ease of processing, abundance, low cost, good mechanical properties and flexibility, conducting polymers have already proved their efficiency in organic electronics as shown in the previous chapters. The tuning of their conductivity over several orders of magnitude through doping and their intrinsically low thermal conductivity compared to inorganic thermoelectric materials (0.2 ~ 0.6 W m^{-1} K^{-1}, around one order of magnitude lower) have rendered them viable for thermoelectric applications. Moreover, they do not seem to thoroughly follow the Wiedemann-Franz law (stating that the electronic contribution of the thermal conductivity is proportional to the electrical conductivity and the temperature), what allows them to have a less constraining dependence between the thermal and electrical conductivity.[74,182]

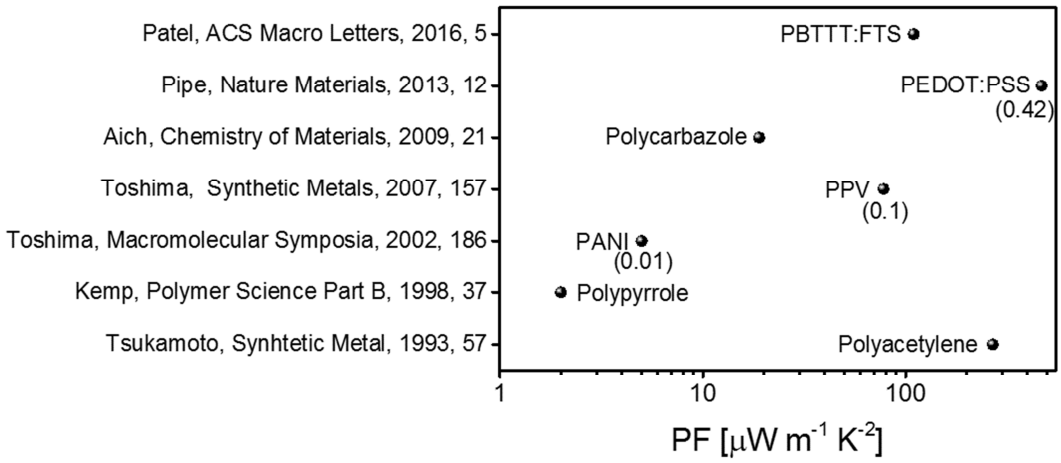

Figure IV.8. State of the art thermoelectric properties of some p-type conducting polymers. PBTTT = poly(2,5-bis(3-tetradecylthiophen-2-yl)thieno[3,2-b]thiophene). FTS = (tridecafluoro-1,1,2,2- tetrahydrooctyl)trichlorosilane

The thermoelectric properties of various conducting polymers have been studied as shown in Figure IV.8.[183] Among all conducting polymers, PEDOT has stood out due to its low thermal conductivity (around 0.37 W m^{-1} K^{-1}) and its moderate Seebeck coefficient (around 20 μV K^{-1}).[18,184,185] The progress made in this thesis on its electrical conductivity optimization (up to 5400 S cm^{-1}) is an additional feature that can benefit its thermoelectric study.[10,63,106]

Highly conductive PEDOT are deposited as films. However, the thermal conductivity of thin films is hard to determine and thick pallets or thick films (sub-millimeter size) are needed, whereas dense block cannot be synthesized from solution-based or VPP processes. Due to the inherently low thermal conductivity of PEDOT, but also due to the difficult characterization of thin films, most studies on the thermoelectric properties of PEDOT mainly focus on the optimization of the numerator in Equation IV.4, namely the power factor $PF = \sigma S^2$.

As seen in Chapter 1, the majority charges carriers in PEDOT are polarons and bipolarons, and PEDOT is a p-type conducting polymer so that its Seebeck coefficient is positive. The Seebeck coefficient and the electrical conductivity are both strongly dependent on the charge carriers' density as previously shown in Figure IV.6. Therefore, they can both be tuned through the charges carriers' density. With increasing the charges carriers' density, the electrical conductivity increases following

Equation I.1, while the Seebeck coefficient decreases. Indeed, the Seebeck coefficient is described as the entropy transported by a charge carrier. In that respect, the more charges carriers there is, the less entropy will be carried by each carrier as the total entropy is shared between their increasing number. An optimization of the power factor (and subsequently the figure of merit) is then possible by charge carrier tuning though chemical doping, electrochemical doping or electrical gating.[102,172,186]

With all the progress done in the last decade, PEDOT was reported to exhibit a figure of merit almost half of the reasonable target for practical applications (i.e. 0.42 as shown in Figure IV.8).

4-2. State of the art of the thermoelectric properties in PEDOT materials

Usually, the electrical conductivity and the Seebeck coefficient of PEDOT films are measured in the plane of the film whereas the thermal conductivity is measured through the plane, if even measured, due to the difficulty to fabricate dense blocks. On the other hand, it has been shown that PEDOT films can be highly anisotropic and therefore, the figure of merit reported in the literature are absolutely not comparable (while some are deduced from the power factors, others are measured with in-plane thermal conductivity and other with through plane thermal conductivity).[182,187,188] However, due to the lack of maturity of the studies on anisotropy in PEDOT thermoelectric properties, such anisotropy will not be discussed in this thesis, but information will be given if the thermal conductivity was estimated, measured in the plane or through the plane of the sample.

Due to the metallic behavior of PEDOT, its Seebeck coefficient is rather low, typically below 20 μV K^{-1}. Before considering PEDOT as a thermoelectric material, its electrical conductivity and Seebeck coefficient were both studied for transport purposes (cf. Figure I.12). However, with its increasing electrical conductivity, more focus was given to that field. Not 10 years ago, PEDOT:PSS pellets were reported to have thermal conductivity around 0.17 W m^{-1} K^{-1} and a Seebeck coefficient up to 15 μV K^{-1}.[189] At first, power factors lower than 10 μW m^{-1} K^{-2} were reported. But at the same time, treating PEDOT:PSS with organic solvents was found to increase the electrical conductivity without being detrimental to the Seebeck coefficient as it induces only conformational and structural changes in PEDOT:PSS as explained in Chapter 1, without deterioration nor improvement of the doping level.[190] Thus, in 2010,

after addition of DMSO in PEDOT:PSS dispersion, Zhang and coworkers achieved a power factor of 47 μW m^{-1} K^{-2} and a figure of merit estimated up to 0.1.[191]

In order to optimize the thermoelectric performance of PEDOT:Tos, Crispin and coworkers tuned the doping level through exposition to tetrakis(dimethylamino)ethylene (TDAE) vapors. The Seebeck coefficient increased with the lowered doping level while the electrical conductivity decreased due to their dependency with the charge carrier density. Both in plane and through plane thermal conductivities were measured and at an optimized doping level, the in-plane figure of merit reached 0.25.[184] Later on, Massonnet et al. studied the influence of different reducing agents and their redox potential on the thermoelectric properties of PEDOT:PSS, whose thermopower increased from 18 to 161 μV K^{-1}.[75] Always for the purpose of controlling the doping level, Kim et al. introduced electrochemical doping. PEDOT:Tos was set as the working electrode of an electrochemical cell and power factors up to 1270 μW m^{-1} K^{-2} were reached.[185] With such high power factor, the figure of merit was estimated to be approximately 1.02.

In the other way around, acids improve the electrical properties of PEDOT:PSS by washing off some excess PSS and/or further doping the material. In that later case, the electrical conductivity increases while the Seebeck coefficient decreases.[190]

Usually, thermopower and the electrical conductivity are interdependent and vary in opposite ways.[63] However, parallel increase of both features has also been reported and was attributed to different physical phenomena taking place into the material.[20,98,106] In 2013, Pipe and coworkers observed a simultaneous increase of both electrical conductivity and Seebeck coefficient of PEDOT:PSS after post-treatment with EG and DMSO. They showed that the transport took place by tunneling due to segregation after solvent addition, and that the removal of PSS after solvent treatment decreased the tunneling distances and hence increased the mobility. At the same time, the charge carrier density was reduced. As the mobility enhancement overwhelms the decrease in charge carriers, both benefits on electrical conductivity and Seebeck coefficient respectively were noticed and an in-plane figure of merit of 0.42 was found.[106] More recently, Kumar et al. observed the same phenomenon after treatment with sulfuric acid.[98]

Other ways to improve the thermoelectric performances of PEDOT include the doping with other counter-anions, the control of the pH of the processing solution and the hybridization of the material with inorganic semiconductors or carbon

nanomaterials.[104,192] By altering the nature of the counter-anion, Culebras and coworkers reported a figure of merit of 0.06 for PEDOT:BTFMSI (bis(trifluoromethylsulfonyl)imide), which was further improved up to 0.22 after reduction with hydrazine.[97] Numerous works on the intercalation of inorganic materials such as Bi_2Te_3, MoS_2, or carbon nanomaterials such as graphene and carbon nanotubes, into PEDOT were led in order to increase the thermopower of the composite results.[63,107,193]

All these progresses done on the improvement of the figure of merit of PEDOT through years are summarized in Figure IV.9.

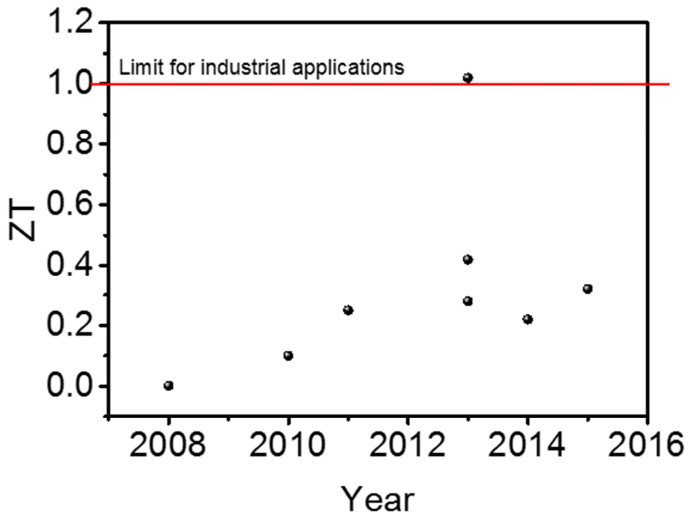

Figure IV.9. PEDOT films and their thermoelectric properties. The references are given in Appendix in Table D1.

N-Type conducting polymers are also investigated for thermoelectricity but they are less numerous than p-type ones. As a matter of fact, electrons are not easily injected in the LUMO (see Figure I.3) which is too high for electrons to be efficiently injected. Strategies developed in the literature include synthesizing polymers with electron-deficient building blocks, reducing the polymer with strong reducing agents, using n-type dopants such as (4-(1,3-dimethyl-2,3-dihydro-1H- benzoimidazol-2-yl)phenyl) dimethylamine (N-DMBI), developing metallo-organic complexes such as nickel-ethenetetrathiolates, or hybridizing with n-type inorganic materials.[194–199]

5. Conclusion and strategy

The industrial limit in order to develop viable thermoelectric devices at low temperatures corresponds to ZT = 1. Since its first introduction as thermoelectric material less than 10 years ago with ZT valuing 1.75 x 10^{-3}, tremendous efforts have been put in order to increase the thermoelectric efficiency of PEDOT. In PEDOT:PSS, enhanced power factors were obtained while treating with organic solvents since the increase of electrical conductivity was not accompanied with a deterioration of the Seebeck coefficient.

Best power factors and figures of merits were nonetheless obtained by optimizing the power factor while tuning the charge carrier density in PEDOT:Tos. As a matter of fact, the electrical conductivity increases and the Seebeck coefficient decreases with the increasing carrier density as shown in Figure IV.6. As synthesized PEDOT being already very oxidized, the main strategy developed in the literature naturally corresponds to the reduction of PEDOT in order to find the best set of thermoelectric properties that optimize the power factor. In that respect, reducing agents, electrochemical reduction and pH control of the oxidizing solution were all strategies that have proved their efficiency for enhancing the figure of merit of PEDOT.

The Seebeck coefficient has been less studied than the electrical conductivity in PEDOT films. It actually has not been studied but just reported and still remains a quite not understood property in organic materials. It is however clear that it strongly depends on the charge carrier density, and while failing to tune it separately from the electrical conductivity, it seems easier to optimize the electrical conductivity before un-doping the material and hence increasing the Seebeck coeeficient until an optimum power factor. With PEDOT:OTf and PEDOT:Sulf previously developed in our group and the conductivity enhancement we managed to achieve during this thesis, the electrical conductivity of our materials are optimized and we therefore aim to investigate the thermoelectric performances and enhance the power factor in this chapter.

From the two post-deposition electronic reduction strategies that have been developed in the literature, reducing agents do not allow a precise control of the doping level since the reduction after exposure to TDAE or hydrazine is quite instantaneous.

Consequently, we will address here the electrochemical reduction of PEDOT:OTf and PEDOT:Sulf for the optimization of their power factor after having reported their thermoelectric performances. Considering the results that will be reported here, further enhancement strategies will be enunciated.

6. Optimization of the thermoelectric properties of our PEDOT materials

6-1. Thermoelectric properties of PEDOT:OTf and PEDOT:Sulf

PEDOT:OTf and PEDOT:Sulf were synthesized by solution-cast polymerization as presented in Materials & Methods and deposited on 2.5 cm x 2.5 cm glass substrates. 7.75 wt. % NMP was added in the oxidative solution in order to optimize the electrical conductivity as reported in Chapter 1. The electrical conductivity was 3270 and 5240 S cm^{-1} respectively. Without the addition of NMP, the electrical conductivity was 1270 and 2270 S cm^{-1} respectively.

The Seebeck coefficient was measured with a dedicated apparatus, the Ulvac-RIKO ZEM-3, whose functioning is explained in Materials and methods. The setup is illustrated in Figure IV.10. The sample is placed in a thermostatic chamber under helium atmosphere. It is placed between two metallic blocks, one being set at room temperature and the other with a temperature made to vary thanks to a Joule heating resistance. Two drops of silver paints are deposited on the PEDOT films in order to allow a better contact between the thermocouples and the PEDOT. Those two thermocouples measure both the temperature gradient and the induced voltage for several temperature gradients. The absolute Seebeck coefficient of PEDOT is then deduced for those measurements after a calibration taking into account the Seebeck coefficient of the thermocouples. The as measured Seebeck coefficient is given with an uncertainty of 10 %.

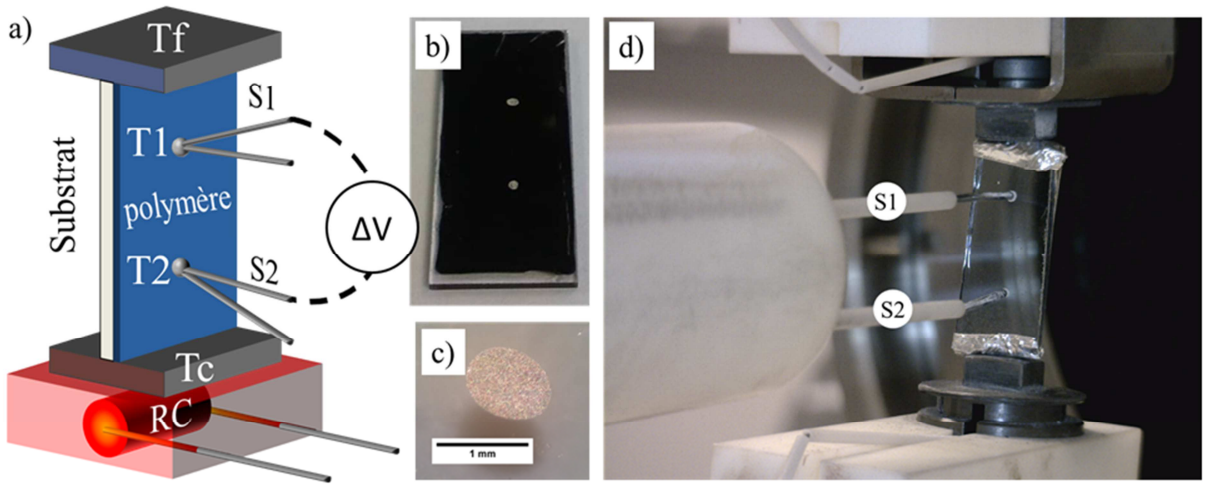

Figure IV.10. Thermopower measurements using ZEM-3. a) Schema of the experimental setup showing the sample, the metal blocks for temperature gradient (Tf = cold temperature and Tc = hot temperature) and the thermocouples for temperature and voltage measurements. b) Drops of silver paints for electrical contacts. c) Magnified image of a drop of silver paint. d) Experimental setup. Reproduced from[18].

Table IV.2. Thermoelectric properties of PEDOT:OTf and PEDOT:Sulf with and without the addition of NMP.

NMP	Materials	Electrical conductivity [S cm^{-1}]	Seebeck coefficient [μV K^{-1}]	Power factor [μW m^{-1} K^{-2}]
No	PEDOT:OTf	1218	17	35
	PEDOT:Sulf	2273	13	38
Yes	PEDOT:OTf	3278	23	177
	PEDOT:Sulf	5247	17	160

With such a setup, Seebeck coefficient of commercial PEDOT:PSS (Clevios PH1000) is measured at 19 μV K^{-1} as reported by Massonnet et al.[18] Without the addition of NMP, the Seebeck coefficient of PEDOT:OTf and PEDOT:Sulf is found to be 17 and 13 ± 10 % μV K^{-1} respectiveley. These values stay in the same order of magnitude than commercial PEDOT:PSS (PH1000). The decrease of the Seebeck coefficient after sulfuric acid treatment (in the case of PEDOT:Sulf then) is consistent with the increase of doping level that has been reported in Chapter 2. After the addition of NMP, the Seebeck coefficient of PEDOT:OTf and PEDOT:Sulf is respectively 23 and 17 ± 10 % μV K^{-1}. The results are summarized in Table IV.2. The same trend is

observed after acid treatment, always correlated with the increase of the doping level as calculated with XPS in Chapter 1. With the addition of NMP however, the Seebeck coefficient is slightly higher. We did not investigate the origin of such light enhancement given the too high uncertainty of the measurement, but if the change is real, it could be attributed to the semi-metallic nature of the polymer. Crispin and coworkers attributed the simultaneous increase of the electrical conductivity and the Seebeck coefficient in PEDOT:Tos to its semi-metallic nature. In a first approximation, the slope of the density of state near the Fermi level is associated to the Seebeck coefficient. At the same time, semi-metallic polymers have a low density of states around the Fermi level. Therefore, a small variation on the density of states can induce a huge variation in the Seebeck coefficient and sometimes, parallel increase of both electrical conductivity and thermopower. This hypothesis is yet to be confirmed in our measurements.

The power factor is calculated from the thermoelectric measurements and is given in Table IV.2 for all four materials. Due to their better electrical properties, PEDOT:OTf and PEDOT:Sulf obtained after the addition of NMP depict the best results, namely 177 and 160 $\mu W\ m^{-1}\ K^{-2}$ respectively. The benefit in electrical conductivity after acid treatment is however lost due to the concomitant decrease of the Seebeck coefficient, which results in a slightly lower power factor. These first results appear highly promising and the power factor could be optimized if the Seebeck coefficient was exceedingly enhanced compared to the decrease of electrical conductivity after reduction.

Regarding these first promising results then, electrochemical reduction for the optimization of the thermoelectric properties of our PEDOT films is very appealing. In the following, only the materials obtained after the addition of 7.75 wt. % NMP are studied.

6-2. Power factor optimization

6-2-1. Cyclic voltammetry (CV) on PEDOT:OTf and PEDOT:Sulf

For electrochemical reduction, PEDOT coated on a glass substrate was used as the working electrode in a three electrode cell. Since PEDOT was conductive enough, no conductive substrate was necessary. Information on the experimental setup can be found in Materials & Methods. The electrolyte and setup was calibrated with the couple ferrocene/ferrocenium (Fc/Fc^+). Cyclic voltammograms of both PEDOT:OTf

and PEDOT:Sulf can be found in Figure IV.11. CV was carried out in order to verify the oxido-reduction window of both PEDOT:OTf and PEDOT:Sulf. For each material, three CV were realized at a scan rate of 20 mV s^{-1} in order to verify the reversibility of the oxydo-reduction process. The reduction peak of PEDOT:OTf is found at -1 V and that of PEDOT:Sulf at -1.13 V. The oxidation peaks were found at -0.50 V and -0.55 V for PEDOT:OTf and PEDOT:Sulf respectively. The oxidation window of PEDOT:Sulf is slightly bigger than that of PEDOT:OTf and the charges' accumulation seems greater in the case of PEDOT:OTf. We however did not investigate those electrochemical considerations and were mainly interested in the working window for controlling the oxidation of our PEDOT materials.

Given the results, we decided to sweep the potential between -1.25 and -0.25 V using chrono-amperometry and applied the specific voltage for 20 s.

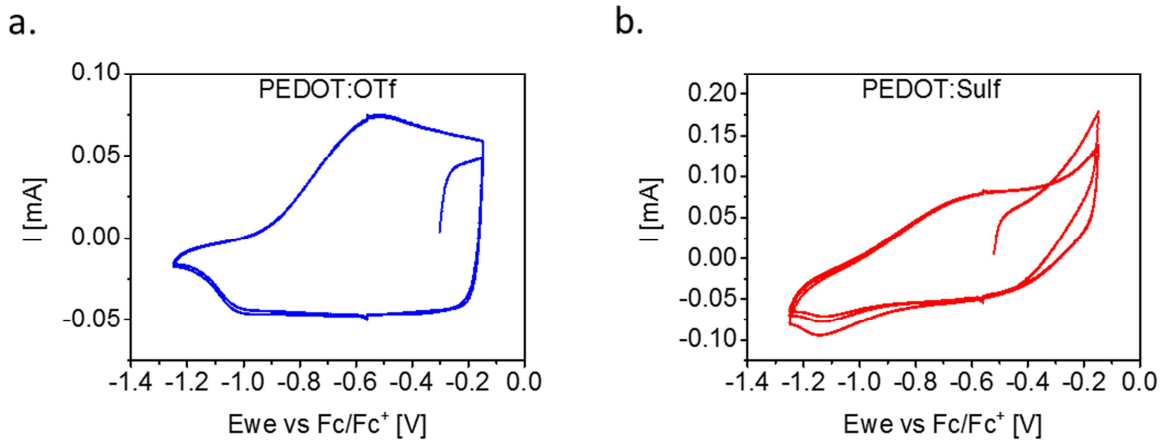

Figure IV.11. CV of PEDOT:OTf and PEDOT:Sulf.

6-2-2. Electrochemical reduction of PEDOT:OTf and PEDOT:Sulf

Each of the sample was made to undergo chrono-amperometry for 20 s at a specified voltage. Due to the electrochromic properties of PEDOT, the color of both PEDOT:OTf and PEDOT:Sulf changes from transparent blue to a darker blue color after reduction as shown in Figure IV.12a. The corresponding UV-Vis-NIR spectra are given in Figure IV.12b.

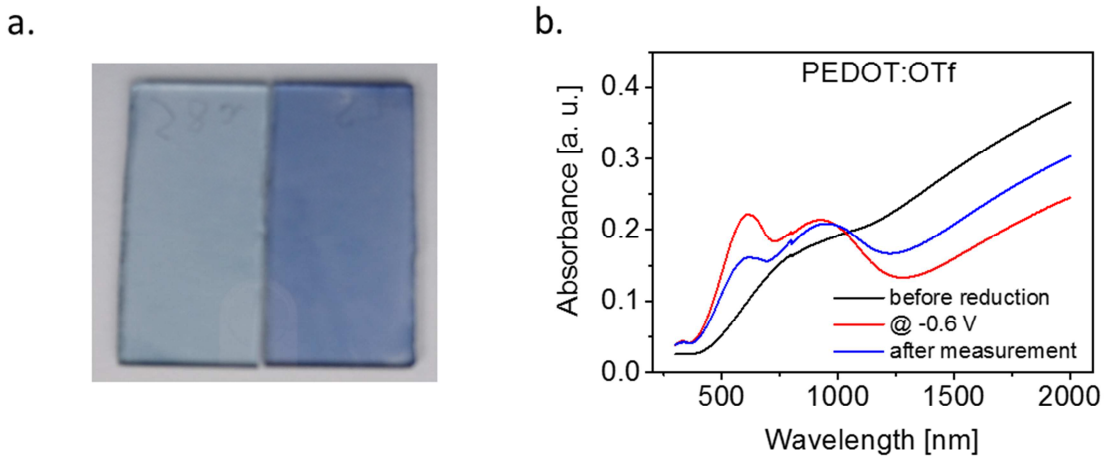

Figure IV.12. a) PEDOT:OTf before (left) and after (right) reduction at -1.15 V. b) UV-Vis-NIR of PEDOT:OTf before reduction, after reduction at -1.15 V and after the measurement of the Seebeck coefficient (the measurement took around 3 h).

We can see the decrease of bipolarons to the detriment of polarons and neutral chains, which shows that the film has been reduced. However, the reduction is not stable as can be seen in Figure IV.12b. As a matter of fact, UV-Vis-NIR experiments were repeated on the reduced sample after all thermoelectric measurements (roughly around 3 h after the electrochemical reduction). The absorbance of the polaronic chains remained slightly constant while that of the neutral chains decreased and that of the bipolarons increased. This is an indication that the polymer film regains more and more its original doping state. This instability has also been shown by Massonnet et al. who studied the stability of the reduction when exposed to sodium sulfite. They showed a rapid decrease of the neutral chains and increase of the polarons and bipolarons in the first five hours, with PEDOT:PSS films in the 10-12 µm thickness range. Given the fact that our materials are far thinner (less than 50 nm), such instability of the reduction is not surprising.

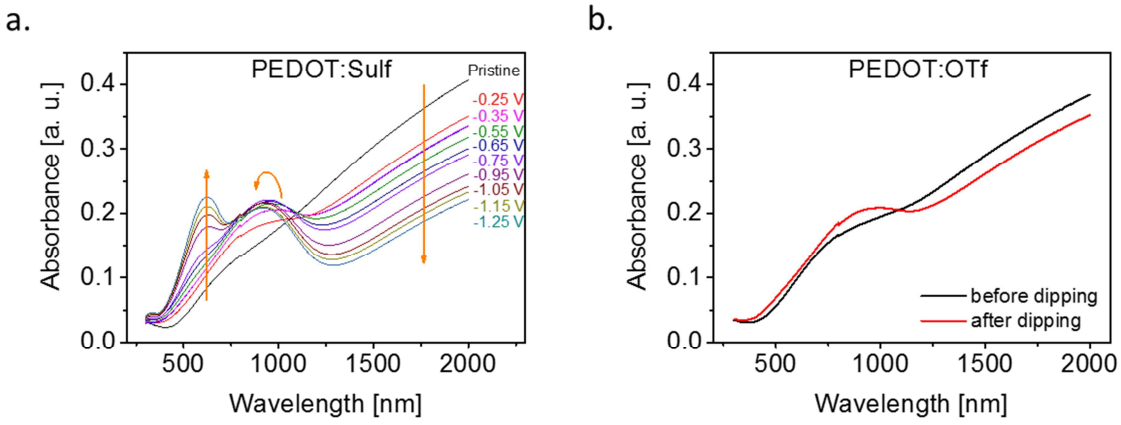

Figure IV.13. a) PEDOT:Sulf at different oxidation states when the applied bias in chronoamperometry is made to vary. b) Differences in the UV-Vis-NIR spectra of PEDOT:OTf before and after dipping in the electrolyte with any potential application.

Figure IV.13a depicts the UV-Vis-NIR spectra of PEDOT:Sulf at different oxidation states. Such curves were obtained by sweeping the working potential between -1.25 and -0.25 V (hence covering the oxido-reduction window). The pristine PEDOT:Sulf before dipping in the electrolyte was also displayed. It appears that the lower the potential is (going from the oxidation peak to the reduction one), the less bipolarons there is and the more neutral chains appear, coherent with a reduction process. The number of polarons however first increases before decreasing. This can be explained by the competition between more polarons originated from the bipolarons and less polarons due to their transition into neutral chains.

We can also note that at -0.25 V, the film is not at least as oxidized as its pristine form as one could guess regarding Figure IV.11 (oxidation peak at -0.55 V). This is probably due to an inherent reduction induced by the dipping into the electrolyte. As a matter of fact, when investigating the reduction state of PEDOT:OTf when dipped in the electrolyte without any potential application (Figure IV.13b), we note the disappearance of bipolarons to the detriment of polarons, sign of a less oxidized sample.

6-2-3. Thermoelectric properties of PEDOT at different oxidation levels

Having successfully reduced the films on several different oxidation levels, we now interest ourselves into their thermoelectric properties.

Samples of PEDOT:OTf (same for PEDOT:Sulf) were deposited on a glass substrate. Each sample was reduced at a different oxidation state. Due to the time consuming

nature of the experiments, the Seebeck coefficient was only measured once for each oxidation state. The thermoelectric properties of pristine PEDOT:OTf and PEDOT:Sulf are given in Table IV.3.

Table IV.3. Thermoelectric properties of pristine PEDOT materials.

Materials	Sheet resistance [Ω sq^{-1}]	Thickness [nm]	Electrical conductivity [S cm^{-1}]	Seebeck coefficient [μV K^{-1}]	Power factor [μW m^{-1} K^{-2}]
PEDOT:OTf	188.5	48	1396	15	31
PEDOT:Sulf	109.8	51	1788	8	12

A first surprising fact is the low electrical conductivities of PEDOT:OTf and PEDOT:Sulf compared to those enunciated in Chapter 2 or even in this chapter. All along the thesis, we have noticed a strong dependence of the electrical properties of our materials with the season. Winter samples depicted very good performances contrary to summer samples. The performances of autumn and spring samples were slightly random (or at least depended on the closest season). We do not have a scientific explanation of this bizarre observation yet.

The second striking fact is the lower Seebeck coefficients compared to those enunciated hereinbefore. These values were measured with a homemade apparatus since the ZEM-3 broke down. That setup was developed by another PhD student working on thermoelectric generators made of PEDOT.[174] The sample is maintained between two copper plates, one being cooled with tap water and the other being heated thanks to a heating block. The temperature gradient is measured with two K-type thermocouples and the voltage measured with a Keithley generator. Even though such setup was efficient in measuring the power generated by a thermoelectric generator, it is not assembled for absolute Seebeck coefficient measurement. As a matter of fact, the Seebeck coefficient of the thermocouples and wires is included in the measurement. Besides, the temperature gradient and the voltage are not measured at the exact same points as in ZEM-3. Moreover, the experiment is long (around 3h compared to 15 min for the ZEM-3), and as seen previously, the reduction state can be partially lost after 3 h. This technique is however enough to give an order of magnitude of the Seebeck coefficient and detect potential variations.

After being dipped in the electrolyte, the electrical conductivity of PEDOT:Sulf (in Table IV.3) is found to decrease down to 860 S cm^{-1}, its Seebeck coefficient to increase

up to 17 µV K^{-1} and its power factor up to 25 µW m^{-1} K^{-2}. These variations are coherent with the fact that the electrolyte already un-dope the PEDOT films.

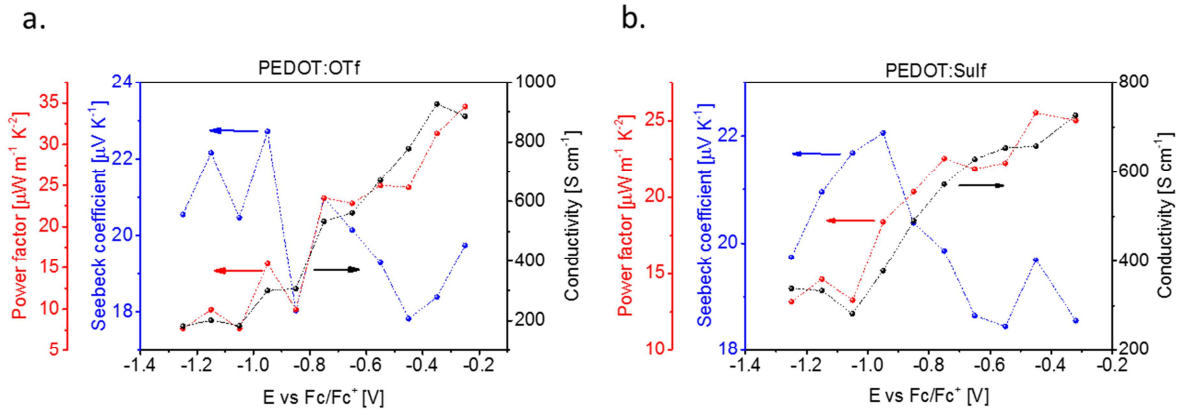

Figure IV.14. Thermoelectric properties of PEDOT:OTf and PEDOT:Sulf.

The thermoelectric performances of PEDOT:OTf and PEDOT:Sulf are given in Figure IV.14. For PEDOT:OTf and PEDOT:Sulf, the electrical conductivity decreases with the decreasing oxidation level until around -1 V, at the reduction peak. When the oxidation level increases however, the electrical conductivity does not surpass its pristine value. This might be due to the already un-doped state of the material when it is dipped in the electrolyte.

Around the oxidation peak, the Seebeck coefficient does not approach nor go under its pristine values, always correlated with the less oxidized material after dipping in the electrolyte. As the working electrode potential decreases, the Seebeck coefficient generally increases as expected, until the reduction peak at around -1 V, before being either stable for PEDOT:OTf, or decreasing for PEDOT:Sulf. The decrease of conductivity is however not accompanied with a subsequent increase of the Seebeck coefficient, so that the power factor is not optimized at all, but rather decreases.

7. Conclusion

Due to its good electrical conductivity, its moderate Seebeck coefficient and its theoretically low thermal conductivity, PEDOT has been investigated as a viable thermoelectric material. In this chapter, we have shown that the highly conductive

PEDOT films synthesized within our group have power factors reaching up to 177 µW m^{-1} K^{-2}. Such good thermoelectric property is slightly deteriorated after acid treatment since the increase in electrical conductivity is made to the detriment of the Seebeck coefficient.

Regarding the thermoelectric properties measured, we controlled the oxidation level in an electrochemical cell in order to optimize the power factor. The decrease of the electrical conductivity with the decreasing oxidation (due to a lower charge carrier density) is however not circumvented with a sufficient increase of the Seebeck coefficient so that the power factor is not optimized, reaching only 35 µW m^{-1} K^{-2} at its best. Moreover, several other problems were encountered, mainly the lack of an efficient characterization technique for thermopower measurement and the non-reproducibility of our results in summer. Besides, several questions still remain. What causes the non-reproducibility of the electrical conductivity around summer? How does the electrolyte un-dope our materials? A study of the Seebeck coefficient and the thermal conductivity is also still lacking. All these are questions to be dealt with for a proper understanding of the thermoelectric properties in PEDOT materials, and are ongoing works.

Though we did not succeed to prove the efficiency of PEDOT:OTf and PEDOT:Sulf as viable thermoelectric materials in this chapter, PEDOT:OTf-based thermoelectric generators were investigated by a PhD colleague and his interesting results can be read in his thesis soon online.[174]

Chapter 5
Stability and ageing mechanisms in PEDOT thin films

1. Introduction

One of the reasons behind the breakthrough of PEDOT is its stability.[44,200] Thanks to that advantage, several applications emerged and intensive studies dealt with the optimization and a better understanding of its properties, this thesis being one of them. When one describes PEDOT as stable, it usually means under a given repeated stress (such as the thermal cycles in Figure III.9) or that a drastic decrease of some properties (mostly the electrical conductivity) is not observed over time. However, several studies have shown that under some particular stresses, films of PEDOT do degrade. A decrease of the electrical conductivity in air, under thermal ageing, under light exposure and under humidity has been observed both in PEDOT:PSS and in PEDOT synthesized through electropolymerization.[201–204] Thermal ageing of PEDOT, electropolymerized and stabilized with $FeCl_4^-$, induced the oxidation of both the counter-ion and the sulfur of the backbone (shown by X-Ray photoelectron spectroscopy (XPS) and X-Ray absorption near edge structure spectroscopy (XANES)), hence leading to irreversible conductivity degradation.[201] In the case of PEDOT:PSS, thermal ageing induced phase segregation between PEDOT and PSS as inferred from transport measurements.[203] Under UV light exposure, XPS on PEDOT:PF_6 synthesized through electro-polymerization showed that the polymer reacts in air and forms sulfone groups in the thiophene units of PEDOT due to photo-oxidation.[204] PEDOT:PSS is also said to undergo photo-oxidation, a mechanism generally observed in conducting polymers since the carbenium is reactive with respect to oxygen.[40] The conjugation lengths are supposed to be shortened, hence leading to a decrease of the electrical conductivity.

The ageing of PEDOT films and the mechanisms remain however relatively unexplored particularly for the recently synthesized PEDOT films through vapor phase polymerization or solution-cast polymerization.[94] Recently Metsik et al. reported an interesting study of the degradation in VPP PEDOT:Tos under different atmospheres and at different temperatures.[116] They however could not correlate their experimental observations of the electrical conductivity degradation to any changes on the chemistry or structure of their material. Therefore, until now, a comprehensive study of the degradation mechanisms and their influence on the electronic transport properties is still lacking.

In that context this last chapter aims to study the degradation mechanisms and their impact on our PEDOT:OTf and PEDOT:Sulf materials and under different environmental stresses, namely under high humidity and under illumination equivalent of one sun exposure (AM 1.5 solar simulator, 1000 W m^{-2}). They will also be compared to commercial PEDOT:PSS materials. Degradation is a long process and ageing experiments should be carried out over several weeks. In that respect, experiments are still ongoing and only preliminary results are presented hereinafter. We will first observe the influence of different ageing conditions on the electrical conductivity of our materials and then we will investigate the chemical and structural changes that have taken place into the films and their influence on the electronic transport properties. A complete understanding of the degradation mechanisms cannot be proposed at that stage.

2. Degradation of the electrical conductivity

PEDOT:OTf and PEDOT:Sulf were synthesized by solution-cast polymerization and deposited on 2.5 cm x 2.5 cm glass substrate. NMP was added at 7 wt. % in the oxidative solution. Commercial PEDOT:PSS (Clevios PH1000) was also deposited by spin coating PEDOT:PSS dispersion and PEDOT:PSS-EG was afterward obtained by dipping PEDOT:PSS into ethylene glycol (EG). Details can be found in Materials & Methods in the appendix. In order to be comparable between the materials, multilayers were deposited until their specular transparence reached roughly 85 - 90 % at 550 nm. This is obtained for a bilayer or tri-layer deposition of each material and the electrical performances are similar to those in Chapter 3.

Figure V.1 displays the stability of PEDOT:PSS, PEDOT:PSS-EG, PEDOT:OTf and PEDOT:Sulf stored in the dark in a drawer at room temperature (RT) and ambient relative humidity (RH). In Figure V.1b, their sheet resistance Rs is normalized to its value at time t = 0 in order to compare the materials. Overall, the four materials are quite stable. After one month in a drawer, the degradation was only about 10 %. PEDOT:PSS and PEDOT:PSS-EG are more stable with only 4 and 7 % degradation of their electrical conductivity after 652 h. PEDOT:OTf and PEDOT:Sulf have a more pronounced degradation of about 10 % after 652 h.

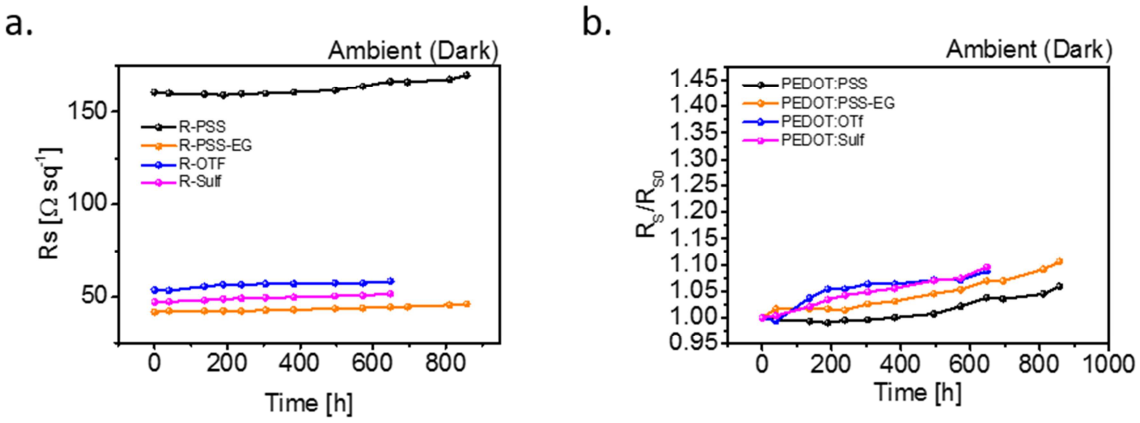

Figure V.1. Ageing in a drawer at room temperature and ambient humidity. The sheet resistance is displayed in a) while the ratio between the sheet resistance and its zero value is displayed in b) for the sake of comparison (normalized). In this figure and in the following ones, lines are drawn as a guide for the eyes.

PEDOT materials seem stable, but they are not meant to be stored in a drawer. Rather, applications such as transparent electrodes, deicing, or thermoelectric generators are targeted, applications in which they are likely to withstand harsh environmental conditions. We therefore investigated the materials under a high humidity exposure and a strong sun illumination. Ageing conditions can be found in Table V.1 and Figure V.2 summarizes the degradation of the electrical conductivity of our materials under those different ageing conditions studied.

Table V.1. Ageing conditions.

Conditions	Atmosphere	Temperature	Relative humidity
Ambient (dark)	Air	RT (between 20 °C and 25 °C)	Between 20 % and 30 %
Inert	Argon (glovebox) O_2 < 0.1 ppm	RT	H_2O < 0.1 ppm
Dry air	Dry air (desiccator)	RT	H_2O < some ppm
1 sun	Air	45 °C	15 %
1 sun – H_2O	Dry air (82 % N_2, 20 % O_2)	45 °C	H_2O < some ppm
1 sun – H_2O –O_2	Inert (N_2)	45 °C	H_2O < some ppm
Dry dark 50 °C	Air (furnace)	50 °C	5 %
Dark humid	Air + deionized water	38 °C	90 %

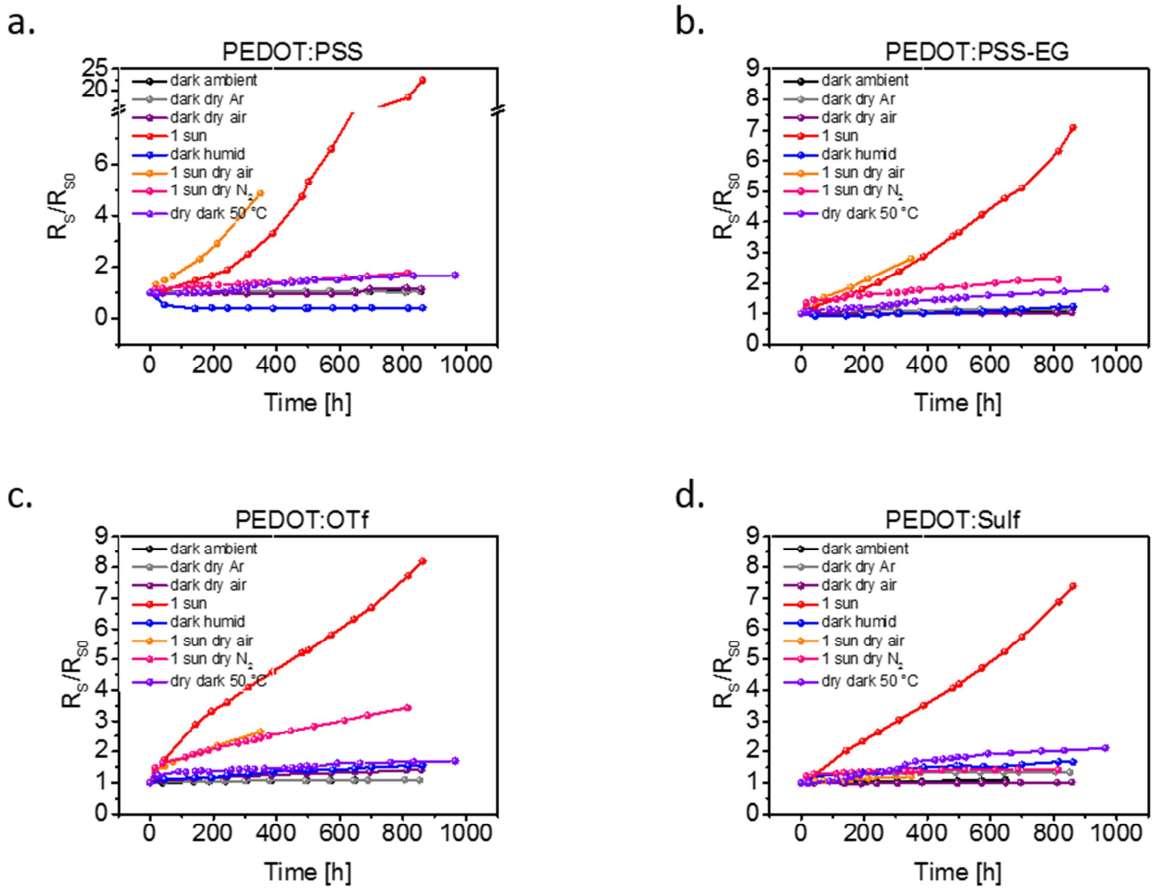

Figure V.2. Summary of the degradation of the sheet resistance (and hence electrical conductivity) of each PEDOT:PSS (a), PEDOT:PSS-EG(b), PEDOT:OTf (c) and PEDOT:Sulf (d) under different ageing conditions.

Overall, the materials are quite stable when stored in the dark at ambient temperature and ambient relative humidity, losing only up to 10 % of their conductivity after 800 h. In the case of PEDOT:PSS and PEDOT:PSS-EG, the electrical degradation is also not important when they are stored in a desiccator under dry air or in a glovebox under argon. Under high humidity and always in the dark, the electrical conductivity of PEDOT:PSS is highly increased (+ 65 %) in the first 100 hours before being stable, probably due to ionic conductivity. This is due to the well-known hydrophilic nature of PEDOT:PSS which retains water after a certain extent of water exposure.[23,79,205] In the case of PEDOT:PSS-EG, the electrical conductivity is slightly enhanced (+ 8 %) in the first 45 h before decreasing slightly following the same trend than when it is stored in a desiccator. The lower increase of the ionic conductivity compared to PEDOT:PSS could be explained by a reduced amount of excess PSSH.[92,206] A huge degradation of the conductivity is observed when the samples are illuminated under one sun at ambient

conditions (-2250 % and -709 % after 865 h for PEDOT:PSS and PEDOT:PSS-EG respectively). The same huge degradation is also observed after illumination under dry air, but not at all under an inert atmosphere. The degradation observed under the inert atmosphere seems to be due to the increase of temperature during the sun illumination as suggested by thermal ageing in the dark and at a temperature similar to the one under the solar simulator (50 °C). Hence, for PEDOT:PSS and PEDOT:PSS-EG, the high temperature and the combination of illumination and oxygen seem to be the main causes of electrical degradation.

In the case of PEDOT:OTf and PEDOT:Sulf, the electrical conductivity is also stable when they are stored in the dark in ambient atmosphere, in a desiccator under dry air or in a glovebox under argon (-10 % after 652 h).The degradation is however higher for PEDOT:OTf in the desiccator (-40 % after 855 h) and PEDOT:Sulf in the glovebox (-27 %). This can be due to the pumping, combined with either the presence or the absence of oxygen. The electrical conductivity is deteriorated under humidity exposure (-58 % and -68 % after 865 h for PEDOT:OTf and PEDOT:Sulf respectively) and after thermal ageing (-68 % and 205 % respectively). Here too, the degradation is more pronounced under one sun illumination. While the illumination under a dry environment highly preserves PEDOT:Sulf, PEDOT:OTf is only slighty protected. Here, the main causes of degradation seem to be high humidity, the high temperature and the combination of illumination and humidity. The illumination seems however to be more detrimental to PEDOT:OTf.

The ageing experiments under different conditions showed us that humidity, thermal ageing and particularly sun exposure are the most detrimental conditions for all materials. The reasons behind the electrical degradations could be either chemical or structural. In the following then, we will investigate the influence of humidity and sun exposure on the chemistry and structure of PEDOT:PSS-EG, PEDOT:OTf and PEDOT:Sulf. The thermal ageing will not be studied, and PEDOT:PSS, whose chemistry and structure is similar to PEDOT:PSS-EG, except for the excess PSSH, will not be studied here either.

3. Chemical changes

In the following, two layers of each material are deposited and all samples have been aged for three weeks in a humid climatic chamber (38 °C, 90 % RH) or under one sun

illumination (AM 1.5, 1000 W m^{-2}, 45 °C, 15 % RH). The aforementioned studies allowed us to state that most changes that appear after humidity ageing are due to the presence of water for all samples, and that most changes that appear after sun exposure are due to the heating and the combination of the illumination and ambient humidity in the case of PEDOT:OTf and PEDOT:Sulf, and the combination of the illumination and oxygen in the case of PEDOT:PSS-EG. The degradation could also be due to oxygen species adsorbed at the surface of the materials. The presence of oxygen will therefore not be totally ignored.

3-1. Doping level variations

The UV-Vis-NIR spectra of PEDOT:OTf, PEDOT:Sulf and PEDOT:PSS-EG can be found in Figure V.3. It is striking that the charge carriers were strongly impacted in both environments. After humidity ageing, the quantity of bipolarons decreases, some neutral chains appear while the quantity of polarons stays roughly constant in the case of PEDOT:OTf, or increases in the case of PEDOT:Sulf and PEDOT:PSS-EG. Comparing these observations to what has already been seen after electrochemical reduction in Chapter 4, one plausible cause is the competition between the conversion of bipolarons into polarons and neutral chains, and the disappearance of polarons that form neutral chains.

After sun exposure, neutral chains do not seem to have been formed in any sample and both polarons and bipolarons decrease, except for PEDOT:PSS-EG where they both increase. Thus all materials seem to undergo un-doping or disappearance of charge carriers after sun or humidity exposure, except for PEDOT:PSS-EG aged under illumination.

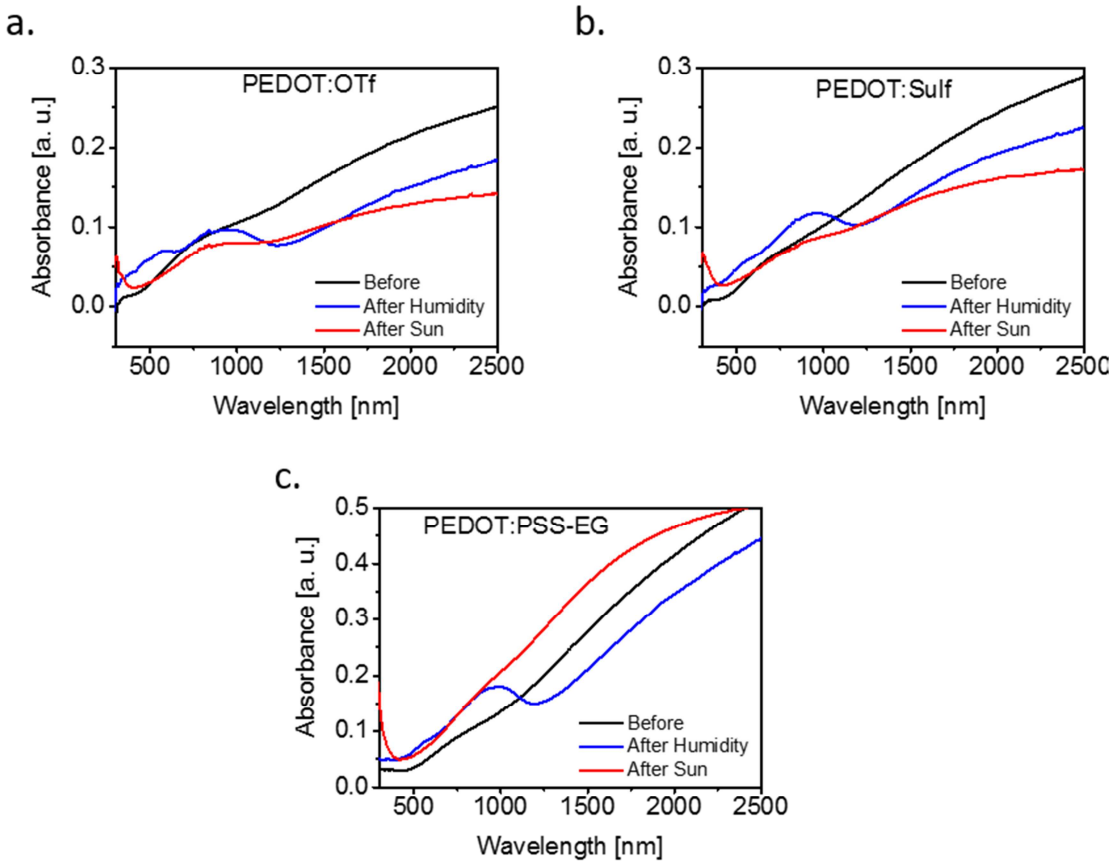

Figure V.3. UV-Vis-NIR spectra of PEDOT:OTf (a), PEDOT:Sulf (b) and PEDOT:PSS (c).

Raman measurements were recorded in order to better assess the changes in charges carriers that are noticed. For each sample, several measurements at different points on the samples were recorded in order to assess the uniformity, and then averaged since a good uniformity was confirmed. Figure V.4 displays the Raman spectra of PEDOT:OTf, PEDOT:Sulf and PEDOT:PSS-EG before ageing. The silicon substrate was detected (521 cm^{-1}), which means that the samples were investigated in their whole depth.[207] The attribution of Raman shifts in PEDOT can be found in Table V. 2.

Table V. 2. Raman shift in PEDOT materials.[76,204,208–212]

Raman shift [cm^{-1}]	Vibration
215 to 1096	Deformation and bending of oxyethylene ring mostly
701	C-S-C deformation
1258	C_α-$C_{\alpha'}$ (interring) stretching
1421	symmetric C_α=C_β stretching
1413	neutral C_α=C_β symmetric stretching
1444	oxidized C_α=C_β symmetric stretching
1511 to 1557	asymmetric C_α=C_β stretching

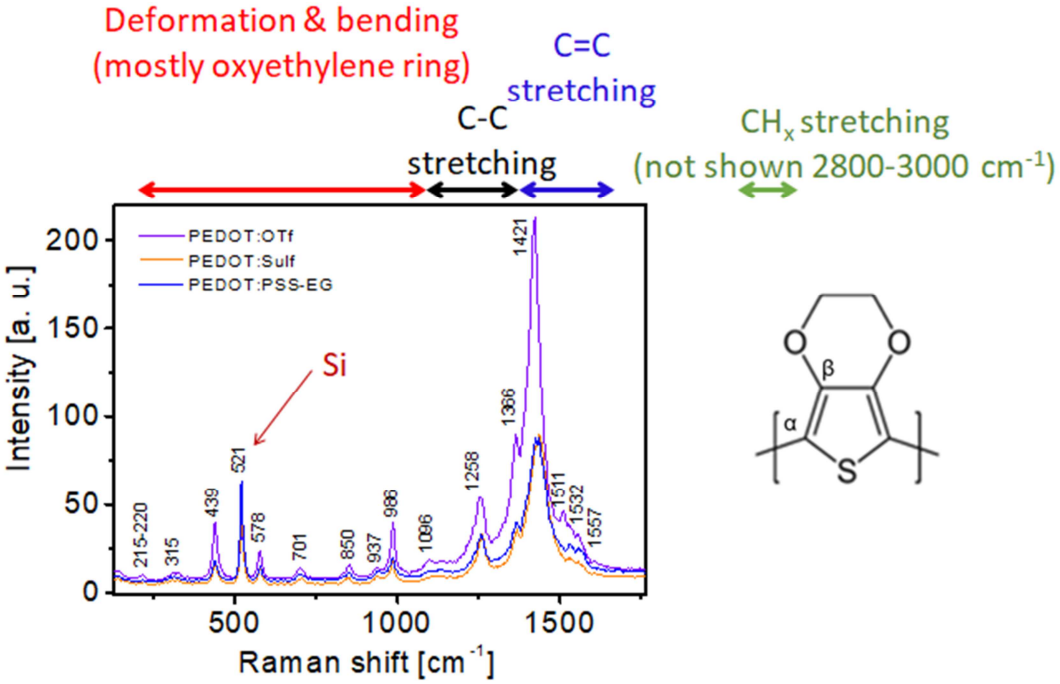

Figure V.4. Raman spectra of PEDOT:OTf, PEDOT:Sulf and PEDOT:PSS-EG before ageing. The Raman shifts induced by the different vibrations in the silicon substrate and in the PEDOT materials are attributed. PEDOT structure is also displayed for the sake of clarity of the different stretchings.

Figure V.5 gives the low resolution Raman spectra of PEDOT:OTf, PEDOT:Sulf and PEDOT:PSS-EG before and after ageing. Only few modifications are noticed after humidity ageing while sun exposure seems to have more impact. In the range 100 – 1100 cm^{-1}, a slightly higher intensity is noticed for PEDOT:OTf and PEDOT:PSS-EG

after sun exposure at 701 cm^{-1} (corresponding to C-S-C deformation). Except for that, no obvious notification is noticed in the range 100 – 1100 S cm^{-1}. This suggests that the structure of the rings is not highly perturbed. More impact of the ageing is however noticed in the C=C stretching region, especially for sun-aged samples.

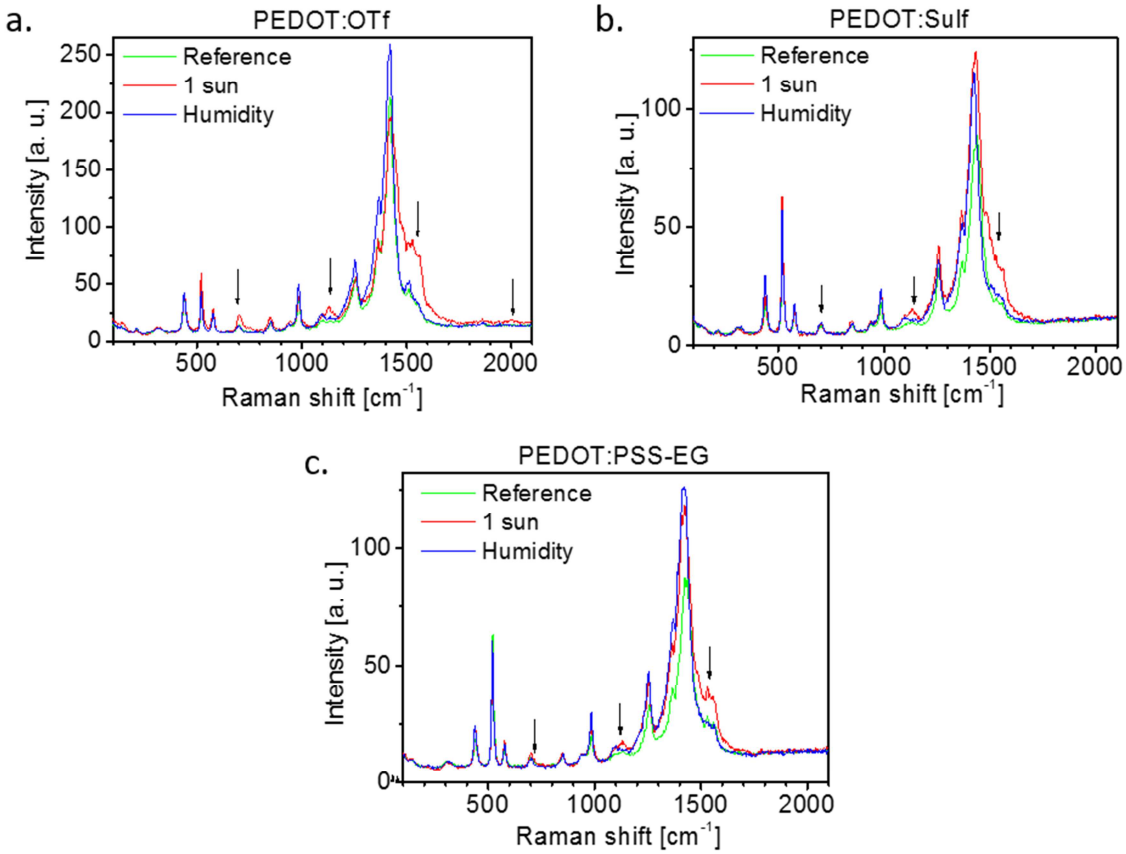

Figure V.5. Low resolution Raman spectra of PEDOT:OTf (a), PEDOT:Sulf (b) and PEDOT:PSS-EG (c) before and after ageing.

Figure V.6 depicts a typical high resolution spectra of PEDOT in the range 1100 – 1700 cm^{-1}. The C-C peaks are unchanged upon doping but the C=C ones are known to shift. As a matter of fact, neutral $C_\alpha=C_\beta$ symmetric stretching (benzenoid form in Figure V.6) is found at 1413 cm^{-1} while oxidized $C_\alpha=C_\beta$ symmetric stretching (quinoid form in Figure V.6) appears at 1444 cm^{-1}.[213] If the deconvolution of both contribution is well done, one could assess a doping level (ratio quinoid/benzenoid contribution). The deconvolution is however not straightforward and it is easier to deal with the shift of the main C=C symmetric stretching toward 1413 cm^{-1} (neutral chains) or 1444 cm^{-1} (oxidized chains). Therefore, a blue shift (to higher wavenumbers) is

associated with higher doping of PEDOT, oxidation, and a shift from benzenoid to quinoid form.[209,211]

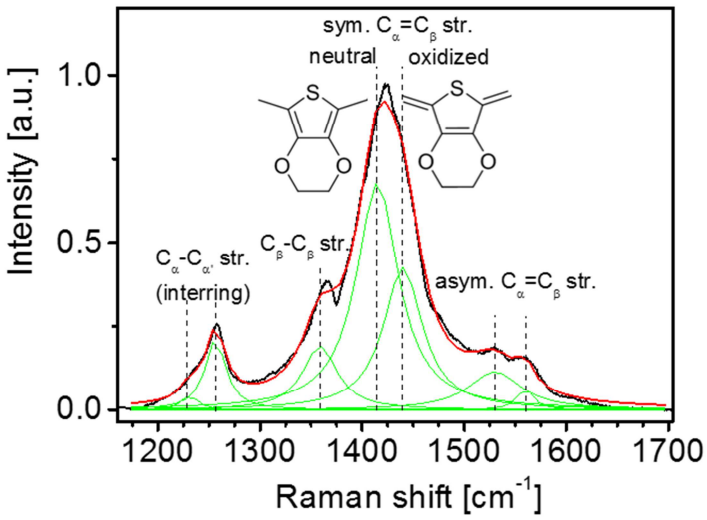

Figure V.6. Deconvolution of C=C stretching Raman shift. The black curve represents experimental values for non-aged PEDOT:OTf. The green curves are the deconvolutions of the different contributions and the red curve represents the fit which sums all green curves. Associated Raman shifts and PEDOT structure are also represented.

Figure V.7 displays the shift of the peak of the symmetric C_α=C_β position before and after ageing. When comparing only reference samples, it appears that the PEDOT:Sulf is the most doped sample and PEDOT:OTf the less doped one. This is coherent with the doping levels that we have measured at 38 % and more for PEDOT:OTf and PEDOT:Sulf respectively. The comparison with PEDOT:PSS-EG is more difficult due to the presence of excess PSS.[56,60] After ageing, the red shift noticed in Figure V.7 corresponds to a systematic de-doping of PEDOT:Sulf and PEDOT:PSS-EG both under humidity and sun exposure, with however a more pronounced impact on humidity-aged samples. This red shift is in accordance with the decrease of charge carriers as shown with UV-Vis-NIR in Figure V.3. In PEDOT:OTf however, only a slight de-doping is observed after ageing under humidity and a strong doping after ageing under one sun. Two contradictions remain between Raman and UV-Vis-NIR measurements, the blue shift (and hence oxidation) observed in sun-aged PEDOT:OTf (Figure V.7) compared to the decrease of charge carriers (and hence reduction)

suggested by UV-Vis-NIR (Figure V.3), and the red shift (and hence reduction) observed in sun-aged PEDOT:PSS-EG (Figure V.7) compared to the increase of charge carriers (and hence oxidation) suggested by UV-Vis-NIR (Figure V.3).

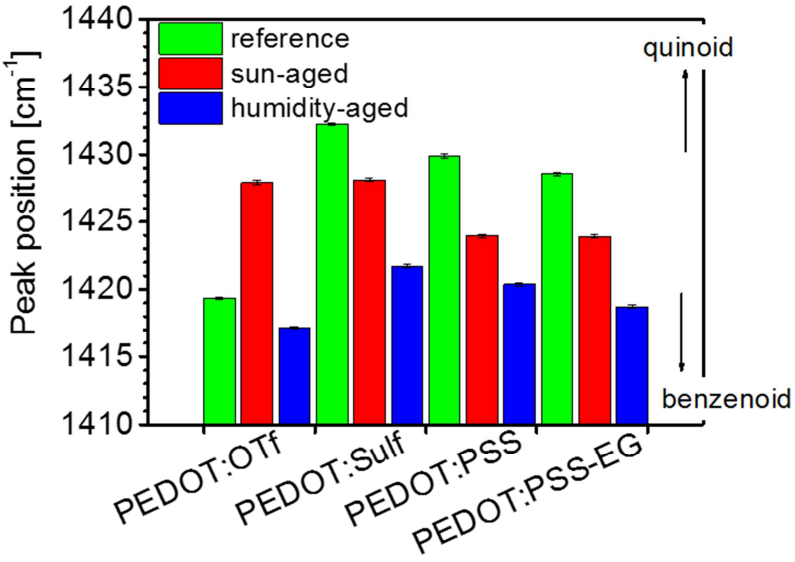

Figure V.7. Peak position of the symmetric C=C stretching in PEDOT materials before and after ageing.

3-2. Chemical variations

Changes in the chemical structure of PEDOT materials were assessed through X-Ray photoelectron spectroscopy (XPS). The survey spectra of PEDOT:OTf, PEDOT:Sulf and PEDOT:PSS-EG can be found in Figure V.8. XPS spectrum of PEDOT:PSS-EG was not recorded before ageing. As expected, fluorine is present in PEDOT:OTf and is absent in PEDOT:Sulf and PEDOT:PSS-EG. The humidity-aged PEDOT:Sulf sample displays however a quite intense fluorine peak, but also a comparatively higher intensity of oxygen or sulfur compared to other samples. This difference is then a scale artefact. Sodium is present in all sun-aged samples and in humidity-aged PEDOT:PSS-EG. Since sodium is not detected in non-aged sample, even for PEDOT:PSS-EG as previously reported by Massonnet, this is attributed to a contamination.[18]

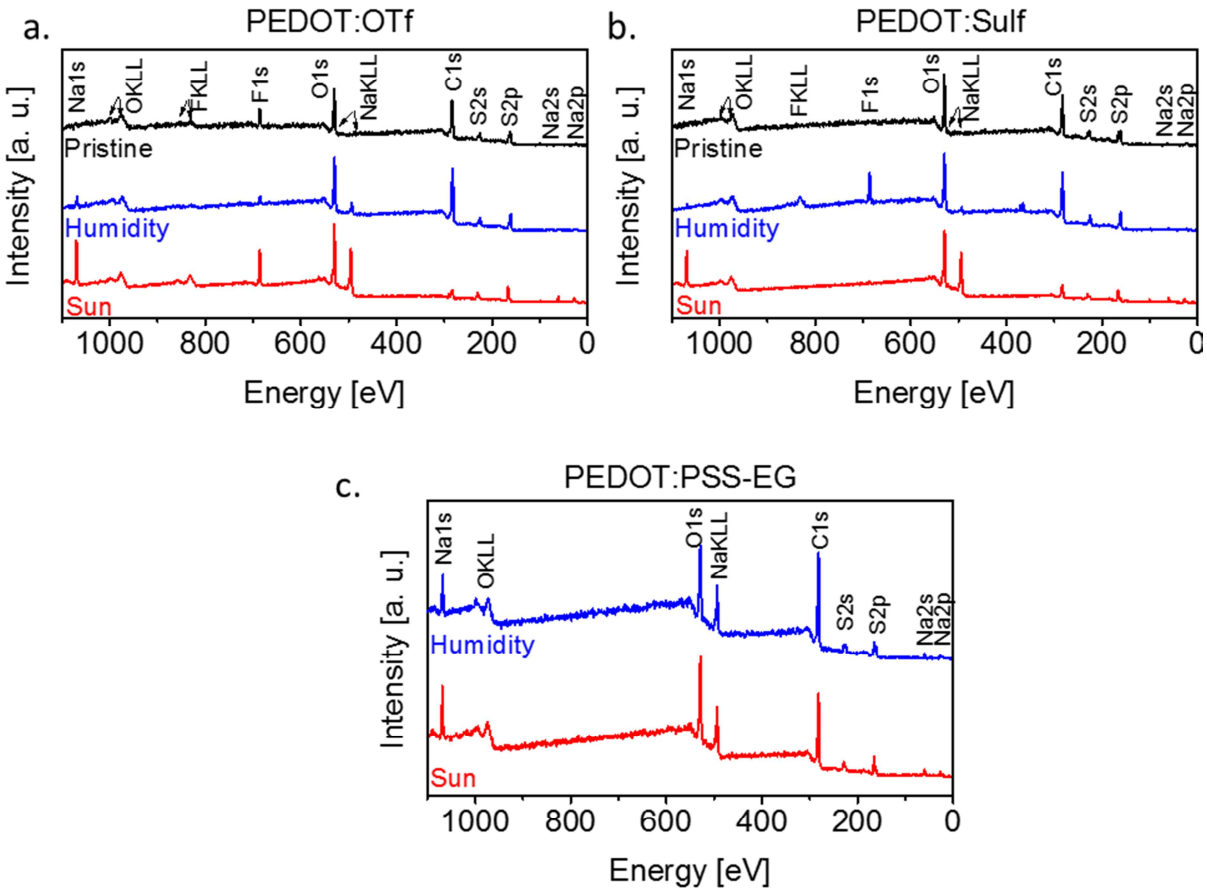

Figure V.8. XPS survey spectra of PEDOT:OTf (a), PEDOT:Sulf(b) and PEDOT:PSS-EG (c) before and after ageing.

3-2-1. PEDOT:OTf

Figure V.9 displays the high resolution spectra of some elements in PEDOT:OTf, namely sulfur, carbon and oxygen. Corresponding fits are also given in the lower curves.

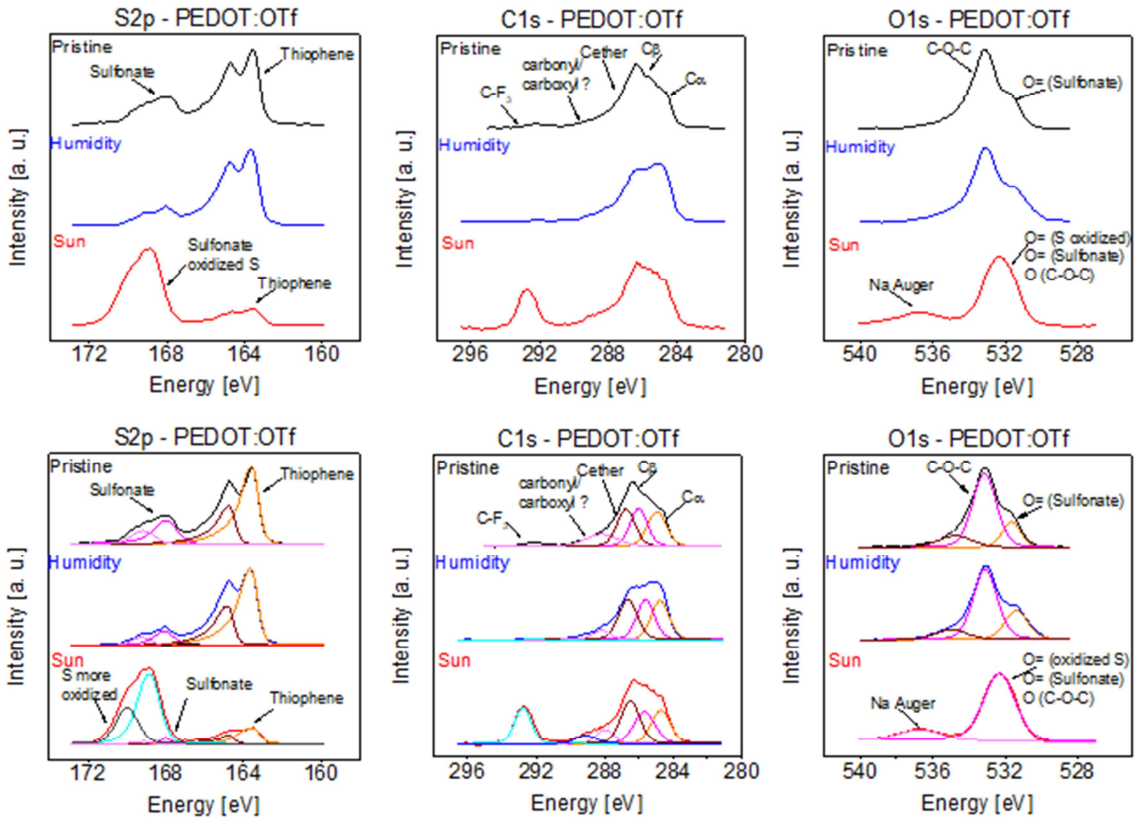

Figure V.9. S2p, C1s and O1s XPS spectra of PEDOT:OTf. Corresponding fits are given in the lower curves as a guide for the eyes.

In the S2p XPS spectrum of non-aged PEDOT:OTf in Figure V.9, the peaks at 163.6 eV and 164.7 eV are attributed to the thiophene ring while the peaks at 167.9 eV and 169.2 eV are attributed to sulfonates in the triflate counter-anions.[10,204] The same peaks are still present after ageing, but the contribution of the sulfonates is highly reduced. The ratio sulfonate/thiophene decreases from 38 % for non-aged PEDOT:OTf to 18 % for humidity-aged PEDOT:OTf and 17 % for sun-aged PEDOT:OTf. Moreover, a new sulfur contribution appears at 168.8 eV and 170.0 eV after sun ageing. It corresponds to a more oxidized state of sulfur that we attribute to sulfates. This new peak accounts for 78 % of the total sulfur contribution. In humidity-aged PEDOT:OTf, the decreased ratio indicates a decreased oxidation level after humidity ageing as also suggested by UV-Vis-NIR and Raman spectroscopy. In the case of sun-aged sample, the origin and role of the sulfates that have appeared are yet to be confirmed. They could act both as a counter-anions, hence increasing the doping level, or another phase, hence reducing the doping level.

The peak related to carbonyl or carboxyl groups appears around 288.0 eV in the C1s spectra and is present in all samples, aged or not, so that it cannot be correlated to ageing mechanisms. In the O1s spectra, the oxygen peak seems slightly shifted toward lower energies. This shift could be attributed to oxygen in a less oxidized state that in C-O-C, sulfates for example.

3-2-2. PEDOT:Sulf

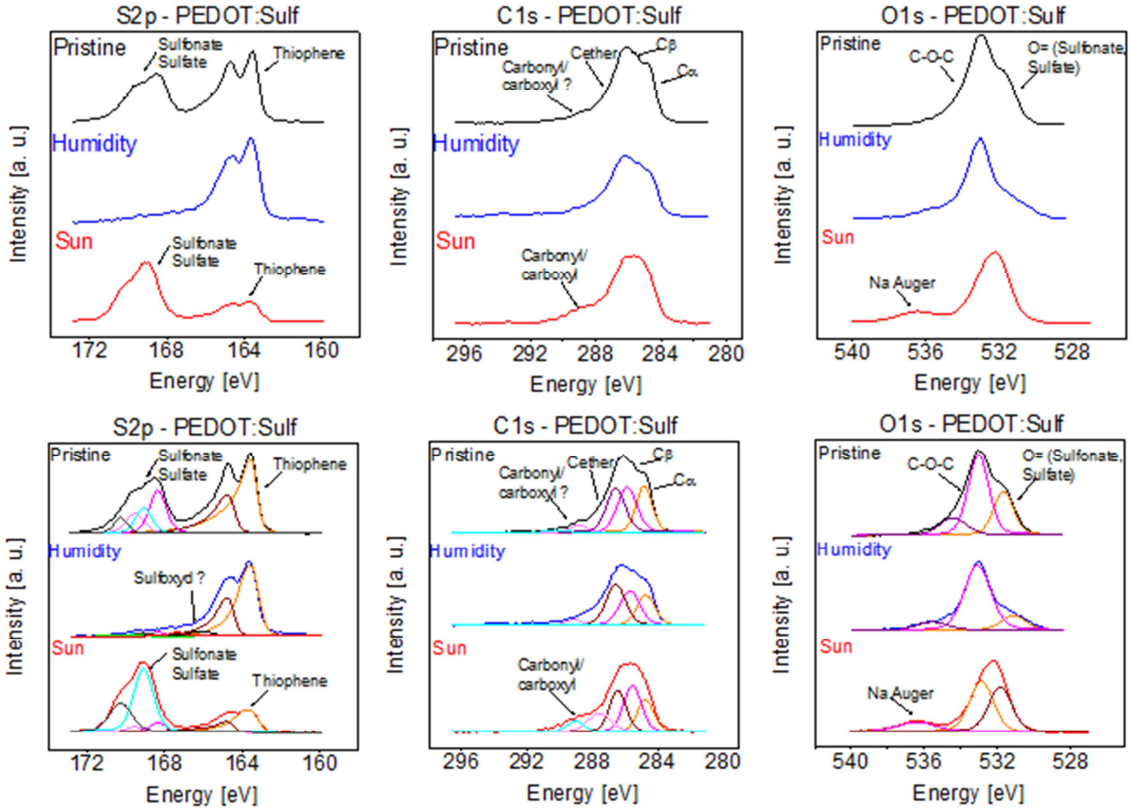

Figure V.10. S2p, C1s and O1s XPS spectra of PEDOT:Sulf. Corresponding fits are given in the lower curves as a guide for the eyes.

In S2p spectra of PEDOT:Sulf in Figure V.10, thiophene and sulfonate and hydrogeno-sulfates contribution are distinguishable. Under humidity ageing however, the counter-anion contribution seems to be highly lessened, decreasing from 62 % to 8%. Moreover, a new doublet appears around 166.2 and 167.4 eV, which we attribute to sulfoxides. After sun exposure, the contribution of sulfonate is highly reduced while that of sulfates is strongly increased.

In Figure V.10, the higher atomic concentration of oxygen in sun-aged PEDOT:Sulf, 50 % compared to 32 % for non-aged PEDOT:Sulf and 26 % for humidity aged PEDOT:Sulf, comforts the apparition of sulfates in sun-aged PEDOT:Sulf similarly to PEDOT:OTf.

PEDOT:PSS-EG

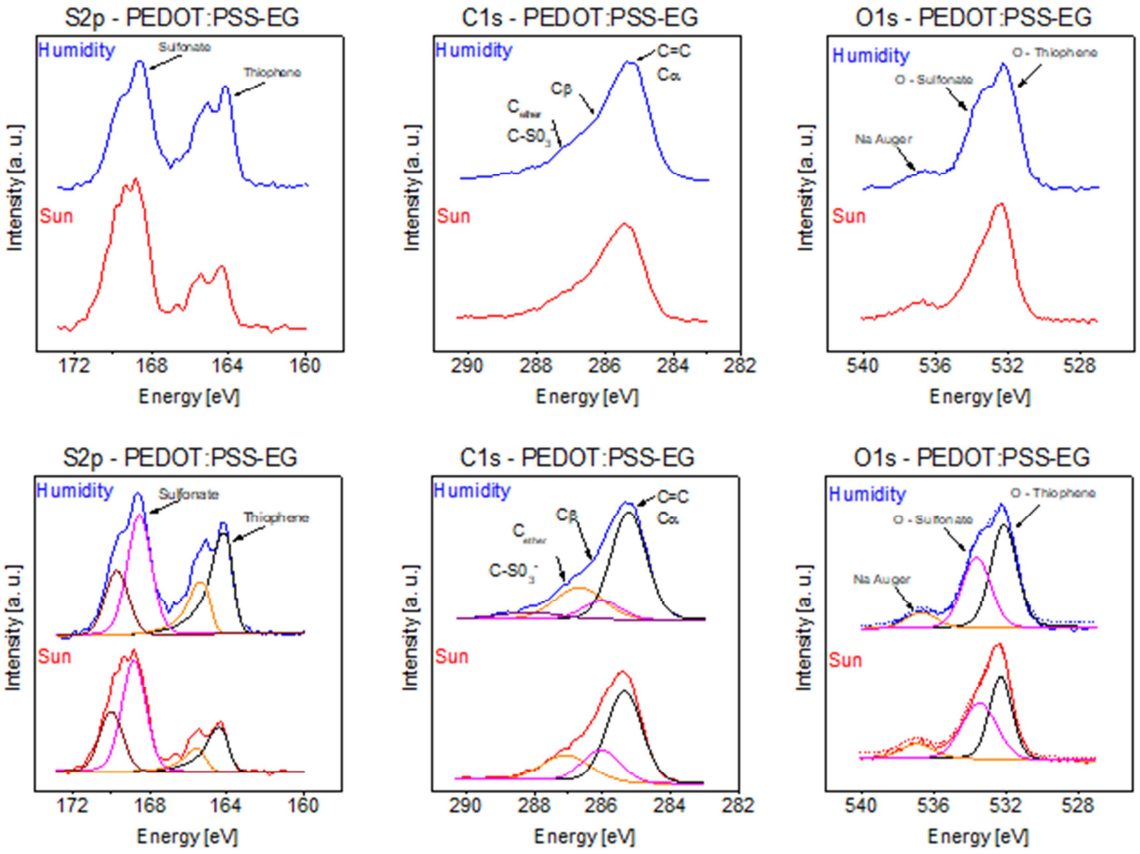

Figure V.11. S2p, C1s and O1s XPS spectra of PEDOT:PSS-EG. Corresponding fits are given in the lower curves as a guide for the eyes.

In Figure V.11, the absence of non-aged sample data for PEDOT:PSS-EG hinders a comparison between samples. Here too, the strong contribution of carbonyl or carboxyl groups in the C1s spectra in both ageing conditions does not allow to attribute their presence to a specific ageing condition. In the S2p spectrum however, the relatively low thiophene concentration in the sun-aged sample suggests the apparition of highly oxidized sulfur. In the literature, sulfone groups appear upon UV exposure (R-SO2-R'), as well as carbonyl and carboxyl groups.[204,212] Since such groups appear at lower energy than sulfonates and since we rather observe a shift to higher energies, we then attribute

the more oxidized sulfur observed to sulfates similarly to sun-aged PEDOT:OTf and PEDOT:Sulf.

3-3. Discussion

Under humidity ageing, we notice a disappearance of the counter-anions in all samples which is consistent with the decrease of charge carriers suggested by UV-Vis-NIR, and the transformation from quinoid to benzenoid conformation proved by Raman spectroscopy. This might suggest that the counter-anions are washed off the films as suggested by their disappearance in XPS spectra. However such phenomenon cannot be explained yet regarding the experimental procedure.

After ageing under one sun, sulfates are detected in all samples. The origin of sulfates and their role is yet to be determined. Given the presence of sodium in the survey spectra of sun-aged PEDOT in Figure V.8, we could expect a salt between sodium and sulfates.

4. Structural Changes

GIWAXS measurements were led on PEDOT:OTf, PEDOT:Sulf and PEDOT:PSS-EG, both before and after ageing. In-plane and out-of-plane measurements were recorded as explained in Chapter 2 and in Materials & Methods. In-plane and out-of-plane GIWAXS measurements are displayed in Figure V.12 for humidity ageing and in Figure V.13 for sun ageing.

Indexation of all peaks can be found in Chapter 2 and an explanation of the data treatment in Appendix. Under humidity ageing (Figure V.12), no changes appear in the diffraction patterns of PEDOT:OTf (both in-plane and out-of-plane) which means that both the π-π stacking and the lamellar stacking are preserved. In the case of PEDOT:Sulf, the π-π stacking is preserved while the lamellar stacking is strongly impacted. The intensity decrease of the diffraction peaks upon increasing 2θ traduces a higher degree of strain in the crystalline lattice. In PEDOT:PSS-EG also the π-π stacking seems preserved. The peaks in the out-of-plane diffraction patterns are too broad to give any quantitative information. The decrease of intensity and the broader peaks after ageing in humidity suggest a softer structure perpendicularly to the plane of the film.

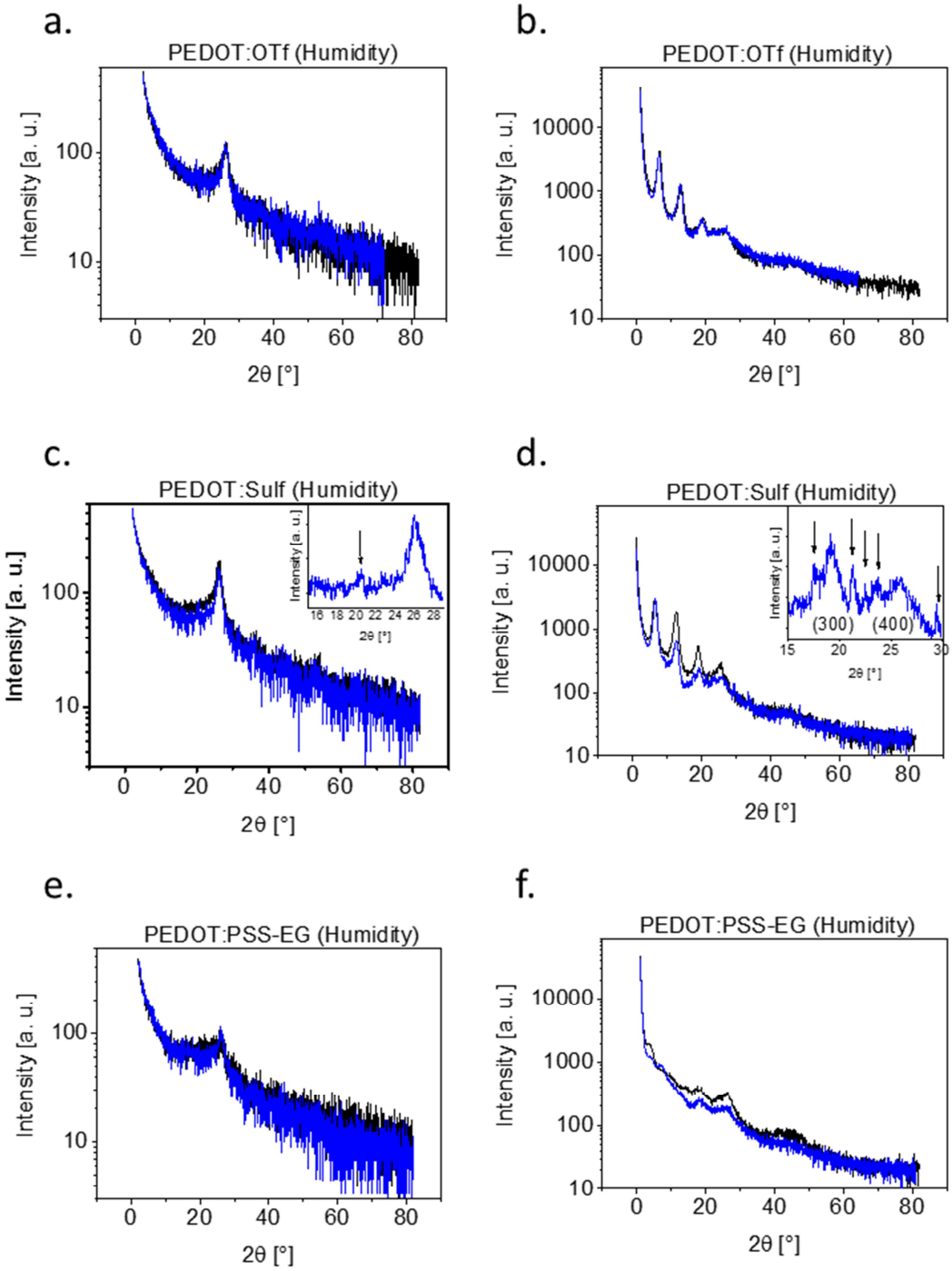

Figure V.12. GIWAXS measurements on PEDOT materials before (black curves) and after humidity (blue curves) ageing. In-plane diffraction patterns of PEDOT:OTf (a), PEDOT:Sulf (c) and PEDOT:PSS-EG (e). Out-of-plane diffraction patterns of PEDOT:OTf (b), PEDOT:Sulf (d) and PEDOT:PSS-EG (f). In the diffraction patterns of PEDOT:Sulf aged under humidity (c,d), new coherent structures are detected. The inset in those figures depicts the peaks of that new structure.

Under sun exposure (Figure V.13), the lamellar order of PEDOT:OTf is preserved but a strong decrease of the π -π stacking peak intensity is observed. This traduces the loss of the coherence in this ordering. In sun-aged PEDOT:Sulf, similar observations can be made regarding the π-π stacking. Concerning the lamellar stacking, the intensity of the peak decreases upon increasing 2θ similarly to humidity-aged PEDOT:Sulf but less pronounced. The π-π stacking of sun-aged PEDOT:PSS-EG is also strongly impacted but no remarkable changes are noticeable in the out-of-plane diffraction patterns.

For all PEDOT:OTf and PEDOT:Sulf samples, the crystallite size associated to the lamellar order is of the order of 9 nm and the degree of stain varies from 5% up to 10%.

New diffraction peaks appear in humidity-aged PEDOT:Sulf and after sun exposure in all samples. They are present at 2θ = 16.9 °, 20.3 °, 23.1 ° and 31.7 ° as shown in the insets in Figure V.13c,d. This indicates the presence of a new crystalline phase which developed under sun exposure and in the case of humidity-aged PEDOT:Sulf. Regarding the chemical elements as well as the sulfate groups detected by XPS, a probable candidate is $NaHSO_4$. Ongoing works will help us define better the structure.

In summary, after ageing under humidity, changes on PEDOT:OTf are not remarkable, PEDOT:PSS-EG becomes softer and a new isotropic crystalline phase appears in PEDOT:Sulf, whose structure is slightly destroyed in the lamellar direction.

After ageing under one sun, that new isotropic crystalline phase appears in all samples. Moreover the π-π stacking and the lamellar stacking are unchanged but the overall coherence of the structure is lost, probably due to disorder induced by the apparition of the new crystalline phase.

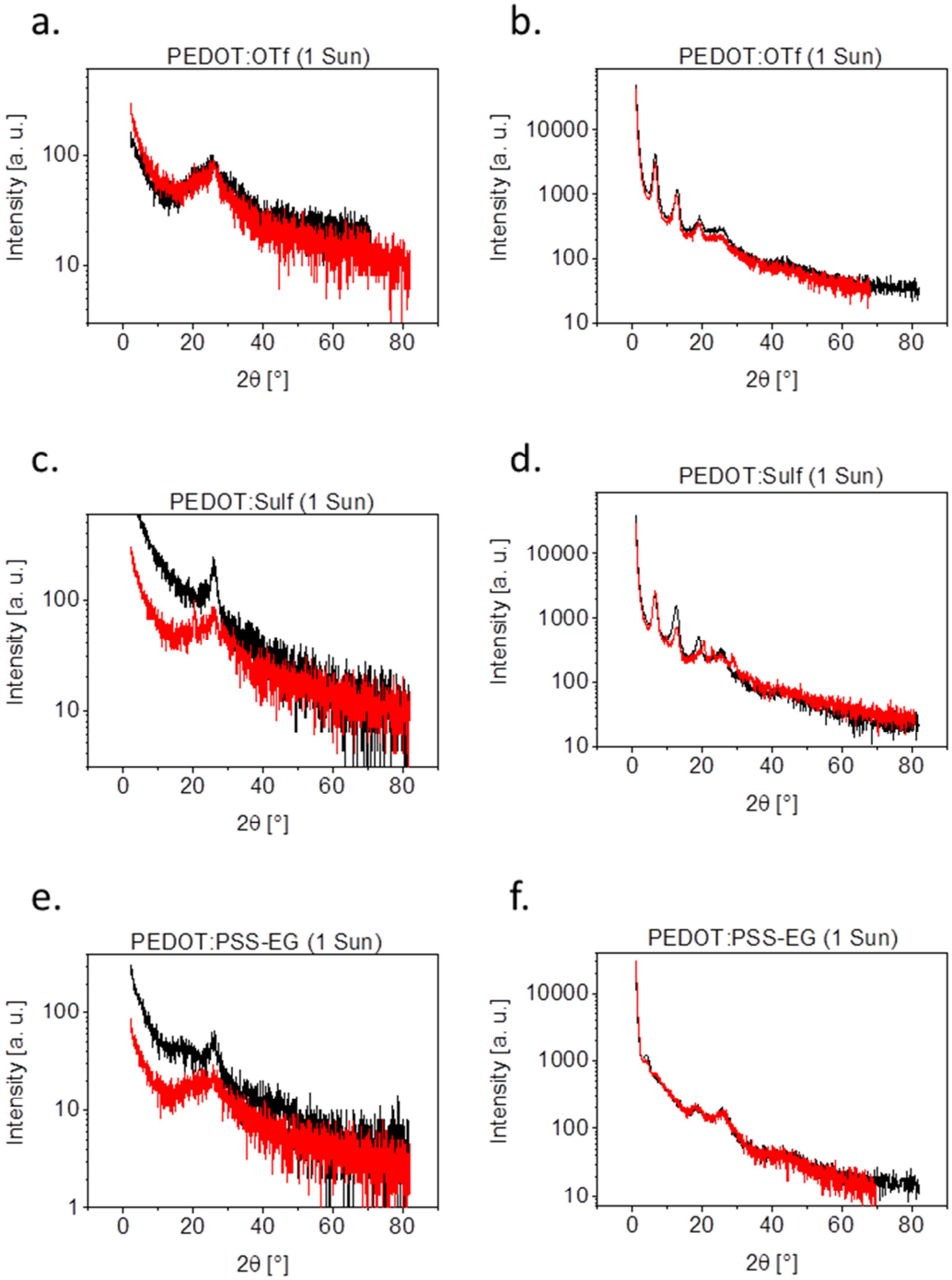

Figure V.13. GIWAXS measurements on PEDOT materials before (black curves) and after one sun ageing (red curves). In-plane diffraction patterns of PEDOT:OTf (a), PEDOT:Sulf (c) and PEDOT:PSS-EG (e). Out-of-plane diffraction patterns of PEDOT:OTf (b), PEDOT:Sulf (d) and PEDOT:PSS-EG (f). Similarly to PEDOT:Sulf aged under humidity, a new coherent structure is detected, whose signature appears around $2\theta = 20.6$ in-pane and around 16.9 °, 20.3 °, 23.1 ° and 31.7 ° out-of-plane.

5. Influence on the electronic transport properties

Information on the disorder and the electronic transport in PEDOT materials can be assessed through the temperature dependence of conductivity as explained in Chapter 1&2.

Figure V.15 depicts the temperature dependence of the conductivity of all three materials before and after the different ageing conditions as well as the associated reduced activation energy. At first glance, humidity-aged PEDOT:OTf and PEDOT:Sulf in Figure V.15a,c behave the same way as their treated counterparts, the drop of the electrical conductivity between room-temperature and near 0 K being less than one order of magnitude. The drop of conductivity after sun-ageing is more consistent and is characteristic of a classical semi-conductor behavior just like PEDOT:PSS-EG in Figure V.15e.

The resistivity ratio $\rho(0\ K)/\rho(300\ K)$ in Table V.3 informs about the disorder in the polymers films as explained in Chapter 2. The disorder increases moderately for PEDOT:OTf and PEDOT:Sulf after humidity ageing and drastically after sun-ageing. For PEDOT:PSS-EG the increase is more severe.

Table V.3. Resistivity ratio of PEDOT:OTf, PEDOT:Sulf and PEDOT:PSS-EG before and after ageing.

	PEDOT:OTf	PEDOT:Sulf	PEDOT:PSS-EG
Prisitine	1.6	1.3	49.0
Humidity-aged	2.2	1.6	2277
Sun-aged	13.0	19.0	8.10^6

This electronic disorder can be correlated with the structural disorder observed after humidity- and sun-ageing in the previous section. The π-π stacking was not deteriorated after humidity ageing while the coherence of the π-π stacking was lost after sun-ageing and mostly for PEDOT:Sulf and PEDOT:PSS-EG.

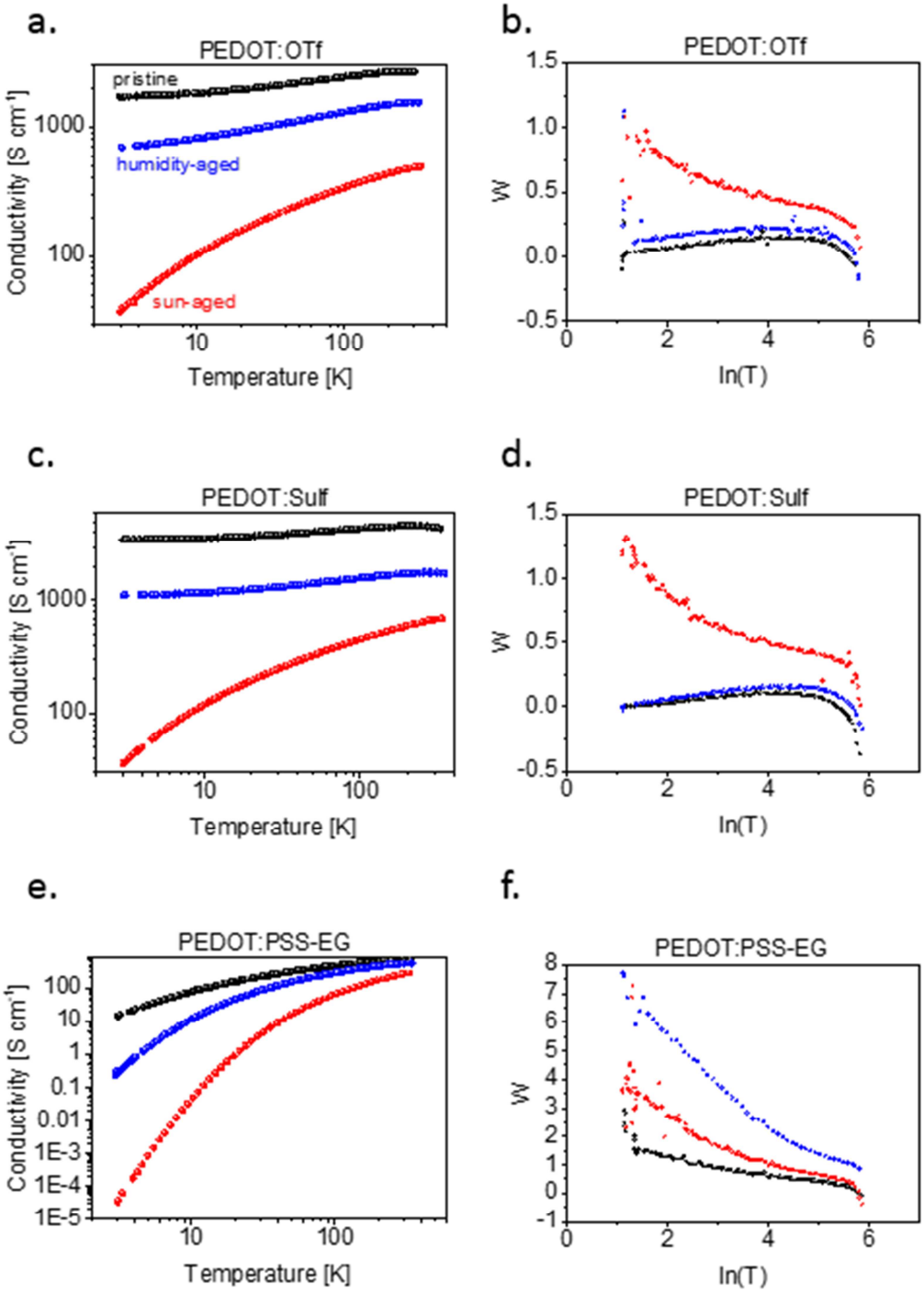

Figure V.14. Temperature dependence of conductivity of PEDOT:OTf (a), PEDOT:Sulf (c) and PEDOT:PSS-EG (e) as well as their associated reduced activation energy (b, d, and f). The legend displayed in a. is respected in each figure.

The reduced activation energy, $W = \frac{d(\ln(\sigma))}{d(\ln(T))}$ as defined in Chapter 1, is displayed in Figure V.15b,d,e for all materials before and after ageing. As demonstrated in Chapter 2, the electronic transport model in PEDOT:OTf and PEDOT:Sulf is

explained by a heterogeneous conduction model with a metallic transport in the crystallites and a disordered metallic transport combined with a tunneling transport outside the crystallites. The signature of the metallic transport is still present after ageing under humidity as confirmed by the positive slope of the reduced activation energy, the non-null conductivity near 0 K and the inflection near room temperature. Such metallic signature however completely disappears after exposure under one sun. In the case of PEDOT:PSS-EG, the dominant transport mechanism is the variable range hopping (VRH).[18,32]All PEDOT:PSS-EG samples depict a signature typical of semiconductors on the insulating side of the metal-insulator transition, namely a negative slope of the reduced activation energy and a strong decrease of the electrical conductivity when the temperature decreases.

We wondered how each component of the transport properties was affected after ageing and therefore developed a model for each material. The results are depicted in Figure V.16.

After humidity-ageing, the metallic transport in the crystallites and in the amorphous regions is still present in PEDOT:OTf as suggested by the reduced activation energy in Figure V.15b. However the transport via tunneling (model first stated by Sheng) in which transport mechanisms take place between highly conductive domains separated by less conductive ones is not encountered anymore. Instead, 3D-VRH (n was found to be 3 in Equation I-3) takes place. This is in accordance with the increase of disorder as reported in Table V.3 and the decrease of doping level as suggested previously. The detailed contribution of each transport mechanisms as deduced from the fitting parameters in Figure V.16a are given in Table V.4. It appears that the electrical conductivity is highly reduced both in the crystallites and in the amorphous regions. Apart from the disorder, un-doping observed with Raman and UV-Vis-NIR spectroscopy could explain such decrease. After sun exposure, even though both the π-π stacking and the lamellar one are not particularly disturbed, no metallic transport occurs and charges flow throughout the film only through 3D-VRH. This could be explained by the too high disorder after sun exposure as suggested by the resistivity ratio in Table V.3, the loss of charge carriers as suggested by UV-Vis-NIR in Figure V.7a and the creation of sulfate groups that might hinder the conduction mechanisms.

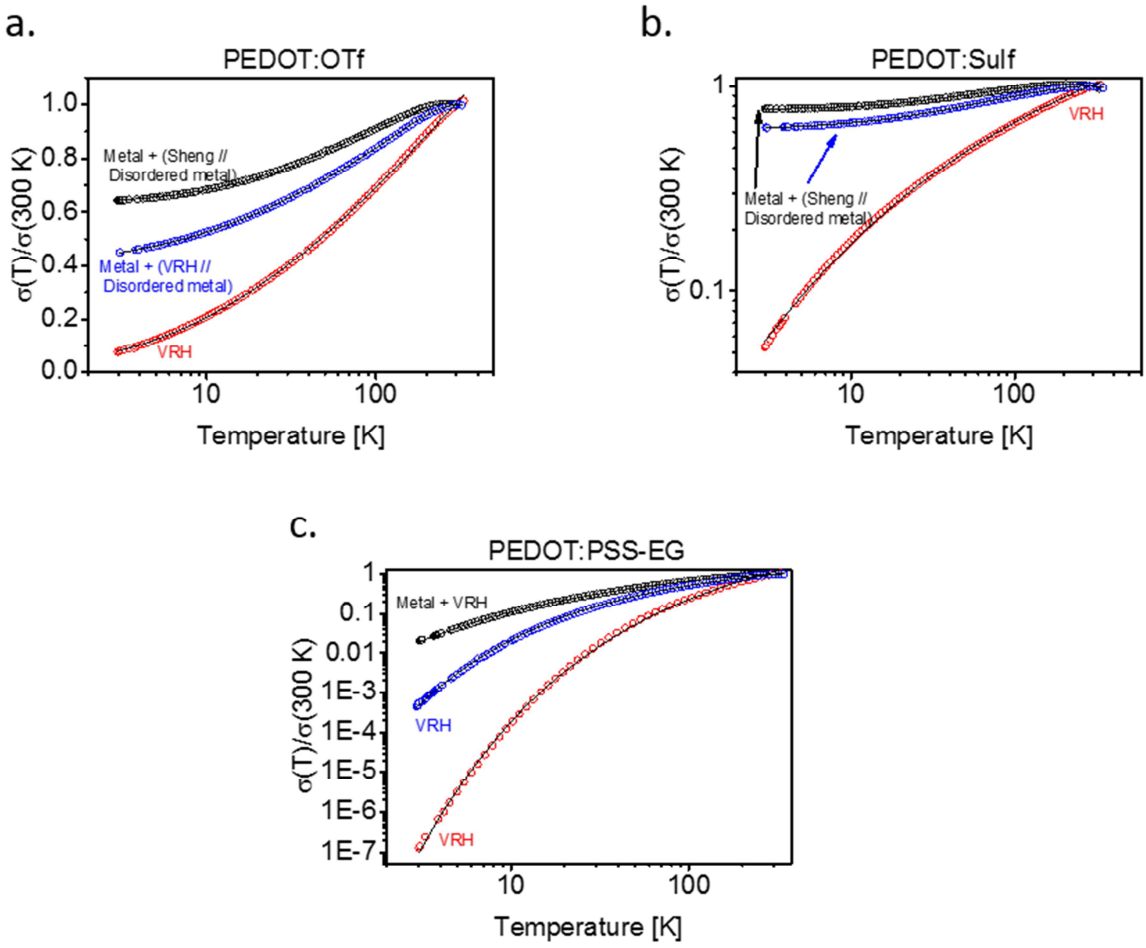

Figure V.15. Transport mechanisms models of PEDOT:OTf (a), PEDOT:Sulf (b) and PEDOT:PSS-EG (c) before ageing (black symbols), after humidity-ageing (blue symbols) and after sun-ageing (red symbols). Symbols represent experimental data while black solid lines represent the model.

Table V.4. PEDOT:OTf: detailed conduction contributions deduced from fitting parameters. The values are given for 300 K.

Ageing conditions	Metallicity [%]	Quasi 1D metal [S cm^{-1}]	Amorphous region [S cm^{-1}]	
			Tunneling or VRH	Disordered metal
Pristine	3	87040	1840 (tunneling)	842
Humidity	1	33465	996 (VRH)	630
Sun	--	--	492 (VRH)	--

In the case of PEDOT:Sulf, humidity ageing was less destructive since tunneling is still encountered. Moreover, as shown in Table V.5, the metallic transport in the crystallites is almost unchanged though the disordered metallic transport suffered the most from the humidity ageing. Here too, the highest loss was imposed by ageing under 1 sun exposure. Similarly to PEDOT:OTf, the high disorder, the loss of charge carriers, and the apparition of a new coherent structure added to the loss of structural coherence as shown by GIWAXS diffraction patterns in Figure V.14c,d could explain the 3D-VRH electronic transport.

Table V.5. PEDOT:Sulf: detailed conduction contributions deduced from fitting parameters. The values are given for 300 K.

Ageing conditions	Metallicity [%]	Quasi 1D metal [S cm^{-1}]	Amorphous region [S cm^{-1}]	
			Tunneling or VRH	Disordered metal
Pristine	5	81993	1362 (tunneling)	3384
Humidity	2	82596	1276 (tunneling)	539
Sun	--	--	692 (VRH)	--

The transport mechanisms in pristine PEDOT:PSS-EG was not previously studied in this thesis. Since VRH was mostly reported for PEDOT:PSS materials, we did not expect to find metallic transport model as shown in Figure V.16c.[79,88] This metallic transport could possibly be explained as long as PEDOT crystallites are found, which is the case as shown by GIWAXS diffraction patterns in Figure V.13e and Figure V.14e. A metallic behavior in the crystallites in series with a 1D-VRH transport in the amorphous regions was found (n was found to be 1.7 for pristine PEDOT:PSS-EG). After humidity and sun ageing the metallic contribution completely extinguished and only 1D-VRH takes place as shown in Table V.6.

Table V.6. PEDOT:PSS-EG: detailed conduction contributions deduced from fitting parameters. The values are given for 300 K.

Ageing conditions	Metallicity [%]	Quasi 1D metal [S cm^{-1}]	VRH [S cm^{-1}]
Pristine	5	14418	726
Humidity	--	--	522
Sun	--	--	293

6. Discussion and conclusions

We showed that PEDOT materials developed by our group, namely PEDOT:OTf and PEDOT:Sulf, together with EG-treated commercial PEDOT:PSS, namely PEDOT:PSS-EG, are quite stable when they are stored under the dark and under moderate temperature and relative humidity up to the ambient ones. In these conditions, we showed that oxygen does not accelerate the ageing since the small degradation of the materials was similar when they were stored in an inert atmosphere.[116]

We also showed that when the storage conditions are harsher degradation takes place and we managed to identify the main degradation factors which are high humidity, heating, and the combination of illumination and oxygen in the case of PEDOT:PSS and PEDOT:PSS-EG, or illumination and humidity in the case of PEDOT:OTf and PEDOT:Sulf.

We then investigated the chemical and structural causes behind these degradations. UV-Vis-NIR and Raman spectroscopy showed us that de-doping systematically occurred under humidity exposure; and XPS showed us a decrease of the counter-anions quantity in the films. Under sun ageing, the doping level was also found altered and sulfate groups were detected in all materials. These chemical modifications were also accompanied by structural ones. While only slight changes in the structure are noticed after humidity exposure, the coherence of the π-π stacking is completely destroyed under illumination. Moreover a new coherent structure crystallizes in humidity-aged PEDOT:Sulf and all sun-aged samples. Given the presence of sodium and sulfate groups in these materials, we expect a salt between sodium and sulfate, but complementary experiments are necessary.

Given all these chemical and structural degradations, the electronic transport mechanism are strongly altered and particularly under sun exposure where only VRH conduction takes place.

This preliminary study allowed us to identify deteriorating factors in PEDOT ageing and to establish the degradations that occurred on the oxidation state, the chemistry and the structure of the materials as well as their influence on the transport mechanism. We observe modifications that cannot be explained yet regarding our experiments and therefore complementary works are needed in order to separate the degradation of the polymer and its counter-anion in each ageing condition and propose a degradation mechanism.

Conclusions and future work

In this thesis we developed highly conductive PEDOT materials and studied their electrical, optoelectronic, thermoelectric, structural and transport properties and their ageing mechanisms.

We began our study with a literature review that showed the importance of PEDOT in the growing market of organic electronics. Commercial PEDOT:PSS is easily processable on large substrates and has an electrical conductivity spreading over several orders of magnitude (from 0.1 to 4840 S cm^{-1}) depending on the treatment it undergoes. Its counter-anion PSS^- which stabilizes its charge carriers is however in excess in the films and is insulating. On the other hand, PEDOT can also be stabilized with small counter-anions such as tosylate (Tos). PEDOT:Tos shows better electrical properties due to a better crystallinity induced by the absence of sterically hindering PSS. In that context and through a previous thesis, our group turned its attention to PEDOT stabilized with triflate (OTf) and synthesized through solution-cast polymerization.[32,75] Very high conductivities up to 1218 cm^{-1} were obtained for PEDOT:OTf and no insulating phase remained after the polymer was rinsed. When it was treated with sulfuric acid, the conductivity increased up to 2273 S cm^{-1}.

Following these research, one of my first objective was to increase the electrical conductivity of PEDOT:OTf so that we reach the current state of the art. For that purpose, our attention has turned toward aprotic polar solvents. PEDOT:OTf is synthesized by spin-coating a solution containing the solvent ethanol, the oxidant iron(III) triflate, the monomer EDOT and the copolymer PEG-PPG-PEG. Since it is known that polar aprotic solvents such as NMP, DMSO, or DMF coordinate with Fe(III), our idea was to add them as co-solvent in the oxidative solution in order to benefit from their coordinating properties. The result was drastic and the addition of 7 – 8 wt. % NMP increases the electrical conductivity up to 3600 S cm^{-1}. By treating the obtained PEDOT:OTf with diluted sulfuric acid, we increase the electrical conductivity up to 5400 S cm^{-1}, which is currently the state of the art of electrical conductivity in PEDOT films.

Afterwards, we thoroughly investigated the causes of such conductivity enhancement as well as the electronic transport properties that arouse from them. The addition of coordinating solvents leads to longer polymerization reactions as shown by UV-Vis-NIR. As a result, the structure is semi-crystalline with bigger crystallites surrounded by amorphous regions as proved by GIWAXS and TEM. The transport mechanisms are enhanced both in the crystallites and in the less well ordered domains. Upon sulfuric

acid treatment, hydrogeno-sulfonate ions from the acid interact preferentially with the amorphous regions and replace thereby the original triflate ions. As a result, the transport mechanisms are mainly improved in the disordered regions. We succeeded in explaining the electronic transport mechanisms in our polymer films with a heterogeneous transport model, a model in which metallic conduction along the chains and inside the crystallites compete with a tunneling transport typical of semiconducting materials with localized highly conductive domains. PEDOT:OTf and PEDOT:Sulf that we synthesized stand near the critical regime of the metal/insulator transition and clearly behave like glassy metals.

With the highly conductive PEDOT films synthesized, another objective was to study both its Joule heating ability and Seebeck effect, two thermoelectric effects that are of prime importance for heating and waste heat harvesting applications respectively. Thus in the third chapter we studied the conversion from electrical to thermal energy using PEDOT films. As a matter of fact, just like every other conductive material, PEDOT materials produce heat when an electrical current flows through them. We showed that our PEDOT materials showed outstanding performances and reached temperature up to 200 °C under 20 V bias. The heating performances were successfully explained by a power model which helped us determine the parameters necessary for good heating performances. It appeared that while the steady state temperature depends mainly on the applied voltage and the active material (its electrical resistance, its thermal resistance and its area), the response time depends mainly on the substrate which accounts for a very high thermal inertia (its mass and its specific heat capacity). Moreover, the good electrical properties are accompanied with interesting optical properties (57 Ω sq^{-1} at 87.8 % transmittance for PEDOT:Sulf and 68 Ω sq^{-1} at 89.6 % transmittance for PEDOT :PSS-EG). Regarding these optoelectronic properties, we proposed the first application of transparent heaters solely made of polymeric materials and demonstrated an application as a visor deicer.

In the fourth chapter, we investigated thermoelectric properties of PEDOT:OTf and PEDOT:Sulf for waste heat harvesting using the Seebeck effect. As a matter of fact, when a semiconductor is kept in a temperature gradient, charge carriers diffuse from the hot to the cold size and then from the cold to the hot size, at a smaller extent, due to the created electrical potential. At steady state, a constant potential difference proportional to the temperature gradient remains, namely the Seebeck voltage. A good electrical conductivity, a good Seebeck coefficient (for inducing a higher Seebeck voltage) and a low thermal conductivity (for keeping the temperature gradient) are all

features that allow a high power conversion efficiency. Thermal conductivity being naturally low in polymers, we mainly focus on the power factor ($S^2\sigma$) in order to assess the efficiency of thermoelectric materials. We found that the highly conductive PEDOT materials that we synthesized have good power factors up to 177 $\mu W\ m^{-1}\ K^{-2}$ for PEDOT:OTf, not enough for practical applications (at least several hundred are needed) but promising anyway. We then wanted to improve the power factor and after a brief literature review, our choice was electrochemical reduction in order to decrease the charge carriers and hence decrease the electrical conductivity while increasing the Seebeck coefficient so that an optimum is found for the power factor. These preliminary results were however not conclusive because of a high seasonal dependence of the electrical conductivity and a large variation for Seebeck coefficient measurements.

Regarding the promising results obtained during this thesis, applications such as transparent electrodes, heaters, transparent heaters or thermoelectric generators are targeted. For such applications, materials with stable functioning are required. We have shown that our materials were stable after multiple cycling at 50 °C and after several bending cycles in the third chapter. We also showed that they are stable when they are stored in the dark at ambient temperature and humidity conditions in the last chapter. We however also noticed a strong degradation of the electrical conductivity under high humidity exposure (up to 60 % after 800 h for PEDOT:OTf and PEDOT:Sulf) and under one sun illumination (up to 800 %). Ageing under different conditions suggested that deteriorating factors were the combination of heating, humidity and illumination and that oxygen does not accelerate the ageing. We also compared the ageing of our materials to that of treated commercial PEDOT:PSS and showed that almost similar mechanisms were observed, but rather than water, oxygen was the main deteriorating factor under sun exposure.

In summary, during these past three years, we managed to develop highly conductive PEDOT and unraveled their structure and transport mechanism. We also demonstrated their good heating properties which, combined to their good optoelectronic ones, render them viable flexible transparent heaters materials. We also showed that they could be interesting thermoelectric materials and regarding all the applications that are proposed for PEDOT materials, we showed their stability under mild conditions and their degradation under harsh atmospheres. Future works are still needed for a better understanding and then a better use of PEDOT materials. Some research should focus on both the Seebeck coefficient and the thermal conductivity. Even though their characterization is problematic in organic materials, their

understanding is a key factor for the development of interesting PEDOT-based thermoelectric materials. The influence of the temperature on the ageing of PEDOT:OTf and PEDOT:Sulf and the enhancement of their stability should also be investigated. This latter one could be realized through encapsulation with flexible transparent films barriers and optically clear adhesives in order to preserve their electrical conductivity, their transparency and their flexibility.

Appendix

A. Materials & Methods

A-1. Deposition techniques

Whether for the study of the materials described all along this thesis or for the different applications highlighted hereinbefore, two deposition techniques were used: spin coating, spray-coating and drop-casting. Examples of samples deposited by spin-coating, spray coating and drop casting can be found in Figure A1. Samples were deposited on glass, polyethylene terephthalate (PET), poly-carbonate (PC) or polyethylene imine (PEI) substrates.

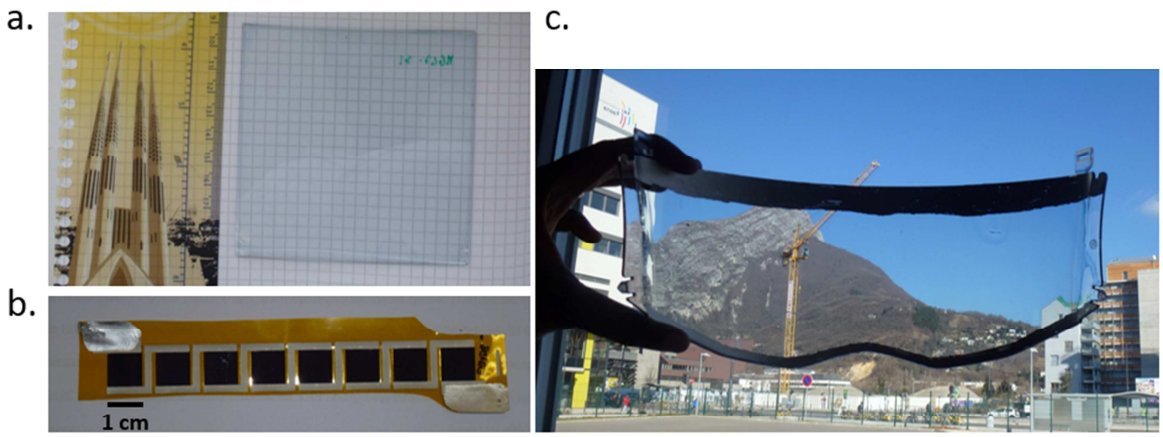

Figure A1. PEDOT:PSS deposited via a) spin-coating on a 10 cm x 100 cm glass substrate, b) spray-coating on a flexible polyethylene imine (PEI) substrate and patterned, and c) drop-casting on a curved motorcycle visor.

A-1-1. Spin-coating

The spin-coating technique uses the centrifugal force of a rotating substrate in order to deposit a uniform coating on a flat surface, as illustrated in Figure A2.

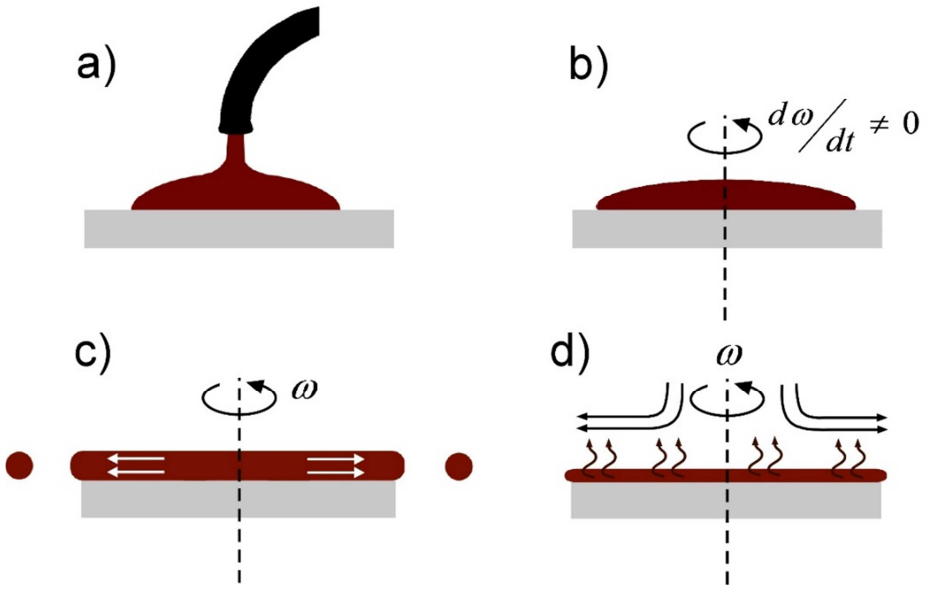

Figure A2. Scheme summarizing a film deposition using the spin-coating technique[3]. a) Dispensation. b) Acceleration. c) Rotation (flow dominated). d) Evaporation.

Samples were deposited on glass, polyethylene terephthalate (PET) or poly carbonate (PC) substrates.

For the deposition of PEDOT:PSS based materials, glass substrates were dipped 10 min in a piranha solution (1/3 vol. % hydrogen peroxide 3. Wt. % in water (H_2O_2) + 2/3 vol. % concentrated sulfuric acid (H_2SO_4)) before being thoroughly washed with deionized water. Such piranha treatment ensures the formation of hydroxyl groups at the surface of the substrate which then becomes hydrophilic.

For the deposition of PEDOT:OTf based materials, the glass substrates were cleaned in an ultrasonic bath (a Kudor),successively dipped in deionized water, acetone, isopropyl alcohol and ethanol for 10 min each.

For the deposition on PET, the substrate was used without further cleaning. In order to not bend the substrate with the spin-coater vacuum, it was adhered onto a glass substrate thanks to toluene drops.

For the deposition on PC, the substrate was cleaned with an O_2 plasma treatment.

[3] Reproduced from « Basic Models of Spin Coating », S. Hellstrom, Stanford University, http://large.stanford.edu/courses/2007/ph210/hellstrom1/

Table A1 summarizes the deposition conditions. The process was repeated for a multilayer deposition and allowed to have thicknesses below 100 nm.

Table A1. Spin coating conditions for both PEDOT:PSS and PEDOT:OTf based materials.

	PEDOT:PSS and derivatives	PEDOT:OTf and derivatives
Acceleration	1000 rpm s^{-1}	1200 rpm s^{-1}
Rotation speed	1000 rpm	4500 rpm
Rotation time	30 s	30 s
Drop of the solution on the substrate	Before the machine is started, after total coverage of the substrate	Once the machine is started and the steady state speed is reached
Annealing	10 min at 120 °C	10 min at 120 °C

A-1-2. Spray coating

The spray-coating technique is suitable when thick homogeneous films, large area films and in particular patterned films are needed. Glass substrates were thoroughly washed with ethanol before being used. PEI substrates were used without further cleaning. In this technique, the solution is stored in a small container and a spray nozzle directs it on a substrate which is heated at 90 °C for PEDOT:PSS based materials and 70 °C for PEDOT:OTf based materials. Such technique allowed to deposit films with thicknesses from ~200 nm 2 μm.

A-1-3. Drop casting

This technique is used when thin homogeneous films on large and curved substrates are needed. The solution is drop casted on the substrate, let drained and the obtained film is annealed in the same conditions as in the spin-coating techniques. Such deposition technique gave films with thicknesses below 100 nm, hence similar to spin-coating, but on non-flat surfaces.

A-2. Materials' synthesis

Materials presented in this manuscript were deposited with spin-coating technique unless stated otherwise.

The polymer PEDOT:PSS Clevios PH1000 was purchased from H.C. Starck, anhydrous ethanol from CARLO ERBAS Reagents, isopropyl alcohol from Honeywell Riedel de Haën and ethylene glycol from Fluka. The monomer ethylene dioxythiophenee (EDOT), the oxidant iron trifluoromethanesulfonate ($Fe(OTf)_3$), the solvent N-methyl-2-pyrrolidone (NMP), and polyethylene glycol− polypropylene glycol−polyethylene glycol (PEG−PPG−PEG) Mw = 5800 were obtained from Sigma-Aldrich. The thermochromic ink was purchased from Gem innov and is constituted of a blue slurry of micro-capsules whose color switching temperature is 43 °C.

When relevant, an OIKE encapsulating film was used. It is constituted of a film barrier sandwiched between two PEN (polyethylene naphthalate), whose total thickness is 225 µm. Its WVTR (water vapor transmission rate) is given at 5.10^{-5} g m^{-2} d^{-1} at 40 °C and 90 % RH. The film barrier adhered to the transparent film heater through an optically clear adhesive from 3M™.

A-2-1. PEDOT:PSS and derivatives

Commercial PEDOT:PSS PH1000 was purchased and blended with IPA (50 vol. % IPA for spin-coating and 75 vol. % IPA for spray-coating). The obtained material is named PEDOT:PSS. This material can be further dipped 30 min in an ethylene glycol (EG) bath and thoroughly rinsed with ethanol before being annealed at 120 °C for 30 min. This material is named PEDOT:PSS-EG.

A-2-2. PEDOT:OTf and derivatives

PEDOT films were prepared by spin-coating an oxidative solution onto a glass, PC or PET substrate. These following steps have been followed:

- Solution preparation
- Substrate preparation
- Film deposition
- Multilayer deposition (when relevant)

A-2-2-a. Solution preparation

The oxidative solution containing the solvent (ethanol), the co-solvent (NMP, DMSO or DMF), the polymerization rate controller (PEG-PPG-PEG), the monomer (EDOT) and the oxidant ($Fe(OTf)_3$) was prepared as followed. First, a solution containing

20 wt. % PEG-PPG-PEG and 80 wt. % ethanol was prepared. It was named solution_EtOH. Then, a solution named solution_cosolv with 20 wt. % PEG-PPG-PEG and 80 wt. % co-solvent was prepared. For the synthesis of PEDOT:OTf, only the solution_EtOH was used. For PEDOT:OTf-cosolv and PEDOT:Sulf-cosolv, the desired amount of solution_EtOH was added to an amount of solution_cosolv. For example, in order to obtain x wt. % of co-solvent in the final solution, (0.8-x)/x*m of solution_EtOH was added to a weighted amount m of solution_cosolv. The obtained solution was named solution_mix. Finally 126 mg of $Fe(OTf)_3$ was dissolved in 1 mL of solution_mix or in solution_EtOH. The obtained oxidative solution, named solution_ox, was sonicated for 2 h before being used.

A-2-2-b. Substrate preparation

The PEDOT films were deposited onto glass substrates (either Corning Eagle XG or microscope slides, 2.5 cm x 2.5 cm & 1.1 mm thick or 10 cm x 10 cm & 1.1 mm thick), which were washed with ethanol before use.

A-2-2-c. Film deposition

The PEDOT films were deposited by spin-coating. An amount of 0.25 mL of solution_ox was mixed with 5 µL of EDOT during 30 s, sonicated during 10 s before being spin-coated on a glass substrate rotating at 4500 rpm. The resulting film was heated on a hot plate at 70 °C, rinsed twice with ethanol and dried. The obtained film was named PEDOT:OTf or PEDOT:OTf-co-solvent when a co-solvent was added.

A-2-2-d. Multilayer deposition

When relevant, after the film was dried, another layer of polymer was deposited on the first layers.

A-2-3. Acid treatment

Sulfuric acid was diluted in deionized water to obtain 0.1 M solution. The synthesized PEDOT films were dipped into that sulfuric acid solution for 30 min before being dried on a hot plate at 120 °C for 20 min. The obtained film was named PEDOT:Sulf (PEDOT:Sulf-cosolv when a co-solvent was used).

A-3. Electrochemical reduction

For the control of the oxidation level in PEDOT, this latter one was used as the working electrode in a three electrode electrochemical cell. PEDOT was coated on a

glass substrate and since it was conductive enough, no conductive substrate was necessary. A platinum electrode was used as the counter-electrode and Ag/Ag^+ in 3.5 M KCl as the reference electrode. The supporting electrolyte contained 0.1 M tetrabuthylammoniun hexa-fluorophosphate in propylene carbonate. Such electrolyte was used for its large oxido-reduction window in order not to be limited by the oxidation or reduction of the electrolyte. Argon was flowed in the electrolyte for 10 min before the experiment. Thereafter, an argon bed was kept during the whole experiment.

The setup was verified and calibrated using the couple ferrocene/ferrocenium. Cyclic voltammetry on PEDOT allowed to determine the oxido-reduction window of PEDOT. The voltage bias applied for different oxidation level is to be correlated to those cyclic voltammograms and to the calibration with the couple ferrocene/ferrocenium (Fc/Fc^+).

A-4. Characterization techniques

A-4-1. Electrical resistance

For the electrical measurements, two silver contacts were painted on the opposing edges of the samples as can be seen in Figure III-1. Resistance measurements are achieved with an ohm-meter ISO-TECH IDM19. The measurement of the resistance is mostly given for transparent heater applications. Most of the time, the sheet resistance is given as this value is more relevant for characterizing the films.

Sheet resistance is a special case of resistivity for thin film with uniform thickness. Equation A.1 gives the resistance of a wire as function of its resistivity , its length L and its cross section A.

$$R = \rho \frac{L}{A} \tag{A.1}$$

For uniform films the cross section A can be split into the thickness t and the width W of the film.

$$R = \rho \frac{L}{t.W} = \frac{\rho}{t} . \frac{L}{W} = \rho_s \frac{L}{W} \tag{A.2}$$

The sheet resistance (R_S) is more convenient to use for two main reasons. First, the resistance of a material is dependent of its shape whereas the resistivity (and hence the conductivity $\sigma = \frac{1}{\rho} = \frac{1}{t.\rho_s}$) is only material dependent. The sheet resistance and the conductivity can then be used to compare the electrical properties of materials which are dissimilar in size. Second, the sheet resistance is directly measured with a four-point

probe measurement, which allows to directly access the conductivity upon knowing the thickness of the film.

The sheet resistance has here been measured with a Loresta four-point probe apparatus. The current flows through the two outer probes while the voltage is read between the two inner probes. Such geometry has in addition the advantage to set the system free from voltage drops at the contacts and then from contact resistances.

A-4-2. Atomic force microscopy (AFM)

The thickness of the films were measured with an AFM Inova from Brucker™. AFM is a high resolution (nanometer scale) scanning probe microscopy technique used to investigate the topography of a surface. In tapping mode a tip is let to vibrate at its resonance frequency on the surface of the sample and its deflection is monitored and correlated to the read topography. For thickness measurements, the film is scratched and the AFM tip dragged on both sides of that scratch. An example of thickness measurement with this method can be found in Figure A3. The data were analyzed using Gwyddion software.

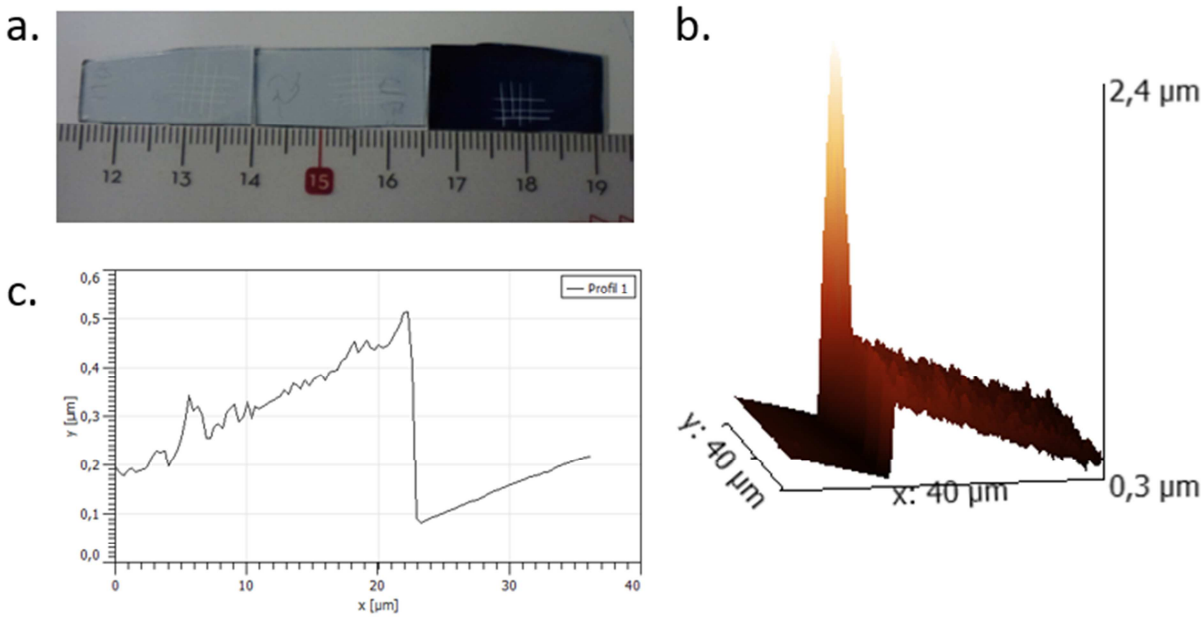

Figure A3. Thickness measurement using AFM. a) Scratched samples for AFM analyses. b) 3D topography image of scratched area. c) Thickness measurement around the scratched area.

We recorded two main data, the topography and the phase as summarized in Figure A4. The topography is the map of the surface of the sample. It was used to extract thickness measurement. The phase on the other hand gives chemical information of the film. Indeed, while oscillating at a driven force, the surrounding regions with different composition can alter the phase signal of the response (different interaction). Phase shifts are then registered as brighter or darker regions and give information on the surface stiffness/softness or a different chemical structure. In other word, uniform color distribution along the probed area implies uniform distribution of the same material.

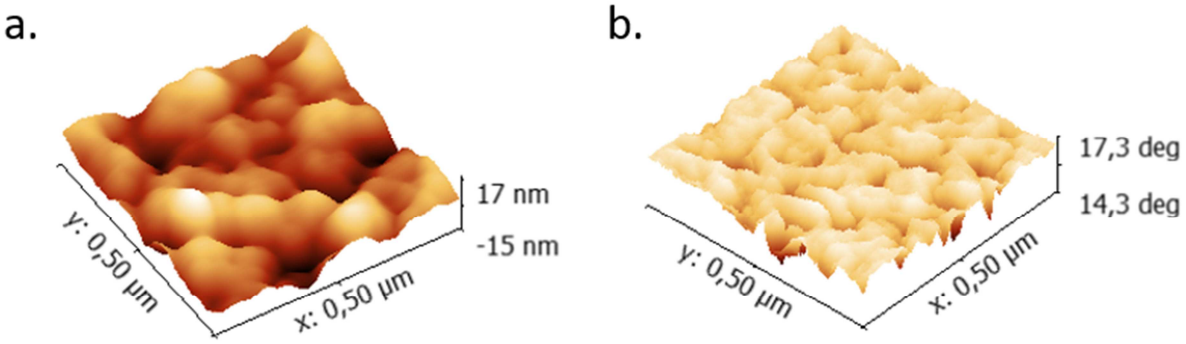

Figure A4. a) Topography and b) phase images of a PEDOT based material.

A-4-3. Electrical conductivity

A-4-3-a. Room temperature (RT)

The room temperature electrical conductivity is deduced from the sheet resistance (obtained with a four-point probe) and the thickness (obtained with an AFM) using Equation A.3.

$$\sigma = \frac{1}{\rho} = \frac{1}{t.\rho_s} \tag{A.3}$$

A-4-3-b. Temperature dependence of conductivity

Low temperature conductivities are measured with a four-point probe setup and monitored from 3 K to RT using a He flow cryostat CF 1200 D from Oxford Instruments. Gold contacts are evaporated on the surface of the material which is then placed under the four-point setup and introduced in the cryostat (see Figure A5). The chamber was pumped a whole night at RT, the temperature was further set to liquid

He temperature (4 K), slightly pumped to fall below 4 K and finally the temperature was increased from 3 K to RT and the resistance monitored at each plateau.

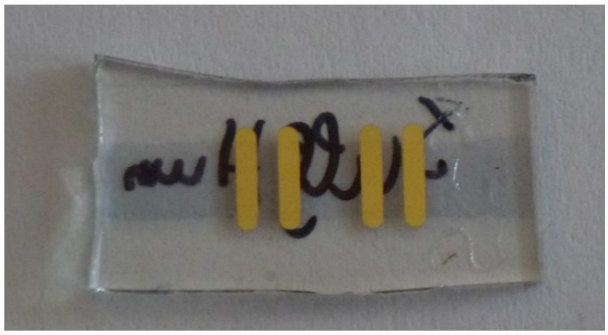

Figure A5. Sample preparation for temperature dependence of conductivity measurement.

A-4-4. Ultraviolet-Visible-Near infrared (UV-Vis-NIR) spectroscopy

UV-Vis-NIR spectra are recorded on a Varian Cary 5000 between 300 nm and 2500 nm. UV-Vis-NIR spectroscopy can give absorbance and specular transmission spectra, but also the diffused and reflective part of the light when an integrating sphere is used.

A-4-5. Raman Spectrometry

Raman spectra are recorded from 3200 to 100 cm^{-1} using a 633 nm excitation line with a low power density on the sample (< 50 μW/ m^2).

Two sets of measurement per sample were led, one standard measurement between 100 and 3200 cm^{-1} and a high resolution (<1 cm^{-1}) measurement of the main region of interest between 1100 and 1700 cm^{-1}. For each sample, several measurements at different points on the samples were recorded to assess the uniformity, and averaged in case of good uniformity.

A-4-6. X-Ray photoelectron (XPS) spectrometry

XPS is a surface analysis spectroscopic technique that measures the elemental composition of a sample. The XPS surface analysis was performed with a VERSAPROBE-II equipment. The samples are irradiated with an X-Rays beam and the energy and number of photoelectrons that escaped are detected. A take-off angle of 45 ° allowed a depth analysis of 5 nm. In order to determine the material composition, we proceeded to the deconvolution of the sulfur XPS peak using the software Multipak.

A sulfur atom will give rise to a spin-split doublet, $S_{2p\ 1/2}$ and $S_{2p\ 3/2}$, in the S_{2p} core level spectrum. The energy splitting is about 1.2 eV, the respective intensities have a ratio of 1:2 and the two components are expected to have the same FWHM and shape. The sulfur in PEDOT films originates from two different sources which are the thiophene rings in the polymer PEDOT chain, or the counter-anion (such as PSS or tosylate). When the chemical environment of an element is changed, its binding energy is altered. The more that element is reduced, the more its binding energy is shifted to lower binding energies. To the contrary the more it is oxidized, the more its binding energy is shifted towards higher values. The S2p doublet of the thiophene units which appears around 163.3 eV is then well distinguished from the one of the sulfonate units in PSS around 167.8 eV.[60,76] Therefore, using XPS surface elemental analysis technique, one can have access to the ratio PEDOT to counter-anion and in case of non-excess counter-anion, to the oxidation level.

The deconvolution in Figure 2 in the main article are carried out with the software Multipak 9.5, which calculated the ratios between the curves' areas of thiophenes' S2p doublet and the others S2p doublets (from OTf and HSO4-), to extract the oxidation levels.

A-4-7. X-Ray diffraction (XRD)

XRD is a technique that reveals the structure of a crystalline material, through which X-Rays are irradiated and whose atoms diffract the beam. The diffraction angles can be correlated to characteristic distances of the materials and the obtained spectra enlighten their structure.

Grazing-incidence wide-angle X-Ray scattering is a structural technique, derived from XRD and suitable for thin films with small structural distances, typically molecular length scales. Indeed the beam explore the surface sample in grazing incidence, hence allowing to collect information from a larger volume. Moreover, wide scattered angles are collected, corresponding to small distances.

GIWAXS measurements are obtained both with a synchrotron radiation using the beamline BM 32 of ESRF, Grenoble, and the laboratory Rigaku Smartlab diffractometer equipped with a copper rotating anode at CEA-INAC. The energy beam used at the ESRF is 18 keV, the incident angle $\omega = 0.1$ °. In our Smartlab laboratory equipment, the parameters are 8 keV and 0.1 ° respectively. GIWAXS data are processed using Igor software and macros developed in our laboratory. When varying

the detector position, both in-plane and out-of-plane information are obtained (Figure A6).

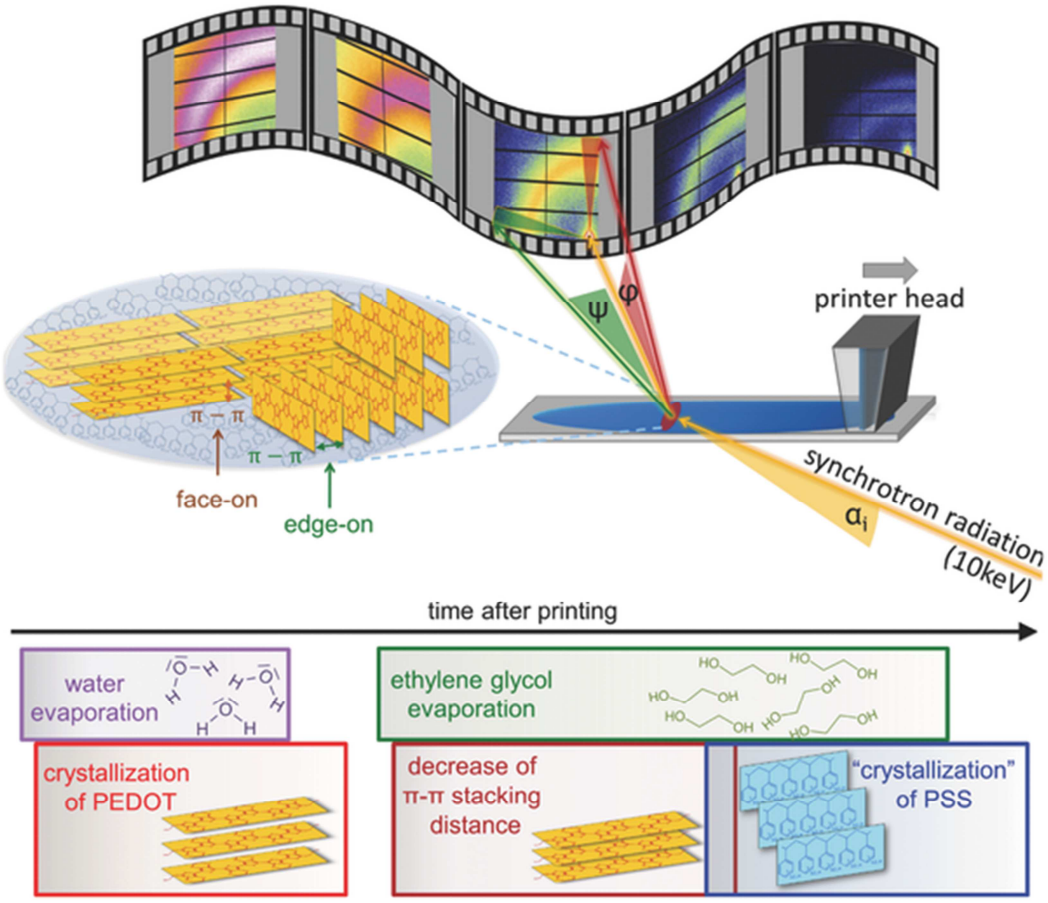

Figure A6. Illustration of the functionning of in-plane and out of plane GIWAXS, reproduced from [214]

Information concerning the sample microstructure can be obtained from the analysis of the peak shape. The widths of the diffraction peaks measured in theta / two theta configuration is thus related to crystallite size and strain due to lattice parameter gradient by Equation A4:

$$FW_{2\theta}(\theta) = \varepsilon \tan\theta + \frac{K\lambda}{L\cos\theta} \quad (A4)$$

Where $FW_{2\theta}$ is the full width at half maximum of the peak corrected from resolution effect, λ the wavelength, K the Scherrer shape factor the value of which is close to 1, L the crystallite size along the direction of the diffusion vector and ε the strain ($\varepsilon = 4.\frac{<d-<d>>}{<d>}$). Scherrer formula is nothing else but the second term. One therefore

has to keep in mind that when applying Scherrer formula one makes the assumption that strain contribution is negligible.

The fit of several peaks corresponding to different orders of diffraction allows the determination of both size and strain contributions. When only one peak is present the use of Scherrer formula gives a minimum value of the perpendicular crystallite size as the whole broadening is attributed to size effect.

Correlation lengths along the π-π stacking direction were calculated using the Scherrer formula. Average crystallite' sizes along the a-direction were calculated using Equation A4.

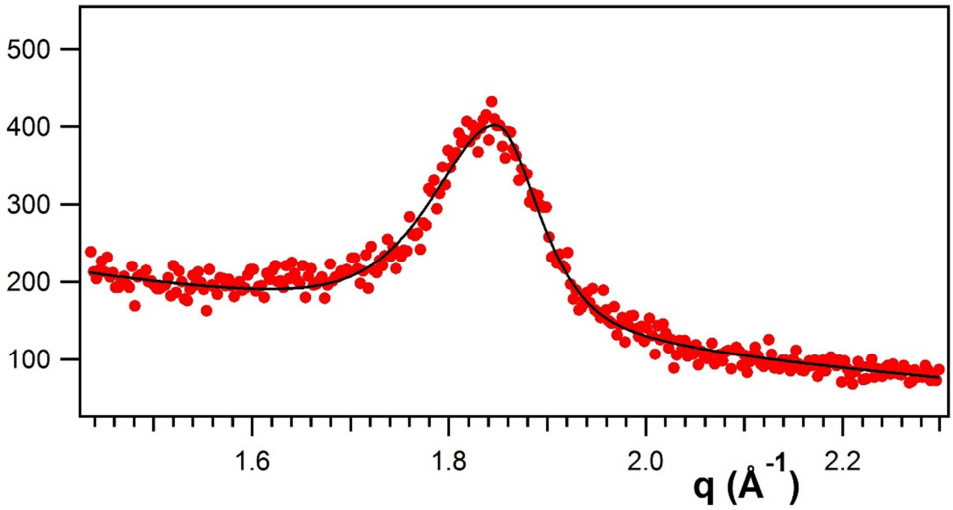

Figure A7. Theta / two-theta in-plane scan measured on PEDOT:OTf-NMP. The solid line corresponds to the result of the peak fitting with the sum of a pseudo-Voigt shape function and a linear background contribution. All the fits were performed keeping the value of the ε shape parameter of the pseudo-Voigt function constant at η = 0,7.

A-4-8. High resolution transmission electron microscopy HRTEM

Images of the structure of the PEDOT films are given by transmission electron microscopy (TEM). TEM is a microscopy technique in which an image is formed from the interaction of a beam of electrons transmitted through a thin sample. High resolution TEM is a TEM technique that can image in the atomic scale.

HRTEM is performed using a double Cs corrected TEM (FEI Titan3 ultimate) operating at 80 kV. The PEDOT thin film was prepared by spin-coating the oxidative

solution on chemical vapor deposition (CVD) grown monolayer graphene transferred on Cu grid with carbon membrane with holes. The signal of graphene was negligible.

A-4-9. Seebeck coefficient

The Seebeck coefficient or thermopower is measured using a Ulvac-RIKO ZEM-3. The functioning principle is given in Figure A8.

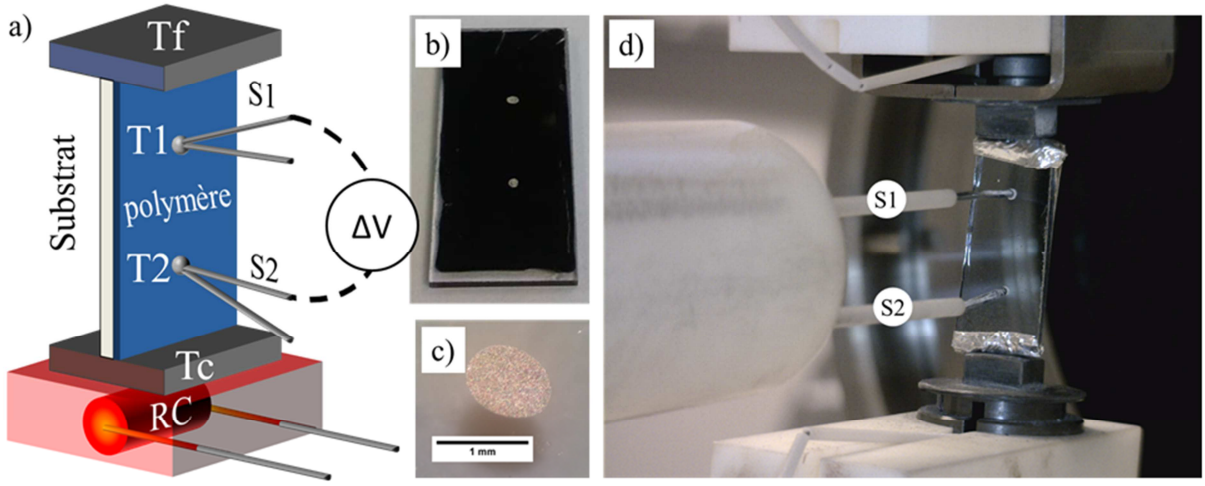

Figure A8. Thermopower measurements using ZEM-3. a) Scheme of the experimental setup showing the sample, the metal blocks for temperature gradient (Tf = cold temperature and Tc = hot temperature) and the thermocouples for temperature and voltage measurements. b) Drops of silver paints for electrical contacts. c) Magnified image of a drop of silver paint. d) Experimental setup. Reproduced from[18]

The sample is placed in a thermostatic chamber under helium atmosphere. It is placed between two metallic blocks, one being set at room temperature and the other with a temperature made to vary thanks to a Joule heating resistance. Two drops of silver paints are deposited on the PEDOT films in order to allow a better contact between the thermocouples and the PEDOT. Those two thermocouples (type R, Pt-Rh (13 %)/Pt couple) measure both the temperature gradient and the induced voltage for several temperature gradients.

An analysis program deduce the absolute Seebeck coefficient of PEDOT after a calibration taking into account the Seebeck coefficient of the thermocouples. The as measured Seebeck coefficient is given with an uncertainty of 10 %.

During the thesis, the ZEM-3 was not always available and the Seebeck coefficient was then measured using a setup developed by another PhD student working on

thermoelectric generators made of PEDOT. The sample is maintained between two copper plates, one being cooled with tap water and the other being heated thanks to a heating block. The temperature gradient is measured with two K-type thermocouples (Nickel-Chromium / Nickel-Alumel) and the voltage measured with a Keithley generator.

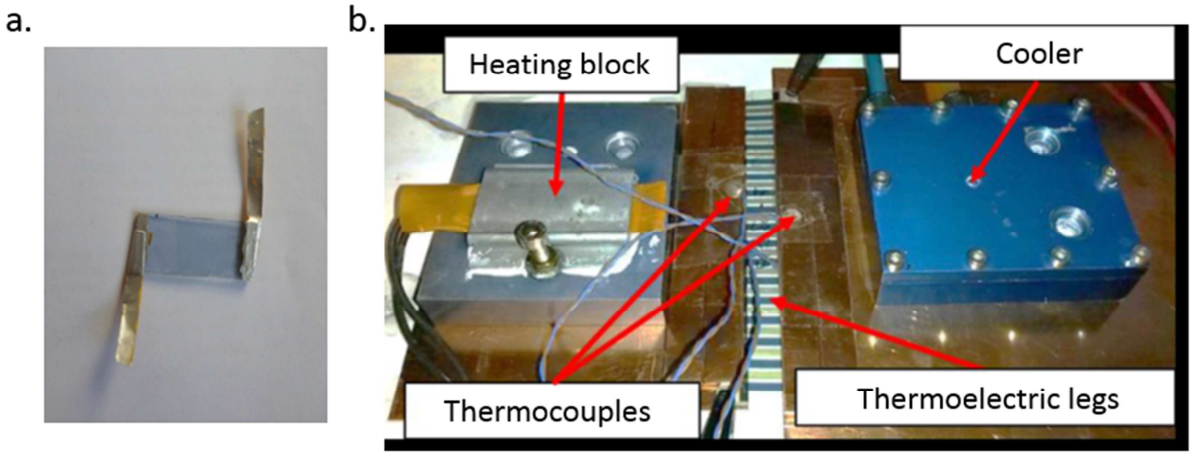

Figure A11. a) Sample prepared for thermoelectric measurements. b) Experimental setup for thermoelectric power measurement.

A-4-10. Transparent heater's characterizations

Blue thermochromik ink (activation temperature at 41 °C) was deposited by spray coating on an encapsulating barrier which was made to adhere to the film. IR images were recorded with a Fluke TI 32 camera.

Bending cycles were performed with a homemade apparatus. The sample was kept between two clamps. Those clamps were connected to a Keithley generator which delivered the voltage and measured the current and the resistance of the sample. One clamp was affixed on a stand while the other was let to slide back and forth at a given frequency (one cycle every 2 seconds). The real time electrical changes were then measured.

B. State of the art of conductivity in PEDOT materials

Table B1. State of the art of conductivity in PEDOT films.

Year	Material	Treatment	Conductivity [S cm^{-1}]	References
1992	PEDOT	electrochemical polymerization	31	Heywang et al.[45]
1992	PEDOT	electrochemical polymerization	200	Heywang et al.[45]
1994	PEDOT	SCP	550	De Leeuw et al.[64]
1995	PEDOT	electrochemical polymerization	780	Granström et al.[59]
1997	PEDOT	Electrochemical polymerization	300	Aleshin et al.[215]
2002	PEDOT:PSS	Organic solvent	80	Kim et al.[19]
2003	PEDOT	Electrochemical polymerization	650	Zotti et al.[60]
2004	PEDOT:PSS	Organic solvent	200	Ouyang et al.[88]
2004	PEDOT:Tos	VPP	1025	Winther-Jensen et al.[66]
2005	PEDOT: Tos	SCP	1000	Winther-Jensen et al.[70]
2006	PEDOT: Tos	VPP	1000	Lindel et al.[216]
2006	PEDOT: Tos	CVD	105	Lock et al.[67]
2007	PEDOT: Tos	CVD	4500	Kim et al.[68]
2007	PEDOT:PSS	Ionic liquids	136	Döbbelin et al.[217]
2008	PEDOT:PSS	Anionic surfactants	80	Fan et al.[82]
2008	PEDOT: Tos	VPP	761	Zuber et al.[109]
2009	PEDOT:PSS	Salt	140	Xia et al.[83]
2010	PEDOT:PSS	Heating	2000	Pyshkina et al.[218]
2010	PEDOT:PSS	Acid	200	Xia et al.[86]
2010	PEDOT:Tos	VPP	669	Fabretto et al.[69]
2011	PEDOT:PSS	Organic pre-	1418	Kim et al.[84]

		and post-treatment		
2011	PEDOT:Tos	VPP	575	Madl et al.[94]
2011	PEDOT:Tos	VPP	1487	Fabretto et al.[111]
2011	PEDOT:Tos	VPP	300	Bubnova et al.[184]
2012	PEDOT:Tos	VPP	1500	Fabretto, et al.[111]
2012	PEDOT:PSS	Ionic liquid	2084	Badre et al.[81]
2012	PEDOT:Tos	VPP	3400	Fabretto et al.[101]
2012	PEDOT:PSS	Acid	3065	Xia et al.[113]
2013	PEDOT:PSS	Organic solvent	900	Kim et al.[106]
2013	PEDOT:Tos	SCP	1500	Yu et al.[90]
2013	PEDOT:PSS	Organic solvents	830	Wei et al.[92]
2013	PEDOT:Tos	SCP	1355	Park et al.[185]
2013	PEDOT:Tos	SCP	2120	Park et al.[185]
2013	PEDOT:Tos	VPP + organic solvent	3305	Hojati-Talemi et al.[112]
2014	PEDOT:PSS	Organic solvent	1647	Lee et al.[206]
2014	PEDOT:PSS	Acid	3500	Mukherjee et al.[143]
2014	PEDOT:PSS		944	Tsai et al.[219]
2014	PEDOT:PSS	Acid	1750	Wang et al.[213]
2014	PEDOT ($FeCl_3$)	VPP, Single crystal	8797	Cho et al.[91]
2014	PEDOT:PSS	Acid	4380	Kim et al.[141]
2015	PEDOT:PSS	Acid	1460	Meng et al.[87]
2015	PEDOT:OTf	SCP	1218	Massonnet et al.[32]
2015	PEDOT:Sulf	SCP + acid	2273	Massonnet et al.[32]
2015	PEDOT:PSS	Shearing	4600	Worfolk et al.[85]
2015	PEDO:PSS	Organic solvent	1500	Xiong et al.[96]
2015	PEDOT:PSS	Acid	1900	Mengistie et al.[190]
2016	PEDOT:PSS	Acid	2600	Kumar et al.[98]
2016	PEDOT:Tos	Organic	640	Petsagkourakis

		solvents + acid		et al.[220]
2016	PEDOT:PSS	Acid	4840	Bae et al.[63]
2017	PEDOT:Tos	SCP + organic solvent	2200	Lee et al.[221]
2017	PEDOT:Tos	SCP + organic solvent	1250	Lee et al.[221]
2017	PEDOT:Sulf	VPP	4050	Farka et al.[33]

C. PEDOT as transparent electrode

Table C1. Optoelectronic properties of PEDOT materials.

Years	Material	Sheet resistance [Ω sq^{-1}]	Transparence @ 550 nm [%]	Figure of merit	References
2006	CVD PEDOT ($Fe(III)Cl_3$)	952	84	2.1	Lock et al.[67]
2011	PEDOT:PSS + EG	285	89.5	11.6	Kim et al.[84]
2011	VPP PEDOT:Tos	--	94	--	Madl et al.[94]
2012	PEDOT:PSS +IL	31	96	294.9	Badre et al.[81]
2012	VPP PEDOT:Tos	45	80	35.5	Fabretto et al.[101]
2012	PEDOT:PSS + Acid	39	80	40.9	Xia et al.[113]
2013	VPP PEDOT:Tos	25	68	35.5	Hojati-Talemi et al.[112]
2014	PEDOT:PSS+DMSO	--	88.3	--	Lee et al.[206]
2014	PEDOT:PSS + Tos acid	78	94	76.9	Mukherjee et al.[143]
2014	PEDOT:PSS +acid	46	90	75.8	Kim et al.[141]
2015	PEDOT:PSS +shearing	17	97.2	775.3	Worfolk et al.[85]
2016	PEDOT:PSS+ sulfuric acid	95	90	36.7	Fallahzadeh et al.[50]
2016	PEDOT:OTf	81	88.4	36.6	This work[11]
2016	PEDOT:PSS-EG	68	89.6	49.1	This work[11]
2016	PEDOT:Sulf	57	87.8	49.2	This work[11]
2017	PEDOT:Sulfate o-CVD	--	87		Farka et al.[33]

D. Thermoelectric properties of PEDOT materials

Table D1. Thermoelectric properties of PEDOT materials.

Year	Conductivity [S cm^{-1}]	Thermopower [µV K^{-1}]	Power factor [µW m-1 K^{-2}]	ZT	Reference
2008	--	--	--	0.00175	Jiang et al.[189]
2010	945	22	47	0.1	Zhang et al.[191]
2011	800	200	324	0.25	Bubnova et al.[184]
2013	--	--	--	0.28	Kim et al.[106]
2013	--	--	469	0.42	Kim et al.[106]
2013	1250	95	1270	1.02	Park et al.[185]
2014	1100	40	150	0.22	Bubnova et al.[20]
2015	--	55	453	--	Mengistie et al.[190]

E. Material selection for thermo-electric applications: Ashby plots

Regarding the possible applications' routes that were enlightened during this thesis, it can be interesting to compare our materials with those already existing for different applications. In particular, they are very interesting for their thermal and electronic properties. Figure E1 displays an Ashby plot of different materials regarding both their electrical resistivity and their thermal conductivity. Such plots are primarily interesting for the classification of materials regarding two or more properties so that, depending on the required properties, a precise selection of interesting materials can be done.

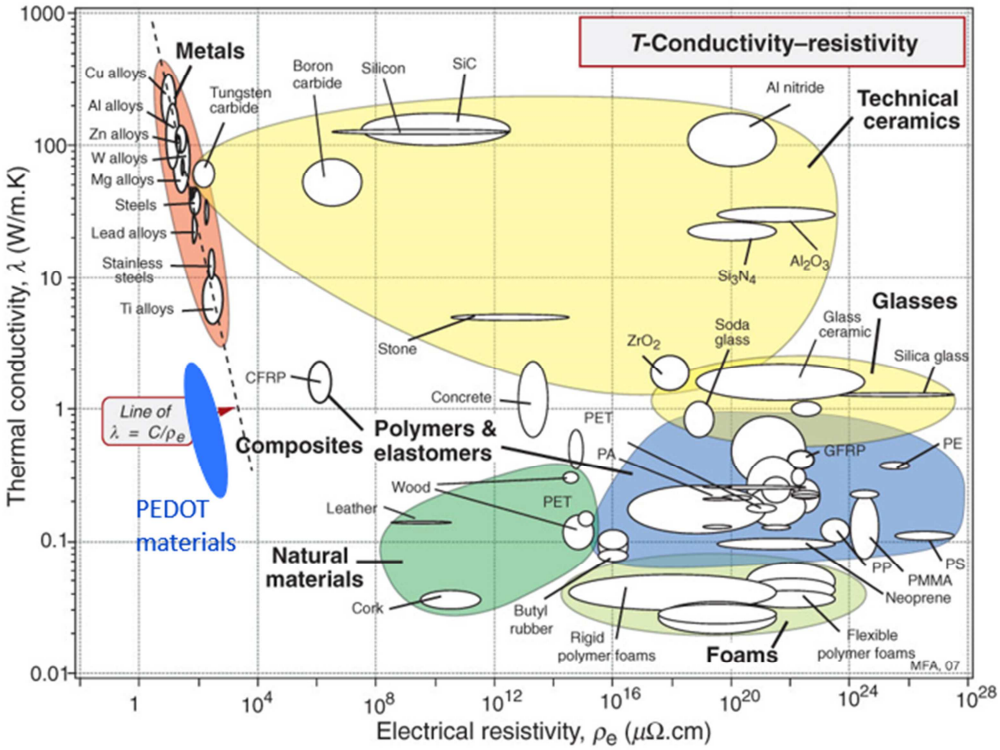

Figure E1. Our PEDOT materials compared to other materials according to their electrical resistivity and their thermal conductivity. The electrical resistivity is deduced from electrical conductivities found during this work (between 3000 and 5000 S cm^{-1}) while the thermal conductivity is inferred from theoretical values of the literature (between 0.35 and 1 W m^{-1} K^{-1}). Reproduced after [4]

[4] http://slideplayer.com/slide/8993568/, Microstructure - Properties – Thermal transport properties. Mast visited on 24th January, 2018

PEDOT is displayed in Figure E1 for the sake of comparison with other thermo-electric materials and also to stir the curiosity of the interested reader.

References

(1) Shirakawa, H.; Louis, J.; Macdiarmid, A. G.; Chiang, C. K.; Heeger, A. J. Synthesis of Electrically Conducting Organic Polymers : Halogen Derivatives of Polyacetylene, (CH)x. *Chem. Commun.* **1977**, *0* (16), 578–580.

(2) Shirakawa, H.; Macdiarmid, A. G. Electrical Conductivity in Doped Polyacetylene. *Phys. Rev. Lett.* **1977**, *39* (17), 1098–1101.

(3) Naarmann, H. Structure and Conductivity of Organic Polymers. *Angew. Chmie Int. Ed.* **1969**, *8* (11), 915–916.

(4) Letheby, H. On the Production of a Blue Substance by the Electrolysis of Sulphate of Aniline. *J. Chem. Soc.* **1862**, *15* (0), 161–163.

(5) Josefowicz, L.; Yu, L. .; Belorgey, G.; Buvet, R. Conductivité Electronique et Propriétés Chimiques de Polyanilines Oligomères. *J. Polym. Sci. Part C* **1967**, *16* (5), 2943–2954.

(6) Bolto, B. A.; McNeill, R.; Weiss, D. E. Electronic Conduction in Polymers III. The Electronic Properties of Polypyrrole. *Aust. J. Chem.* **1963**, *16* (6), 1090–1103.

(7) McNeill, R.; Siudac, R.; Wardlaw, J. H.; Weiss, D. E. Electronic Conduction in Polymers I. The Chemical Structure of Polypyrrole. *Aust. J. Chem.* **1963**, *16* (6), 1056–1075.

(8) Bolto, B. A.; Weiss, D. E. Electronic Conduction in Polymers II. The Electrochemical Reduction of Polypyrrole at Controlled Temperature. *Aust. J. Chem.* **1963**, *16* (6), 1076–1089.

(9) Heeger, A. J. Semiconducting and Metallic Polymers : The Fourth Generation of Polymeric Materials (Nobel Lecture). *Angew. Chemie - Int. Ed.* **2001**, *105* (36), 8475–8491.

(10) Gueye, M. N.; Carella, A.; Massonnet, N.; Yvenou, E.; Brenet, S.; Faure-Vincent, J.; Pouget, S.; Rieutord, F.; Okuno, H.; Benayad, A.; Demadrille, R.; Simonato, J.-P. Structure and Dopant Engineering in PEDOT Thin Films: Practical Tools

for a Dramatic Conductivity Enhancement. *Chem. Mater.* **2016**, *28* (10), 3462–3468.

(11) Gueye, M. N.; Carella, A.; Demadrille, R.; Simonato, J.; Accepted, J. All-Polymeric Flexible Transparent Heaters. *ACS Appl. Mater. Interfaces* **2017**, *9* (32), 27250–27256.

(12) Elschner, A.; Kirchmeyer, S.; Lövenich, W.; Merker, U.; Reuter, K. *PEDOT Principples and Applications of an Intrinsically Conductive Polymer*; 2010.

(13) Pron, A.; Gawrys, P.; Zagorska, M.; Djurado, D.; Demadrille, R. Electroactive Materials for Organic Electronics: Preparation Strategies, Structural Aspects and Characterization Techniques. *Chem. Soc. Rev.* **2010**, *39* (7), 2577–2632.

(14) Attias, A.-J. Polymères Conjugués et Électronique Organique. *Tech. l'ingénieur* **2017**, E1862 V2.

(15) Patil, A.; Heeger, A. J.; Wudl, F. Optical Properties of Conducting Polymers. *Chem. Rev.* **1988**, *88* (1), 183–200.

(16) Brooke, R.; Cottis, P.; Talemi, P.; Fabretto, M.; Murphy, P.; Evans, D. Recent Advances in the Synthesis of Conducting Polymers from the Vapour Phase. *Prog. Mater. Sci.* **2017**, *86*, 127–146.

(17) Bredas, J. L.; Street, G. B. Polarons , Bipolarons , and Solitons in Conducting Polymers. *Acc. Chem. Res.* **1985**, *18* (10), 309–315.

(18) Massonnet, N. Développement et Optimisation de Matériaux À Base de Poly (3,4-Éthylènedioxythiphène) Pour Des Applications Thermoélectriques, Université Grenoble Alpes, 2014.

(19) Kim, J. Y.; Jung, J. H.; Lee, D. E.; Joo, J. Enhancement of Electrical Conductivity of poly(3,4-ethylenedioxythiophene)/poly(4-Styrenesulfonate) by a Change of Solvents. *Synth. Met.* **2002**, *126* (2-3), 311–316.

(20) Bubnova, O.; Khan, Z. U.; Wang, H.; Braun, S.; Evans, D. R.; Fabretto, M.; Hojati-Talemi, P.; Dagnelund, D.; Arlin, J.-B.; Geerts, Y. H.; Desbief, S.; Breiby, D. W.; Andreasen, J. W.; Lazzaroni, R.; Chen, W. M.; Zozoulenko, I.; Fahlman, M.; Murphy, P. J.; Berggren, M.; Crispin, X. Semi-Metallic Polymers. *Nat. Mater.* **2014**, *13* (1), 190–194.

(21) Jain, V.; Sahoo, R.; Mishra, S. P.; Sinha, J.; Montazami, R.; Yochum, H. M.; Heflin, J. R.; Kumar, A. Synthesis and Characterization of Regioregular Water-

Soluble 3,4-Propylenedioxythiophene Derivative and Its Application in the Fabrication of High-Contrast Solid-State Electrochromic Devices. *Macromolecules* **2009**, *42* (1), 135–140.

(22) Karabay, B.; Pekel, L. C.; Cihaner, A. A Pure Blue to Highly Transmissive Electrochromic Polymer Based on Poly(3,4-Propylenedioxyselenophene) with a High Optical Contrast Ratio. *Macromolecules* **2015**, *48* (5), 1352–1357.

(23) Chang, W. B.; Fang, H.; Liu, J.; Evans, C. M.; Russ, B.; Popere, B. C.; Patel, S. N.; Chabinyc, M. L.; Segalman, R. a. Electrochemical Effects in Thermoelectric Polymers. *ACS Macro Lett.* **2016**, *5* (4), 455–459.

(24) Tessler, N.; Preezant, Y.; Rappaport, N.; Roichman, Y. Charge Transport in Disordered Organic Materials and Its Relevance to Thin-Film Devices: A Tutorial Review. *Adv. Mater.* **2009**, *21* (27), 2741–2761.

(25) Noriega, R.; Rivnay, J.; Vandewal, K.; Koch, F. P. V; Stingelin, N.; Smith, P.; Toney, M. F.; Salleo, A. A General Relationship between Disorder, Aggregation and Charge Transport in Conjugated Polymers. *Nat. Mater.* **2013**, *12* (11), 1038–1044.

(26) Yao, Y.; Dong, H.; Hu, W. Charge Transport in Organic and Polymeric Semiconductors for Flexible and Stretchable Devices. *Adv. Mater.* **2015**, *28* (22), 4513–4523.

(27) Andersson, P. Absence of Diffusion in Certain Random Lattices. *Phys. Rev.* **1958**, *109* (5), 1492–1505.

(28) Mott, N. F. Conduction in Non-Crystalline Materials. *Philos. Mag.* **1969**, *19* (160), 835–852.

(29) Park, Y.-W.; Heeger, A. J.; Druy, M. A.; MacDiarmid, A. G. Electrical Transport in Doped Polyacetylene. *J. Chem. Phys.* **1980**, *73* (1980), 946–957.

(30) Menon, R.; Yoon, C. O.; Moses, D.; Heeger, A. J. Transport in Polyaniline near the Critical Regime of the Metal-Insulator Transition. *Phys. Rev. B Condens. Matter* **1993**, *48* (24), 17685–17694.

(31) Ishiguro, T.; Kaneko, H.; Nogami, Y.; Ishimoto, H.; Nishiyama, H.; Tsukamoto, J.; Takahashi, a.; Yamaura, M.; Hagiwara, T.; Sato, K. Logarithmic Temperature Dependence of Resistivity in Heavily Doped Conducting Polymers at Low Temperature. *Phys. Rev. Lett.* **1992**, *69* (4), 660–663.

(32) Massonnet, N.; Carella, A.; de Geyer, A.; Faure-Vincent, J.; Simonato, J.-P. Metallic Behaviour of Acid Doped Highly Conductive Polymers. *Chem. Sci.* **2015**, *6* (1), 412–417.

(33) Farka, D.; Coskun, H.; Gasiorowski, J.; Cobet, C.; Hingerl, K.; Uiberlacker, L. M.; Hild, S.; Greunz, T.; Stifter, D.; Sariciftci, N. S.; Menon, R.; Schoefberger, W.; Mardare, C. C.; Hassel, A. W.; Schwarzinger, C.; Scharber, M. C.; Stadler, P. Anderson-Localization and the Mott – Ioffe – Regel Limit in Glassy-Metallic PEDOT. *Adv. Electron. Mater.* **2017**, *3* (7), 170050.

(34) Sheng, P.; Abeles, B.; Arie, Y. Hopping Conductivity in Granular Metals. *Phys. Rev. Lett.* **1973**, *31* (1), 44–47.

(35) Sheng, P. Fluctuation-Induced Tunneling Conduction in Disordered Materials. *Phys. Rev. B* **1980**, *21* (6), 2180–2195.

(36) Kivelson, S.; Heeger, A. J. Intrinsic Conductivity of Conducting Polymers. *Synth. Met.* **1988**, *22* (4), 371–384.

(37) Kaiser, A. B. Metallic Behaviour in Highly Conducting Polymers. *Synth. Met.* **1991**, *45* (2), 183–196.

(38) Kaiser, A. B.; Graham, S. Temperature Dependance of Conductivity in "Metallic" Polyacetylene. *Synth. Met.* **1990**, *36* (3), 367–380.

(39) Naarmann, H.; Theophilou, N. New Processes for the Production of Metal-Like, Stable Polyacetylene. *Synth. Met.* **1987**, *22* (1), 1–8.

(40) Münstedt, H. Ageing of Electrically Conducting Organic Materials. *Polymer (Guildf).* **1988**, *29* (2), 296–302.

(41) Roth, B. S.; Filzmoser, M. Conducting Polymers - Thirteen Years of Polyacetylene Doping. *Adv. Mater.* **1990**, *2* (8), 356–360.

(42) Jonas, F.; Schrader, L. Conductive Modifications of Polymers with Polypyrroles and Polythiophenes. *Synth. Met.* **1991**, *43* (3), 831–836.

(43) Fichou, D. *Handbook of Oligo- and Polythiophenes*, Weinheim.; 1999.

(44) Groenendaal, B. L.; Jonas, F.; Freitag, D.; Pielartzik, H.; Reynolds, J. R. Poly(3,4-Ethylenedioxythiophene) and Its Derivatives: Past, Present, and Future. *Adv. Mater.* **2000**, *12* (7), 481–494.

(45) Heywang, G.; Jonas, F. Poly(alkylenedioxythiophene)s - New , Very Stable Conducting Polymers. *Adv. Mater.* **1992**, *4* (2), 116–118.

(46) Jonas, F.; Heywang, G.; Schmidtberg, W.; Heinze, J.; Dietrich, M. Procédé Pour La Préparation de Polythiophènes. EP0339340, 1988.

(47) Jonas, F.; Heywang, G.; Schmidtberg, W. Feststoff-Elektrolyte Und Diese Enthaltende Elektrolyt-Kondensatoren. DE 3814730 A1, 1988.

(48) Heywang, G.; Jonas, F.; Heinze, J.; Dietrich, M. Neue Polythiophene, Verfahren Zu Ihrer Herstellung Und Ihre Verwendung. DE 3843412 A1, 1988.

(49) Jonas, F.; Krafft, W. Dispersions de Polythiophènes Nouvelles, Leur Préparation et Leur Utilisation. EP0440957, 1990.

(50) Fallahzadeh, A.; Saghaei, J.; Saghaei, T. Ultra-Smooth poly(3,4-Ethylene Dioxythiophene):poly(styrene Sulfonate) Films for Flexible Indium Tin Oxide-Free Organic Light-Emitting Diodes. *J. Lumin.* **2016**, *169* (Part A), 251–255.

(51) Lee, I.; Kim, G. W.; Yang, M.; Kim, T. Simultaneously Enhancing the Cohesion and Electrical Conductivity of PEDOT:PSS Conductive Polymer Films Using DMSO Additives. *ACS Appl. Mater. Interfaces* **2016**, *8* (1), 302–310.

(52) Zhou, Y.; Cheun, H.; Choi, S.; Potscavage, W. J.; Fuentes-Hernandez, C.; Kippelen, B. Indium Tin Oxide-Free and Metal-Free Semitransparent Organic Solar Cells. *Appl. Phys. Lett.* **2010**, *97* (2010), 153304.

(53) Zhou, Y.; Fuentes-hernandez, C.; Shim, J.; Meyer, J.; Giordano, A. J.; Li, H.; Winget, P.; Papadopoulos, T.; Cheun, H.; Kim, J.; Fenoll, M.; Dindar, A.; Haske, W.; Najafabadi, E.; Khan, T. M.; Sojoudi, H.; Barlow, S.; Graham, S.; Brédas, J.; Marder, S. R.; Kahn, A.; Kippelen, B. A Universal Method to Produce Low–Work Function Electrodes for Organic Electronics. *Science (80-.).* **2012**, *336* (6019), 327–332.

(54) Kim, N.; Kang, H.; Lee, J.-H.; Kee, S.; Lee, S. H.; Lee, K. Highly Conductive All-Plastic Electrodes Fabricated Using a Novel Chemically Controlled Transfer-Printing Method. *Adv. Mater.* **2015**, *27* (14), 2317–2323.

(55) Roncali, J.; Blanchard, P.; Frère, P. 3,4-Ethylenedioxythiophene (EDOT) as a Versatile Building Block for Advanced Functional Pi-Conjugated Systems. *J. Mater. Chem.* **2005**, *15* (16), 1589–1610.

(56) Kirchmeyer, S.; Reuter, K. Scientific Importance , Properties and Growing Applications of poly(3,4-Ethylenedioxythiophene). *J. Mater. Chem.* **2005**, *15* (21), 2077–2088.

(57) Yamamoto, T.; Abla, M. Synthesis of Non-Doped poly(3,4-Ethylenedioxythiophene) and Its Spectroscopic Data. *Synth. Met.* **1999**, *100* (2), 237–239.

(58) Pei, Q.; Zuccarello, G.; Ahlskogt, M.; Inganäs, O. Electrochromic and Highly Stable poly(3,4-Ethylenedioxythiophene) Switches between Opaque Blue-Black and Transparent Sky Blue. *Polymer (Guildf).* **1994**, *35* (7), 1347–1351.

(59) Granström, M.; Inganäs, O. Electrically Conductive Polymer Fibres with Mesoscopic Diameters: 1. Studies of Structure and Electrical Properties. *Polymer (Guildf).* **1995**, *36* (15), 2867–2872.

(60) Zotti, G.; Zecchin, S.; Schiavon, G.; Louwet, F.; Groenendaal, L.; Crispin, X.; Osikowicz, W.; Salaneck, W.; Fahlman, M. Electrochemical and XPS Studies toward the Role of Monomeric and Polymeric Sulfonate Counterions in the Synthesis, Composition, and Properties of poly(3,4-Ethylenedioxythiophene). *Macromolecules* **2003**, *36* (39), 3337–3344.

(61) Mueller, M.; Fabretto, M.; Evans, D.; Hojati-talemi, P.; Gruber, C.; Murphy, P. Vacuum Vapour Phase Polymerization of High Conductivity PEDOT : Role of PEG-PPG-PEG , the Origin of Water , and Choice of Oxidant. *Polymer (Guildf).* **2012**, *53* (11), 2146–2151.

(62) Hohnholz, D.; MacDiarmid, A. G.; Sarno, D. M.; E. Johnes Jr., W. Uniform Thin Films of Poly-3,4-Ethylenedioxythiophene (PEDOT) Prepared by. *Chem. Commun.* **2001**, 2444–2445.

(63) Jin Bae, E.; Hun Kang, Y.; Jang, K.-S.; Yun Cho, S. Enhancement of Thermoelectric Properties of PEDOT:PSS and Tellurium-PEDOT:PSS Hybrid Composites by Simple Chemical Treatment. *Sci. Rep.* **2016**, *6*, 18805.

(64) Leeuw, D. M. De; Kraakman, P. A.; Bongaerts, P. F. G.; Mutsaers, C. M. J.; Klaassen, D. B. M. Electroplating of Conductive Polymers for the Metallization of Insulators. *Synth. Met.* **1994**, *66*, 263–273.

(65) U, L. A. A. P.; Carlsson, F.; Inganas, O.; Arwin, H. Spectroscopic Ellipsometry Studies of the Optical Properties of Doped Poly Ž 3 , 4-Ethylenedioxythiophene . : An Anisotropic Metal. *Thin Solid Films* **1998**, *131-131* (13), 356–361.

(66) Winther-Jensen, B.; West, K. Vapor-Phase Polymerization of 3,4-Ethylenedioxythiophene: A Route to Highly Conducting Polymer Surface Layers. *Macromolecules* **2004**, *37* (12), 4538–4543.

(67) Lock, J. P.; Im, S. G.; Gleason, K. K. Oxidative Chemical Vapor Deposition of Electrically Conducting Poly (3 , 4-Ethylenedioxythiophene) Films. *Macromolecules* **2006**, *39* (16), 5326–5329.

(68) Kim, J.; Kwon, M.; Min, Y.; Kwon, S.; Ihm, D. Self-Assembly and Crystalline Growth of Poly (3 , 4-Ethylenedioxythiophene) Nanofilms. *Adv. Mater.* **2007**, *19* (21), 3501–3506.

(69) Fabretto, M.; Müller, M.; Hall, C.; Murphy, P.; Short, R. D.; Griesser, H. J. In-Situ QCM-D Analysis Reveals Four Distinct Stages during Vapour Phase Polymerisation of PEDOT Thin Films. *Polymer (Guildf).* **2010**, *51* (8), 1737–1743.

(70) Winther-jensen, B.; Breiby, D. W.; West, K. Base Inhibited Oxidative Polymerization of 3,4-Ethylene Dioxythiophene with iron(III)tosylate. *Synth. Met.* **2005**, *152* (1-3), 1–4.

(71) Greczynski, G.; Kugler, T.; Salaneck, W. R. Characterization of the PEDOT-PSS System by Means of X-Ray and Ultraviolet Photoelectron Spectroscopy. *Thin Solid Films* **1999**, *354* (1-2), 129–135.

(72) Jönsson, S. K. M.; Birgerson, J.; Crispin, X.; Greczynski, G.; Osikowicz, W.; Denier van der Gon, a. W.; Salaneck, W. R.; Fahlman, M. The Effects of Solvents on the Morphology and Sheet Resistance in poly(3,4-Ethylenedioxythiophene)-Polystyrenesulfonic Acid (PEDOT-PSS) Films. *Synth. Met.* **2003**, *139*, 1–10.

(73) Gustafsson, J.; Liedberg, B.; Inganas, O. In Situ Spectroscopic Investigations of Electrochromism and Ion Transport in a Poly (3,4-Ethylenedioxythiophene) Electrode in a Solid State Electrochemical Cell. *Solid State Ionics*. 1994, pp 145–152.

(74) Bubnova, O.; Crispin, X. Towards Polymer-Based Organic Thermoelectric Generators. *Energy Environ. Sci.* **2012**, *5* (11), 9345–9362.

(75) Massonnet, N.; Carella, A.; Jaudouin, O.; Rannou, P.; Laval, G.; Celle, C.; Simonato, J.-P. Improvement of the Seebeck Coefficient of PEDOT:PSS by

Chemical Reduction Combined with a Novel Method for Its Transfer Using Free-Standing Thin Films. *J. Mater. Chem. C* **2014**, *2* (7), 1278–1283.

(76) Crispin, X.; Marciniak, S. Conductivity, Morphology, Interfacial Chemistry, and Stability of Poly (3, 4-ethylene Dioxythiophene)–poly (styrene Sulfonate): A Photoelectron Spectroscopy Study. *J. Polym. Sci. Part B Polym. Phys.* **2003**, *41*, 2561–2583.

(77) Greczynski, G.; Kugler, T.; Keil, M.; Osikowicz, W.; Fahlman, M.; Salaneck, W. R. Photoelectron Spectroscopy of Thin Films of PEDOT – PSS Conjugated Polymer Blend : A Mini-Review and Some New Results. *J. Electron Spectros. Relat. Phenomena* **2001**, *121* (1-3), 1–17.

(78) Crispin, X.; Jakobsson, F. L. E.; Crispin, A.; Grim, P. C. M.; Andersson, P.; Volodin, A.; van Haesendonck, C.; Van der Auweraer, M.; Salaneck, W. R.; Berggren, M. The Origin of the High Conductivity of poly(3,4-Ethylenedioxythiophene)-Poly(styrenesulfonate) (PEDOT- PSS) Plastic Electrodes. *Chem. Mater.* **2006**, *18* (4), 4354–4360.

(79) Nardes, A. M.; Janssen, R. a J.; Kemerink, M. A Morphological Model for the Solvent-Enhanced Conductivity of PEDOT:PSS Thin Films. *Adv. Funct. Mater.* **2008**, *18* (1), 865–871.

(80) Nardes, A. M.; Kemerink, M.; Kok, M. M. De; Vinken, E.; Maturova, K.; Janssen, R. A. J. Conductivity , Work Function , and Environmental Stability of PEDOT : PSS Thin Films Treated with Sorbitol. *Org. Electron.* **2008**, *9* (5), 727–734.

(81) Badre, C.; Marquant, L.; Alsayed, A. M.; Hough, L. A. Highly Conductive poly(3,4-ethylenedioxythiophene):Poly (styrenesulfonate) Films Using 1-Ethyl-3-Methylimidazolium Tetracyanoborate Ionic Liquid. *Adv. Funct. Mater.* **2012**, *22* (13), 2723–2727.

(82) Fan, B.; Mei, X.; Ouyang, J. Significant Conductivity Enhancement of Conductive Poly (3 , 4-Ethylenedioxythiophene): Poly (Styrenesulfonate) Films by Adding Anionic Surfactants into Polymer Solution. *Macromolecules* **2008**, *41* (16), 5971–5973.

(83) Xia, Y.; Ouyang, J. Salt-Induced Charge Screening and Significant Conductivity Enhancement of Conducting Poly (3 , 4-Ethylenedioxythiophene): Poly (Styrenesulfonate). *Macromelecules* **2009**, *42* (12), 4141–4147.

(84) Kim, Y. H.; Sachse, C.; MacHala, M. L.; May, C.; Müller-Meskamp, L.; Leo, K. Highly Conductive PEDOT:PSS Electrode with Optimized Solvent and Thermal Post-Treatment for ITO-Free Organic Solar Cells. *Adv. Funct. Mater.* **2011**, *21* (6), 1076–1081.

(85) Worfolk, B. J.; Andrews, S. C.; Park, S.; Reinspach, J.; Liu, N.; Toney, M. F.; Mannsfeld, S. C. B.; Bao, Z. Ultrahigh Electrical Conductivity in Solution-Sheared Polymeric Transparent Films. *Proc. Natl. Acad. Sci.* **2015**, *12* (46), 14138–14143.

(86) Xia, Y.; Ouyang, J. Significant Conductivity Enhancement of Conductive poly(3,4- Ethylenedioxythiophene): Poly(styrenesulfonate) Films through a Treatment with Organic Carboxylic Acids and Inorganic Acids. *ACS Appl. Mater. Interfaces* **2010**, *2* (2), 474–483.

(87) Meng, W.; Ge, R.; Li, Z.; Tong, J.; Liu, T.; Zhao, Q.; Xiong, S.; Jiang, F.; Mao, L.; Zhou, Y. Conductivity Enhancement of PEDOT:PSS Films via Phosphoric Acid Treatment for Flexible All-Plastic Solar Cells. *ACS Appl. Mater. Interfaces* **2015**, *7* (25), 14089–14094.

(88) Ouyang, J.; Xu, Q.; Chu, C.; Yang, Y.; Li, G.; Shinar, J. On the Mechanism of Conductivity Enhancement in Poly(3,4-Ethylenedioxythiophene):poly(styrene Sulfonate) through Solvent Treatment. *Polymer (Guildf).* **2004**, *45* (25), 8443–8450.

(89) Aasmundtveit, K. E.; Samuelsent, E. J.; Pettersson, L. A. A.; Inganäs, O.; Johansson, T.; Feidenhans, R. Structure of Thin Films of Poly (3 , 4-Ethylenedioxythiophene). *Synth. Met.* **1999**, *101* (1-3), 561–564.

(90) Yu, S. H.; Lee, J. H.; Choi, M. S.; Park, J. H.; Yoo, P. J. Improvement of Electrical Conductivity of Poly (3 , 4- Ethylenedioxythiophene) (PEDOT) Thin Film. *Mol. Cryst. Liq. Cryst.* **2013**, *580* (1), 76–82.

(91) Cho, B.; Park, K. S.; Baek, J.; Oh, H. S.; Koo Lee, Y. E.; Sung, M. M. Single-Crystal Poly(3,4-Ethylenedioxythiophene) Nanowires with Ultrahigh Conductivity. *Nano Lett.* **2014**, *14* (6), 3321–3327.

(92) Wei, Q.; Mukaida, M.; Naitoh, Y.; Ishida, T. Morphological Change and Mobility Enhancement in PEDOT:PSS by Adding Co-Solvents. *Adv. Mater.* **2013**, *25* (20), 2831–2836.

(93) Takano, T.; Masunaga, H.; Fujiwara, A.; Okuzaki, H.; Sasaki, T. PEDOT Nanocrystal in Highly Conductive PEDOT_PSS Polymer Films. *Macromolecules* **2012**, *45* (9), 3859–3865.

(94) Madl, C. M.; Kariuki, P. N.; Gendron, J.; Piper, L. F. J.; Jones, W. E. Vapor Phase Polymerization of Poly (3 , 4-Ethylenedioxythiophene) on Flexible Substrates for Enhanced Transparent Electrodes. *Synth. Met.* **2011**, *161* (13-14), 1159–1165.

(95) Shi, H.; Liu, C.; Jiang, Q.; Xu, J. Effective Approaches to Improve the Electrical Conductivity of PEDOT:PSS: A Review. *Adv. Electron. Mater.* **2015**, *1* (4), 1500017.

(96) Xiong, J.; Jiang, F.; Zhou, W.; Liu, C.; Xu, J. Highly Electrical and Thermoelectric Properties of a PEDOT:PSS Thin-Film via Direct Dilution–filtration. *RSC Adv.* **2015**, *5* (75), 60708–60712.

(97) Culebras, M.; Gomez, C. M.; Cantarero, A. Enhanced Thermoelectric Performance of PEDOT with Di Ff Erent Counter-Ions Optimized by Chemical Reduction. *J. Mater. Chem. A* **2014**, *2* (26), 10109–10115.

(98) Kumar, S. R. S.; Kurra, N.; Alshareef, H. N. Enhanced High Temperature Thermoelectric Response of Sulphuric Acid Treated Conducting Polymer Thin Films. *J. Mater. Chem. C* **2016**, *4* (1), 215–221.

(99) Kaiser, A. B. Electronic Transport Properties of Conducting Polymers and Carbon Nanotubes. *Reports Prog. Phys.* **2001**, *64* (1), 1–49.

(100) Lee, K.; Cho, S.; Park, S. H.; Heeger, a J.; Lee, C.-W.; Lee, S.-H. Metallic Transport in Polyaniline. *Nature* **2006**, *441* (May), 65–68.

(101) Fabretto, M. V.; Evans, D. R.; Mueller, M.; Zuber, K.; Hojati-Talemi, P.; Short, R. D.; Wallace, G. G.; Murphy, P. J. Polymeric Material with Metal-like Conductivity for next Generation Organic Electronic Devices. *Chem. Mater.* **2012**, *24* (20), 3998–4003.

(102) Wei, Q.; Mukaida, M.; Kirihara, K.; Naitoh, Y.; Ishida, T. Recent Progress on PEDOT-Based Thermoelectric Materials. *Materials (Basel).* **2015**, *8* (2), 732–750.

(103) Suchand Sangeeth, C. S.; Jaiswal, M.; Menon, R. Correlation of Morphology and Charge Transport in poly(3,4-Ethylenedioxythiophene)-Polystyrenesulfonic Acid (PEDOT-PSS) Films. *J. physics. Condens. matter* **2009**, *21* (7), 072101.

(104) Khan, Z. U.; Bubnova, O.; Jafari, M. J.; Brooke, R.; Liu, X.; Gabrielsson, R.; Ederth, T.; Evans, D. R.; Andreasen, J. W.; Fahlman, M.; Crispin, X. Acido-Basic Control of the Thermoelectric Properties of poly(3,4-Ethylenedioxythiophene)tosylate (PEDOT-Tos) Thin Films. *J. Mater. Chem. C* **2015**, *3* (40), 10616–10623.

(105) Mai, C.-K.; Russ, B.; Fronk, S. L.; Hu, N.; Chan-Park, M. B.; Urban, J. J.; Segalman, R. a.; Chabinyc, M. L.; Bazan, G. C. Varying the Ionic Functionalities of Conjugated Polyelectrolytes Leads to Both P- and N-Type Carbon Nanotube Composites for Flexible Thermoelectrics. *Energy Environ. Sci.* **2015**.

(106) Kim, G.-H.; Shao, L.; Zhang, K.; Pipe, K. P. Engineered Doping of Organic Semiconductors for Enhanced Thermoelectric Efficiency. *Nat. Mater.* **2013**, *12* (8), 719–723.

(107) Yee, S. K.; Coates, N. E.; Majumdar, A.; Urban, J. J.; Segalman, R. a. Thermoelectric Power Factor Optimization in PEDOT:PSS Tellurium Nanowire Hybrid Composites. *Phys. Chem. Chem. Phys.* **2013**, *15*, 4024–4032.

(108) Zhou, J.; Anjum, D. H.; Lubineau, G.; Li, E. Q.; Thoroddsen, S. T. Unraveling the Order and Disorder in poly(3,4-Ethylenedioxythiophene)/poly(styrenesulfonate) Nanofilms. *Macromolecules* **2015**, *48*, 5688–5696.

(109) Zuber, K.; Fabretto, M.; Hall, C.; Murphy, P. Improved PEDOT Conductivity via Suppression of Crystallite Formation in Fe (III) Tosylate During Vapor Phase Polymerization. *Macromol. Rapid Commun.* **2008**, *29* (18), 1503–1508.

(110) Fabretto, M.; Müller, M.; Zuber, K.; Murphy, P. Influence of Peg-Ran-Ppg Surfactant on Vapour Phase Polymerised PEDOT Thin Films. *Macromol. Rapid Commun.* **2009**, *30* (21), 1846–1851.

(111) Fabretto, M.; Jariego-Moncunill, C.; Autere, J. P.; Michelmore, A.; Short, R. D.; Murphy, P. High Conductivity PEDOT Resulting from Glycol/oxidant Complex and Glycol/polymer Intercalation during Vacuum Vapour Phase Polymerisation. *Polymer (Guildf).* **2011**, *52* (8), 1725–1730.

(112) Hojati-Talemi, P.; Bächler, C.; Fabretto, M.; Murphy, P.; Evans, D. Ultrathin Polymer Films for Transparent Electrode Applications Prepared by Controlled Nucleation. *ACS Appl. Mater. Interfaces* **2013**, *5* (1), 11654–11660.

(113) Xia, Y.; Sun, K.; Ouyang, J. Solution-Processed Metallic Conducting Polymer Films as Transparent Electrode of Optoelectronic Devices. *Adv. Mater.* **2012**, *24* (18), 2436–2440.

(114) Ahlskog, M.; Menon, R.; Heeger, A.; Noguchi, T.; Ohnishi, T. Electronic Transport in the Metallic State of Oriented Poly(p-Phenylenevinylene). *Phys. Rev. B* **1996**, *53* (23), 15529–15537.

(115) Ugur, A.; Katmis, F.; Li, M.; Wu, L.; Zhu, Y.; Varanasi, K. K.; Gleason, K. K. Low-Dimensional Conduction Mechanisms in Highly Conductive and Transparent Conjugated Polymers. *Adv. Mater.* **2015**, *27* (31), 4604–4610.

(116) Metsik, J.; Timusk, M.; Käämbre, T.; Mändar, H.; Umalas, M.; Kuus, A.; Puust, L.; Utt, K.; Sildos, I.; Mäeorg, U. Stability of Poly (3 , 4-Ethylenedioxythiophene) Thin Fi Lms Prepared by Vapor Phase Polymerization. *Polym. Degrad. Stab.* **2016**, *126*, 170–178.

(117) Zabrodskii, A. G. Electrical Conductivity of Heavily Doped Compensated N-Type Germanium Produced by Neutron Doping. *Sov. Physics. Semicond.* **1980**, *14* (6), 670–676.

(118) Sun, Y.; Sheng, P.; Di, C.; Jiao, F.; Xu, W.; Qiu, D.; Zhu, D. Organic Thermoelectric Materials and Devices Based on P- and N-Type Poly(metal 1,1,2,2-Ethenetetrathiolate)s. *Adv. Mater.* **2012**, *24*, 932–937.

(119) Sichel, E. K.; Gittleman, J. I.; Sheng, P. Transport Properties of the Composite Material Carbon-Poly(vinyl Chloride). *Phys. Rev. B* **1978**, *18* (10), 5712–5716.

(120) Kaiser, A. B. Systematic Conductivity Behavior in Conducting Polymers: Effects of Heterogeneous Disorder. *Adv. Mater.* **2001**, *13* (12), 927–941.

(121) Shi, W.; Zhao, T.; Xi, J.; Wang, D.; Shuai, Z. Unravelling Doping Effects on PEDOT at the Molecular Level: From Geometry to Thermoelectric Transport Properties. *J. Am. Chem. Soc.* **2015**, *137*, 12929–12938.

(122) Okuzaki, H.; Suzuki, H.; Ito, T. Electromechanical Properties of Poly(3,4-ethylenedioxythiophene)/Poly(4-Styrene Sulfonate) Films. *J. Phys. Chem. B* **2009**, *113* (33), 11378–11383.

(123) Zhou, J.; Mulle, M.; Zhang, Y.; Xu, X.; Li, E. High-Ampacity Conductive Polymer Microfibers as Fast Response Wearable Heaters and Electromechanical Actuators. *J. Mater. Chem. C* **2016**, *4* (6), 1238–1249.

(124) Yeon, C.; Kim, G.; Lim, J. W.; Yun, S. J. Highly Conductive PEDOT : PSS Treated by Sodium Dodecyl Sulfate for Stretchable Fabric Heaters. *RSC Adv.* **2017**, *7* (10), 5888–5897.

(125) Zhou, J.; Fukawa, T.; Kimura, M. Directional Electromechanical Properties of PEDOT / PSS Films Containing Aligned Electrospun Nanofibers. *Polym. J.* **2011**, *43* (10), 849–854.

(126) Zhou, J.; Kimura, M. Transaction Electromechanical Actuation of Highly Conductive PEDOT / PSS-Coated Cellulose Papers. *Sen'I Gakkaishi* **2011**, *67* (6), 125–131.

(127) Laforgue, A. Electrically Controlled Colour-Changing Textiles Using the Resistive Heating Properties of PEDOT Nanofibers †. *J. Mater. Chem.* **2010**, *20*, 8233–8235.

(128) Lin, Y.; Ni, W.; Lee, J. Effect of Incorporation of Ethylene Glycol into PEDOT : PSS on Electron Phonon Coupling and Conductivity. *J. Appl. Phys.* **2015**, *117* (21), 21501.

(129) Taguchi, T.; Ueno, Y.; Hattori, T. DEFROSTABLE OUTSIDE REAR VIEW MIRROR FOR AN AUTOMOBILE. 4634242, 1987.

(130) De, S.; Coleman, J. N. Are There Fundamental Limitations on the Sheet Resistance and Transmittance of Thin Graphene Films ? *ACS Nano* **2010**, *4* (5), 2713–2720.

(131) Sorel, S.; Bellet, D.; Coleman, J. N. Relationship between Material Properties and Transparent Heater Performance for Both Bulk-like and Percolative Nanostructured Networks. *ACS Nano* **2014**, *8* (5), 4805–4814.

(132) Gupta, R.; Rao, K. D. M.; Srivastava, K.; Kumar, A.; Kiruthika, S.; Kulkarni, G. U. Spray Coating of Crack Templates for the Fabrication of Transparent Conductors and Heaters on Flat and Curved Surfaces. *ACS Appl. Mater. Interfaces* **2014**, *6* (16), 13688–13696.

(133) Lagrange, M.; Sannicolo, T.; Lohan, B. G.; Khan, A.; Anikin, M.; Jiménez, C.; Bruckert, F.; Bréchet, Y.; Bellet, D. Understanding the Mechanisms Leading to Failure in Metallic Nanowire-Based Transparent Heaters , and Solution for Stability Enhancement. *Nanotechnology* **2017**, *28* (5), 055709.

(134) Ji, S.; He, W.; Wang, K.; Ran, Y.; Ye, C. Thermal Response of Transparent Silver Nanowire / PEDOT : PSS Film Heaters. *Small* **2014**, *10* (23), 4951–4960.

(135) Celle, C.; Mayousse, C.; Moreau, E.; Basti, H.; Carella, A.; Simonato, J. P. Highly Flexible Transparent Film Heaters Based on Random Networks of Silver Nanowires. *Nano Res.* **2012**, *5* (6), 427–433.

(136) Janas, D.; Koziol, K. K. A Review of Production Methods of Carbon Nanotube and Graphene Thin Films for Electrothermal Applications. *Nanoscale* **2014**, *6* (6), 3037–3045.

(137) Gupta, R.; Rao, K. D. M.; Kiruthika, S.; Kulkarni, G. U. Visibly Transparent Heaters. *ACS Appl. Mater. Interfaces* **2016**, *8* (20), 12559–12575.

(138) Savage, N. Optical Adhesives. *Nat. Photonics* **2009**, *3* (7), 418–419.

(139) Gordon, R. G. Criteria for Choosing Transparent Conductors. *MRS Bull.* **2000**, *25* (8), 52–57.

(140) Angmo, D.; Krebs, F. C. Flexible ITO-Free Polymer Solar Cells. *J. Appl. Polym. Sci.* **2013**, *129* (1), 1–14.

(141) Kim, N.; Kee, S.; Lee, S. H.; Lee, B. H.; Kahng, Y. H.; Jo, Y. R.; Kim, B. J.; Lee, K. Highly Conductive PEDOT:PSS Nanofibrils Induced by Solution-Processed Crystallization. *Adv. Mater.* **2014**, *26* (14), 2268–2272.

(142) Kim, H. K.; Kim, M. S.; Chun, S. Y.; Park, Y. H.; Jeon, B. S.; Lee, J. Y.; Hong, Y. K.; Joo, J.; Kim, S. H. CHARACTERISTICS OF ELECTRICALLY CONDUCTING POLYMER-COATED TEXTILES. *Mol. Cryst. Liq. Cryst.* **2003**, *405* (1), 161–169.

(143) Mukherjee, S.; Singh, R.; Gopinathan, S.; Murugan, S.; Gawali, S.; Saha, B.; Biswas, J.; Lodha, S.; Kumar, A. Solution-Processed Poly (3 , 4-Ethylenedioxythiophene) Thin Films as Transparent Conductors : Effect of P-Toluenesulfonic Acid in Dimethyl Sulfoxide. *ACS Appl. Mater. Interfaces* **2014**, *6* (20), 17792–17803.

(144) Sannicolo, T.; Lagrange, M.; Cabos, A.; Celle, C.; Simonato, J.; Bellet, D. Metallic Nanowire-Based Transparent Electrodes for Next Generation Flexible Devices : A Review. *Small* **2016**, *12* (144), 6052–6075.

(145) Kim, J. H.; Ahn, B. Du; Kim, C. H.; Jeon, K. A.; Kang, H. S.; Lee, S. Y. Heat Generation Properties of Ga Doped ZnO Thin Films Prepared by Rf-Magnetron Sputtering for Transparent Heaters. *Thin Solid Films* **2008**, *516* (7), 1330–1333.

(146) Jang, H.; Jeon, S. K.; Nahm, S. H. The Manufacture of a Transparent Film Heater by Spinning Multi-Walled Carbon Nanotubes. *Carbon N. Y.* **2011**, *49* (1), 111–116.

(147) Bae, J. J.; Lim, S. C.; Han, G. H.; Jo, Y. W.; Doung, D. L.; Kim, E. S.; Chae, S. J.; Huy, T. Q.; Luan, N. Van; Lee, Y. H. Heat Dissipation of Transparent Graphene Defoggers. *Adv. Funct. Mater.* **2012**, *22* (21), 4819–4826.

(148) Zhai, H.; Wang, R.; Wang, X.; Cheng, Y.; Shi, L.; Sun, J. Transparent Heaters Based on Highly Stable Cu Nanowire. *Nano Res.* **2016**, *9* (12), 3924–3936.

(149) Chen, J.; Chen, J.; Li, Y.; Zhou, W.; Feng, X.; Huang, Q.; Zheng, J.; Liu, R.; Ma, Y.; Huang, W. Enhanced Oxidation-Resistant Cu–Ni Core–shell Nanowires: Controllable One-Pot Synthesis and Solution Processing to Transparent Flexible Heaters. *Nanoscale* **2015**, *7* (40), 16874–16879.

(150) Hecht, D. S.; Hu, L.; Irvin, G. Emerging Transparent Electrodes Based on Thin Films of Carbon Nanotubes , Graphene , and Metallic Nanostructures. *Adv. Mater.* **2011**, *23* (13), 1482–1513.

(151) Gupta, R.; Walia, S.; Jensen, J.; Angmo, D.; Krebs, F. C.; Kulkarni, G. U. Solution Processed Large Area Fabrication of Ag Patterns as Electrodes for Flexible Heaters, Electrochromics and Organic Solar Cells. *J. Mater. Chem. A* **2014**, *2* (28), 10930–10937.

(152) Gao, T.; Wang, B.; Ding, B.; Lee, J.; Leu, P. W. Uniform and Ordered Copper Nanomeshes by Microsphere Lithography for Transparent Electrodes. *Nano Lett.* **2014**, *14* (4), 2105–2110.

(153) Lan, W.; Chen, Y.; Yang, Z.; Han, W.; Zhou, J.; Zhang, Y.; Wang, J.; Tang, G.; Wei, Y.; Dou, W.; Su, Q.; Xie, E. Ultra Flexible Transparent Film Heater Made of Ag Nanowire/PVA Composite for Rapid-Response Thermotherapy Pads. *ACS Appl. Mater. Interfaces* **2017**, *9* (7), 6644–6651.

(154) Lordan, D.; Burke, M.; Manning, M.; Martin, A.; Amann, A.; Connell, D. O.; Murphy, R.; Lyons, C.; Quinn, A. J. Asymmetric Pentagonal Metal Meshes for Flexible Transparent Electrodes and Heaters. *ACS Appl. Mater. Interfaces* **2017**, *9* (5), 4932–4940.

(155) Kang, J.; Kim, H.; Kim, K. S.; Lee, S.-K.; Bae, S.; Ahn, J.-H.; Kim, Y.; Choi, J.; Hong, B. H. High-Performance Graphene-Based Transparent Flexible Heaters. *Nano Lett.* **2011**, *11* (12), 5154–5158.

(156) Sui, D.; Huang, Y.; Huang, L.; Liang, J.; Ma, Y.; Chen, Y. Flexible and Transparent Electrothermal Film Heaters Based on Graphene Materials. *Small* **2011**, *7* (22), 3186–3192.

(157) Simonato, J. P.; Celle, C.; Mayousse, C.; Carella, A.; Basti, H.; Carpentier, A. Transparent Film Heaters Based on Silver Nanowire Random Networks. *MRS Online Proc. Libr.* **2012**, *1449*.

(158) Lee, S. M.; Lee, J. H.; Bak, S.; Lee, K.; Li, Y.; Lee, H. Hybrid Windshield-Glass Heater for Commercial Vehicles Fabricated via Enhanced Electrostatic Interactions among a Substrate , Silver Nanowires , and an over-Coating Layer. *Nano Res.* **2015**, *8* (6), 1882–1892.

(159) Kim, T.; Kim, Y. W.; Lee, H. S.; Kim, H.; Yang, W. S.; Suh, K. S. Uniformly Interconnected Silver-Nanowire Networks for Transparent Film Heaters. *Adv. Funct. Mater.* **2013**, *23* (10), 1250–1255.

(160) Mayousse, C.; Celle, C.; Fraczkiewicz, A.; Simonato, J. Stability of Silver Nanowire Based Electrodes under Environmental and Electrical Stresses. *Nanoscale* **2015**, *7* (5), 2107–2115.

(161) Chen, S.; Song, L.; Tao, Z.; Shao, X.; Huang, Y.; Cui, Q.; Guo, X. Neutral-pH PEDOT : PSS as over-Coating Layer for Stable Silver Nanowire Flexible Transparent Conductive Films. *Org. Electron.* **2014**, *15* (12), 3654–3659.

(162) Choi, D. Y.; Kang, H. W.; Sung, H. J.; Kim, S. S. Annealing-Free, Flexible Silver Nanowire – Polymer Composite Electrodes via a Continuous Two-Step Spray-Coating Method. *Nanoscale* **2013**, *5* (3), 977–983.

(163) Argun, B. A. A.; Cirpan, A.; Reynolds, J. R. The First Truly All-Polymer Electrochromic Devices. *Adv. Mater.* **2003**, *15* (15), 1338–1341.

(164) Im, K.; Cho, K.; Kim, J.; Kim, S. Transparent Heaters Based on Solution-Processed Indium Tin Oxide Nanoparticles. *Thin Solid Films* **2010**, *518* (14), 3960–3963.

(165) Yoon, B. Y.; Song, J.; Kim, D.; Kim, J.; Park, J.; Oh, S. Transparent Film Heater Using Single-Walled Carbon Nanotubes. *Adv. Mater.* **2007**, *19* (23), 4284–4287.

(166) Kwon, N.; Kim, K.; Heo, J.; Yi, I.; Chung, I. Study on Ag Mesh/conductive Oxide Hybrid Transparent Electrode for Film Heaters. *Nanotechnology* **2014**, *25* (26), 265702.

(167) Cullen, J. M.; Allwood, J. M. Theoretical Ef Fi Ciency Limits for Energy Conversion Devices. *Energy* **2010**, *35* (5), 2059–2069.

(168) Sousa, T.; Brockway, P. E.; Cullen, J. M.; Miller, J.; Cabrera, A.; Domingos, T. The Need for Robust , Consistent Methods in Societal Exergy Accounting. *Ecol. Econ.* **2017**, *141*, 11–21.

(169) Seebeck, T. J. *Magnetische Polarisation Der Metalle Und Erze Durch Temperatur-Differenz*; pp 265–373.

(170) Seebeck, T. J. Ueber Die Magnetische Polarisation Der Mettale Und Erze Durch Temperatur Differenz. *Ann. Phys.* **1826**, *82* (2), 133–160.

(171) Ørsted, H. C. Nouvelles Experiences de M. Seebeck Sur Les Actions Électro-Magnetiques. *Ann. Phys. Chim.* **1823**, *22*, 375–389.

(172) Venkateshvaran, D.; Broch, K.; Warwick, C. N.; Sirringhaus, H. Thermoelectric Transport Properties of High Mobility Organic Semiconductors. *Proc. SPIE* **2016**, *9943*, 99430U.

(173) Peltier, J. C. A. Nouvelles Expériences Sur La Caloricité Des Courans Électriques. *Ann. Chim. Phys.* **1834**, *2* (LVI), 371–387.

(174) Yvenou, E. Développements de Modules Thermoélectriques Imprimés et Flexibles Pour Des Applications À Température Ambiente, 2017.

(175) Thomson, W. On a Mechanical Theory of Thermo-Electric Currents. *Proc. R. Soc. Edinburgh* **1851**, *III* (42), 91–98.

(176) Ichiro, T. *Introduction To Thermoelectricity*; 2016.

(177) Altenkirch, E. Elektrothermische Kälteerzeugung Und Reversible Elektrische Heizung. *Phys. Zeitschrift* **1911**, *12*, 920–924.

(178) Bubnova, O. Thermoelectric Properties of Conducting Polymers, Linköping University, 2013.

(179) Fleurial, J.-P. Short Course on Thermoelectrics. The International Thermoeelectric Society 1993, pp 1–27.

(180) Snyder, G. J.; Toberer, E. S. Complex Thermoelectric Materials. *Nat. Mater.* **2008**, *7* (February), 105–114.

(181) Forman, C.; Muritala, I. K.; Pardemann, R.; Meyer, B. Estimating the Global Waste Heat Potential. *Renew. Sustain. Energy Rev.* **2016**, *57*, 1568–1579.

(182) Patel, S. N.; Chabinyc, M. L. Anisotropies and Thermoelectric Properties of Semiconducting Polymers. *J. Appl. Polym. Sci.* **2016**, *134* (3), 44403.

(183) McGrail, B. T.; Sehirlioglu, A.; Pentzer, E. Polymer Composites for Thermoelectric Applications. *Angew. Chemie Int. Ed.* **2015**, *54* (6), 1710–1723.

(184) Bubnova, O.; Khan, Z. U.; Malti, A.; Braun, S.; Fahlman, M.; Berggren, M.; Crispin, X. Optimization of the Thermoelectric Figure of Merit in the Conducting Polymer poly(3,4-Ethylenedioxythiophene)., Nature Publishing Group, 2011, Vol. 10, pp 429–433.

(185) Park, B. T.; Park, C.; Kim, B.; Shin, H.; Kim, E.; Park, T. Flexible PEDOT Electrodes with Large Thermoelectric Power Factors to Generate Electricity by the Touch of Fingertips. *Energy Environ. Sci.* **2013**, *6* (3), 788–792.

(186) Bubnova, O.; Berggren, M.; Crispin, X. Tuning the Thermoelectric Properties of Conducting Polymers in an Electrochemical Transistor. *J. Am. Chem. Soc.* **2012**, *134*, 16456–16459.

(187) Mai, C.; Liu, J.; Evans, C. M.; Segalman, R. A.; Chabinyc, M. L.; Cahill, D. G.; Bazan, G. C. Anisotropic Thermal Transport in Thermoelectric Composites of Conjugated Polyelectrolytes / Single-Walled Carbon Nanotubes. **2016**.

(188) Wei, Q.; Mukaida, M.; Kirihara, K.; Ishida, T. Experimental Studies on the Anisotropic Thermoelectric Properties of Conducting Polymer Films. *ACS Macro Lett.* **2014**, *3* (9), 948–952.

(189) Jiang, F.; Xu, J.; Lu, B.; Xie, Y.; Huang, R.; Li, L. Thermoelectric Performance of Poly(3,4-Ethylenedioxythiophene): Poly(styrenesulfonate). *Chinese Phys. Lett.* **2008**, *25* (6), 2202–2205.

(190) Mengistie, D. A.; Chen, C.; Boopathi, K. M.; Pranoto, F. W.; Li, L.; Chu, C. Enhanced Thermoelectric Performance of PEDOT : PSS Flexible Bulky Papers by Treatment with Secondary Dopants. *ACS Appl. Mater. Interfaces* **2015**, *7* (1), 94–100.

(191) Zhang, B.; Sun, J.; Katz, H. E.; Fang, F.; Opila, R. L.; Zt, S. T. Promising Thermoelectric Properties of Commercial PEDOT : PSS Materials and Their Bi2Te3 Powder Composites. *ACS Appl. Mater. Interfaces* **2010**, *2* (11), 3170–3178.

(192) Gao, C.; Chen, G. Conducting Polymer/carbon Particle Thermoelectric Composites: Emerging Green Energy Materials. *Compos. Sci. Technol.* **2016**, *124*, 52–70.

(193) Jiang, F.; Xiong, J.; Zhou, W.; Liu, C.; Wang, L.; Zhao, F.; Liu, H.; Xu, J. Organic Solvent Assisted Exfoliated MoS2 for the Optimized Thermoelectric Performance of Flexible PEDOT:PSS Thin-Film. *J. Mater. Chem. A* **2016**, *4* (14), 5265–5273.

(194) Lei, T.; Xia, X.; Wang, J.; Liu, C.; Pei, J. " Conformation Locked " Strong Electron-Deficient Poly(p-Phenylene Vinylene) Derivatives for Ambient-Stable N-Type Field-Effect Transistors: Synthesis, Properties, and Effects of Fluorine Substitution Position. *J. Am. Chem. Soc.* **2014**, *136* (5), 2135–2141.

(195) Wang, H.; Hsu, J.-H.; Yi, S.-I.; Kim, S. L.; Choi, K.; Yang, G.; Yu, C. Thermally Driven Large N-Type Voltage Responses from Hybrids of Carbon Nanotubes and Poly(3,4-Ethylenedioxythiophene) with Tetrakis(dimethylamino)ethylene. *Adv. Mater.* **2015**, n/a – n/a.

(196) Shi, K.; Zhang, F.; Di, C.; Yan, T.; Zou, Y.; Zhou, X. Supporting Information for Towards High Performance N -Type Thermoelectric Materials by Rational Modification of BDPPV Backbones. *J. Am. Chem. Soc.* **2015**, *137* (22), 6979–6982.

(197) Shi, K.; Wu, Y.; Lu, Z.; Liu, H.; Wang, J.; Pei, J. Enhanced Molecular Packing of a Conjugated Polymer with High Organic Thermoelectric Power Factor. *ACS Appl. Mater. Interfaces* **2016**, *8* (37), 24737–24743.

(198) Schlitz, R. a.; Brunetti, F. G.; Glaudell, A. M.; Miller, P. L.; Brady, M. a.; Takacs, C. J.; Hawker, C. J.; Chabinyc, M. L. Solubility-Limited Extrinsic N-Type Doping of a High Electron Mobility Polymer for Thermoelectric Applications. *Adv. Mater.* **2014**, *26*, 2825–2830.

(199) Wan, C.; Gu, X.; Dang, F.; Itoh, T.; Wang, Y.; Sasaki, H.; Kondo, M.; Koga, K.; Yabuki, K.; Snyder, G. J.; Yang, R.; Koumoto, K. Flexible N-Type Thermoelectric Materials by Organic Intercalation of Layered Transition Metal Dichalcogenide TiS2. *Nat. Mater.* **2015**, *14* (6), 622–627.

(200) Winther-jensen, B.; West, K. Stability of Highly Conductive Poly-3 , 4-Ethylene-Dioxythiophene. *React. Funct. Po* **2006**, *66* (5), 479–483.

(201) Winter, I.; Reese, C.; Heywang, G.; Jonas, F. The Thermal Ageing of Poly (3 , 4-Ethylenedioxythiophene). An Investigation by X-Ray Absorption and X-Ray Photoelectron Spectroscopy. *Chem. Phys.* **1995**, *194* (1), 207–213.

(202) Rannou, P.; Nechtschein, M. Ageing of Poly (3 , 4-Ethylenedioxythiophene): Kinetics of Conductivity Decay and Lifespan. *Synth. Met.* **1999**, *101* (1-3), 474.

(203) Vitoratos, E.; Sakkopoulos, S.; Dalas, E.; Paliatsas, N.; Karageorgopoulos, D.; Petraki, F.; Kennou, S.; Choulis, S. A. Thermal Degradation Mechanisms of PEDOT : PSS. *Org. Electron.* **2009**, *10* (1), 61–66.

(204) Marciniak, S.; Crispin, X.; Uvdal, K.; Trzcinski, M.; Birgerson, J.; Groenendaal, L.; Louwet, F.; Salaneck, W. R. Light Induced Damage in poly(3,4-Ethylenedioxythiophene) and Its Derivatives Studied by Photoelectron Spectroscopy. *Synth. Met.* **2004**, *141*, 67–73.

(205) Wang, H.; Ail, U.; Gabrielsson, R.; Berggren, M.; Crispin, X. Ionic Seebeck Effect in Conducting Polymers. *Adv. Energy Mater.* **2015**, *5* (11), 1500044.

(206) Lee, S. H.; Park, H.; Kim, S.; Son, W.; Cheong, I. W.; Kim, J. H. Transparent and Flexible Organic Semiconductor Nanofilms with Enhanced Thermoelectric Efficiency. *J. Mater. Chem. A* **2014**, *2* (103), 7288.

(207) Khorasaninejad, M.; Walia, J.; Saini, S. S. Enhanced First-Order Raman Scattering from Arrays of Vertical Silicon Nanowires. *Nanotechnology* **2012**, *23* (27), 275706.

(208) Zanfrognini, B.; Colina, A.; Heras, A.; Zanardi, C.; Seeber, R.; López-palacios, J. A UV - Visible / Raman Spectroelectrochemical Study of the Stability of Poly (3 , 4-Ethylendioxythiophene) Films. *Polym. Degrad. Stab.* **2011**, *96* (12), 2112–2119.

(209) Garreau, S.; Louarn, G.; Buisson, J. P.; Froyer, G.; Lefrant, S. In Situ Spectroelectrochemical Raman Studies of Poly (3 , 4-Ethylenedioxythiophene) (PEDT). *Macromolecules* **1999**, *32*, 6807–6812.

(210) Garreau, S. Optical Study and Vibrational Analysis of the Poly (3 , 4-Ethylenedioxythiophene) Wavenumbers (Cm-L). *Synth. Met.* **1999**, *101* (1-3), 312–313.

(211) Łapkowski, M.; Pron, A. Electrochemical Oxidation of Poly Ž 3 , 4-Ethylenedioxythiophene / — "‘ in Situ ’" Conductivity and Spectroscopic Investigations. *Synth. Met.* **2000**, *110* (1), 79–83.

(212) Mitraka, E.; Jafari, M. J.; Vagin, M.; Liu, X.; Fahlman, M.; Ederth, T.; Berggren, M.; Jonsson, M. P.; Crispin, X. Oxygen-Induced Doping on Reduced PEDOT. *J. Mater. Chem. A* **2017**, *5* (9), 4404–4412.

(213) Wang, J.; Cai, K.; Shen, S. Z. Enhanced Thermoelectric Properties of Poly (3 , 4-Ethylenedioxythiophene) Thin Films Treated with H2SO4. *Org. Electron.* **2014**, *15* (11), 3087–3095.

(214) Palumbiny, C. M.; Liu, F.; Russell, T. P.; Hexemer, A.; Wang, C.; Müller-Buschbaum, P. The Crystallization of PEDOT:PSS Polymeric Electrodes Probed In Situ during Printing. *Adv. Mater.* **2015**, *27* (22), 3391–3397.

(215) Aleshin, A. N.; Kiebooms, R.; Menon, R.; Heeger, A. J. Electronic Transport in Doped Poly (3 , 4- Ethylenedioxythiophene) near the Metal- Insulator Transition. *Synth. Met.* **1997**, *90* (1), 61–68.

(216) Lindell, L.; Burquel, A.; Jakobsson, F. L. E.; Lemaur, V.; Berggren, M.; Lazzaroni, R.; Cornil, J.; Salaneck, W. R.; Crispin, X. Transparent, Plastic, Low-Work-Function poly(3,4-Ethylenedioxythiophene) Electrodes. *Chem. Mater.* **2006**, *18* (7), 4246–4252.

(217) Döbbelin, M.; Marcilla, R.; Salsamendi, M.; Pozo-gonzalo, C.; Carrasco, P. M.; Pomposo, J. A.; Mecerreyes, D. Influence of Ionic Liquids on the Electrical Conductivity and Morphology of PEDOT : PSS Films. *Chem. Mater.* **2007**, *8* (17), 2147–2149.

(218) Pyshkina, O.; Kurbakov, A.; Sergeyev, V. Poly(3,4-ethylenedioxythiophene):Synthesis and Properties. *Sci. J. Riga Tech. Univ. Mater. Sci. Appl. Chem.* **2010**, *21*, 51–54.

(219) Tsai, T. C.; Chang, H. C.; Chen, C. H.; Huang, Y. C.; Whang, W. T. A Facile Dedoping Approach for Effectively Tuning Thermoelectricity and Acidity of PEDOT:PSS Films. *Org. Electron. physics, Mater. Appl.* **2014**, *15* (3), 641–645.

(220) Petsagkourakis, I.; Pavlopoulou, E.; Portale, G.; Kuropatwa, B. A.; Dilhaire, S.; Fleury, G.; Hadziioannou, G. Structurally-Driven Enhancement of Thermoelectric Properties within Poly(3,4-Ethylenedioxythiophene) Thin Films. *Sci. Rep.* **2016**, *6*, 30501.

(221) Lee, Y. H.; Oh, J.; Lee, S.; Kim, H.; Son, J. G. Highly Ordered Nanoconfinement Effect from Evaporation-Induced Self-Assembly of Block Copolymers on In Situ Polymerized PEDOT:Tos. *ACS Macro Lett.* **2017**, *6* (4), 386–392.

Avec la demande sans cesse renouvelée de matériaux éco-compatibles pour l'électronique de demain, les polymères conducteurs se sont imposés comme une alternative intéressante aux matériaux déjà existants. Ils doivent leur popularité principalement à leurs propriétés électriques, optoélectroniques, thermo-chromiques, luminescentes et mécaniques, couplées à leur bonne processabilité et leur faible impact environnemental. Parmi eux, le poly(3,4-ethylenedioxythiophene) (PEDOT) est certainement le plus connu est le plus utilisé. De nombreuses études se sont focalisées sur l'optimisation de sa conductivité électrique et des progrès remarquables ont été réalisés. Cependant, la compréhension fine de la relation structure/propriétés de ce matériau reste à élucider. C'est ainsi que dans le cadre de cette thèse nous avons décidé de plusieurs objectifs qui sont (1) la synthèse de PEDOT hautement conducteurs à structure contrôlée et optimisée, (2) l'étude des propriétés électriques, structurales et de transport électroniques dans ces PEDOT, (3) l'étude de leurs propriétés thermoélectriques et (4) l'étude de leur stabilité sous différentes conditions afin de valider leurs potentielles applications. Ainsi, après une revue de la littérature sur le PEDOT, nous étudions l'amélioration de la conductivité électrique du PEDOT:OTf et du PEDOT:Sulf, qui atteint dorénavant des valeurs à hauteur de 5400 S cm^{-1}. Différentes techniques de caractérisation nous ont permis de mener une étude exhaustive de leurs propriétés électriques et structurales ainsi que des mécanismes de transport électronique qui en découlent. Nous nous sommes ensuite intéressés à deux de leurs propriétés thermoélectriques, l'effet Joule et l'effet Seebeck, le premier pour des applications en chauffage et le deuxième pour la récupération d'énergie. L'utilisation pour la première fois du PEDOT comme film chauffant flexible transparent est d'ailleurs présentée. On démontre par exemple que PEDOT:Sulf présente une résistance carrée de 57 Ω sq^{-1} pour 87.8 % de transparence et qu'une température de 138 °C peut être atteinte lorsqu'on applique 12 V. Cette thèse se conclut sur l'étude de la stabilité de nos matériaux de PEDOT sous différentes atmosphères ainsi que l'étude des mécanismes de dégradation.

With the rising demand of flexible, low cost and environmentally friendly materials for future technologies, organic materials are becoming an interesting alternative to already existing inorganic ones. Organic photovoltaics, organic light emitting diodes, organic field effect transistors, organic thermoelectricity, organic transparent electrodes are all evidences of how organic materials are sought for tomorrow. Materials which can fulfill the requirements specifications of future technologies are conducting polymers, which owe their popularity to their outstanding electrical, optoelectronic, thermochromic, lighting and mechanical properties. Moreover, they exhibit good processability even on flexible substrates and low environmental impact. Poly(3,4-ethylenedioxythiophene) (PEDOT) is certainly the most known and most used conducting polymer because it is commercially available and shows great potential for organic electronics. Studies dedicated to PEDOT films have led to high conductivity enhancements. However, an exhaustive understanding of the mechanisms governing such enhancement is still lacking, hindered by the semi-crystalline nature of the material itself. In such a context, this thesis has four objectives which are (1) the synthesis of PEDOT materials with an optimized and controlled structure to enhance the electrical properties, (2) the thorough characterization of the as-synthesized PEDOT in order to understand the charge transport mechanisms, (3) the study of their thermoelectric properties and (4) the study of their stability under different environments and stresses. Thus, after a literature review on PEDOT materials, we present the enhancement of the electrical conductivity of PEDOT:OTf and PEDOT:Sulf up to 5400 S cm^{-1} via a structure and dopant engineering, and then thoroughly study their electrical and electronic transport properties. Subsequently, two thermoelectric properties of PEDOT are investigated, namely its resistive Joule heating ability and its Seebeck effect, for both heating and energy harvesting applications. A novel application of PEDOT as flexible transparent heater is demonstrated in the first case. PEDOT:Sulf for example exhibited a sheet resistance of 57 Ω sq^{-1} at 87.8 % transmittance and reached a steady state temperature of 138 °C under 12 V bias. Finally, this thesis is concluded with the ageing and stability of our PEDOT based materials under different environmental stresses. While PEDOT is stable under mild conditions, heavy degradations can occur under harsh conditions. The degradation mechanisms are then investigated in this last part.